Action, valence, dopamine – *Drosophila* as a study case

Thesis

for the degree of

doctor rerum naturalium (Dr. rer. nat.)

approved by the Faculty of Natural Sciences of Otto von Guericke University Magdeburg

by M.Sc. Fatima Amin
born on 06.09.1991 in Cumilla, Bangladesh

Examiner: Prof. Dr. Bertram Gerber
Prof. Dr. Ansgar Büschges

submitted on: 17.02.2025
defended on: 26.09.2025

Summary

In this thesis, my focus will be on the mechanistic relationships between action, valence and dopamine in adult fruit fly, *Drosophila melanogaster*, and the biomedical implications that the uncovered relationships might have. Here I investigated two main aspects:

1) How action confers valence? - as my main PhD project (Chapter 1)

2) How timing affects valence? (Chapter 2)

In Chapter 1, my work was inspired by William James's theory of emotion:

Common sense says, we lose our fortune, are sorry and weep; we meet a bear, are frightened and run; we are insulted by a rival, are angry and strike. The hypothesis here to be defended says that this order of sequence is incorrect. *(James, 1890, p. 449)*

This theory, strikingly, questioned the conventional way of thinking that emotions cause action. Rather, he proposed it can be the other way around-namely animals take action, and it is the action that causes the emotion!

Therefore, I developed an unconventional experimental twist for action-to-perceived emotional experience (valence) causation by asking a simple question namely can moving backward make flies 'feel bad' about odours experienced during this action?

Hereby, I established a neurobiologically yielding study case to understand how action, valence and dopamine processing are related and its biological significance in solving the long-standing so-called avoidance paradox for a simple animal model- *Drosophila melanogaster*-as an example.

In Chapter 2, I investigated a fundamental aspect of valence processing as such, namely its dependence on the timing of its occurrence and its termination. Here the focus will be on dissociating dopaminergic from non-dopaminergic mechanisms in timing-dependent valence processing.

Regarding both chapters, I will discuss plausible biomedical implications.

Zusammenfassung

In dieser Arbeit konzentriere ich mich auf die mechanistischen Beziehungen zwischen Handlung, Valenz und Dopamin in der erwachsenen Fruchtfliege Drosophila melanogaster und auf die biomedizinischen Auswirkungen, die aufgedeckten Beziehungen haben könnten. Ich habe zwei Hauptaspekte untersucht:

1) Wie wird Valenz durch Handlung vermittelt? - als mein Haupt-Doktorandenprojekt (Kapitel 1)

2) Wie beeinflusst das Timing die Valenz? (Kapitel 2)

In Kapitel 1 wurde meine Arbeit von William James' Theorie der Emotionen inspiriert:

Common sense says, we lose our fortune, are sorry and weep; we meet a bear, are frightened and run; we are insulted by a rival, are angry and strike. The hypothesis here to be defended says that this order of sequence is incorrect. *(James, 1890, p. 449)*

Diese Theorie stellte die herkömmliche Denkweise in Frage, dass Emotionen Handlungen verursachen. Stattdessen schlug er vor, dass es auch andersherum sein könnte - nämlich dass Tiere handeln und die Handlung die Emotion verursacht!

Daher habe ich eine unkonventionelle experimentelle Methode entwickelt, um die Beziehung zwischen Handlung und wahrgenommener emotionaler Erfahrung (Valenz) zu untersuchen, indem ich eine einfache Frage stellte: Kann eine Rückwärtsbewegung dazu führen, dass Fliegen die Gerüche, die sie während dieser Aktion wahrnehmen, als schlecht empfinden?

Damit habe ich einen neurobiologisch ergiebigen Studienfall geschaffen, um am Beispiel eines einfachen Tiermodells - Drosophila melanogaster - zu verstehen, wie Handlung, Valenz und Dopaminverarbeitung zusammenhängen und welche biologische Bedeutung sie für die Lösung des langjährigen sogenannten Vermeidungsparadoxons haben.

In Kapitel 2 habe ich einen grundlegenden Aspekt der Valenzverarbeitung als solche untersucht, nämlich ihre Abhängigkeit vom Zeitpunkt ihres Auftretens und ihrer Beendigung. Hier liegt der Schwerpunkt auf der Unterscheidung von dopaminergen und nicht-dopaminergen Mechanismen

In beiden Kapiteln werde ich plausible biomedizinische Implikationen diskutieren.

Table of contents

General Introduction

Background

Over 120 years ago, William James (*Mind*, 1884), proposed the idea of subjective experience of emotions marked by “distinct bodily expression” (Friedman, 2010). James’s theory was greatly influenced by Darwin’s (1872) *The expression of emotion in man animals* (Dunlap, 1922/1967). A similar model at the similar era was also independently proposed by Carl Lange (1885/1912), which hence was often called as ‘James-Lange theory of emotion’.

This theory faced a lot of challenges from the field of psychophysiology, namely from Cannon-Bard (1939) and Schachter-Singer (1962) study. The major challenge, till today, has been to test it experimentally! In fact, James explicitly stated in *Mind* that his theory applied to emotions that have a distinct bodily expression- otherwise afferent sensory feedback would not be providing the differentiating information of certain emotions (Friedman, 2010). Overall, this confined the theory to more hurdles to be tested. Nevertheless, it inspired a number of subsequent emotion research with mixed results. For example, the facial feedback hypothesis (Strack et al., 1988) which studied whether and how subjective facial expressions can influence their affective experience. According to Darwin’s (1872) - an emotion that is freely expressed by outward signs will be intensified, whereas an emotion whose expression is repressed will be softened. In simpler words, smiling (e.g. pen in mouth task, stark 1988) makes one feel good, or frowning makes one feel bad. Despite some disagreements, this hypothesis has been supported by several experimental paradigms and recently by a large adversarial team conducting a multi lab test to test the hypothesis (Coles et al., 2022). Very recently in mice supportive evidence has been observed where increasing heart rate and inducing specific breathing patterns can result in fearful emotion (Hsueh et al., 2023; Jhang et al., 2024).

However, even after more than a century, it remains an open question **how** action and valence are mutually related, what is the **physiology** behind this relationship and finally what is the **biological significance**?

As per Darwin’s “The expression of the Emotions in Man and Animals, 1872”-

We may conclude that our subject (theory of expression) has well deserved the attention which it has already received from several excellent observers, and that it deserves still further attention, especially from any able physiologist. *(Darwin, 1872)*

And with this inspiration from Darwin, all the above-mentioned questions I addressed in this thesis with a simple but elegant study model- *Drosophila melanogaster*.

Why *Drosophila*?

Understanding the complexity of the nervous system has always been the central goal of neuroscience. To track down the neural circuits underlying learning and memory, adaptive behaviour, locomotion, sensory adaptation and so on, it's then prudent to use a relatively simple model. Along that line, *Drosophila* in research is quite successful (Kohler, 1994) pioneered by the Nobel Prize winning work of Thomas Hunt Morgan to prove the chromosomal theory of inheritance. Since then, *Drosophila* has been widely used. Not only for the easy breeding, short life cycle, continuously developing genetic tools, cost effectiveness but also for combining genetic perturbations with spatio-temporally precise cell-labelling methods (Clark et al., 2022), we have now profound (albeit incomplete) understanding of molecular, anatomical and physiological properties of *Drosophila melanogaster*. Together, it offers a versatile possibility for combined and comprehensive behavioural and neurogenetic analyse of associative memory systems (Heisenberg, 2003; Gerber and Aso, 2017; Cognigni et al., 2018; Boto et al., 2020; Li et al., 2020; Modi et al., 2020; Davis, 2023).

In the following sections, I will give an overview of some of the key genetic tools as they have been used towards this end in this study.

The GAL4-UAS system

Among the various genetic tools, the famous one is a two-part (binary) system namely the GAL4-UAS system (Brand and Perrimon, 1993). This system allows cell or tissue specific targeted gene expressions in embryos, larvae and adult *Drosophila*. With this method, any gene of interest, even a lethal one, can be expressed. This binary system has two parts: 1) the GAL4, a yeast transcription factor, composed of DNA-binding domain (DBD) and activation domain (AD) which can be artificially expressed under the control of a cell-specific promoter, 2) the upstream activating sequence (UAS) transgene construct. The GAL4 protein decides 'where' to target and binds to the UAS combined with a 'what' gene of interest downstream to it. These two parts are maintained in two separate parental strains: the driver and the effector strain respectively. By a simple crossing of a GAL4 driver fly with a UAS effector fly one can thus manipulate exclusively the gene of interest in those targeted cells in the offsprings. By this method, GAL4-DBD recognizes the UAS and AD recruits' the transcriptional machinery to activate the transcription process to express the gene of interest in cell specific manner (Figure 0.1a).

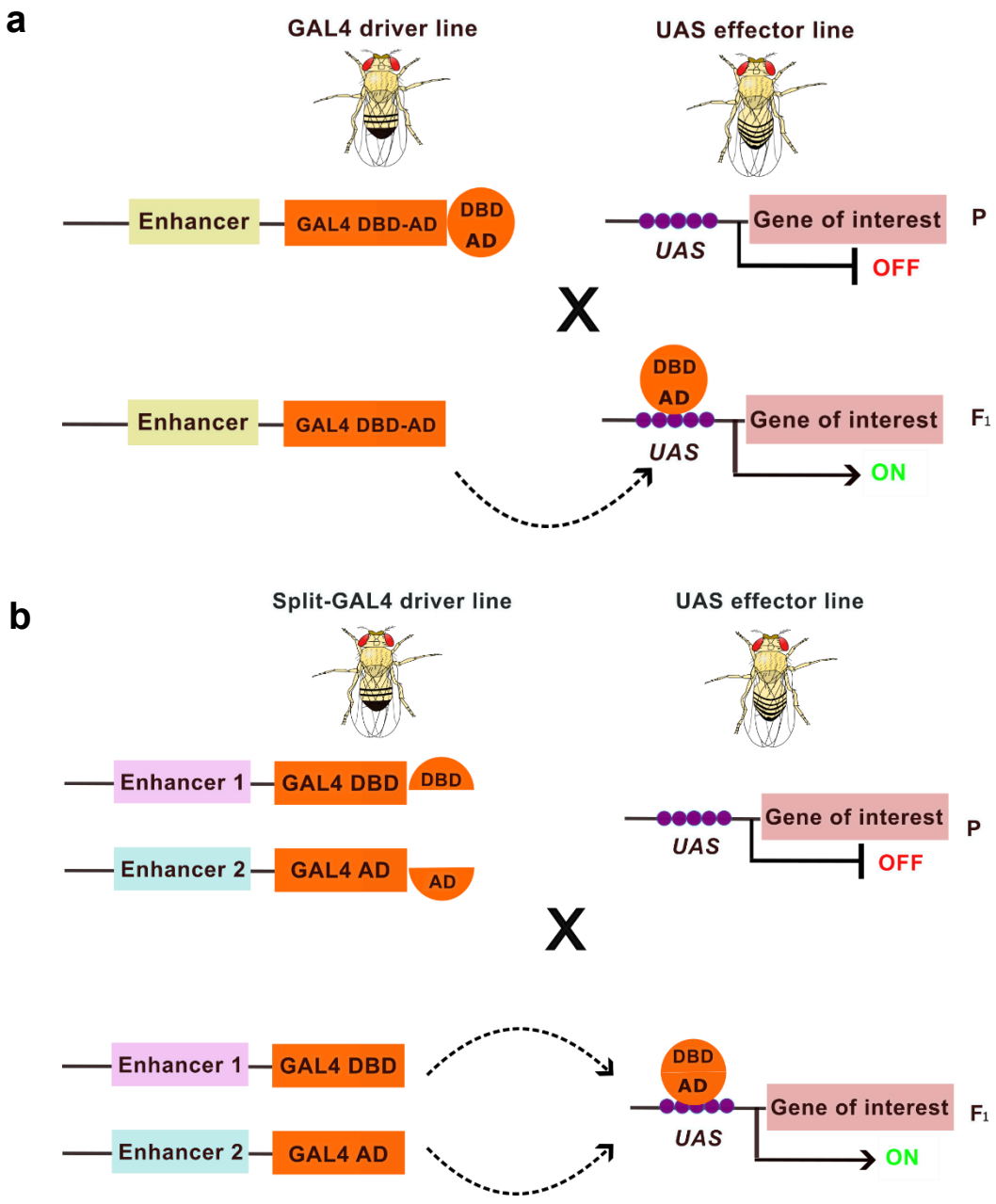

Figure 0.1 | The GAL-UAS system. (a) Parental (P) GAL4 driver fly contains GAL4 transcription factor composed of DBD-AD (orange) under the control of a specific genomic enhancer (yellow). It is crossed with effector fly (P) with UAS (purple) – upstream to a target gene of interest (pink). In the offspring (F_1), GAL4 protein (DBD-AD) binds to the UAS and enables the transcription at UAS of the target gene. **(b)** Split-GAL4 driver line (P) consists of two functional domains DBD and AD of the GAL4 protein under two enhancers 1 (lavender) and 2 (cyan) respectively. It is crossed with another fly (P) with UAS – upstream to a target gene of interest. In the offspring (F_1), only when both domains DBD-AD binds with the UAS, enables the transcription process at tissue specific manner (inspired from Luan et al., 2020, Wikipedia).

A step further cell specificity expression has been achieved with the development of the Split-GAL4/UAS method (Luan et al., 2006; Pfeiffer et al., 2010). In this method, the GAL4 gene is split into its two domains: activation domain (AD) under one enhancer and DNA binding domain under another enhancer. These domains are not able to promote gene expression alone. Only in the intersection of cells, where both domains are expressed, a functional GAL4 protein is produced and upon binding with UAS leads to transgene expression (Figure 0.1b). Thus, the development of the GAL4/split-GAL4-UAS system has given us the opportunity to work with a well-defined population of neurons or even single neurons by expressing a variety of genes of interest (e.g. ChR: light gated cation channel to depolarize neurons, GCaMP: calcium sensitive reporter to monitor neuronal activity, see the upcoming sections for further details) to manipulate or monitor these single neurons or groups of neurons. The collection of GAL4 and split-GAL4 drivers and UAS effector lines is still developing, and many of these are available in Bloomington Drosophila Stock Center (BDSC) and Vienna Drosophila Resource Center (VDRC).

Similarly, there is another binary system namely the lexA-lexAop system (Lai and Lee, 2006). The major advantage of having an independent system is that it allows stimulation of one set of neurons by for example the GAL4/UAS system and recording the other set of neuronal activity at the same time using the lexA-lexAop system, or vice versa (Owald et al., 2015; Barnstedt et al., 2016; Felsenberg et al., 2017,2018).

Optogenetics: tool to manipulate neuronal activity

Among the effector transgenes, optogenetics has gained immense popularity to manipulate neuronal activity with light. Optogenetics is a tool to genetically express light sensitive microbial opsins e.g. ion channels, ion pumps, or enzymes into target specific neurons to either activate or inhibit their physiological state by using light pulses in a millisecond resolution (Deisseroth, 2011; Klapoetke et al., 2014; Riemensperger et al., 2016). Such interference allows us to understand the relationship between induced neuronal activity and the subsequent behavioural changes. The field of optogenetics soared in late 2005 with the introduction of the algae protein Channelrhodopsin 2 (ChR2). ChR2 is a blue light gated cation channel (Nagel et al., 2002, 2003; Boyden et al., 2005; Klapoetke et al., 2014) taken from green algae *Chlamydomonas reinhardtii* which has a seven transmembrane cation channel with light isomerisable chromophore all trans retinal (ATR). This ATR undergoes a conformational change upon blue light absorption leading to opening of Na+ ion channel within millisecond time range (Harz and Hegemann, 1991; Nagel et al., 2002, 2003). In *Drosophila*, ChR2 has been successfully used with additional supplementation of ATR feeding. Recently, an advanced version of ChR2, termed ChR2-XXL has been developed

with high expression, increased photocurrent amplitude and without any complementing food with ATR (Dawydow et al., 2014). However, ChR2-XXL has some limitations such as the visibility of blue light to flies, incompatibility during imaging due to the fluorophore in the green spectrum leading to intrinsic blue absorption and inadequate tissue penetration capacity (Salcedo et al., 1999).

But these obstacles were circumvented with the development of red-shifted ChR namely Chrimson (Klapoetke et al., 2014) having faster kinetics yet effective light sensitivity, deeper tissue penetration, minimum visual interference. Along the minimal interference with the blue-green excitation/emission spectrum of GCaMP, these features make Chrimson the preferred choice for combining neuronal activation with calcium imaging which I will discuss in detail in the next segment.

Another extensive use of optogenetics is to inhibit neuronal firing with light. It is an anion channelrhodopsin variant discovered first in Guillardia theta algae, namely GtACR1 and GtACR2. This provides a green light gated large anion (Cl-) conductance leading to efficient membrane hyperpolarization and thus potent neuronal silencing (Govorunova et al., 2015, 2017). It has faster kinetics with high conductivity and precise anion selectivity (Figure 0.2).

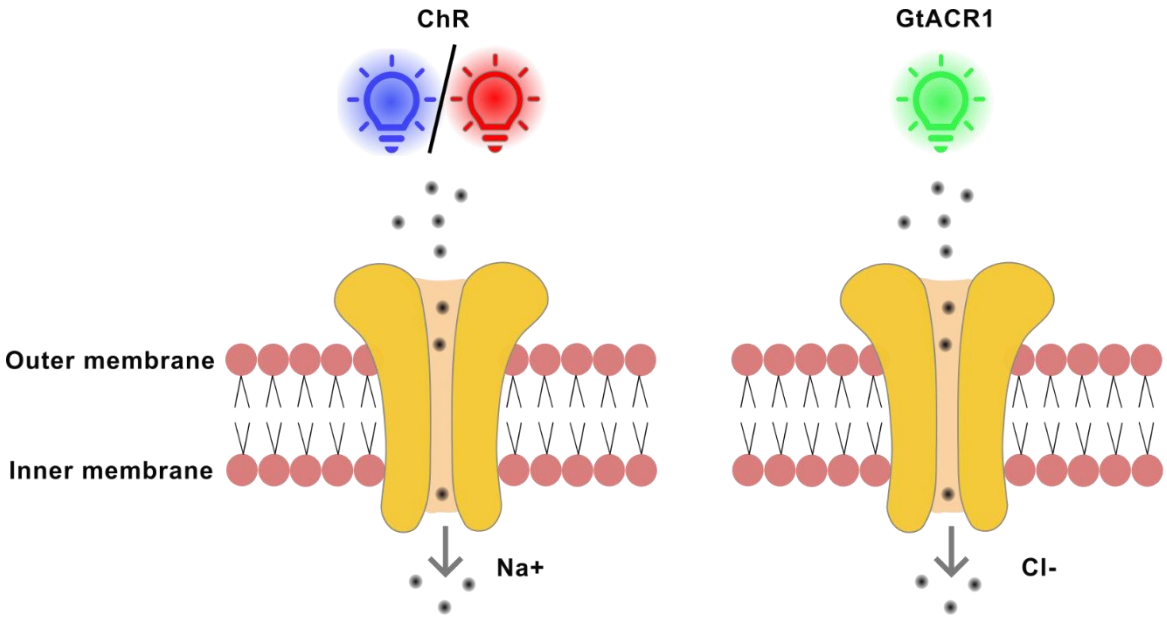

Figure 0.2 | Optogenetics allows to manipulate neuronal activity. (Left) ChR is a light gated cation channel. Blue light (465 nm) induces a conformational change and opens the cation (Na+) channel. This depolarizes the cell and activates the neuron by causing an action potential. Another variant of ChR (Chrimson) performs a similar function with red light (630 nm). (Right) The green light (532 nm) gated anion (Cl-) channel hyperpolarizes the cell and inhibit neuronal activity (figure is inspired from Wikipedia).

Calcium imaging: tool to observe neuronal activity

The central goal of neuroscience revolves around understanding the process of how, why and which neurons communicate with each other to generate either action, emotions or memory. Continuous development of genetic tools has made it possible to record neuronal activity at the milliseconds range for a duration of minutes to weeks range, often in largely intact, behaving animals. One of the popular and reliable optical neural activity recording technique is calcium imaging. Calcium imaging relies on the flux of calcium ions which is the indispensable determinant in intracellular signalling to exert major functions in all types of neurons (Grienberger and Konnerth, 2012). Therefore, visualizing and quantifying the calcium trace on neurons of interest allows us to investigate biologically meaningful neuronal activity even in behaving animals.

Calcium imaging is basically an experimental technique to detect the change of intracellular calcium concentration ($Ca^{2+)}$ by using fluorescent calcium indicators (Grienberger et al., 2022). So, the idea would be the moment neurons fire action potentials there is an increase in intracellular calcium level. And this change of calcium level will then be detected by the fluorophore binding to calcium. The revolution in calcium imaging happened with the discovery of green fluorescent protein (GFP) (Tsien, 1998). The combination of this fluorescence protein and calcium binding protein then led to the development of the single-fluorophore genetically encoded calcium indicators (GECIs) (Mank and Griesbeck, 2008; Tian et al., 2009; Lütcke, 2010). The exemplary member of this GECIs is the GCaMP family (Wang et al., 2003; Chalasani et al., 2007; Fletcher et al., 2009; Dombeck et al., 2010). From Grienberger and Konnerth, 2012, GCaMPs consist of a circularly permuted enhanced green fluorescent protein (EGFP) bound to calcium binding protein calmodulin (CaM) and calmodulin binding peptide M13 (Nakai et al., 2001). This CaM-M13 complex undergoes a calcium-dependent conformational change and exerts changes in the fluorescent emission intensity (Figure 0.3) (Nakai et al., 2001; Tian et al., 2009). Since its original development, GCaMP family has been continually developed with regards to its signal to noise ratio, dynamic range and response kinetics. For instance, GCaMP6s has better Ca^{2+} affinity and fluorescence intensity but it has slower kinetics in comparison to GCaMP6f with rapid kinetics allowing the detection of single action potentials (Chen et al., 2013). Recently, even improved GCaMP sensors have been developed e.g. jGCaMP8s, m, f with improved kinetics and without compromising brightness (Zhang et al., 2023). During in-vivo calcium imaging experiments, GCaMP6f was used in this study.

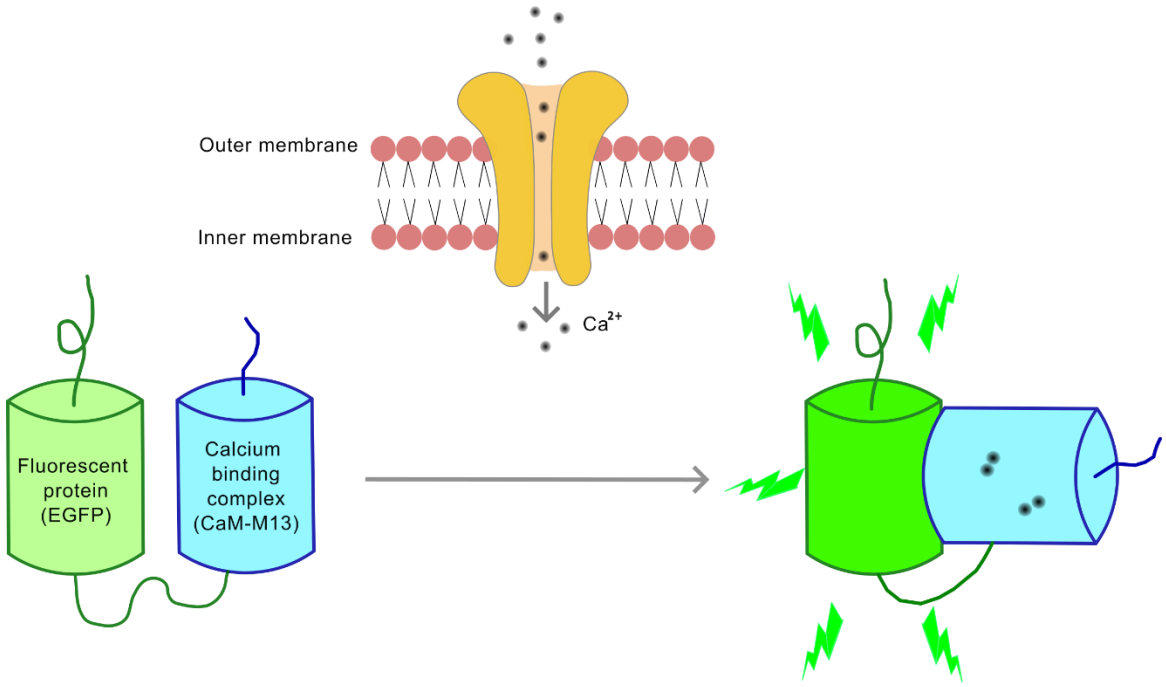

Figure 0.3 | Calcium indicator to monitor neuronal activity. GCaMP consists of a circularly permuted EGFP (light green) linked to calcium binding complex, CaM-M13 (cyan). Upon increased intracellular calcium (Ca^{2+}) level, CaM-M13 complex obtains a conformational change and its proximity to EGFP induces increased fluorescence emission (adapted from Grienberger et al., 2022).

Other than GCaMPs, there are also other calcium indicators: 1) chemical calcium indicators (e.g. Indo-1, Fura-2, Fluo-4), 2) FRET-based GECI (e.g. TN- XXL). To observe neural activity, another way, albeit having a very low signal to noise ratio, would be to measure the voltage changes through patch-clamp electrophysiology or by genetically encoded voltage indicators (GEVIs) (Perron et al., 2009; Akemann et al., 2012).

Connectome: resources to understand brain→behaviour

A connectome is a list of neurons and the chemical synapse between them. Although it sounds easy, in practical this is a challenging task to accomplish considering not only the numbers of neurons but also the problem of identifying the types and transmitters of neurons and how and to what extend they are connected to their upstream and downstream neurons! To date, only three organisms of having only several hundred brain neurons had the full connectome data set available: *Caenorhabditis elegans*; larva of *Ciona intestinalis* and *Platynereis dumerilii* (Winding et al., 2023). A very recent addition on that is the full connectome of the 1st instar larva of *Drosophila.* For the adult fly brain, connectome analysis started in 1991 by analysis a series of electron microscopic (EM) cross sections (Meinertzhagen and O'Neil, 1991). These efforts continued and massively expanded since then and recent advances in molecular genetics, digital

resources and collaborative tools to involve a large community of researchers is making it possible to produce different complete connectome datasets for adult fly brain and ventral nerve cord in male and female flies. Major remaining challenges include stitching together brain and ventral nerve cord datasets, relating their analyses to behaviour, and underlying mechanism. Regardless, already at this stage the available connectomics information provides a highly versatile resource to contextualize current studies into the neurogenetic bases of behaviour. Below is an overview of the available *Drosophila* connectome datasets in Table 0.1.

Table 0.1: Overview of *Drosophila* connectome

Connectome dataset	Source
Whole brain connectome of adult female (CODEX, FlyWire, Neuprint)	Dorkenwald et al., 2024; Schlegel et al., 2024
Male adult ventral nerve cord connectome (MANC)	Cheong et al., 2024; Takemura et al., 2024
Female adult ventral nerve cord connectome (FANC)	Azevedo et al., 2024
1st instar larva	Winding et al., 2023

After this general overview about tools and resources to study *Drosophila*, in the successive parts I will discuss, as the general backdrop of the current thesis, learning processes more generally and with a focus on olfactory associative learning in flies, the organization of the memory centre of fly brain, its dopaminergic system, and the output pathways to descending neurons and behavioural control.

Learning and memory: in *Drosophila*

"Present is the memory of the past; present is the perception of the presence and present is the expectation of the future"

Augustine, Confessions, Book 11, Chapter 20

Learning and memory are inextricably intertwined as it's almost impossible to study one without the other. They are like two sides of a same medal as such the psychochemical changes happens during learning last as memory traces. When these traces are addressed again, the learned behaviour is recalled again as memory. And during the course of life, animals need to organize their behaviour/keep updating their learning based on memory, according to necessity. However, memories are not an old recorder to replay by pressing the past button again and again (Gerber et al., 2004) rather memory is a process of coding, storing and retrieving information about our experience/learning to adjust future behaviour (Lieberman, 2020).

So continuous updates are going on by various known and unknown mechanisms. These kinds of processes include non-associative as well as associative learning (Gluck, 2016). Non-associative learning commonly includes sensitization and habituation. While associative learning is learning about the causal relationship between two events. It includes classical conditioning and operant conditioning. In classical conditioning, animals learn the relationship of two stimuli while operant conditioning is learning between a response and the consequence that follows it. Such associative learning has been observed across the animal kingdom, not only on higher complex organisms but also simple organisms like *Drosophila melanogaster*.

In this thesis, I conducted olfactory classical/ Pavlovian conditioning with adult *Drosophila melanogaster* as a tool to answer the aim of my project which I will discuss in the following parts.

Classical conditioning

Ivan Petrovich Pavlov (1927) with his classical conditioning experiment created worldwide excitement. In his experiment dogs were trained to associate the ringing of a bell (conditioned stimulus, CS) with the presentation of food (unconditioned stimulus, US). The salivation (unconditioned response, UR) could also occur upon naïve presentation of food (US) and no response upon isolated ringing of bell. He discovered that after a conditioning procedure in which CS was repeatedly followed by the US, dogs would also salivate (conditioned response, CR) after only ringing the bell. The fundamental principles of such association were thought to be the following:

i) contiguity: the association can be formed between events that occur together,
ii) frequency: how many times those events occurred
iii) intensity: determined the strength of that association

Until 1966, the picture of classical conditioning was coherent and satisfying with its above-mentioned foundation stones. Then Robert Rescorla came with the concept of contingency. He showed that contiguity is not sufficient for conditioning. Rather he suggested that it's the precise contingency between the stimuli that matters most. As per his theory, contingency is a simple mathematical summary of a relationship between two events, at which degree they occur relative to another- the greater the linkage of occurrence together, the greater contingency. This contingency refers to the probability that a US will occur in the presence of a CS or in the absence of a CS (Lieberman, 2020). Both contiguity and contingencies describe the strength of conditioned responses (Schultz, 2006, 2015).

Olfactory conditioning in *Drosophila*

Quinn et al., (1974) showed that olfactory and visual associative learning can be formed in *Drosophila melanogaster*. While visual learning was less extensive, olfactory associative learning was sophisticated with characteristic features e.g. sustainable but yet rapidly extinguishable or reversed by retraining. However, there were some shortcomings such as the willingness of fly to enter the training tubes with their first behavioural setup (McGuire, 1984; Tully, 1984). This led Tully and Quinn (1985) to introduce a new behavioural paradigm in a T-maze apparatus to test classical conditioning in *Drosophila* more stringently. In this setup, there are electrifiable training tubes where flies experience one odour with electric shock as punishment and another odour without shock. Then there is an elevator compartment to fly transfer and two test tubes that is approached from a choice point (Tully and Quinn, 1985) which reduces the handling of flies. Since then, it has been widely used to test aversive olfactory learning (Tully et al., 1994a, 1994b; Pascual and Préat, 2001; Aso et al., 2014a; Aso et al., 2014b). For olfactory appetitive learning, instead of electric shock, one odour is associated with 1M sucrose painted tube. A similar modified T-maze apparatus has also been used in our lab which allows us to run 4 experiments in parallel, as all the behavioural experiments in this thesis. Also, in this set up, optogenetic manipulation of neurons can also take place by shining light around the tubes (below is an example picture of the used T-maze apparatus, see Figure 0.4).

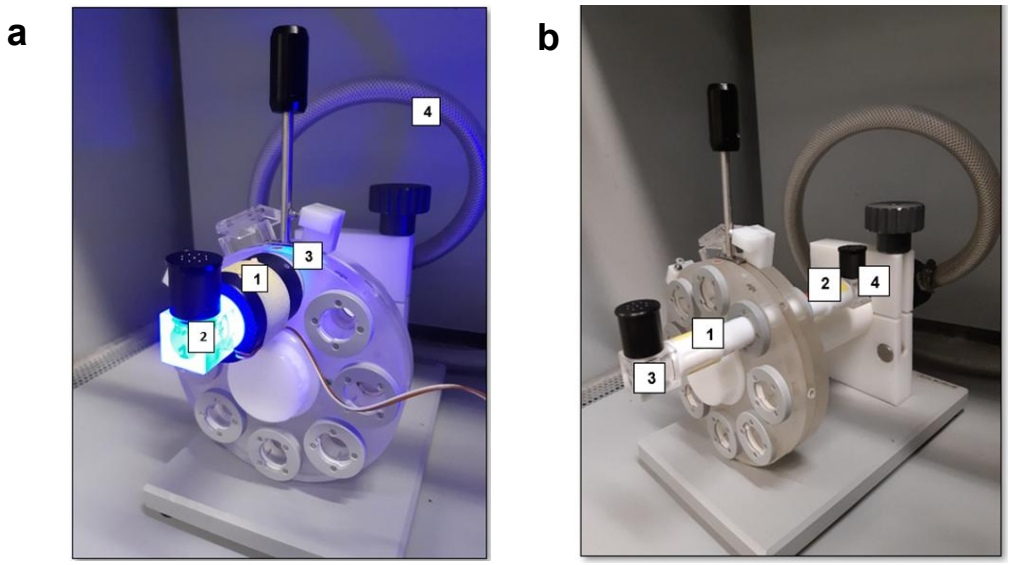

Figure 0.4 **(a)** Training apparatus containing (1) one training tube surrounded by LEDs allowing to use optogenetics, (2) odour container, (3) sliding wheel to move flies from training to test position within the apparatus, (4) attached tubing to vacuum pump for air flow. **(b)** (1,2) represents the test tubes while (3,4) represents the CS+ and CS- Oduors. The whole set up is surrounded by a box to keep the temperature and humidity constant. Tubes for presenting electric shock and additional three training and test tubes were omitted here for clarity.

How does memory formation take place?

The existing knowledge of CS-US pathways involved in olfactory associative learning in *Drosophila* has made it an excellent model organism to study not only at specific neuronal level but also synapse level (Aso et al., 2014a, 2014b; Aso and Rubin, 2016; Gerber and Aso, 2017; Menzel, 2022). And the harmony of precise neuronal activation via synaptic contacts are the pre-requisite of memory storing and implementation to act as a learning. Two brain regions particularly play the key role in the olfactory associative learning- the antennal lobe (AL)- the functional analogue of the olfactory bulb in mammals for the odour perception to proper processing and the mushroom body (MB)- the higher brain area to integrate the CS-US stimulus for olfactory memory formation in insect brain. In the subsequent segments of this thesis, these two pathways will be described in detail.

The olfactory CS pathway in the fly brain

Proper recognition and processing of olfactory information create an internal representation of the external world to most animals (Vosshall et al., 2000; Vosshall and Stocker, 2007). This representation is essential in simpler animals like *Drosophila* to detect food, predators and mating. The relatively simple brain made the olfactory processing in *Drosophila* quite tractable, and it begins with the perception of odour.

Flies primarily sense odour via olfactory sensory neurons (OSNs) located on the 3rd segment of antenna and the maxillary palp on the head (Stocker, 1994; Strausfeld et al., 1998; de Bruyne et al., 1999, 2001; Vosshall et al., 2000; Heisenberg, 2003; Keene and Waddell, 2007). These olfactory organs consist of a large number of sensory hairs, called sensilla (approx. 410 in antenna and 60 in maxillary palp) to house the OSNs. The sensory epithelium of the OSNs exhibit one of the 61 olfactory receptors (ORs) and an odorant co-receptor OR83b (Vosshall et al., 2000; Larsson et al., 2004) which are under the assumption belonging to classic G-protein coupled receptors (GPCRs). The axonal projections from thousands of OSNs expressing the same ORs bilaterally goes to the ~50 glomeruli in the antennal lobe (AL) and sorted according to chemosensitivity. The glomeruli consist of at least 3 classes of neurons- among which OSNs synapse with the excitatory projection neurons (PNs). The other two types are GABAergic local neurons (iLNs) and cholinergic local neurons (eLNs). Together they ‘shape’ complex antennal lobe firing pattern by inhibiting generalized ‘spread’ activity and thus modulate PNs response (Kenne and Waddel, 2007).

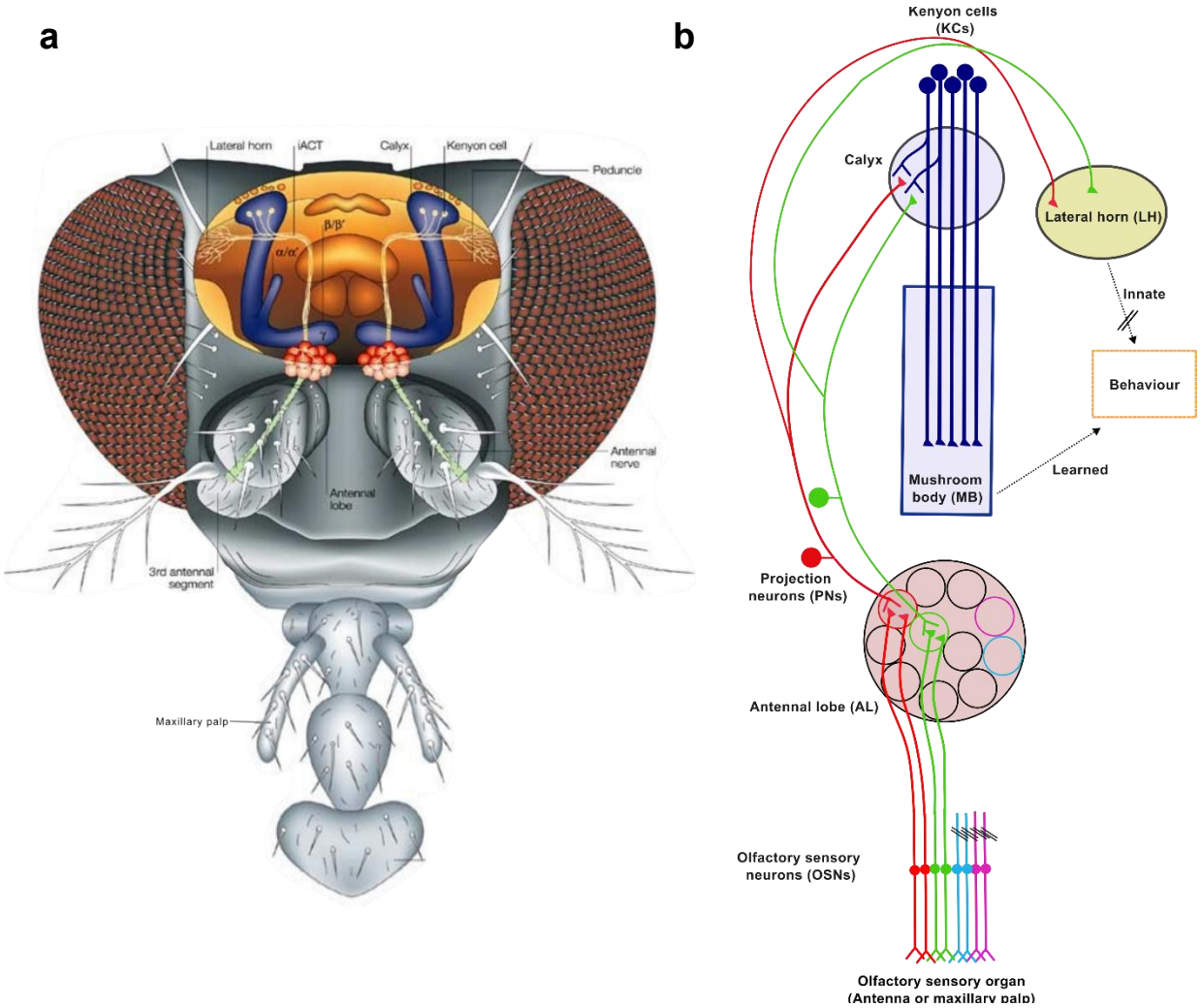

Figure 0.5│ **Olfactory CS pathway**. **(a)** Showing the main neuropils of olfactory pathways in adult *Drosophila* (adapted from Heisenberg 2003, Keene and Waddel 2007). **(b)** Simplified schematic of odour sensing pathways starting from olfactory sensory organs in antenna or maxillary palp and carried by olfactory sensory neurons (OSNs) (focusing only red and green) to antennal lobe (AL) glomeruli (light pink). From there projection neurons (PNs) (red, green) convey the information into calyx (CA) to dendritic claws of mushroom body intrinsic neuron Kenyon cells (KCs) (blue). KCs then project their axons to mushroom body lobes: α/β, α'/β' and γ (see **a**). PNs also carry olfactory information to lateral horn (LH) (yellow). Mushroom body (MB) and lateral horn (LH) plays role in learned and innate behavioural response respectively. In all figures, open triangle indicates the dendritic input and closed triangle the axonal output region. (//) depicts non-mentioned topics in this study.

There are about 150 PNs in adult flies and 3-5 innervate each glomerulus. A possible notion is that PNs respond selectively to the same odour likewise their afferent OSNs (Vosshall 2003; 2007). After that PNs carry the olfactory information in the inner and medial antennocerebral tract (iACT and mACT) to the mushroom body (MB) and to the lateral horn (LH). The current notion is that the experience-independent odour responses are carried by PNs to LH which is comparable

to the piriform cortex and the cortical amygdala in mammals (Sosulski et al., 2011; Seki et al., 2017). But this needs further investigation as recent studies showed an independent context-dependent memory formation in LH (Zhao et al., 2019). On the other hand, the mushroom body (MB) is considered as the memory centre of the insect brain and often compared to the mammalian hippocampus, cerebellum or the piriform cortex (Farris, 2011; Honegger et al., 2011). In recent decades, there have been extensive research on the insect MB, pioneered by honeybee and *Drosophila* (Menzel 1974; Heisenberg, 1980; Heisenberg, 2003; Heisenberg and Gerber 2008) showing that the MB are essential higher brain centre to integrate the CS-US stimulus to associative learning and memory formation (Heisenberg, 2003; (McGuire et al., 2001); Kenne and Waddel 2007) (see Figure 0.5). Classic genetic blocking and lesion experiments proved the necessity of the MB in learning and memory in *Drosophila* too (ERBER et al., 1980; Heisenberg et al., 1985; Dubnau et al., 2001; McGuire et al., 2001; Krashes et al., 2007). They also play a role in sleep, locomotion, decision making or social behaviour (Davis, 1993; Martin et al., 1998; Tang and Guo, 2001; Heisenberg, 2003; Joiner et al., 2006; Fiala, 2007; Zhang et al., 2007; Sun et al., 2020).

To the mushroom body:

Kenyon cells (KCs): mushroom body intrinsic neuron and CS processing

The mushroom bodies are two mirrored symmetrical pedunculus central structures in the insect midbrain (Heisenberg, 2003). They are covered by glial sheath and extend from dorsocaudal to rostroventrally. The MBs are formed by densely packed, cholinergic intrinsic neurons called the Kenyon cells (KCs) (Technau, 1984; Aso et al., 2009; Barnstedt et al., 2016) and are divided into three parts: the calyx, the pedunculus and the lobes (Li et al., 2020). The main calyx (CA) is the primary sensory input region where the KCs have their dendrites to receive maximum olfactory input from PNs. On the other hand, the accessory calyx receives the non-olfactory input such as temperature, humidity, visual and likely gustatory as well (Stocker et al., 1997; Brembs, 2009; Masek and Scott, 2010; Aso et al., 2014a, 2014b; Frank et al., 2015; Kirkhart and Scott, 2015; Vogt et al., 2016; Eichler et al., 2017; Marin et al., 2020).

The KCs are sensory information conveyors and are representative of 3rd order neuron-pyramidal neuron in mammalian brain (Stettler and Axel, 2009). There are ~2000 KCs in each adult fly brain hemisphere and from the CA the axonal fibers of the KCs run in parallel to form a glial sheath covered dense bundle namely pedunculus (Crittenden et al., 1998). The proximal part of the pedunculus is likely to be the action potential initiation point of KCs. The pedunculus further splits into vertical lobe extending to the dorsal top of the brain and a horizontal lobe extending to the

midline. Based on the developmental neuroblasts, there are 3 major KC classes: α/β, α'/β' and γ. Among them the γ KCs are early born contributing exclusively to the medial lobe where the α/β, α'/β' equally contribute to the medial and vertical lobes (Heisenberg, 2003). They are named after their distinct projections to the MB lobes α/β, α'/β' and γ (first described by Heisenberg, 1980; Lin et al., 2007; Tanaka et al., 2008; Aso et al., 2014; Aso et al., 2014b) and in line with the MB role in appetitive and aversive memory formation and read out (Figure 0.6).

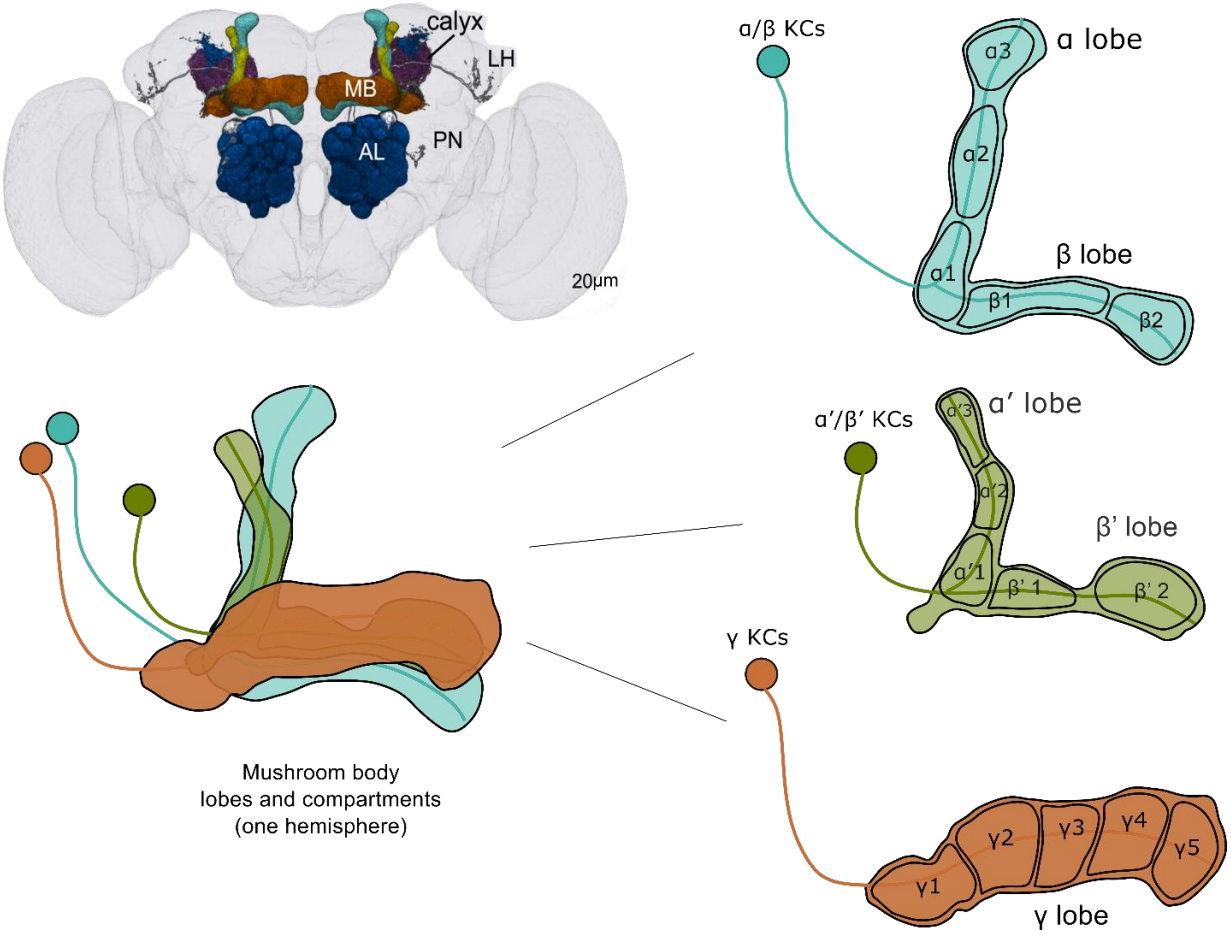

Figure 0.6| **Mushroom body compartments**. **(a)** A 3D anterior view fly brain showing the mushroom body (MB) and other olfactory neuropils (adapted from Gerber and Aso, 2017). **(b)** MB lobes and compartments in one hemisphere. 3 major KC classes: α/β (cyan blue), α'/β' (bottle green) and γ (brown) with their axonal projections form respective lobes which are divided into 15 compartments namely α1-3, β1-2; α'1-3, β'1-2 and γ1-5 (Figure is inspired from Aso et al., 2014a and Li et al., 2020).

Like all sensory systems, olfactory networks face complexity of generation to appropriate detection, storing and recall of a signal. In fly brain, the KCs are well characterized (Turner et al., 2008; Honegger et al., 2011) for their sparse sensory representation. Here, the olfactory information is carried away in an odour-specific manner from ORNs to glomeruli innervated by PNs of same type. KCs receive olfactory signals from ~10 PNs from ~2-5 per glomerulus of multiple glomerulus (Turner et al., 2008). Although KCs are enabled to respond to a wide variety of odour, but KC population maintain a sparse activity pattern to represent odour identity by two mechanisms. Firstly, individual KCs start spiking only upon simultaneously receiving signals from ~2-5 PNs of multiple glomerulus (Gruntman and Turner, 2013). This means only ~5-10% of KCs response upon any given odour (Perez-Orive et al., 2002; Ito et al., 2008; Turner et al., 2008; Honegger et al., 2011). Secondly, an overall KC excitability is checked and balanced by feedback inhibition from GABAergic neuron APL (Tanaka et al., 2008; Liu and Davis, 2009; Papadopoulou et al., 2011; Aso et al., 2014b; Lin et al., 2014). Thus, the very odour-specific responses, sparseness, non-overlapping sets of KCs serve the role of CS conveyor (Perez-Orive et al., 2002; Ito et al., 2008; Turner et al., 2008; Honegger et al., 2011; Hige et al., 2015) (see Figure 0.5).

Mushroom body compartments

The parallel axonal fibres of KCs travel to the MB output regions, the MB lobes. The lobes are devoid of external innervation and are divided into 15 compartments which are formed by the axonal fibers of α/β, α'/β' and γ KCs, the axon terminals of 21 types of dopaminergic neurons (DANs) and the dendrites of the 34 types mushroom body output neurons (MBONs) (Séjourné et al., 2011; Cassenaer and Laurent, 2012; Pai et al., 2013; Aso et al., 2014b; Bouzaiane et al., 2015a; Hige et al., 2015; Owald et al., 2015; Perisse et al., 2016; Li et al., 2020; Davis, 2023). Based on the discrete innervation pattern of DANs and MBONs (for further details, see the subsequent paragraphs), MB lobes form several compartments. The γ lobe consists of 5 compartments γ 1-5 extending from the MB heel/peduncle towards the midline/horizontally. On the other hand, α and α'lobes have 3 compartments each namely α1-3 and α'1-3 and extend upwards/vertically from the heel while β and β'lobes have 2 compartments each extending horizontally from the heel namely β1-2 and β'1-2 respectively (Aso et al., 2014a). These anatomical compartments are shown as the convergent unit of associative learning formation where the sensory stimuli (CS) are represented by the sparse activity of KC and the reinforcement signal carried by dopaminergic neurons (DANs) and read out by the mushroom body output neurons (MBONs) (Aso et al., 2014; Hige et al., 2015;Takemura et al., 2017; Li et al., 2020).

Dopaminergic neurons (DANs): reinforcement signal, US processing

Dopamine is one of the widely distributed biogenic amines in the central nervous system of both vertebrates and invertebrates. It serves versatile functions such as novelty, locomotion, sleep regulation, motivation, learning, memory formation, reward, punishment so as omission (extinction), forgetting and safety (Tanimoto et al., 2004; Gerber et al., 2014; Cohn et al., 2015; Sitaraman et al., 2015; Aso and Rubin, 2016; Felsenberg et al., 2017, 2018; Hattori et al., 2017; Dag et al., 2019; Handler et al., 2019; Jacob and Waddell, 2020). Most significantly its role for conveying reinforcement signals allows animals, including fruit fly, to adjust the causal structure of the world (Dickinson, 2001; Yamamoto and Vernier, 2011; Waddell, 2013; Schultz, 2015; Gerber and Aso, 2017). As human and other vertebrates, dopamine is synthesized from amino acid tyrosine with the help of two rate limiting steps: one via the enzymatic action of tyrosine hydroxylase (TH) and the other by the aromatic amino acid decarboxylase (AADC). Dopamine cannot cross the blood-brain barrier, thus synthesized within the dopaminergic neurons and packed into vesicles to release by exocytosis into the synaptic cleft. From here binds to the dopamine receptors on post synaptic membrane, in fruit fly dopamine receptors in KCs. In *Drosophila*, the dopaminergic neurons (DANs) are the most predominant neuromodulator in the MB and known to convey the reinforcement signal e.g. electric shock, sugar etc at a target specific MB compartment and modulate the KC → MBON synapse for expressing learned behaviour (Kim et al., 2007; Aso et al., 2010a, 2012a, 2014b; Burke et al., 2012; Waddell, 2013; Cohn et al., 2015; Huetteroth et al., 2015; Owald et al., 2015). In principle, the valence of the memory depends on DAN specific compartment activation and odour specific KC activation during the time of dopamine release (see in detail in the following sections) (Heisenberg, 2003;Burke et al., 2012; Lieu et al., 2012; Hige et al., 2015). It has been heavily investigated showing the activation of DANs subpopulation serving as US conveyor in associative learning paradigm (Schroll et al., 2006; Claridge-Chang et al., 2009; Aso et al., 2010a, 2012a, 2014b, 2014a; Burke et al., 2012; Liu et al., 2012).

DAN anatomy

Traditionally, there are 21 types of DANs innervating 15 MB compartments (Aso et al., 2014; see details in Table 0.2). Based on the anatomical location of the cell body, they are clustered into two populations: paired posterior lateral 1 (PPL1) DANs and paired anterior medial (PAM) DANs. There are 6 types of PPL1 DANs (PPL101-PPL106, see Table 0.2) and each type has 1-2 cell bodies. PPL1 DANs innervate mostly the vertical lobe, the junction area, the heel, distal peduncle and lateral part of the horizontal lobe. In contrast, PAM DANs are 15 types, and each have 3-26 cell bodies, targeting mostly the medial portion of the horizontal MB lobes (Riemensperger et al.,

2005; Mao and Davis, 2009; Burke et al., 2012; Aso et al., 2014a; Huetteroth et al., 2015; Li et al., 2020). In classical conditioning, upon different US, different DAN types respond and convey the information of US to specific MBON types. Strict MB compartmentalization leads to dopamine release in specific compartments and thus modifies KC-MBON synapse to modulate behavioural output (see the subsequent paragraphs for more details). There is also calyx (CA) innervating DANs, namely PPL2ab cluster and PPL201 cluster, shown role in salience signalling (Boto et al., 2019). Still, DANs are full of surprises and a lot is yet to explore and understand the input and outputs of them. Their wide range of heterogeneity is also consistent with mammalian midbrain dopaminergic heterogeneity (Lammel et al., 2014; Otto et al., 2020) (see Figure 0.7).

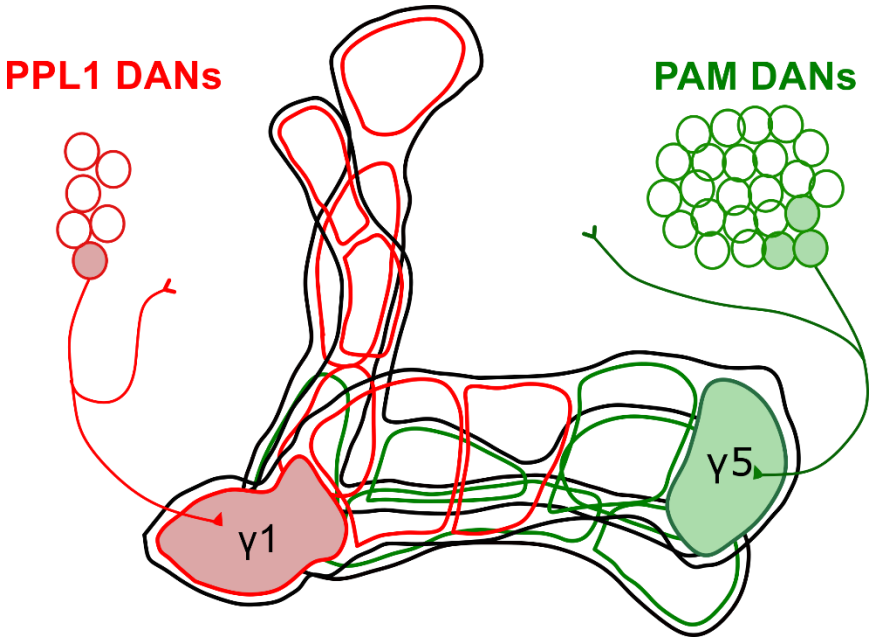

Figure 0.7 | Dopaminergic neurons (DANs). Two clusters of DANs: paired posterior lateral 1 (PPL1) and paired anterior medial (PAM) DANs innervate 15 compartments of the MB. PPL1 DANs (red) convey the punishment reinforcement in compartments drawn in red and PAM DANs (green) convey the reward reinforcement to the compartments in green. Despite all shown 6 types of PPL1 and 15 types of PAM DANs cell bodies, only one cluster of PPL1 (PPL1-01, 1 cell body) innervating the punishment processing γ1 compartment (red filled) and one cluster of PAM (PAM-15, 3 cell body) innervating the reward processing γ5 compartment (green filled) have been shown (Figure is inspired from Felsenberg et al., 2017).

PPL1- DANs for aversive US processing

The observation of Heisenberg and colleagues (reviewed by Heisenberg et al., 1985) made MB a model for aversive olfactory classical conditioning. This establishes MB as the convergence site of CS (odour) and US (electric shock). However, the question remained that how brains organize the association at all? How come the same CS be associated with different US and form different sorts of memory namely aversive or appetitive?

The necessity of DANs in *Drosophila* olfactory aversive conditioning was first described in (Schwaerzel et al., 2003). It was shown that blocking aversive reinforcement signal conveying by PPL1 DANs impaired aversive learning. In this study, they targeted all the PPL1 DANs by using TH-Gal4 (Friggi-Grelin et al., 2003). This observation has been further supported by functional imaging and immunohistochemistry (Riemesperger et al., 2005; Mao and Davis, 2009). Eventually continuous rapid development of DANs specific driver lines and optogenetics provided more evidence of aversive reinforcement by PPL1 DANs, especially in γ1, γ2 compartments along the horizontal lobe and α'1, α'2, α3 of vertical lobe compartments by PPL1-γ1pedc; γ1, PPL1-γ2 α'1, PPL1- α'1, PPL1- α'2 and PPL1- α3 respectively (Aso et al.,2010, 2012; Aso and Rubin, 2016). Besides PPL1, there is another controversial PAM DANs namely MB-M3 and PAM-γ3 innervating β and γ3 compartment (covered by TH-Gal4) which also convey aversive reinforcement (Aso et al., 2010; Waddel, 2013; Yamagata et al., 2016). Furthermore, blocking these DANs by optogenetics and thermogenetic and thus impaired aversive memory formation strengthen the role of the PPL1 and few controversial PAM- DANs as aversive reinforcement provider (Claridge-Chang et al., 2009; Aso et al., 2010; 2012).

PAM- DANs for appetitive US processing

Seminal studies in honeybee and *Drosophila* indicated that octopaminergic neurons (OAN), the invertebrate analogue of norepinephrine is the insect appetitive reinforcement conveyor (Hammer and Menzel, 1998; Schwaerzel et al., 2003; Schroll et al., 2006). However, studies showed that appetitive signal is not so disingenuous! It turns out that OAN only works transiently and provide the taste "sweetness" property of sugar while PAM - DANs signalling is more downstream of OA and provide an additional reinforcing effect- nutritional value in appetitive memory formation (Burke et al., 2012). Also, it is not only the sugar that can serve as rewarding reinforcer but depending on the state of the fly or the concentration of the reinforcer, other stimuli also serve the purpose. For example, salt (Niewalda et al., 2008); amino acids (Toshima and Tanimura, 2012; Schleyer et al., 2015). A yet to discover full aspect is formation of relief learning upon termination of a painful stimulus e.g. shock or optogenetically activating PPL1-DANs (PPL1-01) (Tanimoto et

al., 2004; Yarali et al., 2008; Aso et al., 2016; König et al., 2018; Amin et al., 2025). Although, for termination of a painful stimulus (relief memory) is not yet so clear if or which PAM- DANs convey the signal, my recent study (see Chapter 2) uncovered a complex role of dopamine for such relief together with punishment and trace conditioning (Amin et al., 2025). So far, PAM- γ4, PAM- γ5, PAM- β'2 innervating γ4, γ5 and β'2 compartments along the medial portion of the horizontal lobe have evidence of providing appetitive reinforcement signal (Burke et al., 2012; Huetteroth et al., 2015; Cohn et al., 2015; Tomchik and Davis 2009).

Mushroom body output neurons (MBONs): the MB transit for learned behaviour

The KCs convey the odour information (CS) to the MB lobe compartments and the reinforcement signal (US) is conveyed by DANs. In these convergent sites, there is another key class of neurons that receives synapses from all KCs and this synaptic strength is modulated by the DANs. These are called mushroom-body output neurons (MBONs) (Heisenberg, 2003) and they read out CS-US association and guide the learned behaviour to either approach or avoid a stimulus and thus sheds light on the complex MB functions (Aso et al., 2014b; Hige et al., 2015; Owald et al., 2015).

Typical MBONs

Until 2020, it was known that MBONs are a network of 34 cells of 21 types of neurons per brain hemisphere (Aso et al., 2014a; Takemura et al., 2017) to serve as the core MB output pathway. All these 21 types of MBON except one have 1 or 2 cells per hemisphere. They have dendritic arborization in the MB lobe compartments as per neurotransmitter- GABA, glutamate or acetylcholine and they are also classified according to the assigned neurotransmitter. Their dendritic clustering strikingly resembles the DANs innervation pattern in MB compartments but with reverse polarity (Aso et al., 2014; Felsenberg et al., 2017). Morphologically, the KC, DAN axon terminals and MBON dendritic terminals remain in proximity in the MB compartments (Takemura et al., 2017). However, DAN>KC synapses are far fewer than the KC>MBON synapses. In fact, only ~6% of KC>MBON synapses have DAN terminal in a proximity of 300 nm which implies volumetric dopaminergic modulation of KC>MBON synapse (Hige et al., 2015). Withing MB lobes, MBONs also receive APL and DPM input (Liu and Davis, 2009; Waddell et al., 2000). And a breakthrough was achieved by identifying that dendritic arborization of MBONs receive excitatory cholinergic synapses from KCs (Barnstedt et al., 2016).

Almost all MBONs then target their axons outside of the MB lobes except three MBONs which send their axonal projections in a feedforward manner to the MB lobes and several others have also seen to target specific DANs dendrites (Aso et al., 2014a; Li et al., 2020). MBONs mostly send their axonal projection to the dorsal brain regions and innervates the CRE, SIP, SMP and

make direct connection to the fan-shaped body of the central complex (a brain area, which is known for goal directed locomotion in insect brain) intending to converge on common targets.

In general, vertical lobe and part of horizontal lobe MBONs read out the aversive learning, in line with the MB compartments which are innervated by the PPL1 DANs. While the media part of the horizontal lobe MBONs read out the appetitive learning in line with the compartments innervated by the PAM DANs (see Table 0.2 for detail).

Atypical MBONs

Recent study from Li et al., 2020, identified 14 additional types of MBON, referred as “atypical MBONs” due to their additional dendritic arborization other than KCs input within the MB lobes, spreading proximity brain areas predominantly in LAL, CRE, SIP, SMP, γ lobe. 9 out of 14 atypical neurons receive input from at least 2 other typical or atypical MBONs. Some also receive direct sensory input e.g. MBON24 (β2γ5) has important inputs from SEZONs conveying mechanosensory or gustatory information (Otto et al., 2020; Zheng et al., 2018). There is only one MBON (MBON30) which receives direct central complex input and thus plays a role in linking these two major regions of flybrain. Looking at the innervation partners, 12 out of 14 innervate the horizontal lobe. Interestingly and exclusively, 6 atypical MBONs have significant innervation in ventral neuropils LAL which put them bridging position to directly connect MB to the motor network (which is critical for my thesis, see Chapter 1 and General Discussion). There is also an extensive network of MBON-MBON connections outside of MB lobes which can be in between typical-atypical MBONs or two atypical MBONs by axo-dendritic or axo-axonal connection respectively. Mostly atypical MBONs form a multilayered feedforward network to perform complex input integration. To sum up, atypical MBONs reveal to perform complex input integration with the numerous sensory inputs, modality selective input that is intended to dopamine-modulated learning in combination with both by other MBONs conveying learned information and non-MB input (see Table 0.2 for overview of mushroom body compartments-DANs-MBONs-neurotransmitters).

Table 0.2: Overview of mushroom body compartments-DANs-MBONs-neurotransmitter

Compartments	DANs	MBONs		MBONs NT
		Typical	Atypical	
γ1	PPL1-01 (PPL1-γ1pedc), PPL1-02 (PPL1-γ1)	MBON-11 (MBON- γ1pedc), MBON-11 (MBON- γ1pedc)	MBON-20 (MBON-γ1 γ2) *, MBON-25 (MBON- γ1 γ2) *,	GABA Glut *predicted
γ2	PPL1-03 (PPL1-γ2α'1)	MBON-12 (MBON-γ2α'1)	MBON-30 (MBON- γ1γ2γ3) *, MBON-32 (MBON- γ2) *, MBON-33 (MBON- γ2γ3) *, MBON-34 (MBON- γ2) *, MBON-35 (MBON- γ2*)	GABA Glut Ach *predicted
γ3	PAM-12 (PAM- γ3)	MBON-09 (MBON-γ3β'1)	MBON-30 (MBON- γ1γ2γ3) * MBON-33 (MBON- γ2γ3) *	GABA Glut Ach *predicted
γ4	PAM-07 (PAM-γ4>γ1γ2), PAM-08 (PAM-γ4)	MBON05 (MBON-γ4>γ1γ2) MBON21 (MBON-γ4γ5)*	MBON-29 (MBON- γ4γ5) *	Glut Ach *predicted
γ5	PAM-15 (PAM- γ5β'2a)	MBON-01 (MBON- γ5β'2a)	MBON-24 (MBON- β2 γ5) *, MBON-27 (MBON- γ5d) *, MBON-29 (MBON- γ4 γ5) *	Glut Ach *predicted
α1	PAM-11 (PAM- α1)	MBON-07 (MBON- α1)		Glut
α2	PPL1-05 (PPL1-α'2α2)	MBON-13 (MBON- α'2), MBON-18 (MBON-α2), MBON-19 (MBON-α2p3p)		Ach
α3	PPL1-06 (PPL1-α3)	MBON-14 (MBON-α3)		Ach
β1	PAM-09 (PAM-β1ped), PAM-10 (PAM-β1)	MBON-06 (MBON- β1>α)		Glut
β2	PAM-03 (PAM-β2β'2α), PAM-04 (PAM-β2)	MBON-02 (MBON- β2β'2α)	MBON-24 (MBON- β2 γ5) *,	Glut Ach *predicted
α'1	PPL1-03 (PPL1-γ2α'1)	MBON-12 (MBON-γ2α'1)	MBON-31 (MBON- α'1a) *	GABA Ach *predicted
α'2	PPL1-05 (PPL1-α'2α2)	MBON-13 (MBON- α'2),		Ach
α'3	PPL1-04 (PPL1-α'3)	MBON-16 (MBON-α'3ap), MBON-17 (MBON-α'3m)	MBON-28 (MBON- α'3a) *	Ach *predicted
β'1	PAM-13 (PAM- β'1ap), PAM-14 (PAM- β'1m)	MBON-09 (MBON-γ3β'1)	MBON-10 (MBON- β'1)	GABA
β'2	PAM-02 (PAM-β'2α), PAM-03 (PAM-β2β'2α), PAM-05 (PAM-β'2p), PAM-06 (PAM-β'2m)	MBON-01 (MBON- γ5β'2a), MBON-02 (MBON- β2β'2α), MBON-03 (MBON- β'2mp), MBON-03 (MBON- β'2mp_bilateral)	MBON-26 (MBON- β'2d) *	Glut Ach *predicted

Molecular underpinning of CS-US association for olfactory associative learning

The MB has a three-layered expand-convergence architecture, which is the fundamental basis of the most influential learning network algorithm- the Marr-Albus model (Marr, 1969; Albus, 1971) . Here the expansion-convergence very nicely fits with the ~2000 KCs converging onto 35 different types of MBONs. This is also the site where reinforcement signals enter by DANs to drive the synaptic plasticity which is the prominent feature of this three-layered circuit. Now the question would be how come from this straightforward anatomical neural circuit, olfactory associative learning takes place at all?

Associative learning first and foremost needs a precise relationship between the CS and US. As described in previous sections, by the sparse activity pattern of KCs, sensory stimuli, here odour (CS) is represented and the reinforcement signal (either positive or negative valence, US) is conveyed by DANs in a compartment specific manner (Figure 0.8).

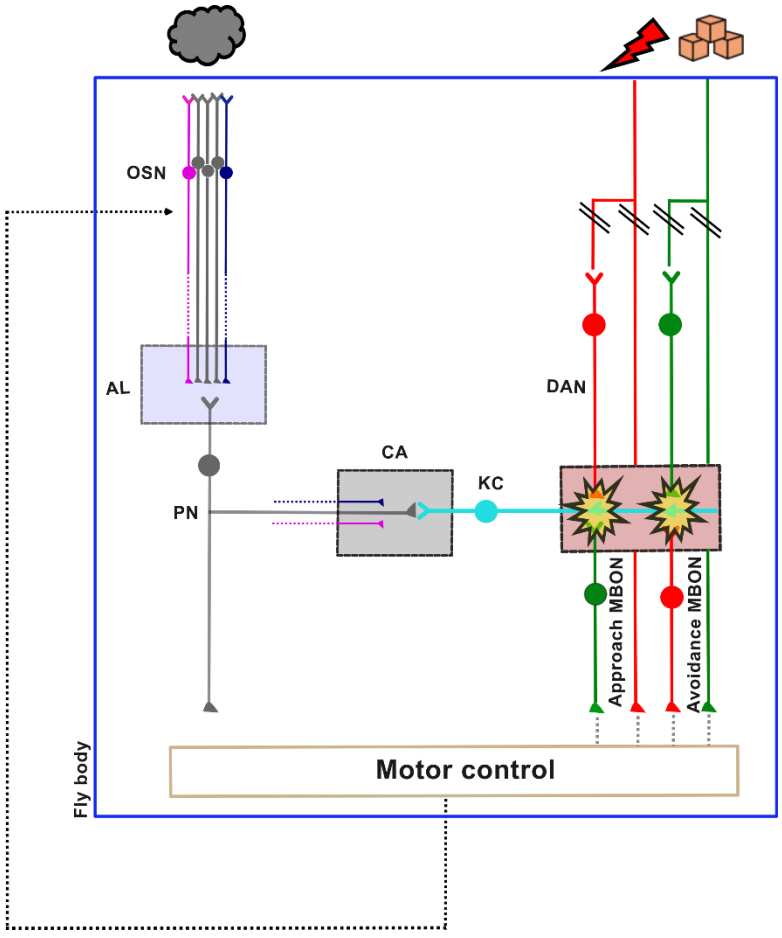

Figure 0.8 | Simplified diagram of CS-US association for olfactory associative learning. *OSN:* olfactory sensory neurons; *AL:* antennal lobe; *PN*: projection neurons; *CA*: calyx; *KC*: Kenyon cell; *DAN*: dopaminergic neuron; *MBON*: mushroom body output neuron. An odour (grey cloud) information carried by OSNs (grey) to AL activates a specific pattern of PNs (grey). PNs convey that information to the KCs (light blue) of a specific mushroom body compartment. KC has a compartment synaptic connection with MBON. Shock (thunderbolt) or reward (sugar cubes) reinforcement carried by punishing or reward DAN respectively to specific MB compartment and lateral horn (not shown). Convergence of odour-shock (red) or odour-sugar (green) occurs at given compartments (yellow star symbols) and long-term depression of corresponding KC-MBON synapse occurs. Thus, it leads to either avoiding or approaching the odour respectively until the memory fades away.

What happens inside the KCs in response to DANs input and how does the KC-MBON synaptic strength get affected by conditioning?

Monoaminergic neurotransmitter, dopamine cannot cross the blood brain barrier and thus is synthesized and packaged within the DANs and released via exocytosis with the help of vesicular monoamine transporter (Vmat) and binds to the dopamine receptors (DA) on the post-synaptic neurons, KCs. There are two types of dopamine receptors: D1-like or D2-like. In mammals D1-like receptors consist of D1, D5 receptors. While D2-like receptors include: D2, D3, D4. The effect of dopamine mostly depends on the type of receptors expressed in the post-synaptic neuron.

In *Drosophila*, D1-like receptors are known as: Dop1R1 (aka dD1 or DUMB) and Dop1R2 (aka DAMB), while D2-like receptors are Dop2R (aka DD2R). Dopamine receptors belong to G-protein-coupled receptors (GPCRs) forming a superfamily of seven-transmembrane proteins. Upon binding of a variety of ligands, they undergo confirmational changes and thus relay the information by initiating intracellular signaling cascades- heterotrimeric G-protein complexes. While D1-like receptors, Dop1R1 and Dop1R2 are coupled to G_s and G_q protein respectively, D2-like receptor, Dop2R is coupled to $G_{i/o}$ (Sugamori et al., 1995; Hearn et al., 2002; Himmelreich et al., 2017). For G-protein mediated signaling, a downstream second messenger is crucial for synaptic plasticity and memory formation, 3'-5'- cyclic adenosine monophosphate (cAMP) (Byrne and Kandel, 1996; Lechner and Byrne, 1998; Heisenberg, 2003; Schwaerzel et al., 2003). This cAMP is activated by adenylyl cyclase and degraded by phosphodiesterase (PDE). In flies, the homologous gene of adenylyl cyclase gene and PDE genes are called rutabaga (rut) and dunce respectively (Levin et al., 1992). This rutabaga encodes mammalian type 1 adenylyl cyclase (AC) is well-studied and considered as the molecular site of convergence of the US and CS pathway is associative learning (Levin et al., 1992; Davis, 1993, 2005; Keene and Waddell, 2007; Tomchik and Davis, 2009).

This rut is exclusively expressed in the KCs at synapses to the MBONs. During associative conditioning, olfactory stimulus (CS) evoked presynaptic calcium (Ca^{2+}) influx through voltage-sensitive calcium channels which in turn activates the Ca/CaM dependent adenylyl cyclase. At the same time, dopaminergic reinforcement signal (US) is conveyed via GPCRs (dissociated by sub-units) activate rut encoded adenylyl cyclase (Livingstone et al., 1984; Levin et al., 1992; Riemensperger et al., 2005). For an effective stimulation of cAMP synthesis, coincident activation of both pathways is indispensable. This in turn, leads to an increase in cAMP production and increased cAMP initiates protein kinase A (PKA) dependent cascade of protein phosphorylation which mediate the short-term molecular changes underlying synaptic plasticity and memory formation (Taylor et al., 1990; Schwaerzel et al., 2002; Tomchik and Davis, 2009; Gervasi et al.,

2010; Boto et al., 2014). Functional imaging from Tomchik and Davis, 2009 showed supportive evidence that rut provides a synergistic increase in cAMP of simultaneous dopamine and acetylcholine stimulated neuronal depolarization are paired, proving the rut is a molecular coincidence detector. Now if this coincident activation occurs within a given compartment of the MB, the synaptic strength of the KCs to the respective MBONs gets altered (Owald and Waddell, 2015; Hige et al., 2015; Hancock et al., 2019; larvae: Eschbach et al., 2020, 2021) (Figure 0.8).

From Hige, (2018) under typical differential olfactory associative learning regime, flies experience an odour together with electric shock (aversive learning) or sugar (reward learning), while another odour without any reinforcement. After that flies are forced to decide in between these two odours. As we saw, distinct DANs convey distinct reinforcement signal, and the type of memory (aversive or reward) are determined by type of activated DAN during conditioning in spatially segregated MB compartments. Upon coincident activation happens in a given compartment, KC-MBON synapses undergoes long term depression (LTD) (Hige et al., 2015). There are two important factors two keep in mind: 1) this odour-evoked synaptic input is strictly temporal contingency dependent, so when the order is odour stimulation and then DAN activation (a delay of 15s, Tomchik and Davis, 2009), leads to a robust induced plasticity. But when the sequence is, otherwise, there is no LTD. 2) The observed plasticity is also spatially specific and happens only in DAN and corresponding MBON specific MB compartments, not the neighbouring ones. Therefore, each MB compartment is represented as a functionally independent unit of plasticity.

Next question would be, how is a valence read out by MBONs? In principle, upon direct activation of each MBON showed their own property of either driving avoidance or approach behaviour rather stereotyped motor pattern (Aso et al., 2014b; Owald et al., 2015). As mentioned before, each independent MB compartment receives olfactory information via sparse activity of KCs and innervated by DANs and equipped with dendrites of MBONs. Along the vertical lobe and proximal part of the horizontal lobe compartments (see Table 0.2), the aversive reinforcement signals are conveyed by PPL1-DANs. For example, PPL1-01 DANs convey aversive signal to γ1pedc compartment. Strikingly, the MBONs innervating the same compartment is oppositely signed. So, the MBONs belonging to the aversive memory compartments, signed to positive valence. Therefore, dopamine induced KC-reward promoting MBON-11 synapse goes to LTD and thus after associative learning decreases the attractive/rewarding output of MBON and form aversive memory (see Figure 0.9) (Dubnau et al., 2001; McGuire et al., 2001; Isabel et al., 2004; Cervantes-Sandoval et al., 2013; Bouzaiane et al., 2015b). Also see Chapter 2 for my detailed work with PPL1-01 DAN.

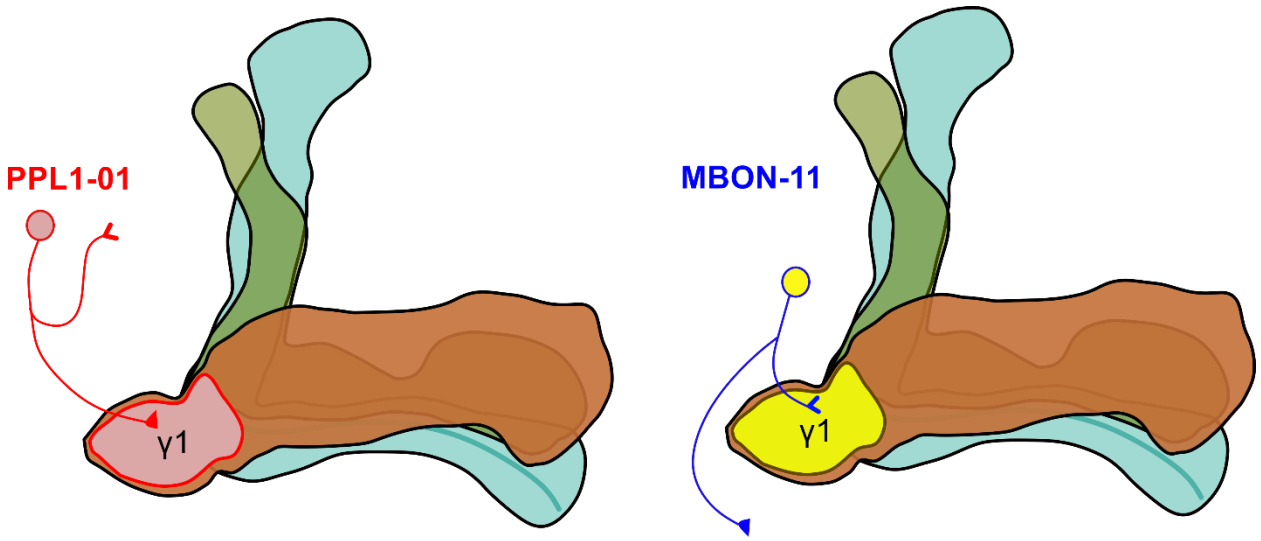

Figure 0.9 | Schematic of PPL1-01 (left) and MBON-11 (right) with outline of mushroom body compartment γ1. Pairing of an odour with activation of PPL1-01 (either optogenetic or electric shock) causes KC-approach promoting MBON-11 synaptic depression. This results in reduced MBON-11 activity when flies experience the odour again and leads to avoidance of that odour (also see Figure 0.8).

Similarly, along the medial part of the horizontal lobe compartments, the positive valence is conveyed by PAM- DANs. For example, PAM-15 (PAM-γ5β'2) innervates the horizontal lobe tip and carries reward/appetitive signal to γ5β'2 compartment and modifies the KC-MBON-01 (MBON- γ5β'2) synapse where MBON-01 arborizes their dendritic innervation at the same compartment. Owald et al., 2015, showed that, after olfactory conditioning for reward learning, this MBON-01 gets depressed and decreases the aversive output and thus form appetitive or reward memory. Another intriguing feature of their bidirectional change, meaning potentiation after aversive conditioning can also happen by inter-compartment lateral connection (Perisse et al., 2016), which needs further study. Altogether, punishment or reward signalling modulatory neurons (DANs) changes the synaptic weight in between the sensory cue representing neurons (KCs) and output neurons (MBONs) and thus made MBON as the critical element of memory formation.

Timing does matter

In the previous section, I described in detail how the CS-US association occurs for olfactory associative learning in *Drosophila*. So, fly learns the valence of an odour as punishing/rewarding when previously it was associated with electric shock/sugar. Therefore, next time when it encounters the same odour, it will avoid/approach the odour. Interestingly, the fundamental property of reinforcers is that their effects are “double-faced” or “Janus-faced” (Konorski et al.,1948; Solomon and Corbit, 1974; Solomon, 1980; Wagner et al., 1981). Thus, the occurrence of punishment can cause pain, but termination of that punishment will give relief from that pain. Similarly, the occurrence of reward causes pleasant feelings and termination of reward causes frustration (Solomon and Corbit, 1973). So, animals not only learn the association of cues (CS) which predict the onset of punishment/reward (US) but also the cues related with the termination of that US. And the precise timing between the CS-US can form memories of opposite valence, a phenomenon called timing dependent valence reversal (Figure 0.10).

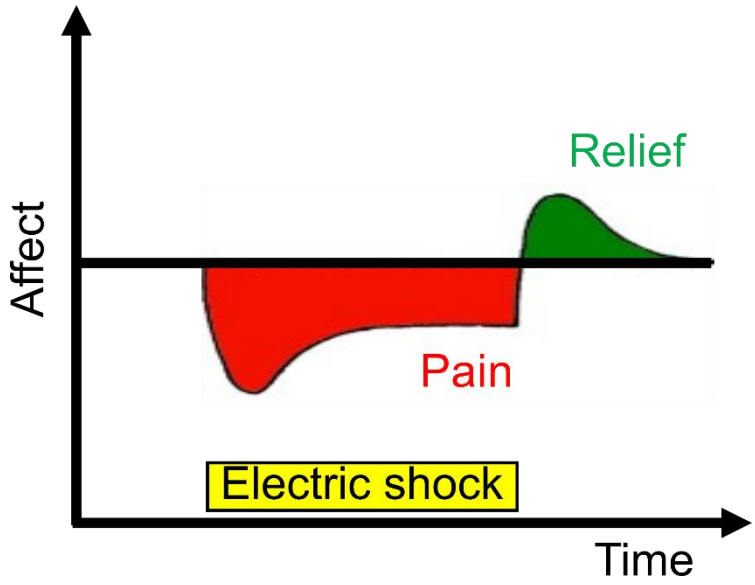

Figure 0.10 | Principle of timing dependent valence reversal. The occurrence of electric shock (yellow) causes pain (red), while its termination gives relief (green) affect (Modified from Solomon and Corbit, 1974). Stimuli associated with pain and relief acquire aversive and appetitive memory, respectively.

This is an across species principle and a rich number of investigation took place across species on punishment and reward learning but much less is known about the underlying mechanism of relief and frustration learning (relief in *Drosophila*: Tanimoto et al., 2004; Yarali et al., 2008; Gerber et al., 2014; Vogt et al., 2015; Aso & Rubin et al., 2016; Handler et al., 2019; in rats: Mohammadi et al., 2015; and in humans: Andreatta et al., 2010 and 2012; frustration in *Drosophila* larvae: Saumweber et al., 2018; and in bees: Hellstern et al., 1998; Felsenberg et al., 2014). Therefore, in Chapter 2, I investigated this fundamental aspect of timing dependent valence reversal focusing on dissociating dopaminergic from non-dopaminergic mechanisms.

Extinction learning

Once the relationship between CS-US is learnt, experiencing CS+ without any reinforcer leads to a drastic impairment of memory performance (Schwaerzel et al., 2002). This was another discovery of Pavlov's termed as the "internal inhibition of conditioned reflexes" (Pavlov, 1927; review: Dunsmoor et al., 2015).

The process by which this learned avoidance or approach is affected by experiencing only CS without reinforcement is called memory extinction. In the past decade, the neuroscience of learning, memory and emotion have seen extensive extinction study. This research interest has not been confined only in the basic mechanism of extinction learning, rather it's clinical significance as the basis of exposure therapy for the treatment of psychiatric disorders e.g. anxiety disorder, addiction, trauma and stress related disorders brought extra attention to study extinction (Milad and Quirk, 2012; Vervliet et al., 2013). According to Pavlov, this extinction process happens by some inhibitory cells in the cortex and by extinction CR is only disrupted but not totally destroyed and can return over time, what he termed as "spontaneous recovery". This notion suggests that original memory trace from CS-US association and extinction memory for CS+ without reinforcer can exist in-parallel. Two consecutive major studies from Felsenberg et al., (2017, 2018) showed light on the underlying neural mechanism for olfactory aversive and reward extinction learning in *Drosophila*. It explained that when flies re-experience an odour alone which was previously associated with punishment reinforcement then aversive memory extinction triggers. This aversive extinction learning engages reward encoding dopaminergic neurons downstream of avoidance promoting MBONs which indicates omission of punishment and form a new positive memory. For example, upon olfactory aversive conditioning, PPL1- γ1pedc conveys negative valence and depresses the CS+ odour>approach promoting MBON- γ1pedc>α/β synapse and skew the behaviour to avoid the odour. However, during aversive extinction learning, they re-evaluate the existing memory and engage PAM neurons innervating γ5 compartments which are functionally connected to the avoidance promoting MBONs and thus form a new positive memory. Consequently, newly formed positive memory competes with the previous aversive memory. This results in the extinction of avoidance behaviour. Thus, two different types of memories are formed and stored in two different compartments in parallel which is supported by functional imaging.

Despite surging extinction research, there are yet a lot to discover. What are the contributing factors to determine when and to what extent extinction should take place, when it relapses, why

it is so difficult to extinguish a memory during fear exposure/ anxiety disorders? Are there any other components e.g. sensory/perceptual, emotional, temporal, conceptual contributing to the memory extinction (Brandon et al., 2000; Delamater, 2012)? An intriguing study (Lattal and Wood, 2013; Delamater and Westbrook, 2014) suggested that fear extinction may only impair the emotional component (fear) while leaving the other components of the CS-US association e.g. sensory input intact. This is a fascinating notion to think about considering that extinction might be a matter of choice also for the animal kingdom!

As the story of my thesis goes on, I will also address this question experimentally in Chapter 1.

Beyond the mushroom body: descending neurons (DNs)

In most bilaterian animals, the central nervous system consists of two major components: an anterior brain and a more posterior nerve cord. To generate complex movement, for example, going towards or away from an odour to execute the innate or learned behaviour, flies need to control the body movement in a coordinated manner. For this the brain needs to communicate with the motor centres as they can follow the command coming from the brain. The evolution of the nervous system is dominated by the “cephalization” process where anterior ganglia fuse to form an information integrating centre- the brain. This cephalic structure then communicates with the motor centres through a versatile population of neurons, called descending neurons (DNs). DNs project their axons as tracts to posterior ganglia within the nerve cord and bring command-like information from brain (Bullock and Horridge, 1965; Namiki et al., 2018). In *Drosophila*, the nerve cord is known as ventral nerve cord (VNC) due to its anatomical ventral position and is born post-embryonically. The adult VNC are organized into major neuropils: 3 thoracic segments: 1) prothoracic, 2) mesothoracic, 3) metathoracic, 4) accessory mesothoracic neuropil (AMNp), and 5) abdominal neuropil (ANp) (Court et al., 2020). In these different segments, DN axons influence local circuits including central pattern generators (CPGs) leading to specific limb or body segment movement (Bouvier et al., 2015; Capelli et al., 2017; Caggiano et al., 2018).

The number of DNs are several orders of magnitude smaller than the brain or posterior ganglia neurons and thus serve as a crucial bottleneck merging the sensory and contextual information to motor system. For example, in the case of insects it’s in the range of 200-500 bilateral pairs (Gronenberg and Strausfeld, 1991; Staudacher and Schildberger, 1998; Gal and Libersat, 2006; Cardona et al., 2009) ~100,000 cells from brain to spinal cord in case of mice (Liang et al., 2011). For *Drosophila*, recent review from Simpson (2024) mentioned that DNs that connect fly’s brain to its ventral nerve cord (VNC) are ~1300 while brain has 130,000 neurons (~1% only) and VNC has 22,000 neurons (see Figure 0.11).

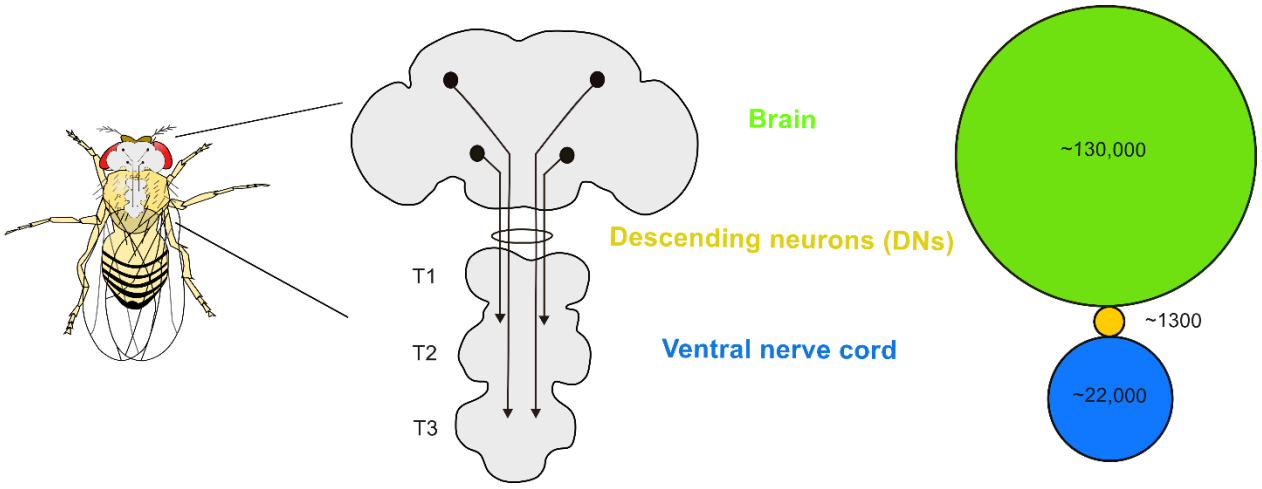

Figure 0.11 | Diagrammatic representation of descending neurons (DNs) organization in adult *Drosophila*. DNs (slinged area, ascending neurons are not shown) extend from brain to ventral nerve cord in highly distributed as well as localized manner (long and short black projection respectively) in three thoracic segments (T1-3). The approximate numbers and proportion of brain neurons, DNs and ventral nerve cord neurons have been depicted in green, yellow and blue respectively (see text for detail).

The DNs convey higher level command e.g. walking, grooming, escape etc rather than precise instructions to execute specific action. There is always an on-going discussion that what type of neurons DNs are. Considering their morphology, many are single and bilaterally presented, while others are divided into small groups. This stereotypically represents the DNs as command-like and population-coding respectively. While the command like is instinctually anticipated as performing high-level, centralized control on motor circuits, population-type might exert low-level, limited range of motor outputs. However, recent advances in DNs research manifest the co-existence of these two modes. For example, some groups of DNs might be fine tuning their actions under the control of command-like DNs as shown in crickets and locusts (Böhm and Schildberger, 1992; Zorović and Hedwig, 2011). In *Drosophila*, there is a single command-like neuron-moonwalker descending neuron (MDNs), which acts both as highly distributed as well as localized manner to coordinate changes in many muscles' movement (Feng et al., 2020). Another possibility could be that different DNs get engaged depending on the sensory context e.g. different DNs are engaged during different odour-evoked vs spontaneous walking or halting behaviour (Israel et al., 2022; Sapkal et al., 2024). The recent advances in anatomical, physiological and behavioural approaches with the ongoing large-scale EM and connectome analysis of adult fly brain (Zheng et al., 2018; Scheffer et al., 2020; Phelps et al., 2021; Schlegel et al., 2024; Dorkenwald et al., 2024) female and male ventral nerve cord analysis (Cheong et al., 2024; Takemura et al., 2024;

Azevedo et al., 2024) have made descending neurons as excellent research field to study the complexity of complete central and peripheral nervous system both in circuit level and behavioural execution level.

Anatomical and functional characterization of fly descending neurons (DNs)

Fly neck connective cross section by electron microscopy revealed that there are ~3000 neurons including ascending and descending neurons. Considering the cell body locations in the brain and dye-filling neurons in the neck together with neurotransmitter identity ~1300 DNs have been classified as cholinergic, GABAergic, glutamatergic and aminergic types (Hsu and Bhandawat et al., 2016). There are some anatomically distinctive DNs due to their huge axon diameter e.g. the pairs of giant fibers implementing the jump escape response in fly. However, most of the experimentally identified command-like DNs are morphologically specialized, bilaterally symmetric pairs consisting of complex neurites. As the name suggests, DNs receive synaptic input in the brain and provide synaptic output in the VNC to motor output transmitted by motor neurons (MNs) (Simpson, 2024). Besides, many DNs also have synaptic output site in a brain region called suboesophageal region (SEZ) which is by origin affiliated with VNC (Hartenstein et al., 2018).

Several DNs input brain regions are: 1) the lateral accessory lobes (LAL) and posterior slope (PS) for navigation and visual motion processing, 2) posterior lateral and ventrolateral protocerebra (PLP, PVLP) for escape and other fast visual response and 3) the gnathal ganglion (GNG) involved in mechanosensory, gustatory and locomotor response (Hsu and Bhandawat, 2016; Namiki 2018). Many DNs also receive input from the local VNC neurons. Meanwhile, the axons of the DNs innervate distinct regions of VNC serving distinguished functions, e.g. ventral leg neuropils targeting DNs coordinate walking and grooming while dorsal tectulum innervating DNs are involved with flight. Most DNs possibly indirectly influence movement via interneurons onto the premotor neurons and implement rhythmic patterns of inter-joint, inter-leg coordination. However, further investigation is needed to obtain more comprehensive knowledge into the DNs anatomical and functional organization. Currently the separate EM connectome datasets of brain and VNC need to be stitched together, which is still quite challenging but will be achieved in near future. Nevertheless, DNs are elegantly critical and experimentally yielding research areas to investigate the underlying mechanism of how animals coordinate their behaviour and in what contexts. For the current instances, in Chapter 1, my focus will be on the backward walking inducing moonwalker descending neurons (MDNs) and I will summarize some other DNs in the general discussion chapter later.

Chapter 1

Avoidance engages dopaminergic punishment in *Drosophila*

Text and figures are part of a manuscript planned for publication with the following author list:
Fatima Amin*, Jasmine T. Stone*, Christian König*, Nino Mancini, Kazuma Murakami, Salil S. Bidaye, M.-Marcel Heim, David Owald, Utsab Majumder, Ilona C. Grunwald Kadow, Anna Pierzchlińska, Ashok Litwin-Kumar, Oliver Barnstedt, Bertram Gerber.
Author contributions as follows: Conceptualization and design: **F.A**., C.K., and B.G.; Methodology: behavioural experiments and *in-vivo* calcium imaging experiments: **F.A.,** C.K., O.B.; connectome analyses and modelling: J.T.S., A.L.K.; immunohistochemistry, EM reconstruction, locomotion tracking: N.M., S.S.B., K.M.; explant calcium imaging: M.-M.H., D.O.; Data analysis and visualization: **F.A.**, C.K., O.B., B.G.; Writing—Original draft: **F.A**. and B.G.; Writing—Review and editing, **F.A.**, J.T.S., C.K., N.M., M.-M.H; U.M., I.C.G.K., A.P., A.L.K., O.B., and B.G.
Supervision, B.G. *Authors contributed equally

Introduction

In his treatise on the relationship between emotions and behaviour, Darwin suggested that not only can a particular emotional state engage a corresponding behaviour, but, conversely, we can adopt the emotional state corresponding to the behaviour we engage in (Darwin 1872; also see James 1884). This hypothesis sparked intense and ongoing debate, a prominent example of which is the question whether smiling can make us feel happier. After decades of controversy a large-scale collaboration recently settled in favour of such facial feedback (Coles et al., 2022). Likewise, in rodents induced increases in heart rate and changes in breathing pattern thought to be indicative of fear can in turn induce it (Hsueh et al., 2023; Jhang et al., 2024). The function of such positive feedback to emotional state is unclear, however, as it seems poised to produce pathological runaway dynamics. Here I discovered that inducing backward movement engages negative valence signals in the fly *Drosophila melanogaster* and investigated the circuit mechanism and function of this effect.

Drosophila lends itself to such analyses as it permits the convenient experimental expression of transgenes to induce, prevent, or measure neuronal activity in the neurons of interest. Combined

with the numerical simplicity of the fly brain and the near complete mapping of its synaptic connectome, behavioural analyses have revealed the basic logic of how these animals learn to seek what is good and to avoid what is bad for them (Heisenberg, 2003; Gerber and Aso, 2017; Cognigni et al., 2018; Boto et al., 2020; Li et al., 2020; Modi et al., 2020; Davis, 2023). Such learning takes place in the mushroom body, a higher brain centre that is evolutionarily conserved across the insects. Its intrinsic neurons, called Kenyon cells (KCs), represent the sensory environment in a sparse and combinatorial manner, and are intersected by predominantly dopaminergic modulatory neurons. A subset of these mediate either negative or positive valence signals, evoked by electric shock punishment or sugar reward, for example, which are conveyed to segregated compartments along the long, parallel axonal fibres of the KCs. Punishment and reward compartments feature output neurons that promote approach and avoidance, respectively. Upon coincidence of KC activity and a dopaminergic punishment signal, for example, the synapse from the KC onto the approach promoting output neuron is depressed, shifting the balance across the output neurons to avoidance when the odour is encountered again (see General Introduction for further details). Despite the elegant simplicity of this logic, the connectome has revealed unexpected circuit complexity (Zheng et al., 2018; Li et al., 2020; Scheffer et al., 2020; Schlegel et al., 2023; Dorkenwald et al., 2024) suggesting a corresponding behavioural and experiential complexity. Here I reasoned that this system should allow for a neurobiologically grounded understanding of the action-valence relationship, and asked whether avoidance can engage negative valence as reflected in the activity of dopaminergic punishment neurons.

The *Drosophila* brain-descending “moonwalker” neurons elicit backward walking when experimentally activated (Figure 1.1, Extended Data Figure 1.1) (Bidaye et al., 2014). I reasoned that such backward locomotion, an element of *Drosophila´*s natural avoidance manoeuvres, might promote negative valence. I tested this idea in a modified Pavlovian conditioning paradigm using odours as conditioned stimuli and, unconventionally, the optogenetic induction of backward locomotion instead of a punishing unconditioned stimulus. These experiments were combined with a collaborative approach with behavioural pharmacology, high-resolution video tracking, functional imaging, connectomics analyses and a normative computational model.

Together, my results suggest that avoidance engages dopaminergic punishment signals, functionally counterbalancing the extinction of aversive memories and minimizing the likely hood of receiving further, potentially life-threatening, punishment. Such a mechanism can resolve the long-standing puzzle of why animals and humans alike often show little sign of extinction but

rather continue to avoid a cue predictive of punishment even when that avoidance is successful and no punishment is received (the “avoidance paradox”: Bolles 1972, (LeDoux et al., 2017).

Materials and methods

Fly strains

Drosophila melanogaster were raised under standard conditions, in constant darkness to avoid any intended optogenetic effects. For behavioural experiments, mixed-sex cohorts of 2-5 day old flies were used. *In vivo* calcium imaging and immunohistochemistry used female flies only due to genetic constraints. Strains to establish experimental genotypes and their driver and effector controls (Dri Ctrl and Eff Ctrl) have been described previously, unless otherwise mentioned. For further genotype details, see Supplemental Table S1.

Conditioning and choice experiments

Male flies of the driver strains were crossed to females of the effector strains and cohorts of ~60-100 flies of their F1 progeny used in a T-maze setup described previously (Schwaerzel et al., 2002, 2003) (CON-ELEKTRONIK, Greussenheim, Germany) allowing for electric shock, optogenetic manipulation and odour delivery, operated at 23-25 °C, 60-80 % relative humidity, and red light invisible to flies, unless mentioned otherwise. As odorants, undiluted 50 µl benzaldehyde (BA) and 250 µl 3-octanol (OCT) (CAS 100-52-7, 589-98-0; Fluka, Steinheim, Germany) were applied to Teflon containers of 5 mm and 14 mm diameter, respectively.

Conditioning with optogenetic activation as reinforcement

Olfactory conditioning with optogenetic activation as reinforcement was conducted as described previously (König et al., 2018) (Figure 1.1-1.5, Figure 1.12, Extended Data Figure 1.4c-d). Flies were loaded to the training tubes and 2 min later one odour (CS+) was presented for 1 min. Unless mentioned otherwise, 15 s later (inter-stimulus-interval (ISI) of -15 s) pulsed light for optogenetic activation was turned on for 1 min (training tubes featured 24 LEDs, either blue: 465±10 nm or red: 627±10 nm, 69.25µW/mm^2 and 53.04 µW/mm^2, as measured with an STS-VIS Spectrometer, Ocean Optics) at 4.99 s / 0.01 s ON / OFF pulses. Another 4 min later the control odour (CS-) was presented. In total, flies underwent three such training trials until given a choice test between the two odours loaded to the arms of the T-maze. After 2 min, the arms of the maze were closed and relative odour preference calculated from the number of flies (#) in each arm:

BA Preference = ([#BA - #OCT] / #Total) x 100 [Equation 1]

Across repetitions of the experiment, cohorts of flies were trained with contingencies of odour and light (*) swapped to calculate the memory score:

Memory score = (BA Preference BA* - BA Preference OCT*) / 2 [Equation 2]

Positive memory scores thus indicate appetitive and negative memory scores aversive associative memory. In Figure 1.2c and Figure 1.3**,** the CS+ was presented for backward pairing (ISIs: +120s; +60, +120s, +240s and +120s respectively). The experiment in Extended Data Figure 1.9b was performed the same, except that green light (530±10 nm, 37.71 μW/mm^2) was used for optogenetic silencing.

Behavioural pharmacology

Pharmacological manipulations were performed as described previously (Amin et al., 2025). For 36-40 h before behavioural experiments flies were offered as their sole food a tissue paper (Fripa, Düren, Germany) soaked with 1.8 ml of either (i) a plain 5 % sucrose solution (CAS: 57-50-1, Hartenstein, Würzburg, Germany), or that solution added with either (ii) 5 mg/ml 3-iodo-L-tyrosine (3IY), an inhibitor of dopamine synthesis (CAS: 70-78-0, Sigma, Steinheim, Germany), or (iii) 5mg/ml 3IY plus the dopamine precursor 10 mg/ml 3,4-dihydroxy-L-phenylalanine (L-DOPA) (CAS: 59-92-7, Sigma, Steinheim, Germany). In all cases, flies were trained and tested as described above for optogenetic activation as reinforcement, at ISIs of either -15 s or 120 s (Figure 1.4a, Supplement Figure 9)**.**

Conditioning with shock or sugar reinforcement and optogenetic silencing during the test

Olfactory conditioning with electric shock or sugar as reinforcement was conducted as described above for optogenetic activation as reinforcement with the following differences. Flies went through only one training trial either with electric shock (12 pulses of 100 V, 1.2 s / 3.8 s ON / OFF) or 2 M sucrose solution presented on filter paper. During the 2 min of choice test, green light was turned on for optogenetic silencing (Figure 1.7, Supplement Figure 5-6). Innate olfactory choice behaviour was assessed the same, save the training (Extended Data Figure 1.3).

Restraining movement (trapping) during training

For the Control case, olfactory training and testing was performed with optogenetic activation as reinforcement as described above. For the Trapped case, flies were gently pushed down to the bottom of the training tubes using a piece of cotton wool and released from this restraint before

the choice test (Figure 1.12a). The experiment in Figure 1.12c used only one training trial to avoid overtraining (König et al 2018). The experiment in Extended Data Figure 1.9a used one training trial of olfactory conditioning with trapping as reinforcer.

Extinction learning

Extinction learning experiments were modified from a previously published procedure (Schwaerzel et al., 2002; Felsenberg et al., 2018) (Figure 1.15a). Training with odour and electric shock was conducted as described above. Subsequently flies were removed from the T-maze setup and kept on a standard food vial for 30 min until returned to the setup and released at the choice point. For the flies of the baseline condition, only air was presented on both sides of the T-maze for 1 min, while independent sets of flies received extinction protocols such that the CS+ was presented either in one arm or in both arms of the T-maze. These extinction protocols were run without green light or with pulsed green light for optogenetic silencing as mentioned before (MDN feedback, and No MDN feedback, respectively). After collecting the flies from both arms of the maze, there followed a 2-min choice test between CS+ and CS- as described above.

In vivo two-photon calcium imaging

A custom-made two-photon microscope with a modified protocol from Barnstedt et al., 2016 was used throughout. 2-7 days old female flies of the indicated genotypes were transferred on freshly prepared standard food mixed with 1mM all trans retinal for 2-3 days in darkness. They were briefly (~20 s) anaesthetized on ice and tethered in a custom chamber (chamber design courtesy: Clifford Talbot, CNCB Oxford, kindly provided by Oliver Barnstedt, manufactured at Sculpteo, France) to open the head capsule under room temperature in carbogenated (95% O2, 5% CO2) buffer solution (103 mM NaCl, 3 mM KCl, 5 mM N-Tris,10 mM trehalose, 10 mM glucose, 7 mM sucrose, 26 mM NaHCO3, 1 mM NaH2PO4, 1.5 mM CaCl2, 4 mM MgCl2, osmolarity 275 mOsm, pH 7.3-4). Flies were fixated to the chamber using wax attached to eyes, wings and parts of the thoracic body wall, but were able to move their legs. After confirming genetic markers and expression under a tabletop fluorescence microscope of both GCaMP and tdtomato in experimental genotype and only GCaMP expression in control flies, they were transferred to a two-photon microscope (see Extended Data Figure 1.5a).

For optogenetic activation, a high-power LED (LEDD1B T-Cube LED Driver, 1200 mA Max Drive Current) was relayed through the imaging objective onto the specimen, triggered manually. The power at the specimen was measured to be 10.5 mW/mm^2. After preparation and transfer to the two-photon microscope, flies were left to rest for 3-5 min. 10 s after recording baseline fluorescence, five 200 ms (Figure 1.9, Figure 1.10, Extended Data Figure 1.6c, Figure 1.11) or 20

ms (Extended data Figure 1.5, Extended Data Figure 1.6d) light pulses were delivered at 40 Hz while recording calcium transients for a total of 60 s. Fluorescence was excited using 75 fs pulses, 80 MHz repetition rate, centred on 920 nm generated by a Ti-Sapphire laser (Chameleon Vision S, Coherent) and images of 550 X 550 pixels were acquired at 40 Hz, controlled by custom-written software in LabView (National Instruments). Dopaminergic neurons were imaged at the level of the horizontal mushroom body lobe focusing on γ1-5, β'2 compartments. Regions of interest (ROI) were manually drawn in the relevant areas using ImageJ and further analysed using Microsoft Excel, Statistica and custom-written Python scripts. Baseline fluorescence F_0 was defined as the mean F from the first 2 s of recording. Calcium responses were quantified by comparing the average $\Delta F/F_0$ from 2 s before until light onset (pre) and the average $\Delta F/F_0$ from the light offset to 2 s thereafter (post). $\Delta\Delta F/F_0$ was defined as the post-stimulus average fluorescence minus the pre-stimulus average fluorescence.

In Fig.1.11a-e, the experiments were performed as mentioned above, in addition with a leg movement restraining protocol, similar to the one used in behavioural experiments before. Leg movements were monitored using a monochrome CCD camera (Basler acA 780-75gm) positioned approximately 5-10 cm from the fly. Camera position was aligned for each fly before the start of recordings and images acquired at 100 Hz with 1040 x 1040 pixels using pylon Camera Software Suite (Basler). Videos were synchronised to two-photon imaging recordings by the two-photon laser's visible on- and offset. Files were saved in compressed MP4 format before further processing.

Explant two-photon calcium imaging

For Extended data Figure 1.7, flies of the indicated genotypes were anesthetized on ice for 5 mins and dissected with forceps in carbogenated saline (103 mM NaCl, 3 mM KCl, 5 mM N-Tris, 10 mM trehalose, 10 mM glucose, 7 mM sucrose, 26 mM NaHCO3, 1 mM NaH2PO4, 1.5 mM CaCl2, 4 mM MgCl2, 295 mOsm, pH 7.3). Either the brain was isolated without the ventral nerve cord, or the brain was extracted with the ventral nerve cord attached (Extended Data Figure 1.7a, Extended Data Figure 1.7b). Samples were put into a transparent imaging chamber and kept in place by a nylon grid. The chamber was then filled with carbogenated saline. After 5 min recordings started under a Femtonics two photon microscope using 920 nm pulsed laser light with a 30 Hz imaging rate. Optogenetic activation was performed with a Thorlabs red light LED of 625 nm (1.41 mW/cm2) controlled by a HEKA patch master EPC9 v12x9. Due to the orientation of the samples, the γ1, β2, and β'2 compartments are located in a different focal plane than the other γ compartments. Therefore, using 200-ms pulses of red light for optogenetic activation, two z-planes were recorded starting either with γ1, β2, and β'2, or the γ2, γ3, γ4, and γ5 plane. Starting

with the respectively second plane, we repeated this for 1000 ms of red light. Raw imaging files were downsampled to 15 Hz and converted into TIFF files using a custom-written Python script. Using NOSA (Oltmanns et al., 2020), changes in the fluorescence signal of the respective compartments were determined and exported as Excel files. Data were further analysed and visualised using custom-written Python scripts. Baseline fluorescence F_0 was defined as the mean F from the first 2 s of recording. Calcium responses were quantified by comparing the average $\Delta F/F_0$ from 2 s before until light onset (pre) to the average $\Delta F/F_0$ from light offset to 2 s (Δ long) or 0.5 s thereafter (Δ short) (post). $\Delta\Delta F/F_0$ was defined as the Δ short, Δ long post-stimulus average fluorescence minus the pre-stimulus average fluorescence.

Immunohistochemistry

Moonwalker^A, MDN1^A (Figure 1.1a, Figure 1.5, Extended Data Figure 1.1a, Extended data Figure 1.1c), were crossed to Chrimson^A, whereas Moonwalker^B and MDN1^B was crossed Chrimson^D (Extended Data Figure 1.4a, b). Brains and ventral nerve cords from adult progeny (5-7 days old) were dissected and immunostained as described (Wu et al., 2016) (https://www.janelia.org/project-team/flylight/protocols). Tissues were dissected in PBS on ice, fixed in 4 % PFA (20-30 min at room temperature), and washed in 0.5 % PBST (3 x 10-15 min at room temperature). After being left overnight in blocking solution (10 % NGS in PBST) at 4 °C, tissues were incubated with the primary antibody for 24 h at 4 °C and washed in 0.5 % PBST (3 x 10-15 min, at room temperature, and overnight at 4 °C). Tissues were incubated with the secondary antibody for 24 h at 4 °C and washed in 0.5 % PBST (3 x 10-15 min at room temperature, and overnight at 4 °C). After a final washing step (1x 5-10 min in PBS), tissues were mounted on a slide using the DPX mounting protocol (https://www.janelia.org/project-team/flylight/protocols) before imaging. Image z stacks were acquired with a LSM780 confocal microscope (Zeiss, NY, USA) at 1024 × 1024-pixel resolution. Image processing was performed using ImageJ (Fiji ImageJ).

For Moonwalker^A and MDN1^A crossed to Chrimson^A, polyclonal chicken anti-GFP was used as primary antibody (Thermo Fisher Scientific, AB_2534023) diluted 1:1000 in 0.5 % PBST for neuronal labelling and a monoclonal mouse anti-Bruchpilot (nc82) antibody (Developmental Studies Hybridoma Bank, AB_2314866) diluted 1:500 in 0.5 % PBST to label neuropil. A polyclonal goat anti-chicken Alexa488 (Thermo Fisher Scientific, AB_2576217) and a polyclonal goat anti-mouse Alex568 (Thermo Fisher Scientific, AB_2534072) were used as secondary antibodies, both diluted 1:500 in 0.5 % PBST.

For Moonwalker^B, MDN1^B crossed to Chrimson^D, a polyclonal rabbit anti-dsRed was used as primary antibody (CloneTech, AB_10013483) diluted 1:500 in 0.5 % PBST for neuronal labelling

and a monoclonal mouse anti-Bruchpilot (nc82) antibody (Developmental Studies Hybridoma Bank, AB_2314866) diluted 1:500 in 0.5 % PBST for neuropil labelling. A polyclonal goat anti-rabbit Alex568 (Thermo Fisher Scientific, AB_10563566) and a polyclonal goat anti-mouse Alex647 (Thermo Fisher Scientific, AB_141725) were used as secondary antibody diluted 1:500 in 0.5% PBST.

EM reconstruction

Renderings of the MDN neurons in the brain and all their pre- and postsynaptic sites (Figure 1.5 (EM), Figure 1.6a, Extended Data Figure 1.1b) were displayed using Codex.ai from FAFB/FlyWire (v783) (Zheng et al., 2018; Buhmann et al., 2021; Dorkenwald et al., 2024; Eckstein et al., 2024; Schlegel et al., 2024). LAL-MDN synapses (Figure 1.6e) and MBON-LAL synapses were displayed using a custom Python script to interact with the FlyWire dataset through the CAVEclient Python package (Dorkenwald et al., 2024).

Rendering of MDN descending arbours in the ventral nerve cord and all their pre- and post-synaptic sites (Figure 1.6a) were displayed using a custom Python script to interact with the FANC dataset through the FANC Python package (Phelps et al., 2021; Azevedo et al., 2024). Code will be made available upon request.

Video recording of fly locomotion

Experimental procedures followed (Bidaye et al., 2020). Newly hatched 1–3-day-old flies of the indicated genotypes and drug treatment (following Behavioural pharmacology protocol as mentioned earlier) were individually placed on a circular arena and given five 10-s light stimulations for optogenetic activation, each pulsed at 50 Hz and 5 ms pulse width, at 50 s intervals. A single trial was considered as 10 s periods with stimulation-light off followed by the 10 s light stimulation (Extended Data Figure 1.2a, Extended Data Figure 1.2c). For the experiments shown in Figure 1.4b and Extended Data Figure 1.2a, light of 530 nm and 0.65 mW/mm^2 was used for optogenetic stimulation, whereas for the experiments shown in Extended Data Figure 1.2b and Extended Data Figure 1.2c light of 630 nm and 0.80 mW/mm^2 was used. Continuous low-intensity light at 530 nm and 0.1 mW/mm^2, in itself insufficient for optogenetic activation, was used throughout to avoid jumping responses upon stimulation-light onset; in addition, low-intensity infrared light of 850 nm and 0.05 mW/mm^2 was used for video recording at 1280 x 1024 pixel resolution and 30 fps. Stimulation-light was controlled and synchronized to the camera (FLIR BlackFly-S Camera, FL3-U3-13Y3M-C, Richmond, BC, Canada) using a customized Arduino board. Individual fly locomotion was tracked using FlyTracker software (Eyjolfsdottir et al., 2014)

and data was analysed and plotted in Matlab for translational velocity (mms/s). Code will be made available upon request.

Connectome analyses

Analysis of the connectivity from MBONs to MDNs in Figure 1.6 b-d were produced using FlyWire v783 (Dorkenwald et al., 2024; Schlegel et al. 2024). Let A_{ij} be the number of synapses onto postsynaptic neuron i from presynaptic neuron j, thresholded at 10 synapses per entry. Define the normalised weight matrix $W_{ij}=A_{ij}/\Sigma_k A_{ik}$, so that each row of W sums to 1 and the 2-step influence from neuron j to neuron i as \(W^2\)$_{ij}$. Figure 1.6c shows as a percentage for the 6 MBON types with the most influence on the MDNs, averaged across MDNs and within MBON type. Figure 1.6d shows the percent input from an MBON to MDN via the indicated LAL type which is calculated as the ratio between the 2-step influence from MBON to MDN without that LAL and the 2-step influence with all intermediaries. The same MBONs, LALs and averaging as in Figure 1.6c are used. Connections via the intermediaries that have a large MBON to MDN influence are shown. Code will be made available upon request.

Modelling

In the model, (Figure 1.14a-d, Figure 1.15b, c) KCs synapse onto MBONs with activities m^{ap} and m^{av} that promote approach and avoidance, respectively. In the following, we suppress time indices unless they are required for clarity. MBON activities are determined by $m^{ap}=\Sigma_i w_i^{ap} k_i$, and similarly for m^{av}, where k_i is the activity of KC i, and w_i^{ap} and w_i^{av} are its weights onto MBONs. Odours activate random non-overlapping subsets of N_{odour} KCs. The firing rate of active KCs is $1/N_{odour}$, and the firing rate of inactive KCs is 0.

The activities of punishment- and reward-responsive DANs d^p and d^r on time step t are given by:

$$d_t^p = cp_t - (1-c)r_t + \frac{1}{2}\left(\pi_t^{av} - \pi_t^{ap}\right) + 2MDN_t$$

$$d_t^r = cr_t - (1-c)p_t + \frac{1}{2}\left(\pi_t^{ap} - \pi_t^{av}\right) + MDN_t,$$

where $c=0.8$, and $p\geq 0$ and $r\geq 0$ represent external punishment and reward. The MDN terms model MDN feedback and influence both DANs, but with a larger magnitude for the punishment-responsive DAN, as in experiments (Figure 1.10). The prediction components π^{ap} and π^{av} are calculated as $\pi_t^{ap}=\Sigma_i \gamma w_{i,t}^{ap} k_{i,t+1} - \Sigma_i w_{i,t}^{ap} k_{i,t}$, and similarly for π^{av}, where $\gamma=0.99$ (Figure 1.14c, Figure 1.14d) or $\gamma=0.8$ (Figure 1.15b, Figure 1.15c) is the temporal discount factor.

KC-to-MBON weights are updated as $w^{ap}_{i,t+1}=w^{ap}_{i,t}-\eta d^{p}_{t} k_{i,t}$ and $w^{av}_{i,t+1}=w_{i,t}{}^{av}-\eta d^{r}_{t} k_{i,t}$, where $\eta=0.1$ is the learning rate. After this update, on each time step the weights are also normalised such that $w_i^{ap}+w_i^{av}\rightarrow 2$ asymptotically: $w_i^{ap}\leftarrow w_i^{ap}+0.025\left(2-w_i^{ap}-w_i^{av}\right)$ and $w_i^{av}\leftarrow w_i^{av}+0.025\left(2-w_i^{ap}-w_i^{av}\right)$ (not shown). The difference $V=m^{ap}-m^{av}$ represents the model's estimate of the current odour's value and controls its approach and avoidance behaviour. At each timepoint, the model fly approaches the odour source, stays in place, or avoids the odour source with probabilities $\left[p_{approach},p_{stay},p_{avoid}\right]$. When $V>0.01$, these probabilities are $[0.8,0.1,0.1]$. When $V<-0.01$, they are $[0.1,0.1,0.8]$. Otherwise, they are $[0.4,0.2,0.4]$.

For models with MDN feedback, $MDN_t=0.1$ if, on the previous timestep, the "avoid" action was selected and $V<-0.001$. The latter condition improves model performance by not reinforcing random "avoid" actions (not shown), although our qualitative results do not depend on this choice. For models without MDN feedback, $MDN=0$ and the model is equivalent to temporal difference learning (Sutton and Barto, 2018).

Extinction experiments (Figure 1.15a-c) consist of three phases – one training phase and one extinction phases – each with 35 timesteps, followed by a test phase. During the training phase, an odour is presented and an external punishment of magnitude -0.4 is delivered every three timesteps, starting on the second timestep. During the extinction phase, odour is either present or absent on each side of the arena according to each protocol (Figure 1.15a), with no external reinforcement. During the test phase, each model's probability of choosing the punishment-predicting odour is given by a softmax function $P=\frac{exp(V/0.3)}{1+exp(V/0.3)}$, where V is the final estimated value of the punished odour following timestep 108. In between phases, a timestep in which no odour is present occurs. Code will be made available upon request.

Statistical analyses

Non-parametric statistical tests were used throughout (Statistica 11.0; StatSoft Hamburg, Germany, and R 2.15.1, www.r-project.org). To analyse the behavioural experiments, the Kruskal-Wallis test (KW) was applied for comparisons between more than two groups. For subsequent pairwise comparisons between groups, Mann-Whitney U-tests (MW-U) were performed. To test whether the values of a given group differed from chance levels, i.e., from zero, one-sample sign tests (OSS) were used. Within-animal comparisons used the Wilcoxon signed-rank test.

Significance levels of multiple tests were adjusted by a Bonferroni-Holm correction to keep the experiment-wide type 1 error limited to 0.05 (Holm, 1979). Data are presented as box plots with the median shown as the middle line and the 25% / 75% and 10% / 90% quantiles as box

boundaries and whiskers, respectively. In cases of within-animal comparisons, data of individual flies are also displayed and connected across repeated measurements. For conditioning and choice experiments, a sample size of N= 1 included ~60-100 flies; video recordings of fly locomotion were done on the indicated number of individual flies. For model fly extinction experiments, a sample size of N= 1 included 20 individual model flies.

For two-photon calcium imaging data, the $\Delta\Delta F/F_0$ values were used for all statistical analyses on the indicated number of individual flies. The $\Delta\Delta F/F_0$ were compared between experimental and control groups across compartments by using Mann-Whitney U-test and significance levels were adjusted by a Bonferroni-Holm correction (Figure 1.9, Figure 1.10, Extended Data Figure 1.5, Extended Data Figure 1.7). In Figure 1.11, $\Delta\Delta F/F_0$ were compared within animal among before, during and after trapping by Wilcoxon signed-rank tests with Bonferroni-Holm correction. Throughout, boxplots show the 25th-75th or 10th-90th percentiles (box), the median (line) and the minimum and maximum (whiskers). In Extended Data Figure 1.6c'', d'', Friedman test was used. Additional information and sample sizes are mentioned in corresponding figure legends.

Results

Moonwalker neuron activation engages a dopaminergic punishment signal

To investigate action-valence relationships, I first tested whether backward locomotion induced by moonwalker neuron activation can confer negative valence. Flies were trained in a differential conditioning task such that one odour was followed by pulsed optogenetic activation of the moonwalker neurons (Figure 1.1a), triggering backward locomotion (Bidaye et al., 2014). A second, control odour was presented alone, followed by a choice test between both odours (Figure 1.1b). This revealed an aversive memory for the odour that had been associated with moonwalker neuron activation in the experimental genotype, but not in genetic controls treated the same (Figure 1.1c).

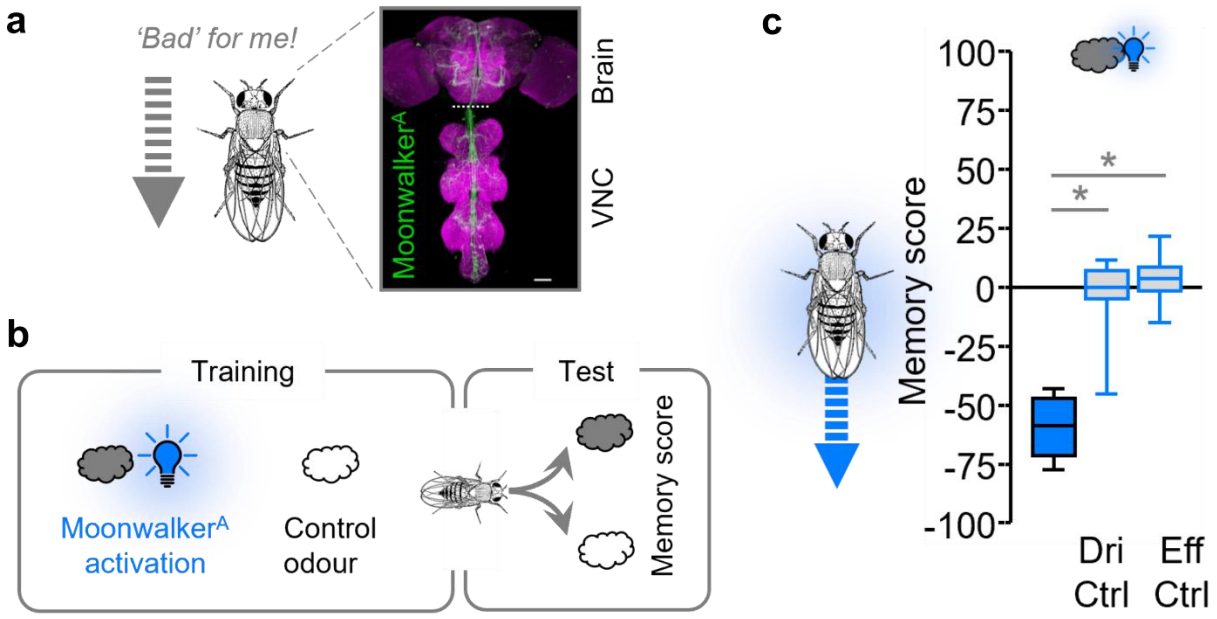

Figure 1.1 | Moonwalker neuron activation confers negative valence.

a, Proposed action-valence relationship and expression of the transgenic driver to induce backward locomotion. Moonwalker^{A}>Chrimson^{A}; magenta: neuropil labelling (anti-Bruchpilot), green: moonwalker neuron labelling (anti-GFP). VNC: ventral nerve cord. Higher resolution version is in Extended Data Figure 1.1a.

b, Rational of learning experiments. Clouds: odours. Light bulb: optogenetic activation of all moonwalker neurons (Moonwalker^{A})

c, Aversive memory by pairing odour with moonwalker neuron activation (blue: Moonwalker^{A}>ChR2XXL^{A}, grey: Driver control: Moonwalker^{A}>+, Effector control: +>ChR2XXL^{A}, +: absence of driver or effector construct) (N= 20,18,18). Data were analysed across groups by Kruskal-Wallis tests (P< 0.05), followed by pairwise comparisons (Mann-Whitney U-tests, *P< 0.05 with Bonferroni-Holm correction) (ns: P> 0.05). Scale bars in (a): 50µm and stippled lines in (a) indicate stitching of images of brain and VNC from the same animal, processed separately.

Box-whisker plots show median, interquartile range (box) and 10th/90th percentiles (whiskers). Underlying BA preference score and memory scores separated by sex are shown in Extended Data Figure 1.11. Additional genotype information is in Supplemental Table S1 and statistical results in Supplemental Data Table S1.

Next, I tested the stability of this aversive memory by using different training-test intervals and it was subsided over 4-8 hours (Figure 1.2a). I also confirmed this aversive moonwalker memory by using another optogenetic effector (Figure 1.2b, also see Supplement Figure 1-4 for further parametric analysis).

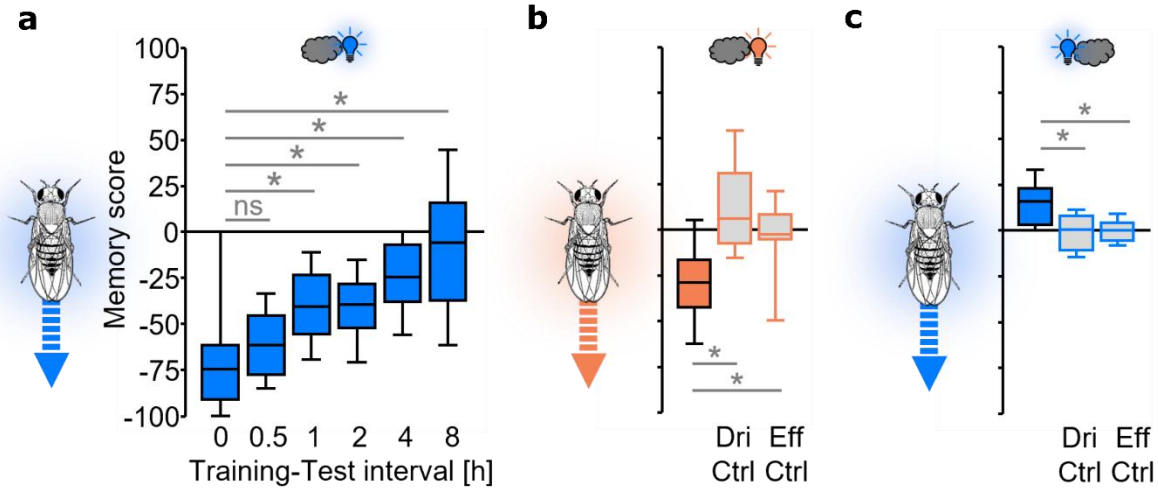

Figure 1.2 | Parametric analysis of moonwalker neuron reinforcement.

a, Stability of moonwalker neuron activation conveying negative valence. As in Figure 1.1, for the indicated training-test intervals (blue: Moonwalker^{A}>ChR2XXL^{A}) (N= 19,20,20,20,20,19).

b, As in (Figure 1.1), using Chrimson^{A} as effector (orange: Moonwalker^{A}> Chrimson^{A}, grey: Driver control: Moonwalker^{A}>+, Effector control: +>Chrimson^{A}) (N= 17,17,18).

c, As in (Figure 1.1), for a training procedure in which the odour followed moonwalker neuron activation (blue: Moonwalker^{A}>ChR2XXL^{A}, grey: Driver control: Moonwalker^{A}>+, Effector control: +>ChR2XXL^{A}, +: absence of driver or effector construct) (N= 18,15,15).
Data were analysed across groups by Kruskal-Wallis tests (P< 0.05), followed by pairwise comparisons (Mann-Whitney U-tests, *P< 0.05 with Bonferroni-Holm correction) (ns: P> 0.05). Box-whisker plots show median, interquartile range (box) and 10th/90th percentiles (whiskers). Underlying BA preference and memory scores separated by sex are shown in Extended Data Figure 1.12. Supplementary information for parametric analysis is shown in Supplement Figure 1-4. Additional genotype information is in Supplemental Table S1 and statistical results in Supplemental Data Table S1.

Interestingly, the punishing effect of moonwalker neuron activation has the same temporal 'fingerprint' as electric shock punishment. That is, while the presentation of an odour before an electric shock induces strong aversive memory for the odour, presenting an odour after the shock, at the moment of relief, induces a characteristically weaker appetitive memory (Gerber et al., 2019). Such timing-dependent valence reversal reflects an across-species principle (Gerber et al., 2019) that also applies to moonwalker neuron activation (Figure 1.2c, Figure 1.3).

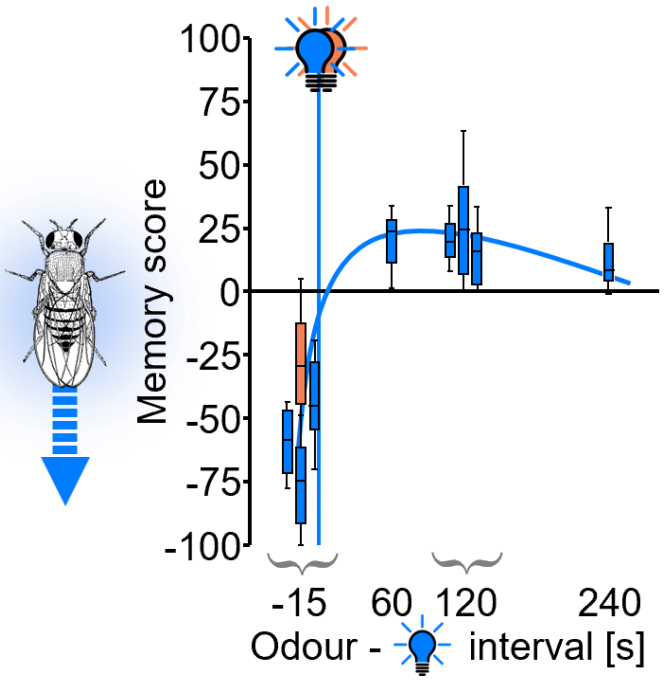

Figure 1.3| Mapping out the temporal profile of moonwalker neuron reinforcement.
Results for the experimental genotypes arranged according to the indicated intervals between odour and optogenetic activation (N= 23,23,23,18; 24; 24; 24,24; 24) (includes data re-plotted from Figure 1.1-1.4; for the -15 s and 120s intervals). Also see Extended Data Figure 1.12d for underlying BA preference and memory scores separated by sex for 60s, 120s, 240s intervals).
Light bulb: optogenetic activation of all moonwalker neurons (Moonwalker^{A}). Box-whisker plots show median, interquartile range (box) and 10th/90th percentiles (whiskers). Additional genotype information is in Supplemental Table S1 and statistical results in Supplemental Data Table S1.

As punishment is conveyed to the mushroom body KCs by dopaminergic neurons (Riemensperger et al., 2005; Claridge-Chang et al., 2009; Aso et al., 2010; Aso et al., 2012), next I hypothesized that learning from moonwalker activation is dopamine dependent. After acutely supplementing fly food with the drug 3IY, an inhibitor of the TH enzyme required for dopamine biosynthesis (but without effect on odour preference (Thoener et al., 2021), impaired punishment and abolished relief learning by moonwalker neurons (Figure 1.4a). Both these effects were fully rescued by additional supply of L-DOPA (Figure 1.4a). Critically, high-resolution video recording showed that moonwalker-induced backward locomotion itself was unaffected by 3IY (Figure 1.4b,

Extended Data Figure 1.2). These results show that moonwalker neuron activation both elicits backward locomotion and engages a dopaminergic punishment signal for associative learning.

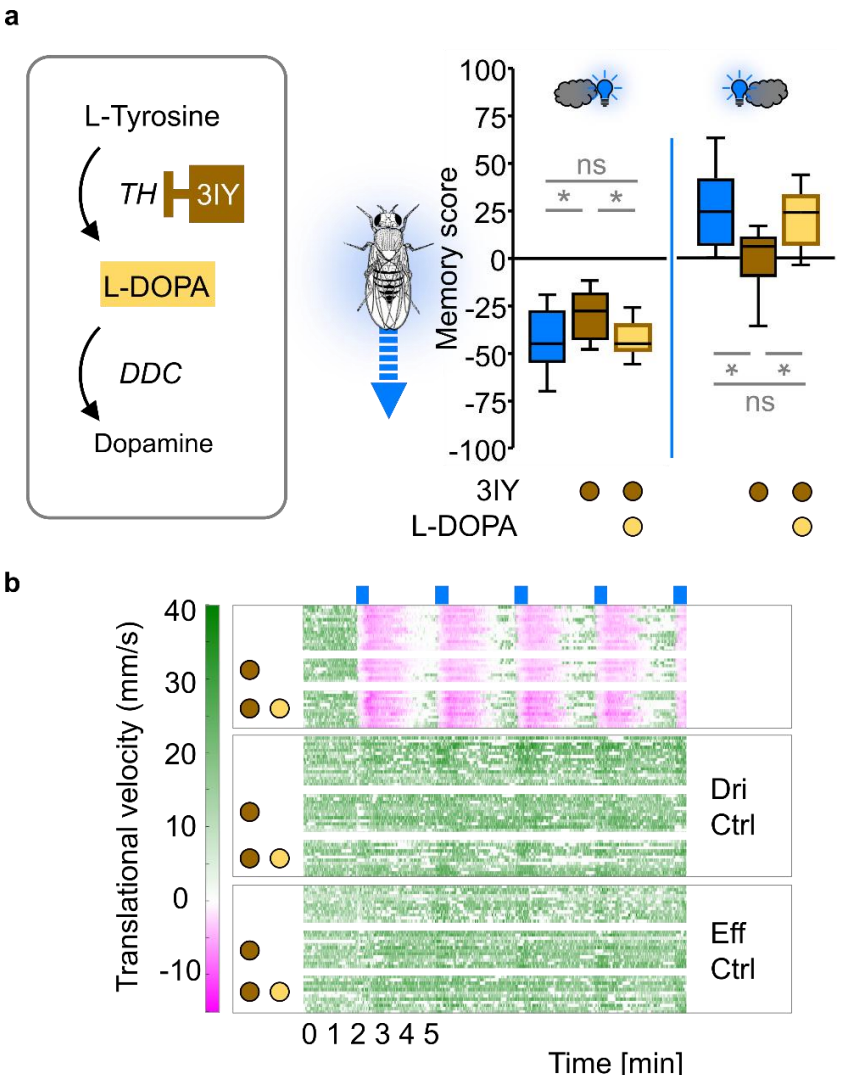

Figure 1.4 | Moonwalker neuron activation engages a dopaminergic punishment signal.

a, Inhibition of dopamine biosynthesis by 3-iodo-L-tyrosine (3IY), and effects of 3IY on learning from moonwalker activation (Moonwalker^{A}>ChR2XXL^{A}, intervals -15s or 120s; blue: control, brown: 3IY, light brown: additional supply of 3,4-dihydroxy-L-phenylalanine (L-DOPA)) (N= 23,24,23; 20,19,20). DDC: dopamine decarboxylase. TH: tyrosine hydroxylase. Clouds and light bulbs represent odours and optogenetic activation in all experiments. Data were analysed across groups by Kruskal-Wallis tests (P< 0.05), followed by pairwise comparisons (Mann-Whitney U-tests, *P< 0.05 with Bonferroni-Holm correction) (ns: P> 0.05). Box-whisker plots show median, interquartile range (box) and 10th/90th percentiles (whiskers). Underlying BA preference and memory scores separated by sex are shown in Extended Data Figure 1.13. Additional genotype information is in Supplemental Table S1 and statistical results in Supplemental Data Table S1.

b, Analysis of locomotion upon the treatments in **(a)**. Shown is translational velocity (mm/s), colour coded from magenta/backward to green/forward walking in relation to moonwalker activation (blue bars). Rows

correspond to individual flies; the top three sets of rows show Moonwalker^{A}>ChR2XXL^{A} flies, genetic controls, as in (Figure 1.1c), are shown below (N= 12,8,12,16,12,12,12,12,12,12). Corresponding average translational velocity is shown in Extended data figure 1.2a. Analysis of locomotion upon treatments as translational velocity (mm/s) and average translational velocity by using other effector Chrimson^{A} are shown in Extended data Figure 1.2b, c. Data will be made available upon request.

The fly strain used for moonwalker neuron activation drives expression in a relatively large number of neuronal subpopulations (Bidaye et al., 2014) (Figure 1.1a, Extended Data Figure 1.1a). These neurons can be assigned to seven cell types, of which moonwalker descending neurons (MDNs) have been previously demonstrated as sufficient to induce backward locomotion (Bidaye et al., 2014). I found that activation of the only four MDNs also produced a punishment memory when paired with odour (Figure 1.5, Extended Data Figure 1.1b, Extended Data Figure 1.1c), thus allows to focus on the subsequent analysis on these neurons. These analyses will uncover a reciprocal interaction between the MDNs and the flies´ olfactory memory centre, the mushroom body.

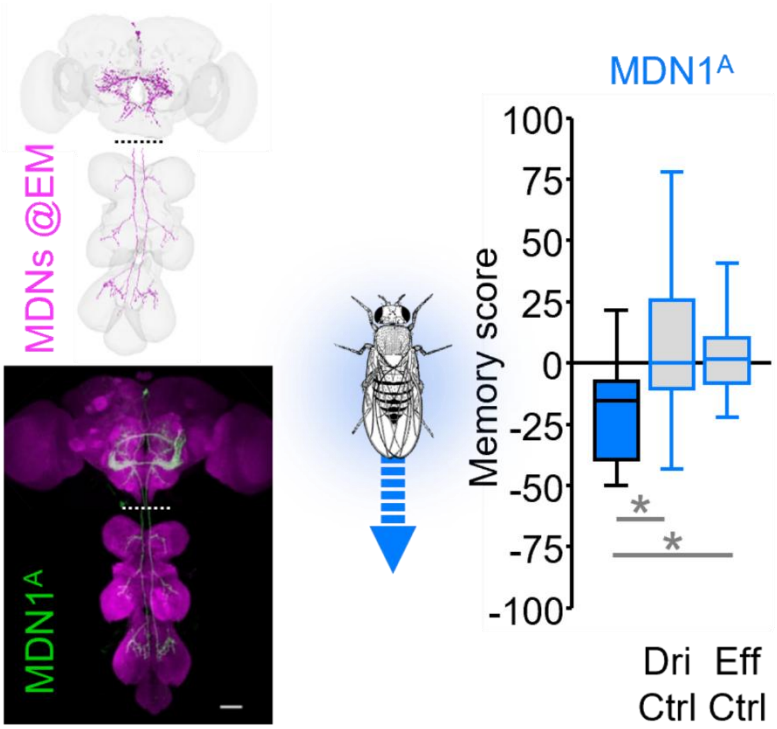

Figure 1.5| **Selective MDNs activation confer negative valence**.
(Left top) EM reconstruction of the moonwalker descending neurons (MDNs, magenta) (grey mesh: brain and VNC; higher resolution versions are in Extended Data Figure 1.1b, c). and (Left bottom) expression of the transgenic driver covering them (MDN1^{A}>Chrimson^{A}, details as in Figure 1.1a-b). Learning experiments as in (Figure 1.1), showing aversive memory through MDNs activation (blue: MDN1^{A}>ChR2XXL^{A}, grey: Driver control: MDN1^{A}>+, Effector control: +>ChR2XXL^{A}) (N= 21,17,17). Data

were analysed across groups by Kruskal-Wallis tests (P< 0.05), followed by pairwise comparisons (Mann-Whitney U-tests, *P< 0.05 with Bonferroni-Holm correction) (ns: P> 0.05).
Scale bars in (left bottom): 50µm and stippled lines in (b) indicate stitching of images of brain and VNC from the same animal, processed separately.
Box-whisker plots show median, interquartile range (box) and 10th/90th percentiles (whiskers). Memory scores separated by sex and odour choices are shown in Extended Data Figure 1.14. Additional genotype information is in Supplemental Table S1 and statistical results in Supplemental Data Table S1. See also Supplement Figure 8 and Supplement Figure 9 for parametric analysis of $MDN1^{A}$. Also Supplement Figure 12-14 shows additional work with other moonwalker drivers.

To understand this reciprocal interaction, I decided to first focus on how the mushroom body is connected to the MDNs (Figure 1.6 and Figure 1.7) and then investigate how the MDNs in turn affect mushroom body processing (Figure 1.9, Figure 1.10, Figure 1.11, Figure 1.12, Figure 1.14 and Figure 1.15).

MDNs are part of aversive memory output pathways

What is the behavioural relevance of associating backward locomotion with a punishment signal? Here the hypothesis was that aversive memory expression pathways may engage backward locomotor control to avoid negatively associated odours. To understand if and how the fly's memory centre, the MB, may engage MDNs, we turned to the recently published *Drosophila* whole-brain connectome (Li et al., 2020). These data show that MDN dendrites innervate the lateral accessory lobe (LAL), where most of their inputs are received, whereas most of their axonal output terminals are in the ventral nerve cord (VNC) (Figure 1.6a). The analysis of the fly connectome suggests that the MDNs are mainly influenced by only 6 of the 35 types of MB output neurons (MBONs) (Figure 1.6b), all of which are of the atypical kind (Li et al., 2020) (see General Introduction for more details). For the most part, their influence is exerted by MBON26 and MBON35 and is mediated via 8 types of local neuron of the LAL, of which LAL160,161 as well as LAL171,172 and LAL051 are the main hubs (Figure 1.6c-e). A substantial share of the synaptic pathways from the MB to the MDNs involve MBONs of the punishment memory compartments γ1, γ2 and γ3 (MBON30, MBON35, MBON32) (also see Table 0.2). Moreover, 4-5 of these 6 MBONs, as well as LAL171,172 and LAL051 were previously suggested as circuit elements by which associative memories are behaviourally expressed (MBON26, MBON27, MBON31, MBON32 and likely MBON35: Li et al., 2020).

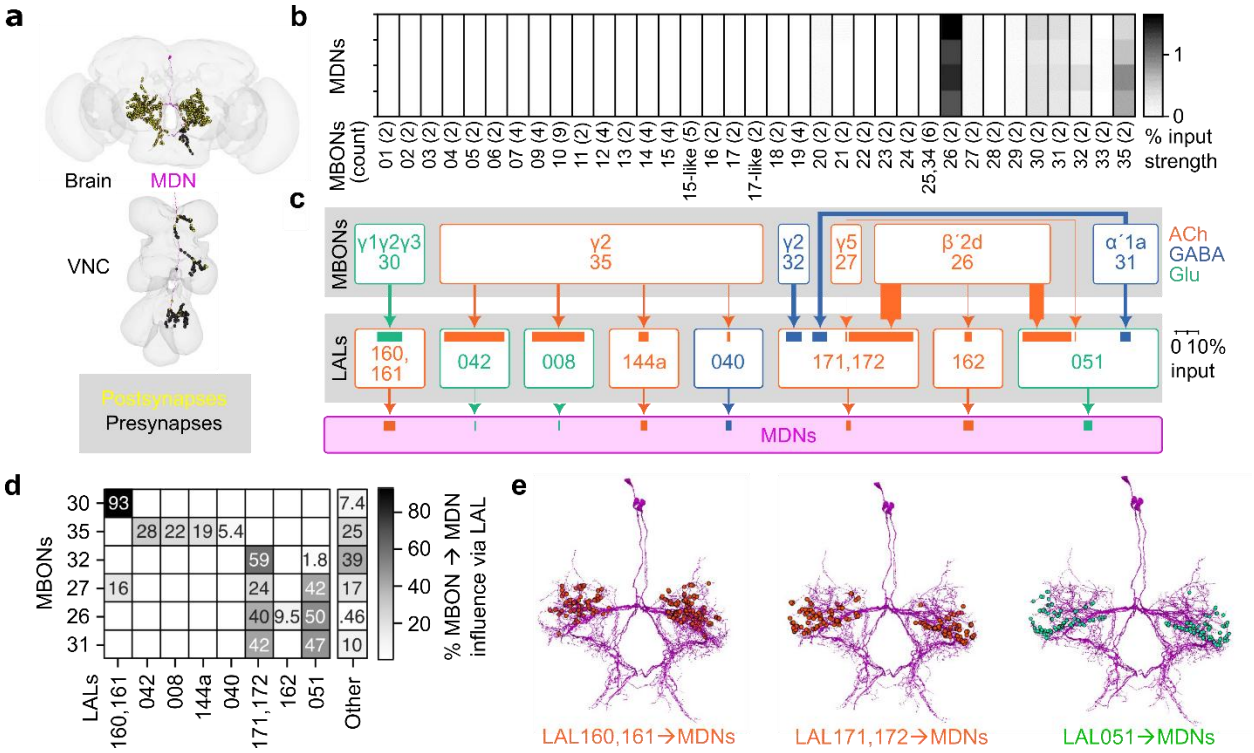

Figure 1.6 | Two-step top-down circuits from MBONs-LALs-MDNs.

a, EM reconstruction of a moonwalker descending neuron (MDN, magenta). VNC: ventral nerve cord. Yellow and black circles: post- and pre-synaptic sites.

b, Heatmap of percent input for 2-step pathways reaching each MDN (rows) from each mushroom body output neuron type (MBONs, columns), determined from FlyWire-v783 after removing connections <10 synapses. Bracketed numbers refer to the number of neurons summed across hemispheres.

c, Pathways from MBONs via neurons of the lateral accessory lobe (LALs) to the MDNs, combined for both hemispheres (omitting connections with <20 synapses total). Arrows are proportional to the total number of synapses (thinnest: 43 synapses, thickest: 2002 synapses). Horizontal bars show percent of input to the downstream partner, calculated as an average over the downstream neuron type, summed over the upstream neuron type. ACh: acetylcholine, orange. GABA: gamma-aminobutyric acid, blue. Glu: glutamate, green.

d, Percent of 2-step input to MDNs from each MBON type that passes through the indicated LAL. Percentages are calculated after averaging across MDNs. “Other” represents all other 2-step MBON to MDN pathways.

e, Locations of synapses (dots) from the indicated LAL to the MDNs, colour coded for LAL transmitter as in (c). Neuron IDs will be provided upon request.

Therefore, I next tested whether the MDNs are part of memory-efferent pathways.

For this, flies underwent differential conditioning with odours as conditioned stimuli and electric shock as unconditioned stimulus – an established Pavlovian association paradigm to induce aversive olfactory short-term memory local to the punishment compartments of the MB (Heisenberg, 2003; Gerber and Aso, 2017; Cognigni et al., 2018; Boto et al., 2020; Modi et al., 2020; Davis, 2023). When MDNs were optogenetically silenced during the choice test, the behavioural expression of odour-shock memory was impaired, whereas no such effect was seen in genetic controls (Figure 1.7a). Likewise, the behavioural expression of appetitive odour-sugar memory was unaffected (Figure 1.7b), as was innate olfactory choice behaviour (Extended Data Figure 1.3). These results show that MDNs contribute to the behavioural expression of aversive odour-shock memory (Figure 1.7).

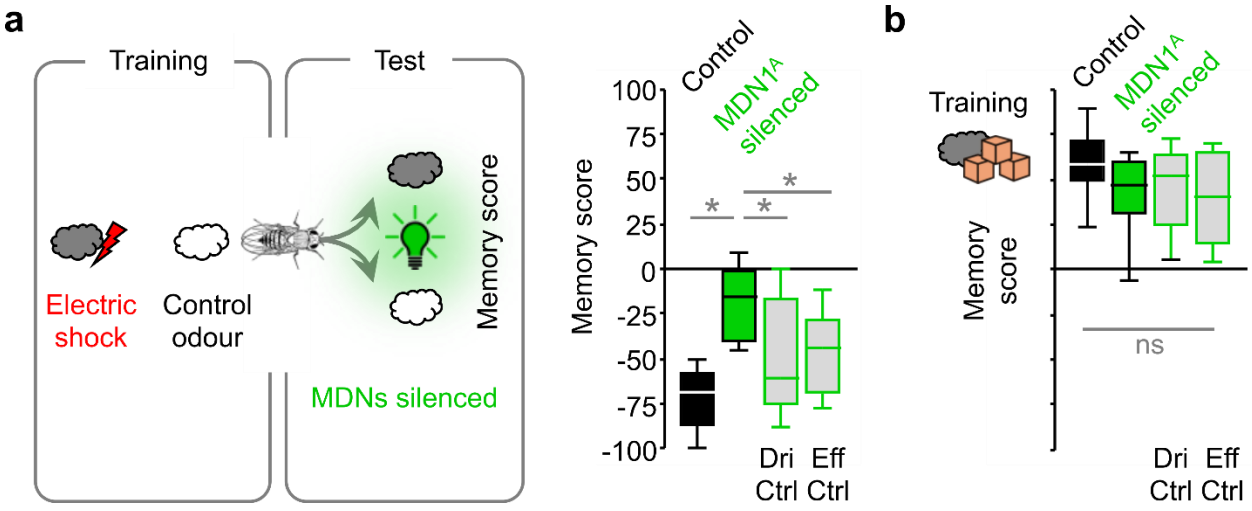

Figure 1.7 | MDNs are part of memory-efferent circuits for learned avoidance memory expression.

a, Rationale and outcome of odour-shock learning experiments. Clouds: odours. Lightning bolt: electric shock. Light bulb: optogenetic silencing of MDNs. Relative to the Control condition (black), silencing MDNs during the test reduced odour-shock memory scores ($MDN1^{A}$ silenced, green) (genotype in both cases: $MDN1^{A}$>GtACR1) to levels less than in genetic controls (grey: Driver control: $MDN1^{A}$>+, Effector control: +>GtACR1) (N= 13,22,21,21).

b, As in **(a)**, but for pairings of odours with sugar reward (orange cubes), showing that appetitive memory scores remained unaffected (N= 8,9,8,10).
Data were analysed across groups by Kruskal-Wallis tests (P< 0.05), followed by pairwise comparisons (Mann-Whitney U-tests, *P< 0.05 with Bonferroni-Holm correction) (ns: P> 0.05). Box-whisker plots show median, interquartile range (box) and 10th/90th percentiles (whiskers). Underlying preference and memory scores separated by sex are shown in Extended Data Figure 1.15. Additional genotype information is in Supplemental Table S1 and statistical results in Supplemental Data Table S1.
Also see Supplement Figure 5,6 for additional work with $Moonwalker^{A}$.

Next, I focused on how, in turn, MDNs affect MB processing. Given that activation of MDNs in the presence of an odour produces an aversive memory for that odour (Figure 1.5), I asked whether activating MDNs drives feedback to punishing dopaminergic neurons (DANs) (Figure 1.8).

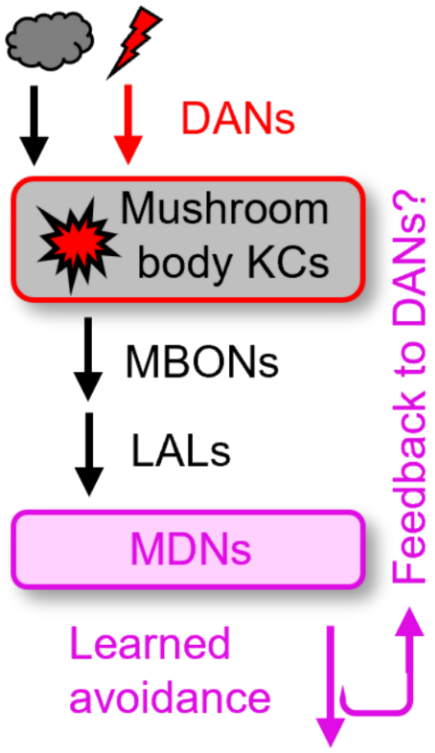

Figure 1.8 | Activating MDNs drives feedback to DANs?

Activating MDNs favours activity in punishing DANs

To test for MDN-to-DAN feedback, I combined optogenetic activation of MDNs with *in vivo* two-photon calcium imaging of DANs in the mushroom body's γ1 and γ2 compartments, known to mediate punishing effects (Claridge-Chang et al., 2009; Aso et al., 2010; Aso et al., 2012.

Therefore, I generated transgenic flies that allowed me to both optogenetically activate MDNs via the red light-activated channelrhodopsin Chrimson and simultaneously image specific DANs via the calcium indicator GCaMP6f through a small window cut into the dorsal head capsule. After mounting the flies underneath a two-photon microscope with their heads, thorax and wings fixed but their legs free to move (Figure 1.9a-b), I observed that activating MDNs resulted in strong calcium responses in both **γ1** (PPL1-01: Figure 1.9c) and **γ2** DAN (PPL1-03: Figure 1.9d). Neither in these nor in any of the following experiments did I observe calcium responses in control flies without the optogenetic effector.

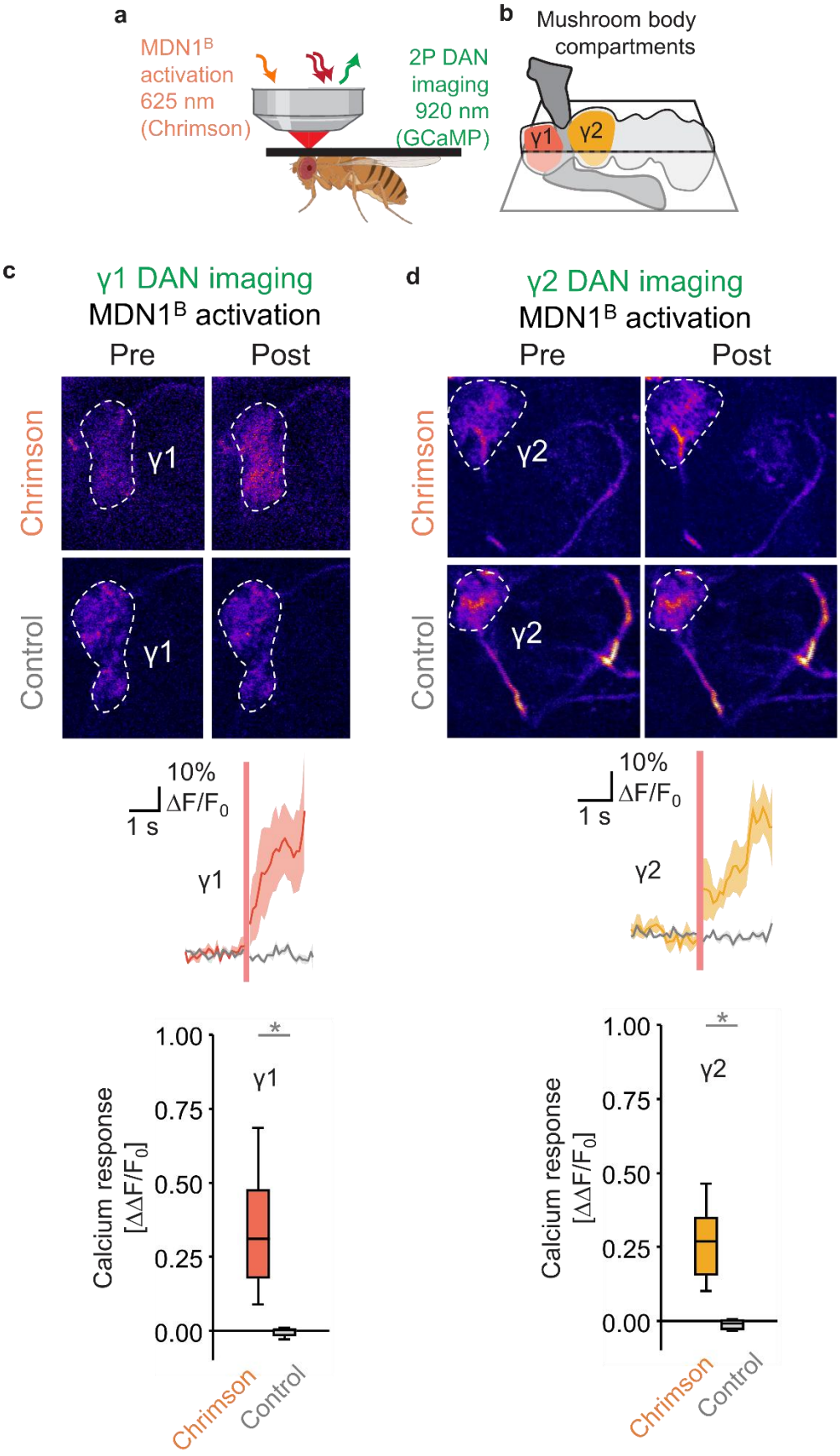
a
MDN1B activation 625 nm (Chrimson)
2P DAN imaging 920 nm (GCaMP)
b
Mushroom body compartments
γ1
γ2
c
γ1 DAN imaging
MDN1B activation
Pre
Post
Chrimson
Control
γ1
10% ΔF/F0
1 s
Calcium response [ΔΔF/F0]
1.00
0.75
0.50
0.25
0.00
*
Chrimson
Control
d
γ2 DAN imaging
MDN1B activation
Pre
Post
Chrimson
Control
γ2
10% ΔF/F0
1 s
Calcium response [ΔΔF/F0]
1.00
0.75
0.50
0.25
0.00
*
Chrimson
Control

Figure 1.9 | Activating MDNs increases calcium response in punishing DANs.

a-b, Combined optogenetics and *in vivo* imaging setup **(a)**. Red light pulses of 200 ms were used to activate Chrimson-expressing MDNs, while calcium signals were measured in GCaMP6f-expressing mushroom body DANs (**b**; compartments colour coded) using continuous two-photon excitation scanning.
c-d, Average intensity projections of sample recordings 2 s before (Pre) and 2 s after the first MDN activation (Post) in flies expressing Chrimson in **γ1 (c)** or **γ2 (d)** DANs, and in Control flies not expressing Chrimson (grey); dashed lines indicate compartment boundaries (top panels). Calcium transients ($\Delta F/F_0$) upon optogenetic MDN activation (red vertical bars) in flies expressing Chrimson (colored traces) and in Controls (grey traces) (middle panels). Activation of MDNs results in significant calcium responses ($\Delta\Delta F/F_0$) in DANs of the **γ1** (**c**; N= 6 flies each) and **γ2** compartments (**d**; N= 8,7 in Chrimson and Control flies) compared to those in Controls (bottom panels). Experimental genotypes: $MDN1^{B}$>$Chrimson^{C}$; **γ1**>GCaMP(**c)** and $MDN1^{B}$>$Chrimson^{C}$; **γ2**>GCaMP (**d)**. Control genotypes: $MDN1^{B}$>+; **γ1** >GCaMP (**c)** and $MDN1^{B}$>+; **γ2** >GCaMP (**d)**.

Box-whisker plots show median, interquartile range (box) and 10th/90th percentiles (whiskers). Calcium transients are plotted as mean +/- SEM. Data were analysed by Mann-Whitney U-tests (*P< 0.05) (**c-d**). Quantification at bottom panels in (**c-d**) is based on the first optogenetic activation trials. Additional genotype information is in Supplemental Table S1 and statistical results in Supplemental Data Table S1.

To confirm these observations regarding the **γ1** and the **γ2** DAN, and to extend the focus beyond these two DANs, next I used a fly strain that expresses the GCaMP6f calcium reporter more broadly across the DANs and thus permits signals to be monitored in all five compartments of the **γ** lobe and the **β'2** compartment (Figure 1.10b). Upon activation of MDNs, I observed the strongest responses in the DANs of the **γ1**, **γ2** and lateral regions of the **γ3** compartment, all of which were previously shown to mediate punishing effects (Claridge-Chang et al., 2009; Aso et al., 2010; Aso et al., 2012; Li et al., 2020), whereas signals in rewarding DANs (medial **γ3, γ4, γ5**, and **β'2** compartments: (Burke et al., 2012; Liu et al., 2012; Li et al., 2020) were considerably weaker (Figure 1.10, Extended Data Figure 1.5, Extended Data Figure 1.6).

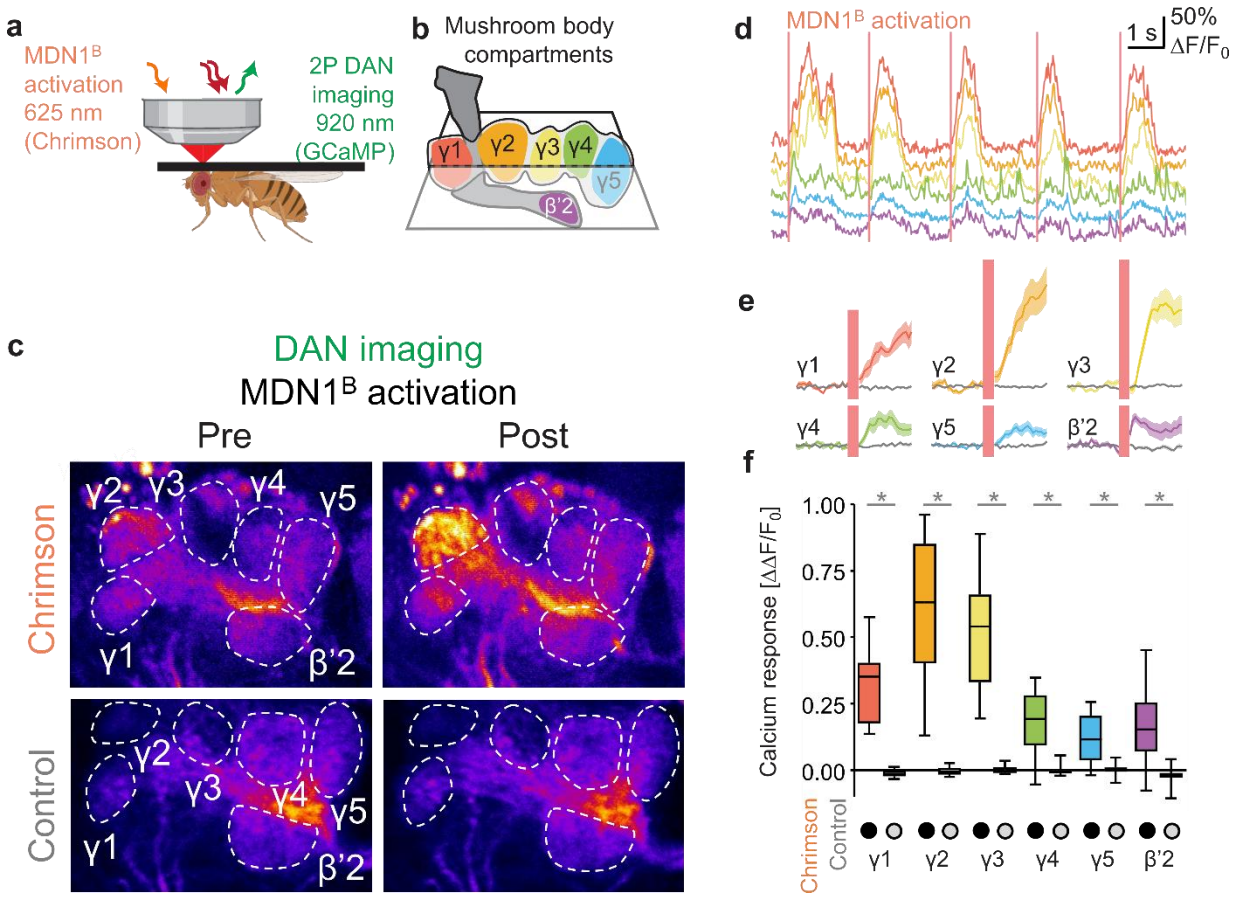

Figure 1.10 | Activating MDNs favours activity in punishing DANs.

a-b, Combined optogenetics and *in vivo* imaging setup. Red light pulses of 200 ms were used to activate Chrimson-expressing MDNs, while calcium signals were measured in GCaMP6f-expressing mushroom body DANs (**b**); compartments highlighted in colour) using continuous two-photon excitation scanning.

c, Average intensity projections of sample recordings 2 s before (Pre) and 2 s after the first MDN activation (Post) in flies expressing Chrimson in DANs, and in Control flies not expressing Chrimson (grey); dashed white lines indicate compartment boundaries.

d, Sample traces of raw calcium transients ($\Delta F/F_0$) across the DANs of the compartments colour coded as in (b) upon five times MDN activation (red bars).

e, Calcium transients ($\Delta F/F_0$) upon optogenetic MDN activation (red vertical bars) in flies expressing Chrimson (colored traces) and in Controls (grey traces).

f, Activation of MDNs revealing strong calcium responses ($\Delta\Delta F/F_0$) in DANs of the **γ1**, **γ2** and **γ3** (N= 10,8 in Chrimson and Control flies). Experimental genotype: $MDN1^{B}$>$Chrimson^{C}$; DANs>GCaMP. Control genotype: $MDN1^{B}$>+; DANs>GCaMP.

Box-whisker plots show median, interquartile range (box) and 10th/90th percentiles (whiskers). Calcium transients are plotted as mean +/- SEM (except **d**). Data were analysed by Kruskal-Wallis tests ($P< 0.05$), followed by pairwise comparisons (Mann-Whitney U-tests, *$P< 0.05$ with Bonferroni-Holm correction). Quantification is based on the first optogenetic activation trials.

Additional information is in Extended Data Figure 1.4, Extended Data Figure 1.5, Extended Data Figure 1.6, Extended Data Figure 1.8. Additional genotype information is in Supplemental Table S1 and statistical results in Supplemental Data Table S1.

Here I found that activating MDNs favours activity in punishing over rewarding DANs, suggesting a mechanism for how MDN activation produces aversive memories for concomitantly presented odours.

Next, I asked whether such DAN activation is mediated by internal, recurrent feedback from MDNs to DANs, or whether the execution of MDN-evoked movement generates external sensory feedback that, in turn, activates DANs.

No evidence for internal, recurrent feedback from MDNs to DANs

The initial hypothesis was that there is internal, recurrent feedback from MDNs to DANs, but systematic queries of the brain connectome of the fly (Scheffer et al., 2020; Dorkenwald et al., 2024; Schlegel 2024) did not reveal any credible connection to support such a notion (see Methods section for inclusion criteria). Current knowledge (See General Introduction and General Discussion) of ascending input from the ventral nerve cord (VNC) to the brain also does not offer evidence for a connection from the MDNs to the DANs; however, a systematic assessment of VNC-to-brain connectivity remains out of reach. We therefore tested whether any yet to be identified internal MDN-to-DAN connection might be functionally relevant. When we optogenetically activated MDNs and imaged from DANs in an *explant* isolated brain preparation or in an *explant* isolated brain-plus-VNC preparation, no significant calcium responses were observed in any DAN, however (Extended Data Figure 1.7). Therefore, next consideration was external, reafferent feedback from the execution of MDN-evoked movement.

MDN-evoked movement is required for DAN activation

As a next step, I returned to combined optogenetic activation of MDNs with *in vivo* calcium imaging of DANs while transiently restraining leg movements (Figure 1.11). Under conditions of unrestrained leg movements, I confirmed reliable and strong activation of DANs in the **γ1**, **γ2**, and **γ3** compartments (Before trapping: Figure 1.11a, Figure 1.11d, Figure 1.11e). These responses were abolished when leg movements were transiently restrained by a piece of cotton wool gently applied to the flies (Trapped: Figure 1.11b, Figure 1.11d, Figure 1.11e) and largely recovered after removing the restraint (After trapping: Figure 1.11c, Figure 1.11d, Figure 1.11e). These results show that the execution of MDN-evoked leg movements is required for activating the DANs of the **γ1**, **γ2**, and **γ3** compartments. Indeed, the onset of leg movements precedes the rise in

calcium responses of these DANs by as much as 500 ms (Extended Data Figure 1.8), consistent with reafferent, sensory feedback from executed leg movements as the cause of these signals, but longer than plausible for an internal, recurrent MDN-to-DAN feedback (Figure 1.11).

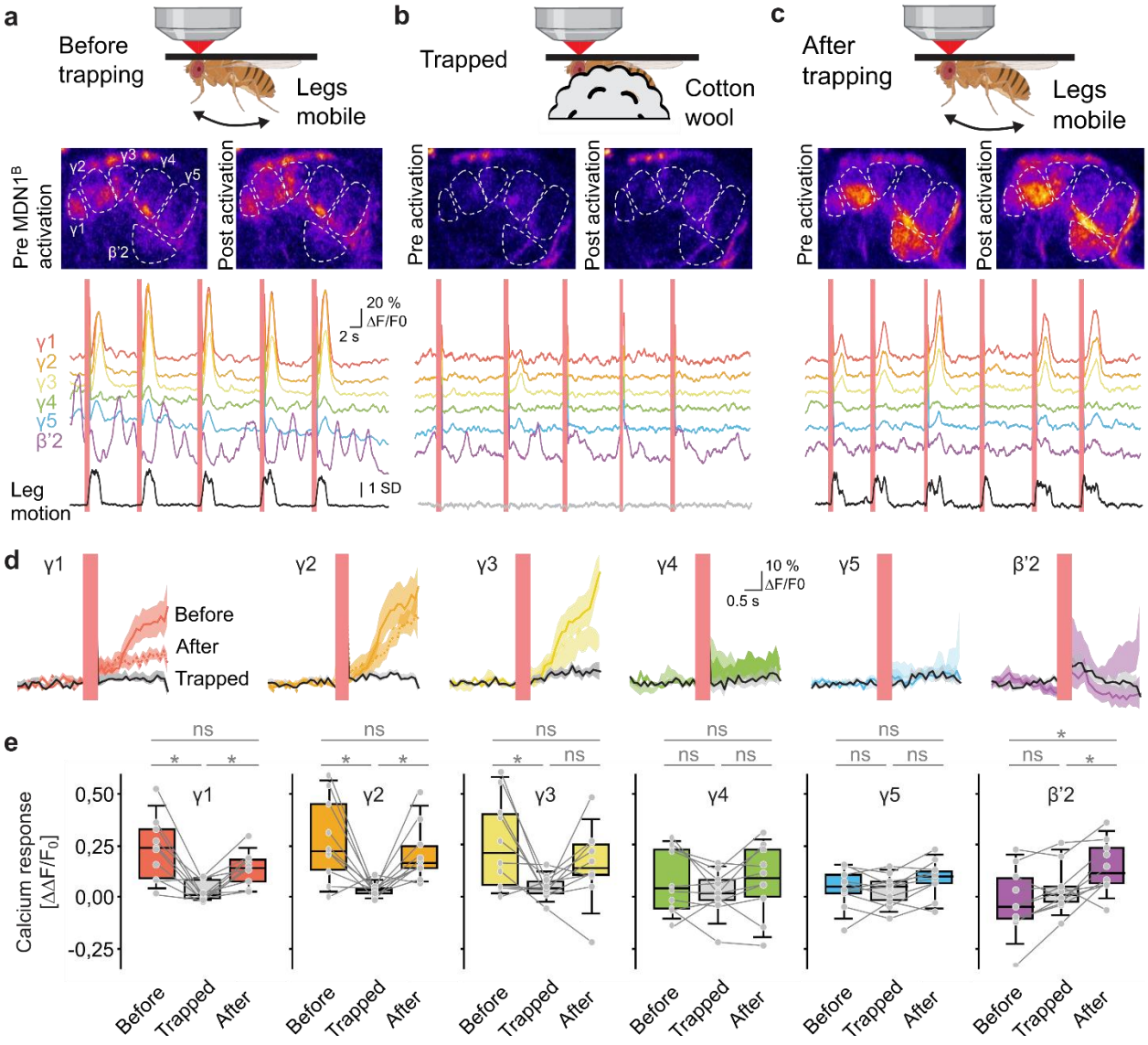

Figure 1.11 | MDN-evoked movement is required for DAN activation.

a-c, Two-photon *in vivo* imaging before (**a**), during (**b**), and after (**c**) leg movement was restrained (Trapped) using a piece of cotton wool (top panels). 200 ms of red light stimulation was used to activate MDNs via Chrimson, while calcium signals were measured in the DANs of the indicated mushroom body compartments with GCaMP6f. Leg movements were calculated as the legs' motion energy of videos captured by an infrared camera. Average intensity projections of the same field of view are shown across conditions, from 2 s before (Pre) and 2 s after MDN activation (Post); dashed white lines indicate compartment boundaries (middle panels). Sample traces of raw calcium transients ($\Delta F/F_0$) in the DANs

of the indicated compartments and leg motion energy (bottom panels) with MDN activation indicated by red vertical bars.
d, Calcium transients (mean +/- SEM) in DANs of the indicated compartments upon the first MDN activation (red vertical bars) before (coloured lines), during (black lines, Trapped), and after (dotted lines) restraining leg movement.

e, MDN-evoked calcium responses ($\Delta\Delta F/F_0$) in DANs of the indicated compartments recorded across trapping conditions. Data points from individual flies are connected by lines (N= 10 flies).
Genotype **(a-e)**: MDN1^{B}>Chrimson^{C}; DANs>GCaMP.

Box-whisker plots show median, interquartile range (box) and 10th/90th percentiles (whiskers) and each dot represents each sample fly. Data were analysed by Wilcoxon signed-rank tests with Bonferroni-Holm correction (*P< 0.05) (ns: P> 0.05).
Additional information in Extended Data Figure 1.4, Extended Data Figure 1.7, Extended Data Figure 1.8. Additional genotype information is in Supplemental Table S1 and statistical results in Supplemental Data Table S1.

Movement is required for punishment by MDNs

Next, I asked whether the execution of MDN-induced movement is also required for the punishing effect of MDN activation, using a procedure to transiently restrain movement during training (Figure 1.12a-b). Flies were trained such that one but not the other odour was paired with optogenetic activation of MDNs, followed by a choice test between both odours. This confirmed the previously observed punishing effect of activating the MDNs (Figure 1.5, Extended Data Figure 1.4c-d) – but only when training took place under control conditions such that flies could freely move in the training apparatus (Control; Figure 1.12b). In contrast, no memories were formed when flies' movement was gently restrained during the training period (Trapped@training; Figure 1.12b). No adverse effects of restraint were observed when activating known punishment DANs directly (Figure 1.12c), suggesting that, in principle, aversive olfactory memory formation is still possible under these conditions. To our initial surprise (but consistent with the lack of spontaneous DAN activity under restraint (Figure 1.11b)), restraint is not punishing in itself (Extended Data Figure 1.9a)**.**

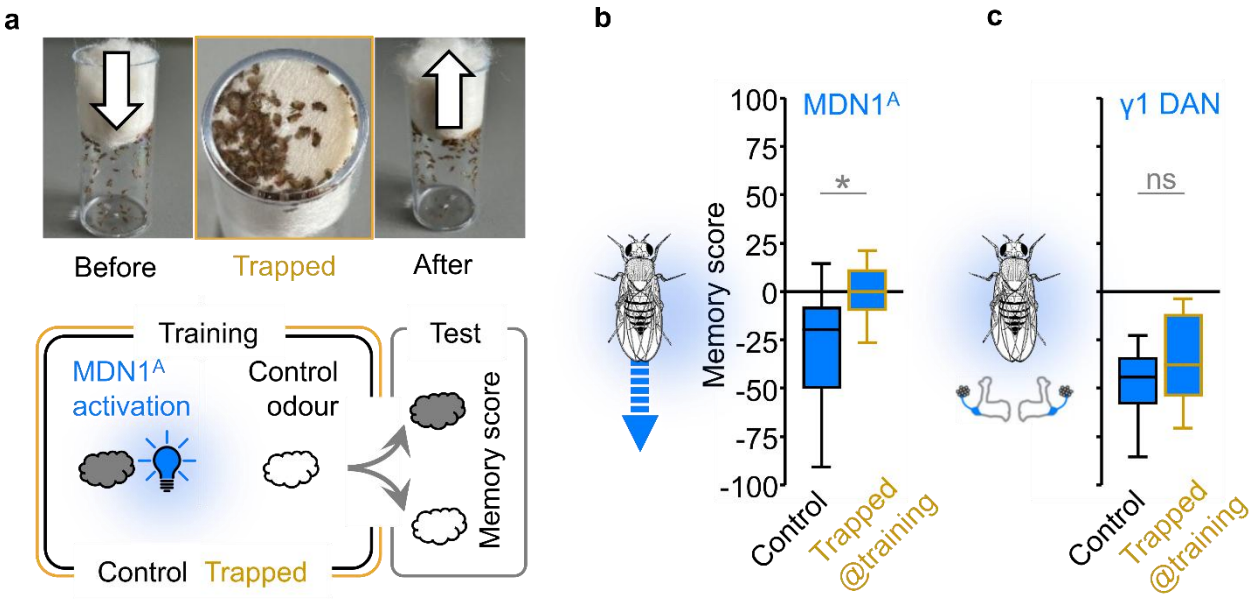

Figure 1.12 | Movement is required for punishment by MDNs.

a, Procedure to transiently restrain movement in the behavioural setup (top, Trapped) and rational of learning experiments (bottom). Clouds: odours. Light bulb: optogenetic activation of neurons indicated in **(b, c)**.
b-c, Pairing odour with optogenetic activation of MDNs establishes aversive memory under Control conditions but not when movement was restrained during the training period (**b**). No effect of such restraint was observed for activating the DANs of the γ1 compartment **(c)**. Genotypes: $MDN1^{A}$>$ChR2XXL^{A}$ (N= 29,29) **(b)** and γ1>$ChR2XXL^{A}$ (N= 24,24) **(c)**.
Data were analysed by pairwise comparisons (Mann-Whitney U-tests, *P< 0.05 with Bonferroni-Holm correction) (ns: P> 0.05). Box-whisker plots show median, interquartile range (box) and 10th/90th percentiles (whiskers). Underlying preference and memory scores separated by sex are shown in Extended Data Figure 1.16. Additional genotype information is in Supplemental Table S1 and statistical results in Supplemental Data Table S1.

These results show that the execution of MDN-evoked movements is required both for MDN activation to engage punishing γ1-3 DANs, and for MDN activation to have a punishing effect. Together with my earlier findings, this uncovers a reafferent positive feedback from learned avoidance to the teaching signals inducing aversive memory (Figure 1.13) – raising the question of the adaptive significance of such feedback.

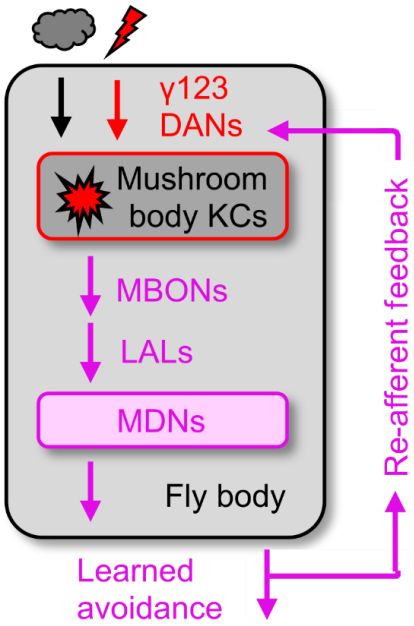

Figure 1.13| **Re-afferent feedback from learned avoidance to dopaminergic teaching signals.**

MDN-mediated feedback maintains learned avoidance

We hypothesized that positive feedback from learned avoidance to aversive teaching signals may counterbalance extinction learning. That is; after pairing a conditioned stimulus (CS) and a punishing unconditioned stimulus (US), animals typically retreat from the CS in order to avoid the US. Such avoidance breaks the initially learned CS-US contingency and should initiate extinction learning. However, despite a broken CS-US contingency, learned avoidance of the CS is often maintained across multiple encounters, referred to as the "avoidance paradox" (Bolles 1972; Le Doux et al., 2017). We hypothesized that MDN feedback facilitates maintained avoidance and developed a reinforcement learning model to probe its performance with or without such feedback, as well as an experimental test of this notion.

In the model, connections from odour-responsive KCs onto two representative MBONs that promote approach or avoidance are modulated by two representative DANs (Figure 1.14a). DANs receive signals encoding external reinforcement as well as predicted reinforcement calculated from MBON activity. One DAN is activated by punishment, whereas the other is activated by reward. Collectively, these DANs represent the prediction error of standard reinforcement learning models. In addition, in our model the DANs receive reafferent positive feedback from MDN-

mediated learned avoidance, that is, when the learned value of the odour is negative, and avoidance behaviour is executed.

We tested this model in a one-dimensional virtual environment with two odours (Figure 1.14b, Figure 1.14c). Reward or punishment was paired with either of these odours and was received only when the model fly reached the edge of the environment. At each time point, the model fly chooses to either stay in its current location, approach, or avoid the odour it senses. For the case of odour-reward pairings, the behaviour of model flies is not altered when MDN feedback is disabled (Figure 1.14d, left). Disabling MDN feedback has drastic consequences in the aversive domain, however. Without MDN feedback and thus with extinction learning operating in isolation, updates to KC-MBON connection weights, odour value and learned avoidance quickly return to pretraining level (Figure 1.14d, right). As a result, the model fly lacking MDN feedback much sooner receives additional punishment. In model flies with MDN feedback, maintained avoidance is driven by dopamine transients reinforcing the negative value of the punished odour each time an avoidance action is taken (Figure 1.14d, right).

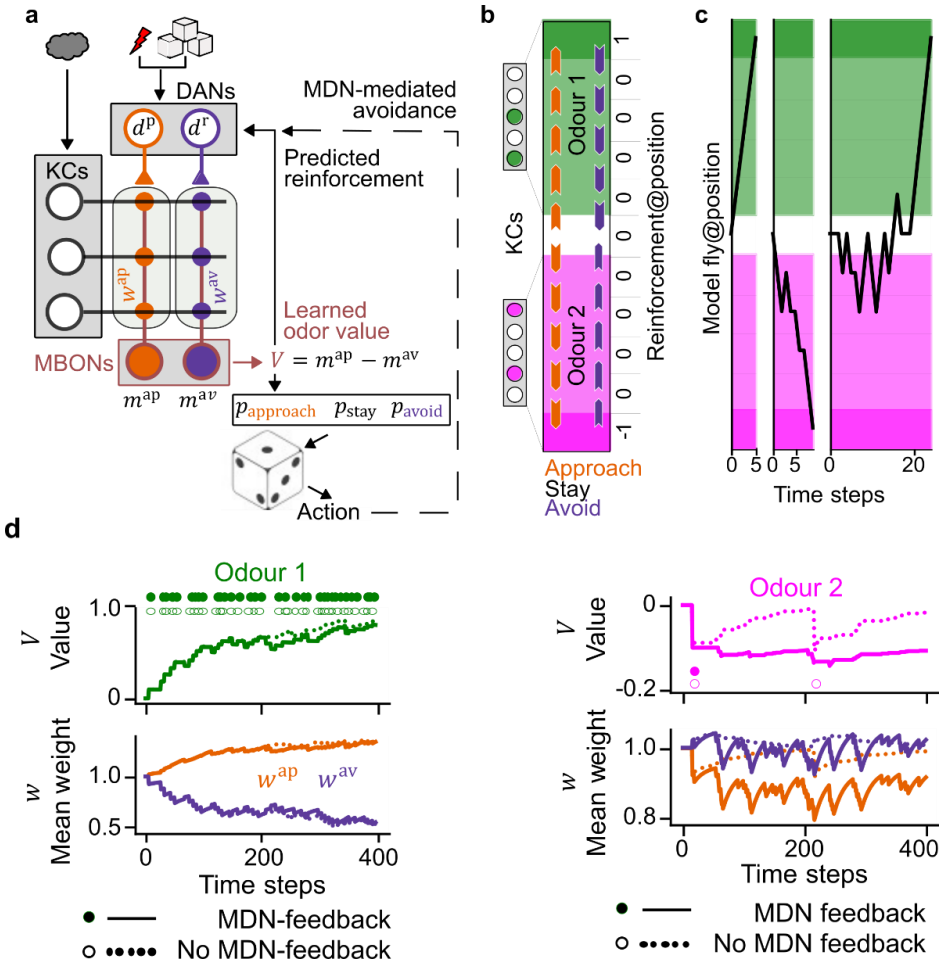

Figure 1.14 | MDN-mediated feedback facilitates maintained avoidance.

a, Model schematic. Punishment and reward activate DANs with firing rates d^{p} and d^{r}, respectively. MBONs with firing rates m^{ap} and m^{av} promote approach and avoidance, respectively. KC-to-MBON weights (w^{ap}, w^{av}) are depressed by co-activation of DANS and odour-responsive KCs. Approach or avoidance behaviour is determined probabilistically by the value (V) derived from MBON activity. Dice by Steaphan Greene, CC-BY-SA-3.0.

b, Schematic of one-dimensional model environment. Reinforcement (punishment -1, reward 1) is received at either end. Different odours (green, magenta) activate different KCs. Arrowheads show possible action choices.

c, Example trials of single model flies navigating the arena. Trials end upon first reinforcement (left and right: reward, middle: punishment). Left and middle are before learning, right is after learning.

d, Evolution of model parameters over multiple trials of the paradigm shown in **(b)**. Circles denote ends of trials when the model fly received reward (top, odour 1) or punishment (bottom, odour 2). The value (V) of the rewarded odour 1 is learned through changes in KC-to-MBON weights (w^{ap} and w^{av} , averaged across odour-responsive KCs) regardless of MDN feedback. Without MDN feedback, avoidance of the punished odour 2 is less persistent and the model fly receives a second punishment earlier (~time step 200). Code will be made available upon request.

The above results thus suggest that MDN feedback counterbalances extinction learning. Therefore, next we tested this by modelling approach and behavioural experiments.

MDN-mediated feedback counterbalances extinction learning

Here, we simulated model flies undergoing aversive conditioning followed by extinction protocols, either with MDN feedback intact or without it (Figure 1.15a). After an extinction protocol with MDN feedback intact, intermediate memory scores were observed. Without such feedback, memory scores were further reduced, uncovering the full effects of extinction learning (Figure 1.15b, Figure 1.15c). These results hold both in situations when, during the extinction protocol, an opportunity is given to avoid the punishment-predicting odour, and when the model flies are forced to choose between two equally punishment-predicting options (the latter protocol eliminates differences in odour exposure with or without MDN feedback).

I next proceeded with behavioural experiments following the same protocol (Figure 1.15a). The outcomes of corresponding behavioural experiments with MDNs intact or with optogenetic silencing of the MDNs during the extinction protocol matched these model predictions (Figure 1.15d). Of note, silencing the MDNs does not in itself confer valence (Extended Data Figure 1.9b).

Together, this concludes that the adaptive significance of reafferent, positive feedback from learned avoidance to punishing teaching signals is to counterbalance extinction learning and to maintain successful learned avoidance.

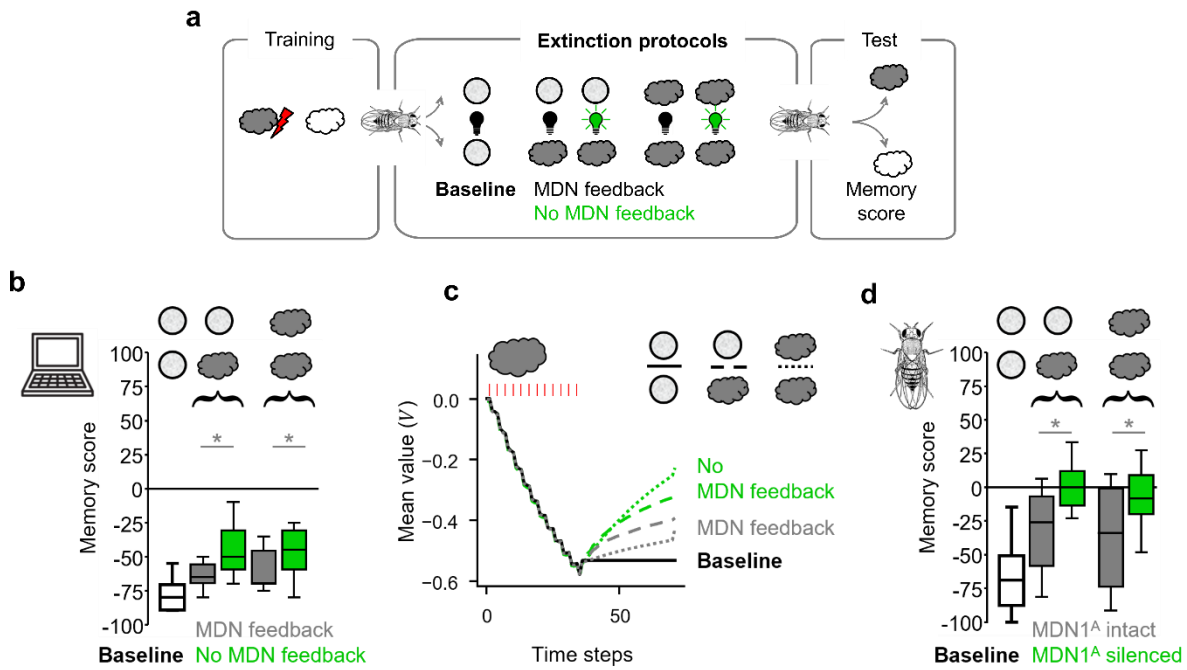

Figure 1.15| **MDN-mediated reafferent feedback counterbalances extinction learning.**

a, Schematic of training, extinction protocols and test. Clouds: odours. Grey circle: choice option without odour. Black and green light bulbs: conditions with or without MDN feedback.

b, Results of simulations of protocols in (a). MDN feedback maintains memory scores at intermediate levels; without it, the full extent of extinction learning is uncovered. Results averaged over 20 experiments per protocol, with 20 model flies per experiment.

c, Mean learned odour value (V) during the protocols in (a, b). During acquisition (time steps 1-36), 12 pulses of punishment (red bars) are delivered in the presence of odour. During the extinction protocol (after time step 36), MDN feedback counterbalances the return of odour value to pre-training levels. Line thickness exceeds ±2 s.e. Code will be made available upon request.

d, Behavioural experiment as in (**a,b**), using optogenetic silencing of the MDNs, using optogenetic silencing of the MDNs. Genotype: $MDN1^{A}$>GtACR1 (N= 34,34,31,18,16). Box-whisker plots show median, Interquartile range (box) and 10th/90th percentiles (whiskers). Data were analysed by Kruskal-Wallis tests ($P< 0.05$), followed by pairwise comparisons (Mann-Whitney U-tests, *$P< 0.05$ with Bonferroni-Holm correction). Additional information in Extended Data Figure 1.9, additional genotype information is in Supplemental Table S1 and statistical results in Supplemental Data Table S1.
Underlying BA preference and memory scores separated by sex and odour choices are shown in Extended Data Figure 1.17.

Discussion

Error types and avoidance paradox

Inspired by the hypothesis of mutual causation between action and valence (Darwin 1872, James 1884), in this study, I discovered that backward locomotion and avoidance engages punishing dopaminergic teaching signals (Figures 1.9, Figure 1.10, Figure 1.11, Extended Data Figure 1.5, Extended Data Figure 1.6). These teaching signals can support aversive memories even if no external punishment is received (Figures 1.1-1.5, Figure 1.11, Figure 1.12, Extended Data Figure 1.4) and can support continued avoidance to save the animal from receiving another, potentially lethal, punishment (Figure 1.14-1.15). However, continued avoidance in a situation that is in fact benign would be maladaptive. The types of errors from these policies, i.e. not avoiding although it is warranted or avoiding unnecessarily, cannot both be simultaneously minimized, a notion reflected in the "avoidance paradox" (Bolles 1972). We suggest that two separate systems reduce these errors. In the γ1-3 compartments, avoidance engages aversive teaching signals to maintain aversive odour memory and promote future avoidance (this study), thus reducing the former error. In the γ5 compartment, extinction memories that oppose further avoidance of the odour are established (Felsenberg et al., 2018), reducing the latter error. This allows these policies to be selected according to situational, motivational, and mnemonic variables.

This study reveals that, during extinction, aversive memories are not unaffected or left to decay but instead are actively maintained: Enacted avoidance engages punishing teaching signals that support memory for the cues that had triggered the avoidance. This is compatible but qualitatively extends notions of the parallel neuronal organization of aversive memory and extinction learning (Tovote et al., 2015; Felsenberg et al., 2018). It is likewise compatible with the proposal that successful avoidance establishes a state of relief/ safety that reinforces avoidance as the action that brought about the relief/ safety state (LeDoux et al., 2017; Bouton et al., 2021; (Laing et al., 2024) in flies avoidance-promoting MBONs of the reward compartments seem poised to receive such reinforcement): In concert, these processes ensure that when the cue is encountered again, avoidance is repeated.

Memory-efferent pathways

A selective set of MBONs and LALs with acetylcholine, GABA or glutamate as predicted transmitters establishes 2-step connections from the MBONs to the MDNs (Figure 1.6). With the assumption that acetylcholine has the excitatory and GABA the inhibitory effects typical of insect central brain synapses; for glutamate, inhibitory effects are assumed (Liu and Wilson, 2013; Shiu

et al., 2024). Accordingly, all but one of the pathways originating in MBONs of the punishment compartments γ1-3 feature either an excitatory MBON upstream of an inhibitory LAL, or vice versa (Figure 1.6c). Through such sign-inversion, a learning-induced depression of KC-MBON synapses will promote MDN activity and backward locomotion as an early component of avoidance before turning around and assuming a new forward walking direction (Extended Data Figure 1.10).

Silencing MDNs during the choice test impaired but did not abolish the behavioural expression of odour-shock memory (Figure 1.7a). This suggests that learned avoidance can be expressed by pathways parallel to the MBON-LAL-MDN pathways (Figure 1.6b-c). This has indeed been shown for the typical MBON of the γ1 compartment (MBON-11) (Aso et al., 2014) and its target MBONs of the γ5 and β'2 compartments (MBON-01, MBON-03) (Owald et al., 2015; Perisse et al., 2016). Such a parallel organization highlights the complexity and importance of the decision of whether to avoid.

Reafferent pathways and DAN signalling

In this study, I demonstrated reafferent, positive feedback from MDN-induced movement to aversive dopaminergic teaching signals (Figure 1.11, Figure 1.12). Which sensory pathways register these movements? Visual input from movement-over-ground is likely irrelevant because functional imaging experiments did not allow for such movement. Of the leg proprioceptive organs (Büschges and Ache, 2024), the campaniform sensilla are also unlikely to be involved, as they sense load that likewise was absent during imaging. Rather, leg hair plates and chordotonal organs seem likely candidates because they monitor joint and leg movements, respectively. Indeed, optogenetic activation of the chordotonal organs selectively activates punishing DANs in larval *Drosophila* (Eschbach et al., 2020).

The feedback from MDN-induced movement to punishing DANs (Figures 1.11, Figure 1.12, Figure 1.14, Figure 1.15) adds complexity to the picture of mushroom body DAN function (Riemensperger et al., 2005; Cohn et al., 2015; Felsenberg et al., 2017; Hattori et al., 2017; Li et al., 2020; Otto et al., 2020; Driscoll et al., 2021; Jiang and Litwin-Kumar, 2021; Siju et al., 2021; Zolin et al., 2021; Meschi et al., 2024). As a heterogeneous population, the mushroom body DANs establish a nuanced, combinatorial coding space for salient features of the animal´s present and predicted environment, its current state and needs, as well as its situationally relevant past experiences. Collectively, these influences shape present and future action selection. Similar heterogeneity is observed in dopamine neurons in the ventral tegmental area of mammals (Stuber, 2023). Given this complexity, and the circuit position of the mushroom body DANs far

removed from the sensory and motor periphery, the relationship between movement and DAN activity can be expected to be heavily modulated by situational, behavioural and motivational variables (Siju et al., 2021; Zolin et al., 2021).

Implications

Extinction is a central component of exposure therapies, effective first-line treatments of anxiety disorders. However, resilience to post-therapy adverse experiences and the generalization beyond the therapeutic context are not yet satisfactory (Craske and Mystkowski, 2006; Vervliet et al., 2013; Carpenter et al., 2018; Craske et al., 2018; Levy et al., 2022). Correspondingly, in rodents, extinguished aversive behaviours often return upon re-exposure to punishment (reinstatement) or upon contextual change (renewal) (Bouton et al., 2021; Laing et al., 2024). The engagement of punishment signals through avoidance behaviour as reported in the present study seems poised to maintain aversive memories in a state susceptible to such reinstatement and renewal. Extrapolated to the human condition, the clinical implication is that preventing avoidance during exposure therapy can reduce relapse rates because it prevents the engagement of avoidance-induced punishment signalling. Conceptually, my findings call for an integrated view of behaviour organization, memory function and emotion regulation.

Chapter 1 Extended Data Figures

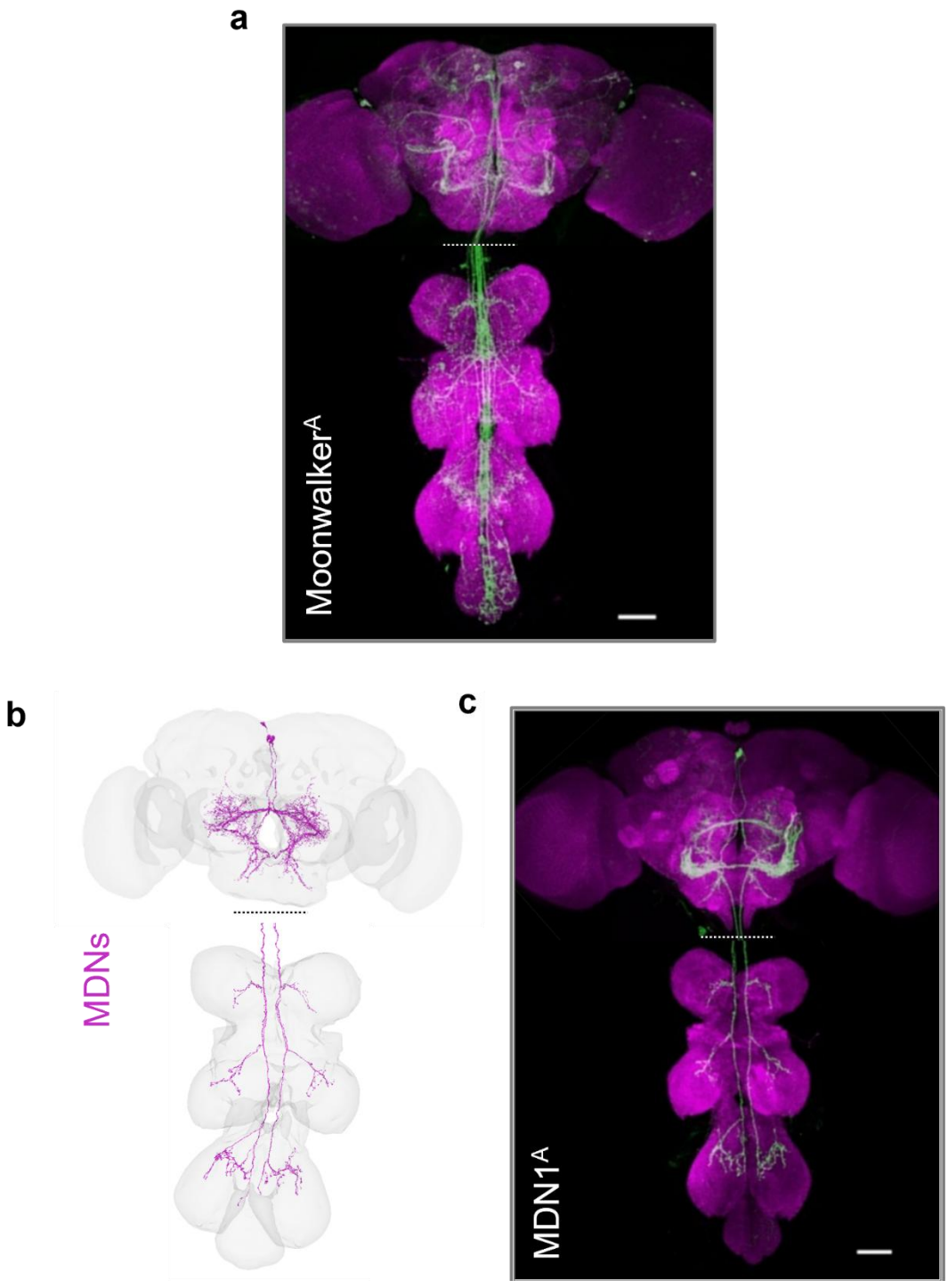

Extended Data Figure 1.1 | Expression patterns of Gal4 drivers and EM reconstruction of MDNs. **a-c**, Higher-resolution images of the anatomy panels of Figure 1.1a (**a**) and Figure 1.5 (**b-c**). Anti-GFP expression (green) driven by Moonwalker^{A} (**a**) and MDN1^{A} (**c**) is shown along with neuropil labelled with anti-Bruchpilot (magenta). Shown in (**b**) is the EM reconstruction of the MDN neurons (magenta) in the context of the neuropil (grey mesh). Other details as in the legend of Figure 1.1a and Figure 1.5.

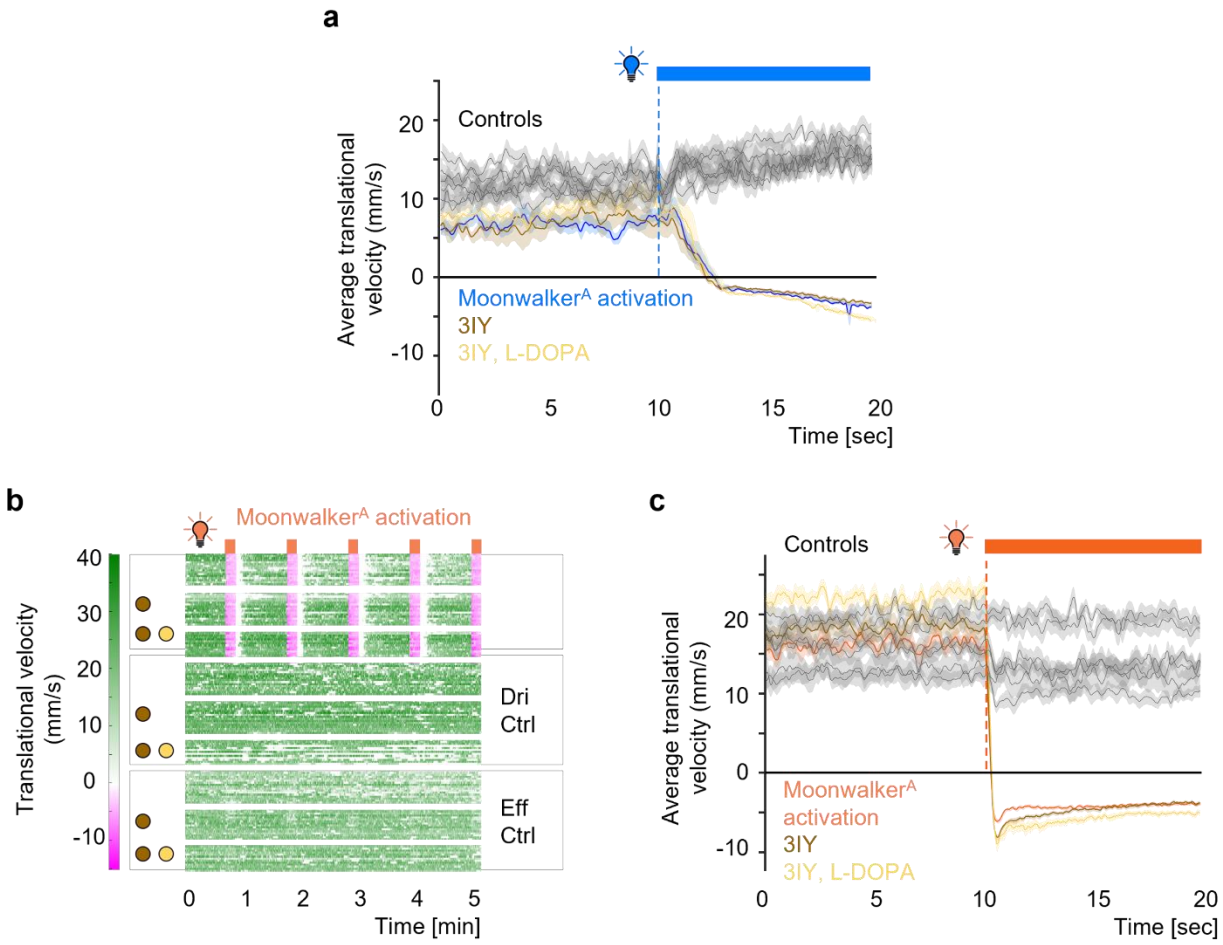

Extended Data Figure 1.2 | Moonwalker-induced locomotion is unaffected by 3IY.

a, Averaged translational velocity (mm/s) (solid lines) 10 s before and during 10-s optogenetic activation (blue bar). For the experimental genotype (Moonwalker^A>ChR2XXL^A, coloured traces) optogenetic activation leads to negative translational velocity, i.e. backward walking, regardless of the indicated drug treatment (brown: 3IY, light brown: additional supply of L-DOPA). In genetic controls (Moonwalker^A/+, +/>ChR2XXL^A) no backward walking is observed, likewise regardless of drug treatment (black traces) (N= 12,8,12,16,12,12,12,12,12). For each fly, data are averaged across the 5 trials shown in Figure 1.4b and plotted as mean +/- SEM.

b, Translational velocity (mm/s), colour coded from magenta/backward to green/forward walking in relation to optogenetic activation (orange bars). Rows correspond to individual flies. The top three sets of rows show the experimental genotype (Moonwalker^A>Chrimson^A) upon the drug treatment colour coded as in **(a)**; bottom rows likewise show genetic controls (Dri Ctrl: Moonwalker^A/+, Eff Ctrl: +/>Chrimson^A) (N= 16,16,12,16,16,12,16,16,12).

c, as in **(a)**, but for the data shown in **(b).**

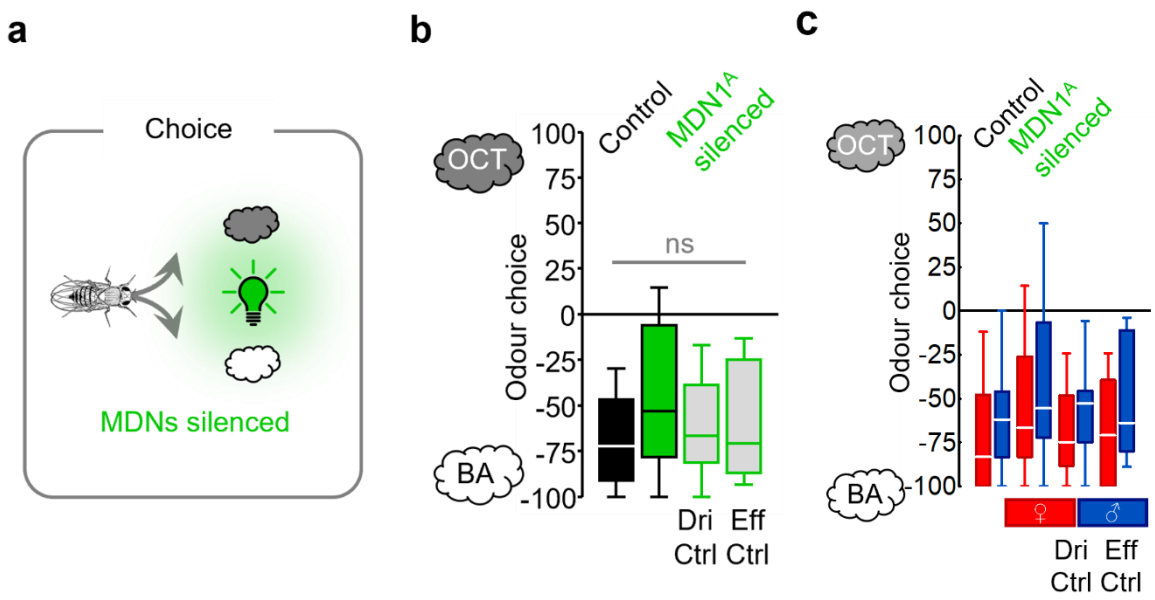

Extended Data Figure 1.3 | Innate olfactory choice behaviour is unaffected by MDNs silencing.

a-**b**, Rationale (**a**) and outcome (**b**) of innate odour choice preference assay. Clouds: odours. Light bulb: optogenetic silencing of MDNs. Relative odour preferences in experimentally naïve flies do not differ for the experimental genotype (MDN1^{A}>GtACR1) under Control conditions without light stimulation (black) versus the MDN1^{A} silenced condition (green), or from genetic controls under light stimulation (grey) (Dri Ctrl: MDN1^{A}/+, Eff Ctrl: +/>GtACR1) (N= 18,19,23,22). Box-whisker plots show median, interquartile range (box) and 10th/90th percentiles (whiskers). Data were analysed across groups by a Kruskal-Wallis test (ns: P> 0.05).

c, Odour choice are separated by sex. Box plots represent the median as the middle line, 25%/75% quantiles as box boundaries, and 10%/90% quantiles as whiskers. Red fill of the box plots shows data from females; blue fill indicates data from male. Additional genotype information is in Supplemental Table S1 and statistical results in Supplemental Data Table S1.

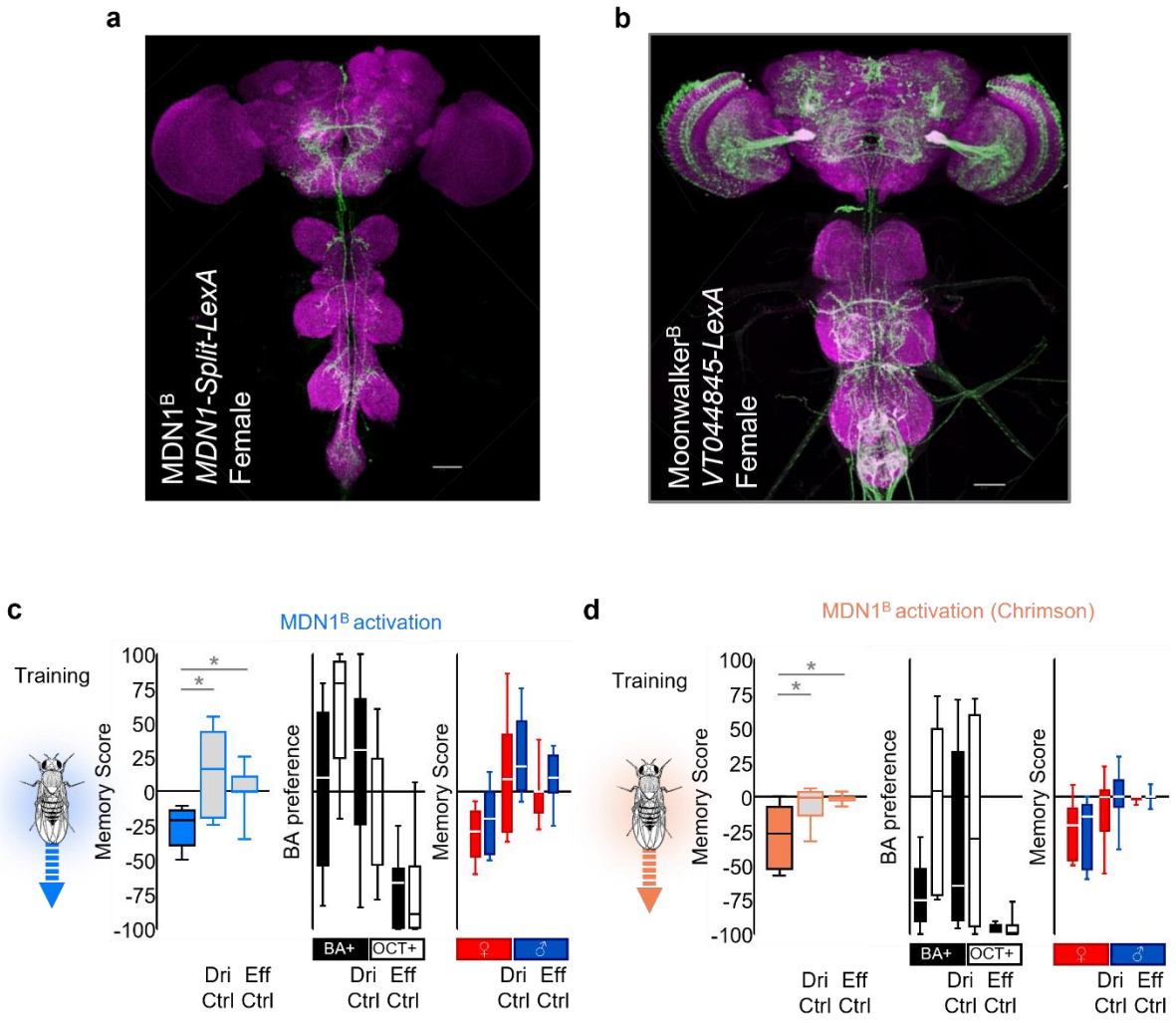

Extended Data Figure 1.4 | Characterization of lexA drivers for moonwalker neuron activation and MDN activation.

a-b, Anti-GFP expression driven by MDN1^{B} (**a**) and Moonwalker^{B} (**b**) (green) along with neuropil labelled with anti-Bruchpilot (magenta). Other details as for Figure 1.1a, Figure 1.5.

c-d, Outcome of pairing odour with MDN1^{B} activation using either ChR2XXL (blue: MDN1^{B}>ChR2XXL^{B}) (c), or Chrimson (orange: MDN1^{B}>Chrimson^{B}) (d) and resulting in aversive memory in the experimental genotype but not in genetic controls (Dri Ctrl: MDN1^{B}/+, Eff Ctrl: +/>ChR2XXL^{B} (c) or Chrimson^{B} (d)) (N= 12,12,10; 12,10,11). Box-whisker plots show median, interquartile range (box) and 10th/90th percentiles (whiskers). Data were analysed across groups by Kruskal-Wallis tests (P< 0.05), followed by pairwise comparisons (Mann-Whitney U-tests, *P< 0.05 with Bonferroni-Holm correction). Other details as for Figure 1.5.

BA preference and memory scores from Extended Data Figure 1.4c and Extended Data Figure 1.4d, respectively, separated by sex. Box plots represent the median as the middle line, 25%/75% quantiles as box boundaries, and 10%/90% quantiles as whiskers. Black fill of the box plots shows BA preference when BA (Benzaldehyde) was associated with optogenetic, and white fill of the box indicates BA preference when OCT (3-octanol) was associated with optogenetic. Red fill of the box plots shows data from females; blue fill indicates data from males. The blue/orange glow fly indicates when blue/red light was used for moonwalker activation. Additional genotype information is in Supplemental Table S1 and statistical results in Supplemental Data Table S1.

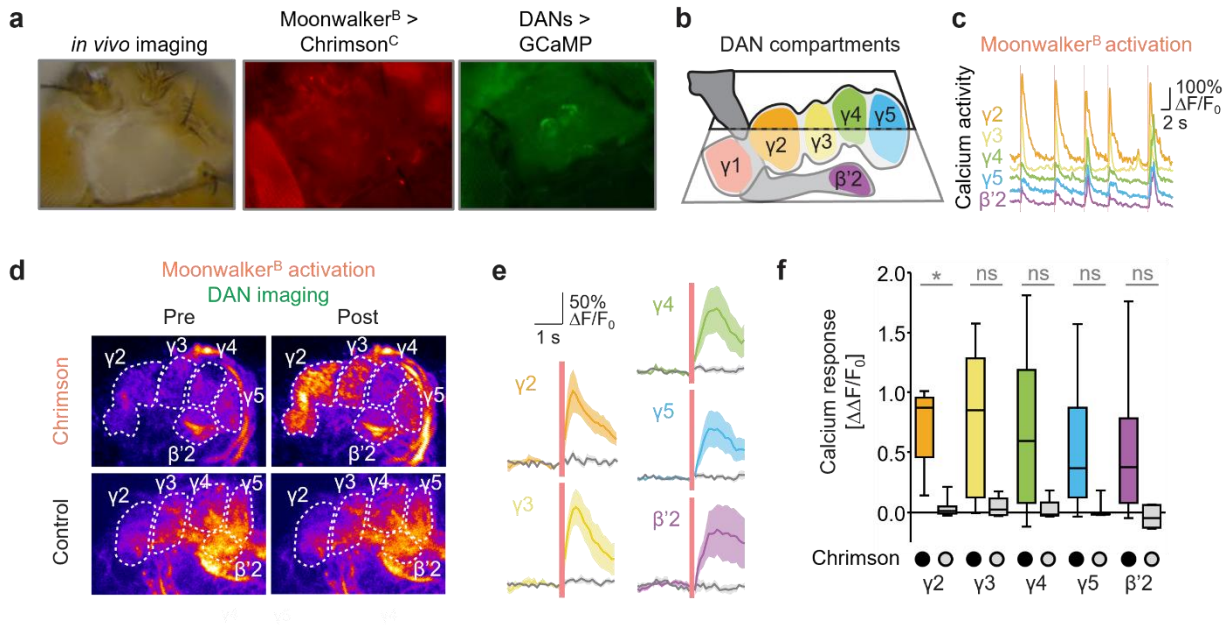

Extended Data Figure 1.5 | DANs calcium response upon full set of moonwalker neuron activation

a, *In vivo* imaging preparation. Dorsal cuticle above the *Drosophila* brain was removed to allow optical access, white light image (left). Fluorescent channels show the expression of Chrimson in Moonwalker^{B} neurons (middle) and GCaMP in DANs (right). For the compartments covered at the chosen imaging plane **(b)** sample traces of raw calcium transients are shown for 5 trials of 20ms optogenetic activation (red vertical lines) of Chrimson-expressing the full set of moonwalker neurons (Moonwalker^{B}) **(c)**.

d, Average intensity projections of sample recordings 2 s before (Pre) and 2 s after the first Moonwalker^{B} activation in flies expressing Chrimson across DANs and in Control flies not expressing Chrimson; dashed white lines indicate compartment boundaries. Experimental genotype: Moonwalker^{B}>Chrimson^{C}; DANs>GCaMP (top). Control genotype: Moonwalker^{B}/+; DANs>GCaMP (bottom).

e, Calcium transients ($\Delta F/F_0$) from the indicated compartments upon activation in the experimental genotype (coloured traces, N= 7) and in Controls (grey traces, N= 6). Calcium transients are plotted as mean +/- SEM (except **c**).

f, Activation of Moonwalker^{B} neurons result in significant calcium responses ($\Delta\Delta F/F_0$) of DANs of only the **γ2** compartment. **(e, f)** are based on first optogenetic activation trial.
Box-whisker plots show median, interquartile range (box) and 10th/90th percentiles (whiskers). Calcium transients are plotted as mean +/- SEM. Data were analysed by Kruskal-Wallis tests ($P < 0.05$), followed by pairwise comparisons (Mann-Whitney U-tests, *$P < 0.05$ with Bonferroni-Holm correction). Additional genotype information is in Supplemental Table S1 and statistical results in Supplemental Data Table S1.

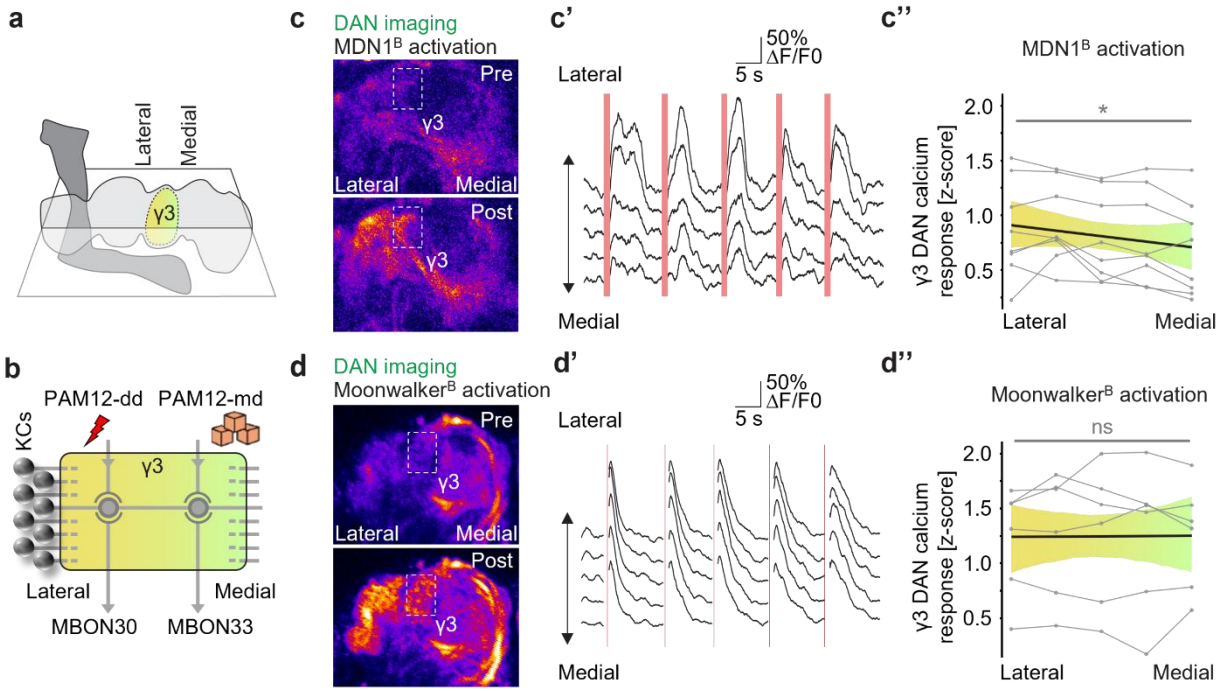

Extended Data Figure 1.6| Compartmental topology of DAN engagement by MDNs and moonwalker neuron activation.

a-b, Imaging plane and topology of the **γ3** compartment **(a)** and its internal organization according to (Li et al., 2020) **(b).** Other KCs connect to only either PAM12-dd or -md (not shown).

c-c'', *In vivo* calcium imaging of flies expressing GCaMP6f across the DANs and optogenetic activation of MDNs, re-analysed from Figure 1.10 (genotype: MDN1^{B}>Chrimson^{C}; DANs>GCaMP). Average intensity projections of sample recording 2 s before/ after activation (Pre/ Post) **(c)**. For the **γ3** compartment region of interest (stippled rectangle in **c**), calcium transients ($\Delta F/F_0$) for spatial bins from lateral (top) to medial (bottom) are displayed for consecutive activation trials (red vertical bars) **(c')**.
Z-scored average calcium responses show stronger DAN engagement in lateral than medial bins (N=8) (**c''**).

d-d'', As in **(c-c'')**, for activation of the full set of moonwalker neurons (Moonwalker^{B}>Chrimson^{C}; DANs>GCaMP) showing uniform DAN activation throughout **γ3**, re-analysed from Extended Data Figure 1.5. (N=6$^{\#}$). $^{\#}$one missing data point, where γ3 was not discernible.
Data were analysed by Friedman tests (*P< 0.05) (**c'', d''**). Additional genotype information is in Supplemental Table S1 and statistical results in Supplemental Data Table S1.

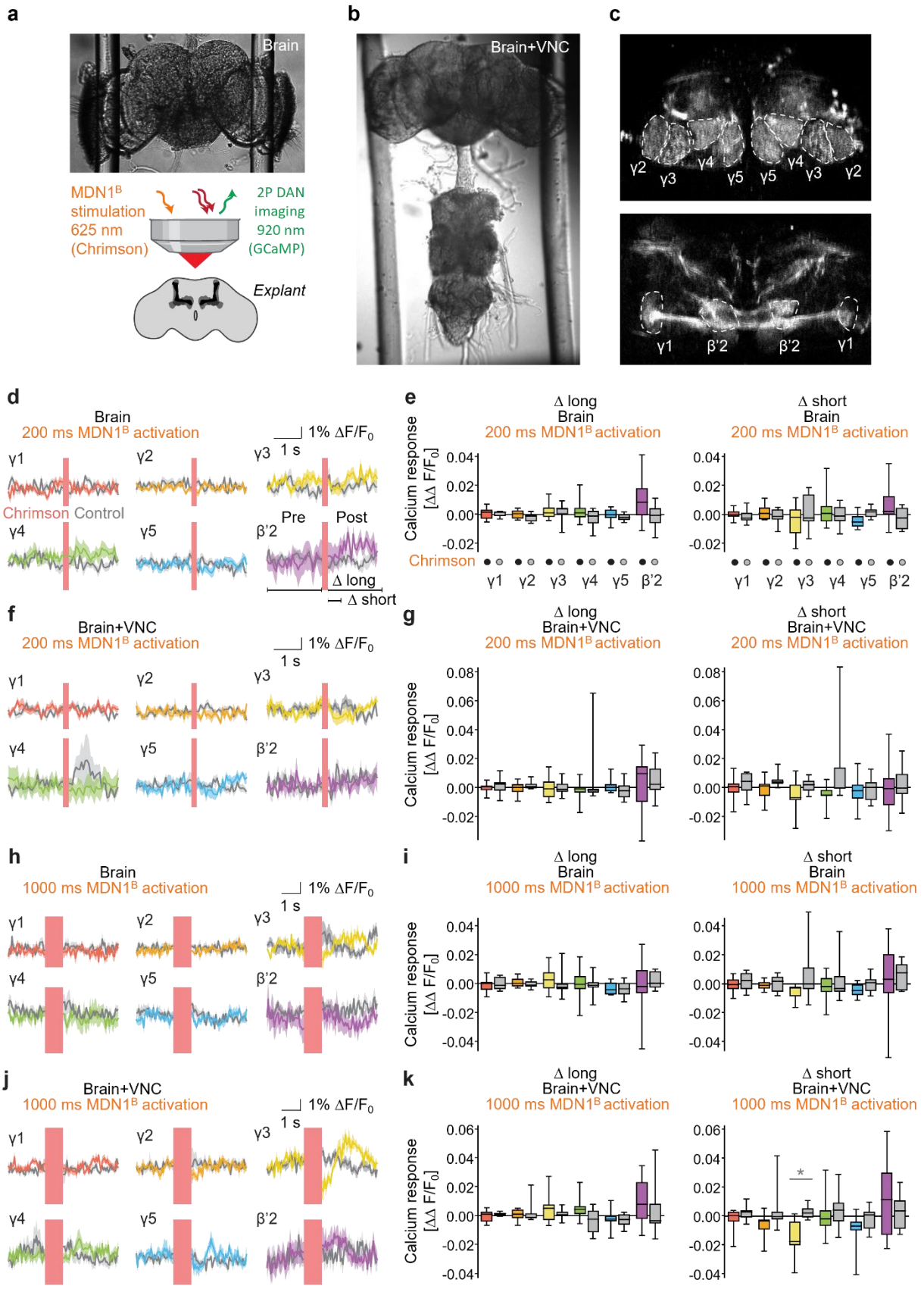
a
Brain
MDN1B stimulation 625 nm (Chrimson)
2P DAN imaging 920 nm (GCaMP)
Explant
b
Brain+VNC
c
γ2 γ3 γ4 γ5 γ5 γ4 γ3 γ2
γ1 β'2 β'2 γ1
d
Brain
200 ms MDN1B activation
1% ΔF/F0
1 s
γ1 γ2 γ3
Chrimson Control
Pre Post
γ4 γ5 β'2
Δ long
Δ short
e
Δ long
Brain
200 ms MDN1B activation
Δ short
Brain
200 ms MDN1B activation
Calcium response [ΔΔ F/F0]
Chrimson
γ1 γ2 γ3 γ4 γ5 β'2
f
Brain+VNC
200 ms MDN1B activation
g
Δ long
Brain+VNC
200 ms MDN1B activation
Δ short
Brain+VNC
200 ms MDN1B activation
h
Brain
1000 ms MDN1B activation
i
Δ long
Brain
1000 ms MDN1B activation
Δ short
Brain
1000 ms MDN1B activation
j
Brain+VNC
1000 ms MDN1B activation
k
Δ long
Brain+VNC
1000 ms MDN1B activation
Δ short
Brain+VNC
1000 ms MDN1B activation
*

Extended Data Figure 1.7 | Activating MDNs in explant preparations does not engage DANs.

a-b, Overview of imaging setup of explant brain (**a**) and explant brain with VNC (**b**) preparation. $MDN1^{B}$ was activated using Chrimson with 200 ms or 1000 ms red light stimulation while calcium transients were monitored across the DANs by GCaMP6f. Images shown are captured under brightfield illumination.

c, Average intensity projections of representative brain preparations of the experimental genotype ($MDN1^{B}$>$Chrimson^{C}$; DANs>GCaMP) under two-photon illumination, with a focus on γ2, γ3, γ4 and γ5 DANs (top) and γ1 and β'2 DANs (bottom). Dashed lines indicate compartment boundaries.

d-e, Calcium transients ($\Delta F/F_0$) from 2 s before to 2 s after activation of $MDN1^{B}$ with 200 ms of red light (red vertical bar) in brains of the experimental genotype (traces colour-coded by compartment; N= 10) or control brains (gray traces, N= 10) ($MDN1^{B}$/+; DANs>GCaMP) **(d)**. Calcium responses ($\Delta\Delta F/F_0$) in these brains comparing 2 s before activation to 2 s after activation (Δ long, left) or 0.5 s after activation (Δ short, right). No significant differences between Chrimson-expressing and control brains were found.

f-g, As in (**d-e**), for brain-plus-VNC preparations (N= 10,10).

h-k, As in (**d-g**), for 1000-ms red light, revealing a significant decrease in calcium responses in γ3 DANs of brain-plus-VNC preparations after 1000 ms stimulation, and when considering Δ short (bottom right panel).
Box-whisker plots show median, interquartile range (box) and 10th/90th percentiles (whiskers). Calcium transients are plotted as mean +/- SEM. Data were analysed by Kruskal-Wallis tests ($P< 0.05$), followed by pairwise comparisons (Mann-Whitney U-tests, *$P< 0.05$ with Bonferroni-Holm correction). Additional genotype information is in Supplemental Table S1 and statistical results in Supplemental Data Table S1.

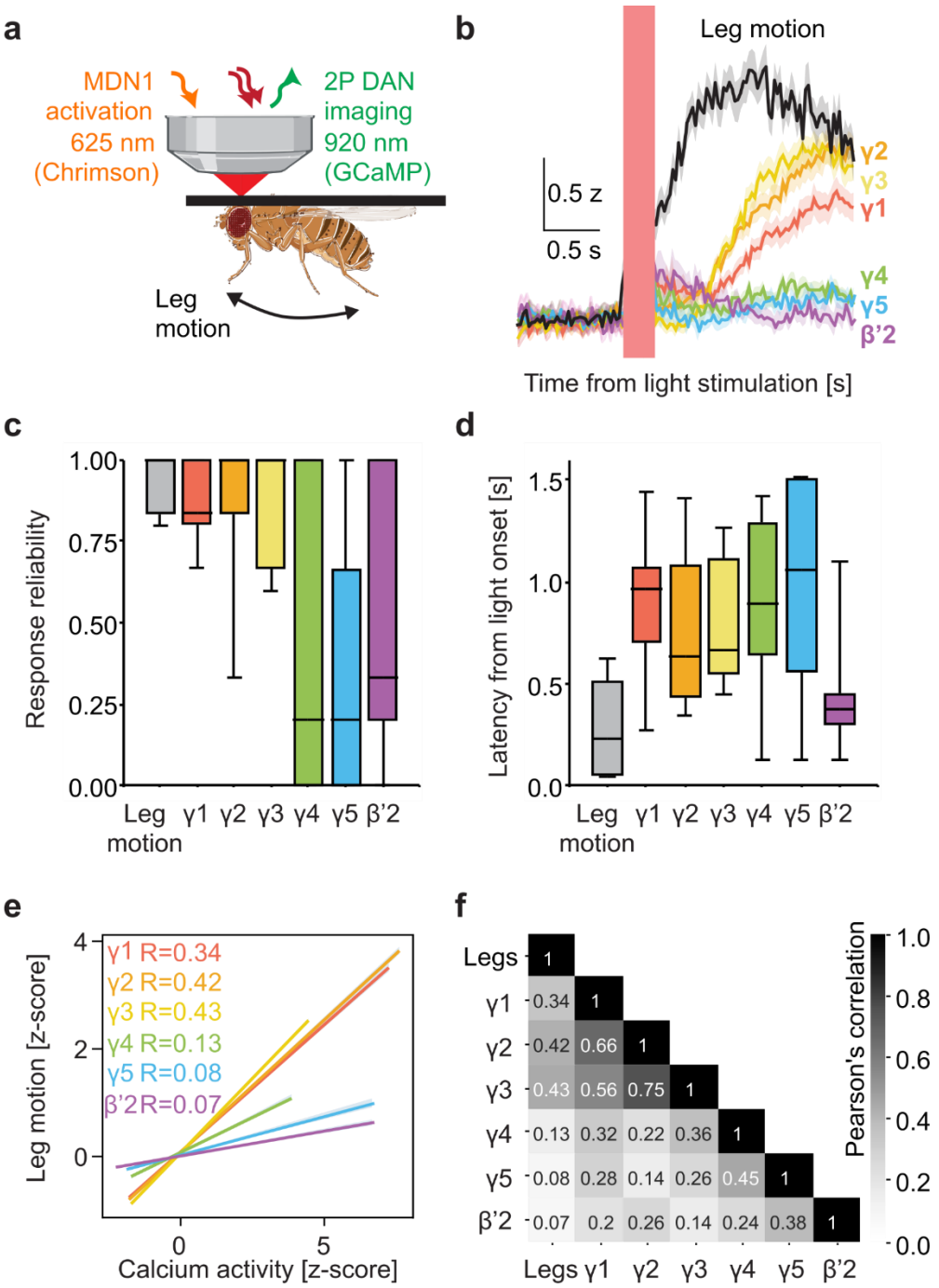

Extended Data Figure 1.8 | MDN- evoked leg movements engage DANs response.

a, Graphical representation of *in vivo* two photon imaging setup. Same as Figure 1.10 and Figure 1.11 (a-e) genotypes, $MDN1^{B}$ was activated using Chrimson with a 200 ms red light activation while calcium transients were simultaneously monitored in horizontal lobe DANs. Animals were free to move their legs. Genotype in **(b-f)**: $MDN1^{B}$>$Chrimson^{C}$; DANs>GCaMP.

b, Average calcium (colour) and leg motion (black) traces around time of first light activation (red vertical line) of MDN1^{B}. Shown are z-scored values, leg motion refers to motion energy calculated from the legs.

c,d, Reliability (c) and latency (d) to induce significant responses upon LED stimulation. Significant responses are defined as those reaching at least 2 standard deviations above the pre-2 s average within a 2 s time window after stimulation. Reliability refers to the probability for each stimulation trial within a recording and latency refers to the time the threshold is first crossed after stimulation.

e,f, Pearson's correlation of DAN calcium traces with leg motion **(e)** and with each other **(f)**. *N* = 11 flies. Data were analysed from Figure 1.10 (N=3$^{\#}$) and Figure 1.11 (a-e) (N=8$^{\#}$) before trapping.
$^{\#}$9 missing data point out of 20, where leg motion was not recorded. Additional genotype information is in Supplemental Table S1.

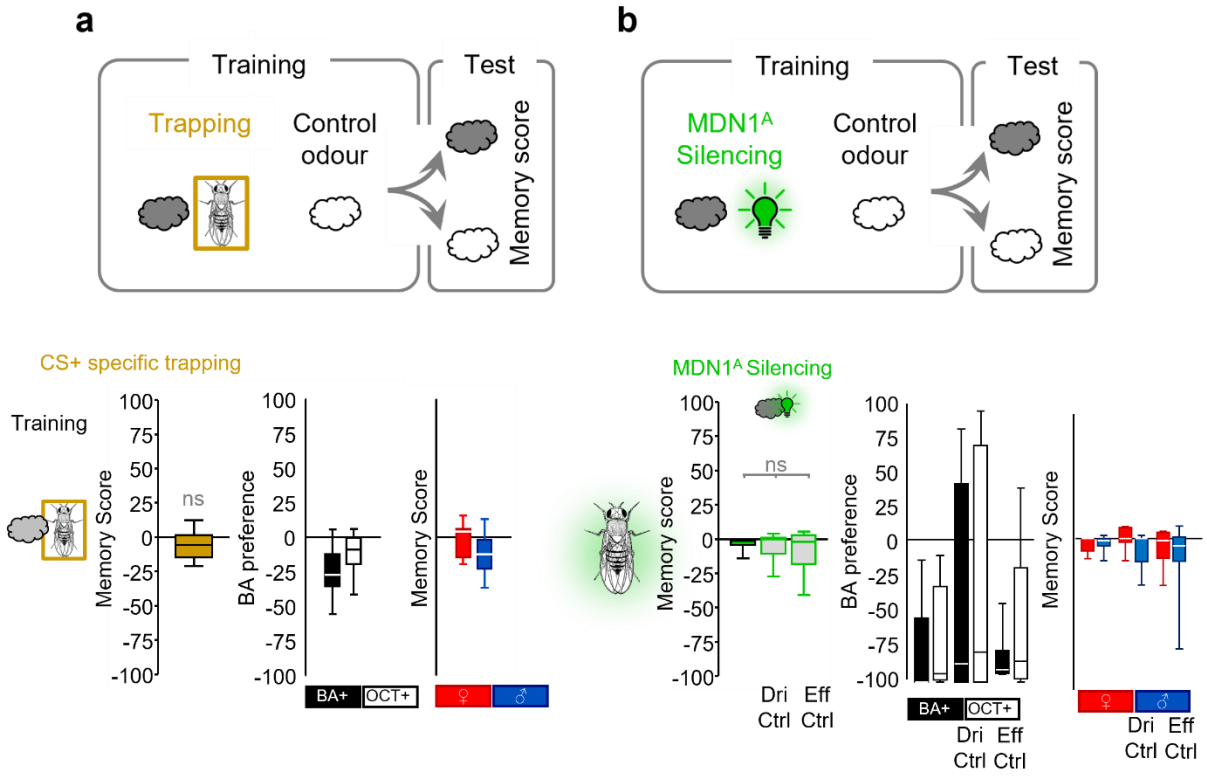

Extended Data Figure 1.9 | Trapping itself and silencing MDN1^{A} do not convey punishing signal.

a, Rationale and outcome of CS+ specific trapping (genotype: Canton S, N= 13). Box-whisker plots show median, interquartile range (box) and 10th/90th percentiles (whiskers). “ns” indicates non-significance in one sample sign test (OSS).

b, Rationale and outcome of silencing MDN1^{A} in comparison to genetic controls. Clouds: odours. Light bulb: optogenetic silencing of MDNs. green: MDN1^{A}>GtACR1, grey: Driver control: MDN1^{A}/+, Effector control: +/>GtACR1) (N= 12,12,12). Box-whisker plots show median, interquartile range (box) and 10th/90th percentiles (whiskers). Data were analysed across groups by Kruskal-Wallis tests (P< 0.05), followed by pairwise comparisons (Mann-Whitney U-tests, *P< 0.05 with Bonferroni-Holm correction) (ns: P> 0.05).

Underlying BA preference and memory scores of (a,b) separated by sex are shown, respectively, where box plots represent the median as the middle line, 25%/75% quantiles as box boundaries, and 10%/90% quantiles as whiskers. Black fill of the box plots shows BA preference when BA (Benzaldehyde) was associated with optogenetic, and white fill of the box indicates BA preference when OCT (3-octanol) was associated with optogenetic. Red fill of the box plots shows data from females; blue fill indicates data from males. Additional genotype information is in Supplemental Table S1 and statistical results in Supplemental Data Table S1.

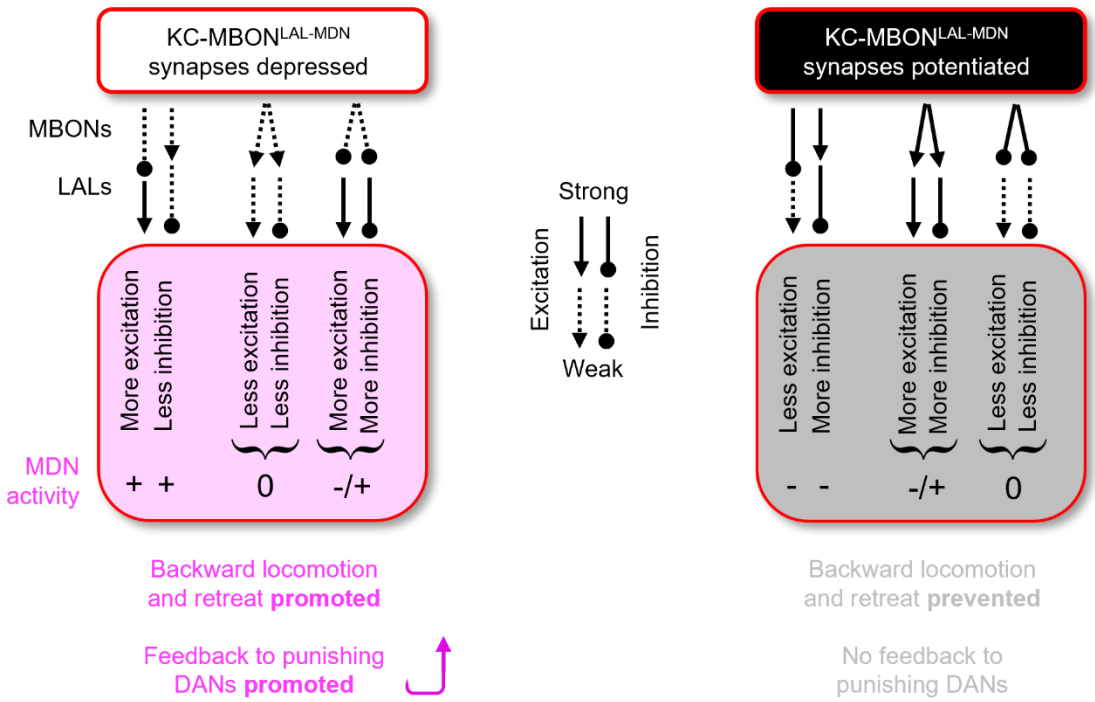

Extended Data Figure 1.10 | Scenarios of how KC-MBON plasticity affects MDNs.

Schematic summary of Figure 1.6c under the assumption that acetylcholine (ACh) has excitatory while GABA and glutamate (Glu) have inhibitory effects. Shown are scenarios of depressed (left) or potentiated (right) synapses between the KCs and the MBONs upstream of MDNs (KC-MBON$^{LAL-MDN}$). Through pathways with sign-inversion (inhibitory MBON to excitatory LAL or vice versa) depressed/ potentiated KC-MBON synapses promote/ prevent MDN activity and avoidance. For MBONs that give rise to parallel pathways with excitatory and inhibitory effects on MDNs the scenario is different: Using synapse number as a proxy for connection strength, these have nearly equal influences on the MDNs (Figure 1.6d). Through these MBONs, the MDNs receive both, more excitation and more inhibition (originating in inhibitory MBONs when the KC-MBON synapses are depressed, and in excitatory MBONs when they are potentiated). Terminals from LAL171,172 and LAL051 as the main conduits in these pathways are located in close proximity to one another on the MDN dendrites (Figure 1.6e). Nonlinear dendritic interactions based on this proximity may render the MDNs particularly sensitive to modulation.

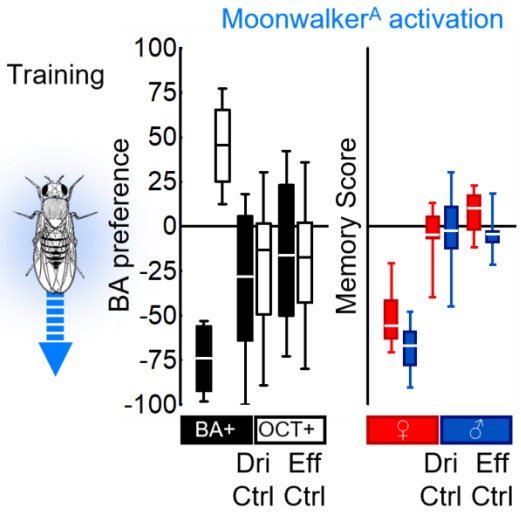

Extended Data Figure 1.11 | BA preference and memory scores from Figure 1.1 separated by sex

BA preference and memory scores from Figure 1.1, respectively, separated by sex. Box plots represent the median as the middle line, 25%/75% quantiles as box boundaries, and 10%/90% quantiles as whiskers. Black fill of the box plots shows BA preference when BA (Benzaldehyde) was associated with optogenetic and white fill of the box indicates BA preference when OCT (3-octanol) was associated with optogenetic. Red fill of the box plots shows data from females; blue fill indicates data from males. The blue glow fly indicates when blue light was used for moonwalker activation. Other details as in the legend of Figure 1.1. Additional information in Supplemental Table S1 and Supplemental Data Table S1.

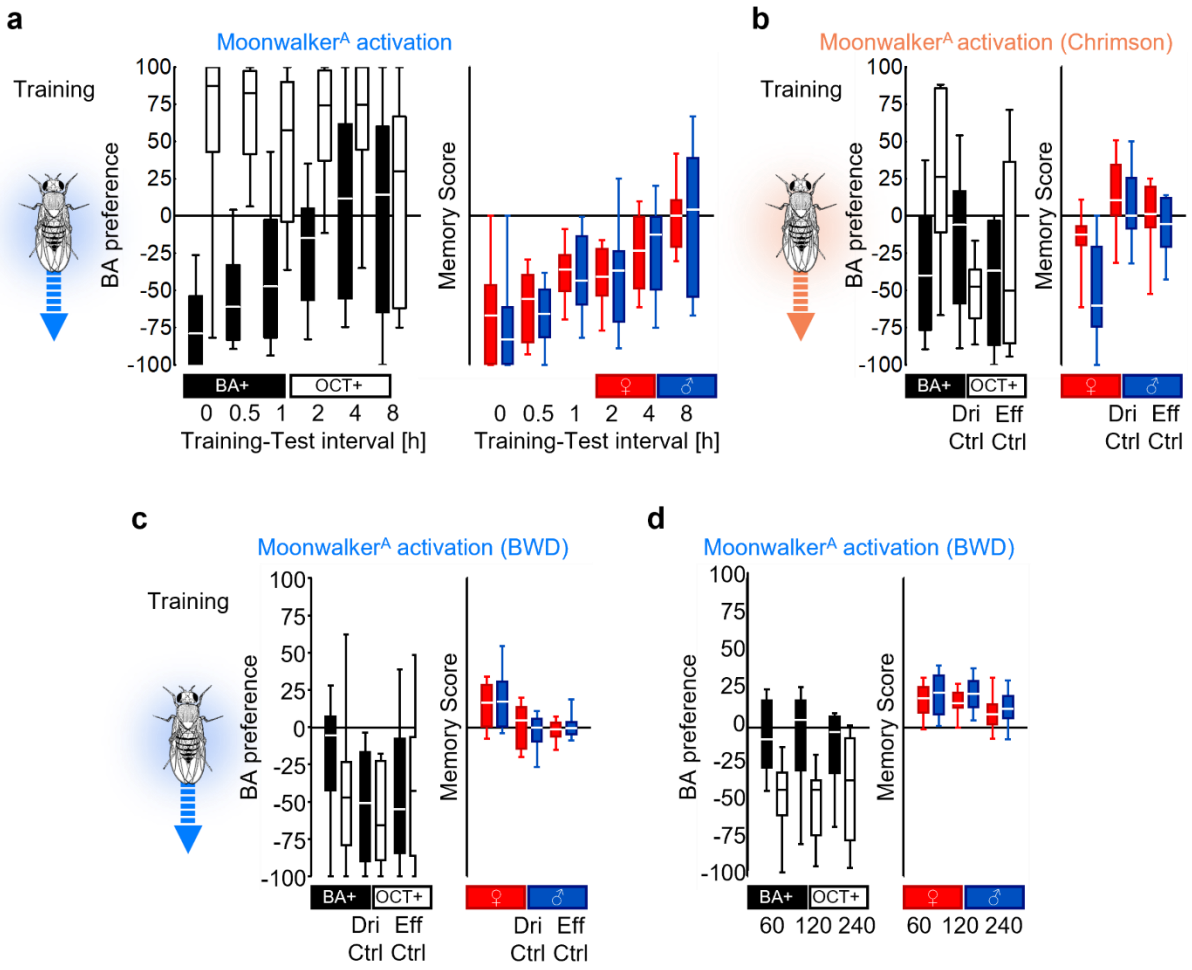

Extended Data Figure 1.12 | BA preference and memory scores from Figure 1.2 and Figure 1.3 (60s, 120s, 240s intervals) separated by sex

(a-c) BA preference and memory scores from Figure 1.2a-c, respectively, separated by sex.
d, BA preference and memory scores from Figure 1.3 (60s, 120s, 240s intervals), respectively, separated by sex. Box plots represent the median as the middle line, 25%/75% quantiles as box boundaries, and 10%/90% quantiles as whiskers. Black fill of the box plots show BA preference when BA (Benzaldehyde) was associated with optogenetic, and white fill of the box indicates BA preference when OCT (3-octanol) was associated with optogenetic. Red fill of the box plots shows data from females; blue fill indicates data from males. The blue/orange glow fly indicates when blue/red light was used for moonwalker activation. Other details as in the legend of Figure 1.2 and Figure 1.3. Additional information in Supplemental Table S1 and Supplemental Data Table S1.

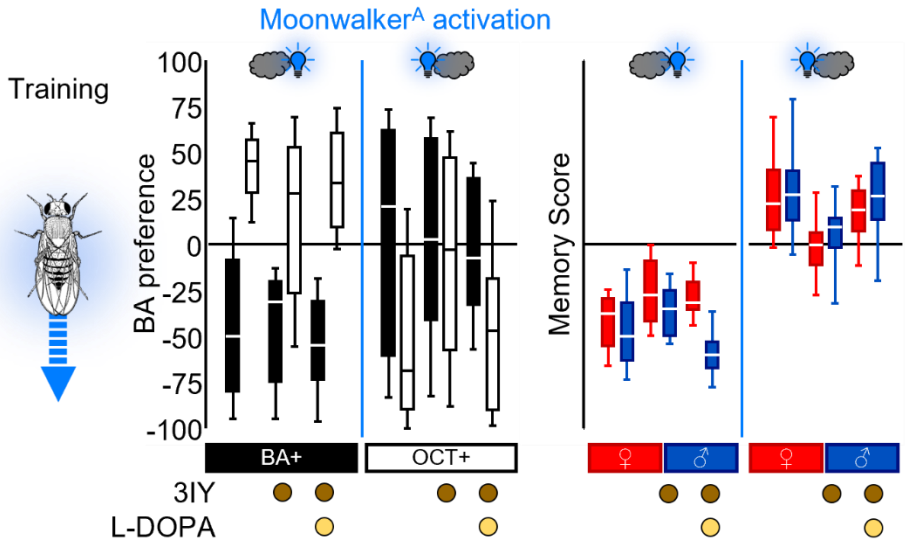

Extended Data Figure 1.13 | BA preference and memory scores from Figure 1.4a separated by sex.

BA preference and memory scores from Figure 1.4a, respectively, separated by sex. Box plots represent the median as the middle line, 25%/75% quantiles as box boundaries, and 10%/90% quantiles as whiskers. Black fill of the box plots show BA preference when BA (Benzaldehyde) was associated with optogenetic, and white fill of the box indicates BA preference when OCT (3-octanol) was associated with optogenetic. Red fill of the box plots shows data from females; blue fill indicates data from males. The blue glowing fly indicates when blue light was used for moonwalker activation. No circles below the panels refer to the control conditions, brown fill refers to feeding with 3IY, and yellow fill to feeding with L-DOPA in addition. Other details as in the legend of Figure 1.4a. Additional information in Supplemental Table S1 and Supplemental Data Table S1.

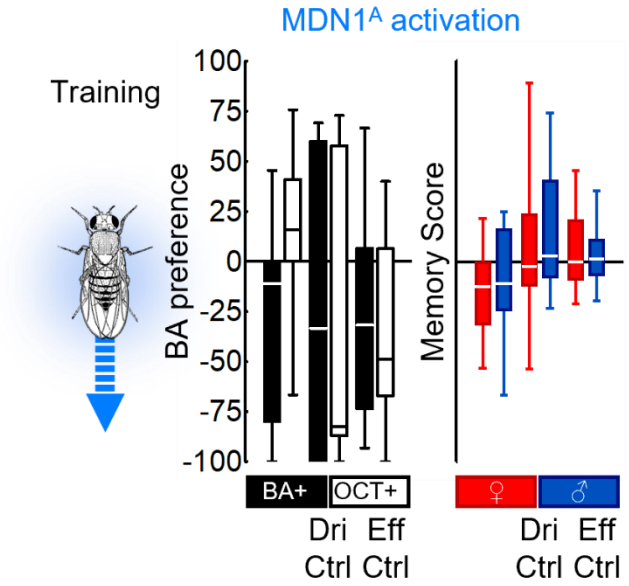

Extended Data Figure 1.14 | BA preference and memory scores from Figure 1.5 separated by sex
BA preference and memory scores from Figure 1.5, respectively, separated by sex. Box plots represent the median as the middle line, 25%/75% quantiles as box boundaries, and 10%/90% quantiles as whiskers. Black fill of the box plots show BA preference when BA (Benzaldehyde) was associated with optogenetic, and white fill of the box indicates BA preference when OCT (3-octanol) was associated with optogenetic. Red fill of the box plots shows data from females; blue fill indicates data from males. The blue glowing fly indicates when blue light was used for moonwalker activation. Other details as in the legend of Figure 1.5. Additional information in Supplemental Table S1 and Supplemental Data Table S1.

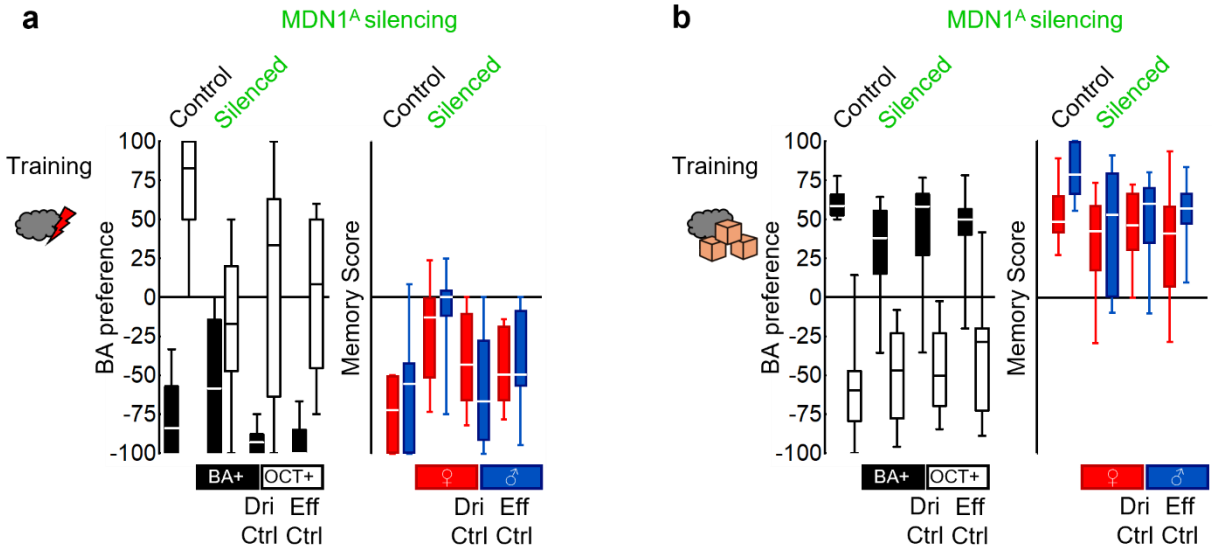

Extended Data Figure 1.15 | BA preference and memory scores from Figure 1.7 separated by sex.
(**a,b**) BA preference and memory scores from Figure 1.7a and 1.7b respectively, separated by sex. Box plots represent the median as the middle line, 25%/75% quantiles as box boundaries, and 10%/90% quantiles as whiskers. Black fill of the box plots show BA preference when BA (Benzaldehyde) was associated with electric shock, and white fill of the box indicates BA preference when OCT (3-octanol) was associated with electric shock. Red fill of the box plots shows data from females; blue fill indicates data from males. The red thunderbolt depicts electric shock, brown cubes indicates sugar and cloud as odour. Other details as in the legend of Figure 1.7. Additional information in Supplemental Table S1 and Supplemental Data Table S1.

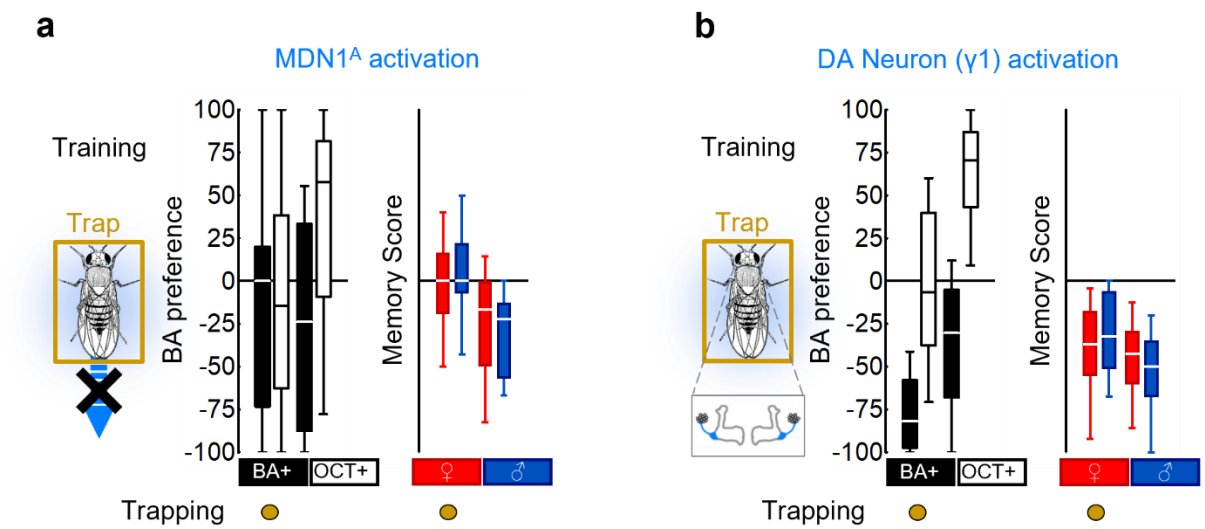

Extended Data Figure 1.16 | BA preference and memory scores from Figure 1.12 separated by sex

(**a,b**) BA preference and memory scores from Figure 1.12b-c, respectively, separated by sex. Box plots represent the median as the middle line, 25%/75% quantiles as box boundaries, and 10%/90% quantiles as whiskers. Black fill of the box plots show BA preference when BA (Benzaldehyde) was associated with optogenetic, and white fill of the box indicates BA preference when OCT (3-octanol) was associated with optogenetic. Red fill of the box plots shows data from females; blue fill indicates data from males. Brown boundary and dot below indicate when fly's movement was restrained. Other details as in the legend of Figure 1.12. Additional information in Supplemental Table S1 and Supplemental Data Table S1.

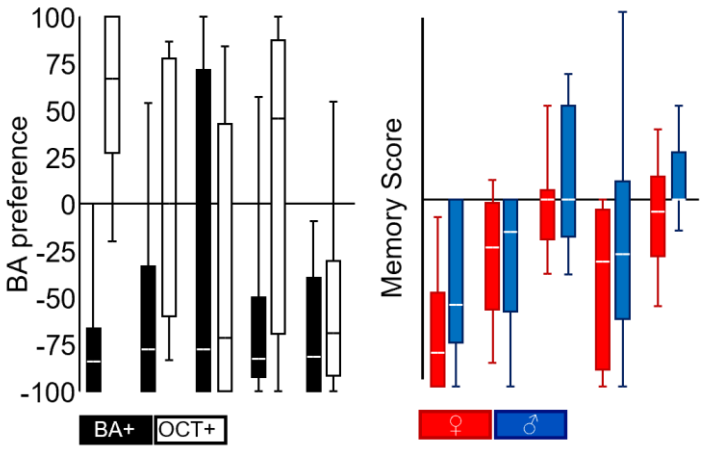

Extended Data Figure 1.17 | BA preference and memory scores from Figure 1.15d separated by sex

BA preference and memory scores from Figure 1.15d, respectively, separated by sex. Box plots represent the median as the middle line, 25%/75% quantiles as box boundaries, and 10%/90% quantiles as whiskers. Black fill of the box plots show BA preference when BA (Benzaldehyde) was associated with electric shock, and white fill of the box indicates BA preference when OCT (3-octanol) was associated with electric shock. Red fill of the box plots shows data from females; blue fill indicates data from males. Other details as in the legend of Figure 1.15d. Additional information in Supplemental Table S1 and Supplemental Data Table S1.

Chapter 2

Temporal profile of reinforcement in *Drosophila*

Text and figures with minor edits based on:
Fatima Amin[=], Christian König[=], Jiajun Zhang, Liubov S. Kalinichenko, Svea Königsmann, Vivian Brunsberg, Thomas D. Riemensperger, Christian P. Müller, Bertram Gerber. Compromising tyrosine hydroxylase function extends and blunts the temporal profile of reinforcement by dopamine neurons in *Drosophila*. J Neurosci. 2025 Jan 3: e1498242024.
doi: 10.1523/JNEUROSCI.1498-24.2024.
Author contributions as stated in the original, in press publication: **F.A**., C.K., T.D.R., C.P.M., and B.G. designed research; **F.A.**, C.K., J.Z., L.S.K., S.K., and V.B. performed research; **F.A.**, C.K., J.Z., L.S.K., S.K., V.B., T.D.R., C.P.M., and B.G. analyzed data; **F.A**., C.K., and B.G. wrote the paper. [=]Authors contributed equally.

Introduction

It is adaptive to consider both evidence for and evidence against causality for a proper representation of the causal structure of the world. Acting in conformity with the causal structure of the world is important for survival in animals and humans alike. Indeed, distortions in the assignment of causes to effects can have consequences ranging from the comical to the lethal. Following early insight into the importance of 'constantly conjoined events' (Hume, 1739-40/ 1978), causal learning is often studied in paradigms that vary the temporal relationship between cues and motivationally salient events (Shanks et al., 1989; Dickinson, 2001). This may concern evidence in favour of a causal relationship with a punishment, for example, or evidence against such causality. That is, a cue X that has preceded a punishment is evidence for punishment, whereas it is evidence against such causation if the punishment came first and cue X followed it. Accordingly, at the behavioural level and in associative learning experiments, aversive memory for cue X is the result when X occurs before punishment, whereas a characteristically weaker and opposing, appetitive memory is the result when cue X is presented only upon the termination of punishment, at the moment of 'relief' (Solomon and Corbit, 1974). Such timing-dependent valence reversal reflects a cross-species principle of reinforcement processing with broad implications in

biomedicine and computational science (Malaka, 1999; Gerber et al., 2014; Silver et al., 2016; König et al., 2019).

In the fruit fly *Drosophila melanogaster*, timing-dependent valence reversal is mostly studied for the association between odour cues and electric shock punishment. After odour→ shock training the flies show learned avoidance of the odour, whereas learned approach is observed after shock→ odour training (Tanimoto et al., 2004). These memories are called punishment and relief memory, respectively (Gerber et al., 2014; Gerber et al., 2019). Punishment learning in *Drosophila* involves the coincidence of olfactory processing and shock-evoked dopaminergic reinforcement in the mushroom body, the highest brain centre of insects (Heisenberg, 2003; Cognigni et al., 2018; Boto et al., 2020; Li et al., 2020; Modi et al., 2020; Menzel, 2022; Davis, 2023). Pairings of odour presentation with the activation of the mushroom body input neuron PPL1-01 can establish aversive associative memory for the odour in a process that involves dopamine signalling from PPL1-01 to the mushroom body neurons (Tanaka et al., 2008; Aso et al., 2010b, 2019; Hige et al., 2015; König et al., 2018) (synonyms for PPL1-01 are PPL1-γ1pedc and MB-MP1) (Figure 2.1a). However, although relief memory is observed for odours presented upon the termination of PPL1-01 activation (Aso and Rubin, 2016; König et al., 2018), it is controversial whether this is mediated by dopamine, too, or involves cotransmitters of dopaminergic neurons such as nitric oxide (Aso et al., 2019). On the one hand, relief memory remained intact when in PPL1-01 both the optogenetic effector for activating it and an RNAi construct were co-expressed to knock-down the transcript for the tyrosine hydroxylase enzyme (TH) required for dopamine biosynthesis (König et al., 2018, loc. cit. figure 5). On the other hand, relief memory through PPL1-01 termination was abolished in loss-of-function mutants for TH (Aso et al., 2019, loc. cit. figure 5, supplementary figure 3C) (also see Handler et al., 2019). It is therefore imperative to clarify the contribution of dopamine in timing-dependent valence reversal by PPL1-01. A distinguishing feature of the present study is that I map out the full 'fingerprint' of PPL1-01 reinforcement across multiple temporal intervals (Figure 2.1b). Yet the findings in this study not only reconcile what appeared to be contradictory conclusions in König et al. (2018) and Aso et al. (2019). They further reveal a dissociation between two forms of punishment learning, namely for procedures with versus procedures without a time gap between odour presentation and PPL1-01 activation ('trace' versus 'delay' conditioning, respectively), moderated by both dopamine and serotonin. This unexpectedly complex modulation of reinforcement processing, I discussed in this chapter with respect to psychiatric implications that may pertain if related modulations were to occur in humans.

Materials and methods

Fly strains

In a mass culture on standard food, *Drosophila melanogaster* were reared at 60-70% relative humidity and 25°C, and under a 12h:12h light: dark cycle, unless mentioned otherwise. In the behavioural assays, 1-to-3-day-old adult flies were collected, regardless of sex, and handled in mixed-sex cohorts of approximately 60-100 flies with approximately equal numbers of females and males. Transgenic fly strains were used to express either the blue-light-gated cation channel ChR2-XXL, or both ChR2-XXL and an RNAi construct against the TH enzyme in the dopaminergic mushroom body input neuron PPL1-01. Specifically, males of the driver strain MB320C-split-GAL4 (covering the PPL1-01 neuron) (Bloomington stock centre no. 68253; Aso et al., 2014) were crossed to females of the effector strains, which were either UAS-ChR2-XXL (Bloomington stock centre no. 58374, Dawydow et al., 2014) or featured UAS-TH-RNAi in addition (Bloomington stock centre no. 25796; Riemensperger et al., 2013). The flies from these crosses (henceforth PPL1-01>ChR2-XXL and PPL1-01>ChR2-XXL/TH-RNAi) were used for experiments and kept in light-shielded vials to avoid optogenetic activation by room light. Genetic controls carrying only the PPL1-01 driver or only the ChR2-XXL effector had previously been tested (König et al., 2018) and did not show memory upon pairing odour with blue light.

Pharmacological manipulations

In this study, unless mentioned otherwise, I used 3-iodo-L-tyrosine (3IY), an inhibitor of the TH enzyme which is rate-limiting for the synthesis of dopamine (Figure 2.1c), in a procedure that followed Thoener et al. (2021). Specifically, in different sets of newly hatched flies, either a plain 5% sucrose solution (CAS: 57-50-1, Hartenstein, Würzburg, Germany; in EVIAN water) was offered to the flies as their sole food, or it was offered in mixture with 5mg/ml 3IY (CAS: 70-78-0, Sigma, Steinheim, Germany; stored at -20°C) or in mixture with 5mg/ml 3IY plus 10mg/ml 3,4-dihydroxy-L-phenylalanine (L-DOPA), a precursor of dopamine (CAS: 59-92-7, Sigma, Steinheim, Germany). Mixtures were prepared by a shaker at high speed for approximately 60min. Specifically, flies were transferred to small plastic vials (diameter: 25mm; height: 60mm; volume: 30ml; K-TK, Retzstadt, Germany) with tissue paper (Fripa, Düren, Germany) soaked with 1.8ml of the solutions mentioned above, kept at 25°C and used for experiments after 36-40h. This procedure is henceforth called the tissue paper method.

As an inhibitor of the enzyme tryptophan hydroxylase (TPH), which is rate-limiting for serotonin synthesis, I used para-chlorophenylalanine (PCPA, a.k.a. DL-4 Chlorophenylalanine, fenclonine) (CAS: 7424-00-2, ThermoFischer, Acros Organics, Geel, Belgium; stored at 4°C), in a procedure

that followed Pooryasin and Fiala, (2015). Specifically, newly hatched flies were transferred to large plastic vials (diameter: 46mm; height: 102mm; volume: 170ml; K-TK, Retzstadt, Germany) with wet tissue paper and starved for 48h at 18°C. After starvation, separate sets of flies were either transferred to small vials containing 1ml of freshly prepared standard food medium mixed with 200µl of 5% sucrose solution and 200µl of water (EVIAN) and left with this as their sole food, or they were kept with this mixture plus in addition either 1.25mg/ml of 3IY, or 1.25mg/ml of 3IY plus 60mg/ml of PCPA, or 60mg/ml of PCPA. In all cases, the flies were kept at 25°C room temperature and used for experiment 4 days later. Mixtures were prepared by a shaker at high speed for approximately 30min. This procedure is henceforth called the food method.

The methods used can be expected to compromise TH function and thus to reduce dopamine levels, systemically or in the PPL1-01 neuron, but they are not expected to result in a total absence of dopamine. It is also likely that they leave intact the function of cotransmitters of dopamine neurons, such as nitric oxide (Aso et al., 2019). Thus, the present experiments make it possible to ascertain a role of TH and of dopamine in timing-dependent valence reversal but do not allow any remaining reinforcing effects to be assigned to residual dopamine or to any unaffected cotransmitter.

Behavioural experiments

Behavioural experiments were performed following König et al. (2018), for the association of odour with the optogenetic activation of PPL1-01 unless mentioned otherwise. In brief, these experiments took place in a custom-made set-up (CON-ELEKTRONIK, Greussenheim, Germany) (modified from Tully and Quinn, 1985) that allowed the simultaneous handling of four cohorts of flies, each with approximately 60-100 flies. During training, dim red light was used to allow minimal vision for the experimenter while the ChR2-XXL channels remained mostly closed. Blue light for opening the ChR2-XXL channels and thus for neuronal activation was turned on only briefly and in the temporal relationship to odour presentation as described below and in the Results section. In all cases, blue light was presented in a pulsatile manner as 12 pulses, each 1.2s long and followed by the next pulse with a 5s onset-to-onset interval. Once the training had concluded, the testing was carried out in darkness.

As odorants, 50µl benzaldehyde (BA) and 250µl 3-octanol (OCT) (CAS 100-52-7, 589-98-0; Fluka, Steinheim, Germany) were applied to 1cm-deep Teflon containers of 5mm or 14mm diameter, respectively.

The crucial variable for the behavioural experiments is the relative timing (or inter-stimulus-interval, ISI) of the pairing between an odour and the optogenetic activation of PPL1-01 by blue light (Figure 2.1b, Extended Data Figure 2.1). The ISI is defined as the time interval between the

onset of the blue light and the onset of the paired odour presentation. In principle, either the paired odour was presented first followed by blue light stimulation (forward conditioning, defined as negative ISIs), or the blue light was presented first followed by presentation of the paired odour (backward conditioning, positive ISIs). Specifically, separate groups of flies were trained with one of seven ISIs (-155s, -100s, -15s, 80s, 120s, 240s, 300s). Given the 60s-duration of blue light stimulation and the 60s-duration of the paired odour presentation, this resulted in gaps between the two events of -95s and -40s for the two longest forward conditioning ISIs (-155s, -100s) ('trace' conditioning), in a partial overlap for the -15s ISI ('delay' conditioning), and in gaps of 20s to 240s for the backward conditioning ISIs ('relief' conditioning). In all cases, a second odour was presented as a reference, unpaired from blue light during training. The use of BA and OCT as the paired and the reference odour was balanced across repetitions of the experiment.

After one cycle of training, which lasted for a total of 15min, the flies were given a 4min accommodation period and were then shifted to the choice point of a T-maze apparatus, with the paired and the reference odour on either side. After 2min, the arms of the T-maze were closed and the numbers of flies (#, as the sum of male and female flies) in each arm was counted by an assistant blind to the experimental conditions to calculate the preference for BA as:

$$PREF = ((\#BA - \#OCT) / \#Total) \times 100 \quad (1)$$

Positive PREF scores thus indicate preference for BA over OCT, and negative scores indicate preference for OCT over BA. From these scores, taken after either BA or OCT had been paired with PPL1-01 activation in separate cohorts of flies (BA+, or OCT+, respectively), an associative memory score was calculated to average out odour-specific and non-associative effects as:

$$\text{Memory score} = (PREF_{BA+} - PREF_{OCT+}) / 2 \quad (2)$$

Negative memory scores thus indicate conditioned avoidance of the paired odour, and positive scores indicate conditioned approach to it.

The difference between the memory scores of the TH-compromised condition and the memory scores of the control condition was determined to quantify the effect of compromising TH function on memory scores.

Measurement of biogenic amine levels

A high-performance liquid chromatography (HPLC) analysis of brain-wide biogenic amine levels was performed after drug feeding using the tissue paper method. For each of the respective treatments, 6 male and 6 female brains were dissected in Ca^{2+}-free saline and separated by sex, immediately frozen in -80°C liquid nitrogen. The samples were analyzed using HPLC with electrochemical detection to measure dopamine and serotonin levels. The column was an ET 125/2, Nucleosil 120-5, C-18 reversed phase column (Macherey & Nagel, Düren, Germany). The mobile phase consisted of 75mM NaH2PO4, 4mM KCl, 20µM EDTA, 1.5mM sodium dodecyl sulfate, 100µl/l diethylamine, 12% alcohol and 12% acetonitrile, adjusted to pH 6.0 using phosphoric acid (Carl Roth GmbH, Karlsruhe, Germany). The electrochemical detector (Intro) (Antec, Alphen, The Netherlands) was set at 500 mV versus an ISAAC reference electrode (Antec, Alphen, The Netherlands) at 30°C. This setup allows the simultaneous measurement of dopamine and serotonin (Amato et al., 2020; Kalinichenko et al., 2021).

Experimental design and statistical analysis

Throughout the study, non-parametric statistical tests were used (Statistica 11.0; StatSoft Hamburg, Germany, and R 2.15.1, www.r-project.org). For comparisons across more than two groups, the Kruskal-Wallis test (KW) was applied. For subsequent pair-wise comparisons between groups, Mann-Whitney U-tests (MW-U) were performed. To test whether values of a given group differed from chance levels, i.e., from zero, one-sample sign tests (OSS) were used. When multiple tests of the same kind were performed within one experiment, significance levels were adjusted by a Bonferroni-Holm correction to keep the experiment-wide type 1 error limited to 0.05 (Holm, 1979). In no case were data compared within-subjects. Data are presented as box-dot plots which represent the median as the middle line and the 25%/75% and 10%/90% quantiles as box boundaries and whiskers, respectively; single data points are displayed as dots. For the behavioural experiments, each such sample N= 1 is based on cohorts of approximately n= 120-200 individual flies, with approximately equal numbers of females and males. For the HPLC measurements each N= 1 is based on 6 female and 6 male flies. Sample sizes of the respective experiments are stated in the Figure legends. Per-experiment details of experimental design and statistical results can be found in Tables 2.1-5.

Results

The temporal profile of PPL1-01 reinforcement extends and blunts upon pharmacological inhibition of TH

Blue-light-gated ion channel ChR2-XXL expressed flies for optogenetic activation of the PPL1-01 neuron showed punishment memory after odour→PPL1-01 training (Figure 2.1d; ISI -15s). Acute feeding of 3IY, an inhibitor of the TH enzyme required for dopamine synthesis, impaired such punishment memory (Figure 2.1d; ISI -15s) (for a repetition see Extended Data Figure 2.2). Of note is that 3IY feeding leaves task-relevant sensory-motor faculties intact (Thoener et al., 2021). In a further repetition of the experiment, an additional feeding of L-DOPA could rescue the effect of 3IY feeding on punishment memory (Figure 2.1e; ISI -15s). In contrast, relief memory after PPL1-01→odour training was unaffected by feeding of 3IY (Figure 2.1d, Figure 2.1e; ISI 120s).

Next, I mapped out the effect of 3IY feeding on the temporal profile of PPL1-01 reinforcement more systematically. This was achieved, based on the association of odour and PPL1-01 activation across multiple intervals between these events. This revealed that this temporal profile is both, extended and blunted by 3IY feeding. The intervals that I used before, this once more replicated the finding that 3IY feeding leads to a decrease in punishment memory, and that there is no such detrimental effect on relief memory (Figure 2.1f; ISIs of -15s and 120s, respectively). Strikingly, however, 3IY feeding increased punishment memory when there was a -40s gap between the offset of the odour and the start of PPL1-01 activation (Figure 2.1f; ISI -100s), and decreased relief memory for relatively long intervals between PPL1-01 activation and odour presentation (Figure 2.1f; ISI 240s, corresponding to a 180s gap).

In a follow-up experiment, I, confirmed these three kinds of effect exerted by 3IY feeding and showed that they can be rescued by additionally feeding L-DOPA (Figure 2.1g) (see Extended Data Figure 2.3 and Extended Data Figure 2.4 for the underlying preference score and memory scores separated by sex, respectively). HPLC measurements of whole-brain homogenates upon 3IY feeding reveal a selective decrease in dopamine but not in serotonin levels, which was likewise rescued by additionally feeding L-DOPA (Figure 2.2) (see Extended Data Figure 2.5 for data separated by sex).

These results suggest that optogenetic activation of PPL1-01 establishes both punishment memory and relief memory through a 3IY-sensitive, TH-dependent, dopaminergic process. To our surprise, I found that the compromising of TH function had opposite effects upon training with a -40s gap between odour and PPL1-01 activation (ISI -100s, punishment memory after trace conditioning) as compared to training without such a gap (ISI -15s, punishment memory after delay conditioning) (Figure 2.1f, Figure 2.1g).

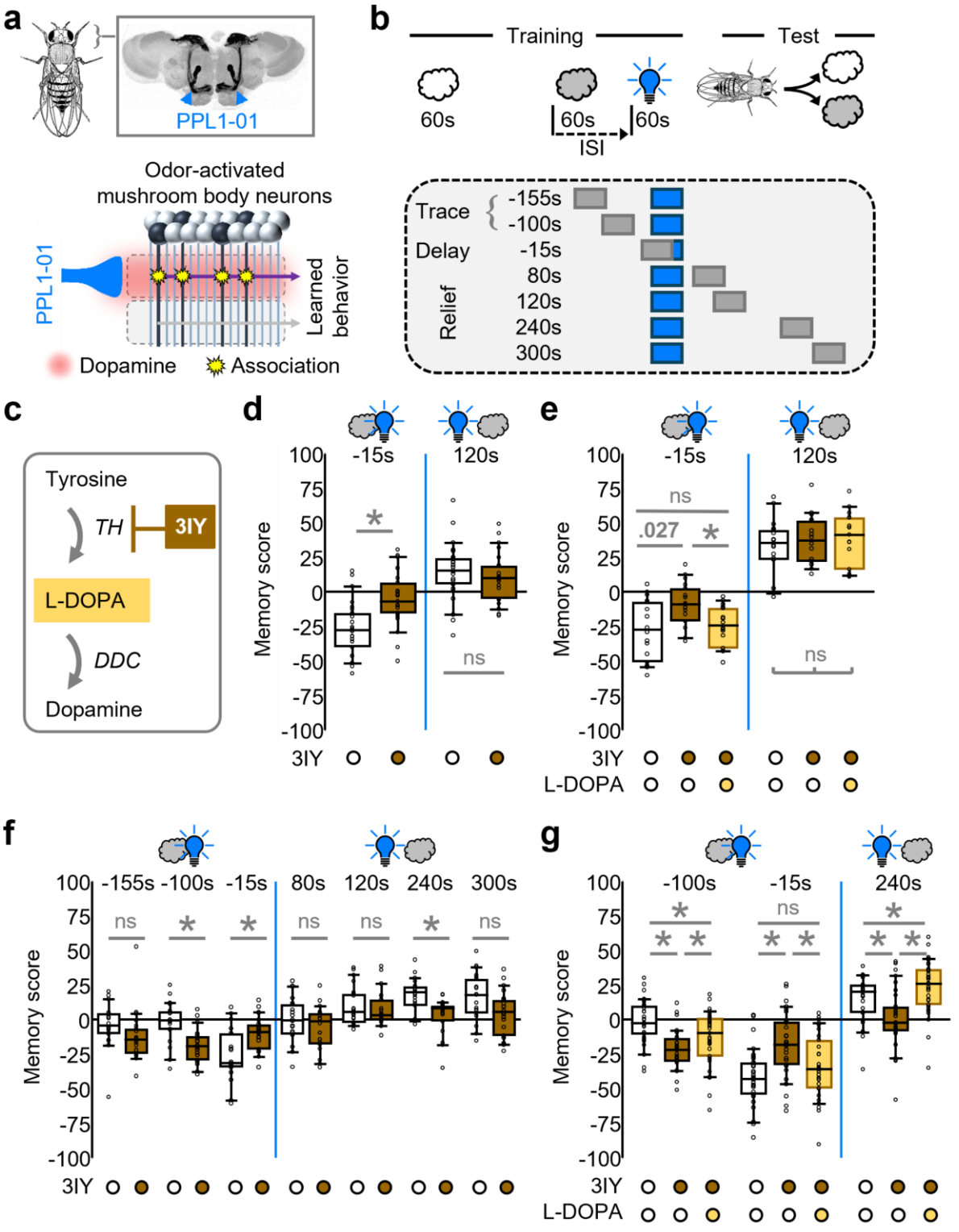
a
PPL1-01
Odor-activated
mushroom body neurons
PPL1-01
Learned
behavior
Dopamine
Association
b
Training
Test
60s
60s
60s
ISI
Trace
Delay
Relief
-155s
-100s
-15s
80s
120s
240s
300s
c
Tyrosine
TH
3IY
L-DOPA
DDC
Dopamine
d
-15s
120s
Memory score
3IY
ns
e
-15s
120s
Memory score
ns
.027
ns
3IY
L-DOPA
f
-155s
-100s
-15s
80s
120s
240s
300s
Memory score
ns
3IY
g
-100s
-15s
240s
Memory score
ns
3IY
L-DOPA

Figure 2.1 | The temporal profile of reinforcement by PPL1-01 extends and blunts upon pharmacologically inhibiting the TH enzyme.

a, Schematics of a fly, its brain, and the mushroom bodies (top) and a highly simplified working hypothesis of association formation during punishment learning (bottom) (for references see body text). The intrinsic neurons of the mushroom bodies represent odours in a sparse and combinatorial manner (mushroom body neurons in black). The dopaminergic PPL1-01 neuron (blue), which can be activated by e.g. electric shock punishment, intersects the axons of the mushroom body neurons in what is called the γ1pedc compartment. Associative coincidence of odour activation and signalling from PPL1-01 (red shade within the compartment) induces associative presynaptic depression (stars) at the synapses from the odour-activated mushroom body neurons towards an approach-promoting output neuron of the compartment (purple). As no such depression takes place in a neighbouring compartment in relation to its avoidance-promoting output neuron, this shifts the balance across the mushroom body output neurons to net avoidance as the learned behaviour. In total, the mushroom body has 15 compartments, only two of which are sketched. The compartment depicted at the top represents the two compartments known to receive input from punishing stimuli (γ1pedc and γ2); the compartment depicted at the bottom represents compartments known to receive reward input (γ4, γ5).

b, Procedure for presenting the reference odour (open clouds), the paired odour (grey clouds), and optogenetic activation of PPL1-01 (blue light bulb). The interval between the onset of the paired odour and the onset of PPL1-01 activation is called the inter-stimulus-interval (ISI). For more details see Extended Data Figure 2.1.

c, Schematic of dopamine biosynthesis and of the inhibition of tyrosine hydroxylase (TH) by 3-iodo-L-tyrosine (3IY). The dopamine precursor 3,4-dihydroxy-L-phenylalanine (L-DOPA) should compensate for the effects of 3IY on dopamine levels. DDC: dopamine decarboxylase. Drug feeding was performed by the tissue paper method.

d, Relative to controls, punishment memory after odor→PPL1-01 training (ISI -15s) is decreased upon feeding of 3IY (N= 25, 25). Relief memory after PPL1-01→odor training (ISI 120s) is unaffected (N= 25, 23).

e, The decrease in punishment memory by 3IY can be rescued by additionally feeding L-DOPA (ISI -15s) (N= 16, 16, 16). Relief memory is unaffected by 3IY, and by combining 3IY and L-DOPA (ISI 120s) (N= 16, 16, 15).

f, Mapping out the effect of 3IY on the temporal profile of PPL1-01 reinforcement (N= 20, 20; 20, 20; 19, 20; 20, 20; 20, 20; 20, 20; 20, 20). 3IY decreases punishment memory (ISI -15s, delay conditioning) and leaves relief memory with an ISI of 120s unaffected. For a longer relief ISI of 240s a decrease in relief memory is revealed. For a training procedure with a -40s time gap between odour and PPL1-01 (ISI -100s, trace conditioning), an increase in memory scores by 3IY is observed.

g, The effects of 3IY on memory scores after trace, delay, and relief conditioning (ISIs of -100s, -15s, and 240s, respectively) can be largely rescued, or even overcompensated, by L-DOPA (N= 30, 31, 31; 30, 31, 31; 30, 31, 30).

Plotted in (d-g) are the memory scores according to equation 2, reflecting associative memory for the odour paired with optogenetic activation of PPL1-01; positive and negative memory scores reflect appetitive and aversive memory, respectively. Box plots represent the median as the middle line, 25%/75% quantiles as box boundaries, and 10%/90% quantiles as whiskers. Open box plots and circles refer to the control condition, brown and light brown fill to groups fed with 3IY or with 3IY plus L-DOPA, respectively. Flies were of the genotype PPL1-01>ChR-2XXL.

* and “ns” indicate significance and non-significance, respectively, in MW-U tests at an error rate of 5%, adjusted according to Bonferroni-Holm, except for (e, ISI 120s) where “ns” indicates non-significance in a KW test. In (e, ISI -15s), the exact p-value is presented, which after Bonferroni-Holm correction is just about non-significant. Given that in all five other cases of comparison between these treatment groups statistical significance is reached (Figure 2.1d, Figure 2.1f, Figure 2.1g, Extended Data Figure 2.2, Figure 2.5b), our

interpretation is that the narrow “miss” of significance in this case is a false negative. Statistical results are documented in Table 2.1, respectively. The underlying preference scores and memory scores separated by sex are shown in Extended Data Figure 2.3 and Extended Data Figure 2.4, respectively. The anatomical image of the mushroom body in (a) is modified from Heisenberg and Gerber (2008).

Table 2.1: Summary experimental design and statistics Figure 2.1

Figure	ISI	KKW test	MWU test			OSS test	
			Groups	*U*	*p*	Group	*p*
2.1d	-15	H(3, N=98) =39.658; p<0.05	Control vs 3IY	132.5	0.05/2	Control	<0.05/4
						3IY	0.152
	120		Control vs 3IY	132.5	0.409	Control	<0.05/3
						3IY	0.035
ExtFig 2.2	-15		Control vs 3IY	4	<0.05/1	Control	0.0625
						3IY	1
2.1e	-15	H(2, N=48) =7.839; p<0.05/2	Control vs 3IY	69	0.027	Control	<0.05/3
			3IY vs 3IY+L-DOPA	59	<0.05/3	3IY	0.21
			Control vs 3IY+L-DOPA	121	0.806	3IY+L-DOPA	<0.05/5
	120	H(2, N=47) =0.579; p=0.749				Control	<0.05//2
						3IY	<0.05/6
						3IY+L-DOPA	<0.05/4
2.1f	-155	H(13, N=279) =110.221; p<0.05	Control vs 3IY	112	0.018	Control	0.824
						3IY	<0.05/11
	-100		Control vs 3IY	74	<0.05/7	Control	0.647
						3IY	<0.05/14
	-15		Control vs 3IY	91	<0.05/5	Control	<0.05/10
						3IY	0.012
	80		Control vs 3IY	161	0.298	Control	0.824
						3IY	1
	120		Control vs 3IY	180	0.598	Control	0.041
						3IY	0.263
	240		Control vs 3IY	79	<0.05/6	Control	<0.05/13
						3IY	0.041
	300		Control vs 3IY	124	0.04	Control	<0.05/12
						3IY	0.167
2.1g	-100	H(2, N=92) =20.261; p<0.05/3	Control vs 3IY	154	<0.05/3	Control	0.585
			3IY vs 3IY+L-DOPA	315	<0.05/2	3IY	<0.05/6
			Control vs 3IY+L-DOPA	314	<0.05/1	3IY+L-DOPA	<0.05/3
	-15	H(2, N=92) =16.874; p<0.05/1	Control vs 3IY	190	<0.05/3	Control	<0.05/8
			3IY vs 3IY+L-DOPA	287	<0.05/2	3IY	<0.05/5
			Control vs 3IY+L-DOPA	366	0.155	3IY+L-DOPA	<0.05/9
	240	H(2, N=91) =17.914; p<0.05/2	Control vs 3IY	277	<0.05/2	Control	<0.05/4
			3IY vs 3IY+L-DOPA	192	<0.05/3	3IY	0.720
			Control vs 3IY+L-DOPA	315	<0.05/1	3IY+L-DOPA	<0.05/7

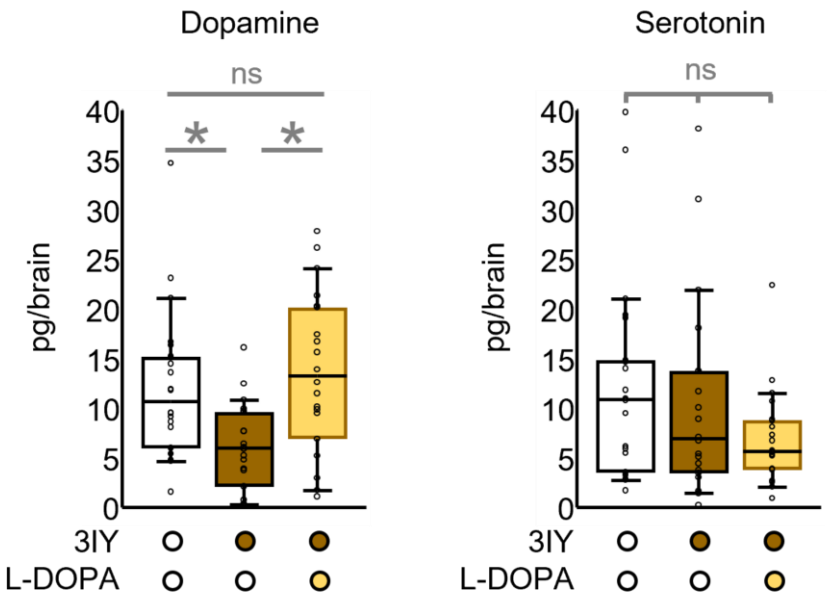

Figure 2.2 | Whole-brain levels of dopamine get reduced by pharmacologically inhibiting the TH enzyme.

Whole-brain levels of dopamine and serotonin after feeding 3-iodo-L-tyrosine (3IY), an inhibitor of the tyrosine hydroxylase (TH) enzyme required for dopamine biosynthesis. Feeding of 3IY reduced dopamine levels, an effect that was restored by feeding the dopamine precursor 3,4-dihydroxy-L-phenylalanine (L-DOPA) in addition (N= 20, 20, 20). Drug feeding, performed by the tissue paper method, was without effect on serotonin levels (N= 20, 20, 20). Box plots represent the median as the middle line, 25%/75% quantiles as box boundaries, and 10%/90% quantiles as whiskers. Open box plots and circles refer to the control condition, brown and light brown fill to groups fed with 3IY or with 3IY plus L-DOPA, respectively. Flies were of the genotype PPL1-01>ChR-2XXL.
* indicates significance in MW-U tests at an error rate of 5%, adjusted according to Bonferroni-Holm. “ns” indicates non-significance in such a MW-U test (dopamine) or in a KW test (serotonin). Data and statistical results are documented in Table 2.2, respectively. Data separated by sex are shown in Extended Data Figure 2.5.

Table 2.2: Summary experimental design and statistics Figure 2.2

Figure	KKW test	MWU test		
		Groups	*U*	*p*
2.2_DA	H(2, N=60)=11.853; p<0.05	Control vs 3IY	100	<0.05/2
		3IY vs 3IY+L-DOPA	85	<0.05/3
		Control vs 3IY+L-DOPA	169	0.409
2.2_5-HT	H(2, N=60)=3.211; p=0.201			
ExtFig2.5_DA_Female	H(2, N=30)=5.499; p=0.064			
ExtFig2.5_DA_Male	H(2, N=30)=8.41; p<0.05/2	Control vs 3IY	14	<0.05/3
		3IY vs 3IY+L-DOPA	21	0.031
		Control vs 3IY+L-DOPA	44	0.678
ExtFig2.5_5-HT Female	H(2, N=60)=0.901; p=0.637			
ExtFig2.5_5-HT Male	H(2, N=60)=2.392; p=0.302			

The temporal profile of PPL1-01 reinforcement extends and blunts likewise upon local knock-down of TH

Next, I asked whether the three observed effects of compromising TH function on memory scores, namely on punishment memory after i) trace and ii) delay conditioning, as well as on iii) relief memory, require dopaminergic signalling from PPL1-01 itself. Therefore, both the optogenetic effector and an RNAi construct for the knock-down of the TH enzyme (Riemensperger et al., 2013) were co-expressed in PPL1-01 and thus, I mapped out the temporal profile of PPL1-01 reinforcement. This again revealed an increase in punishment memory after trace conditioning (ISI -100s), a decrease in punishment memory after delay conditioning (ISI -15s), as well as a decrease in relief memory (ISI 300s) (Figure 2.3a, Figure 2.3b) (see Extended Data Figure 2.6 and Extended Data Figure 2.7 for the underlying preference scores and memory scores separated by sex, respectively).

Tother, these results show that compromising TH function extends and blunts the temporal profile of reinforcement by PPL1-01 (see Figure 2.4a): trace conditioning (ISI -100s) is improved, delay conditioning is impaired, and relief conditioning is abolished for longer intervals (ISIs 240s and 300s).

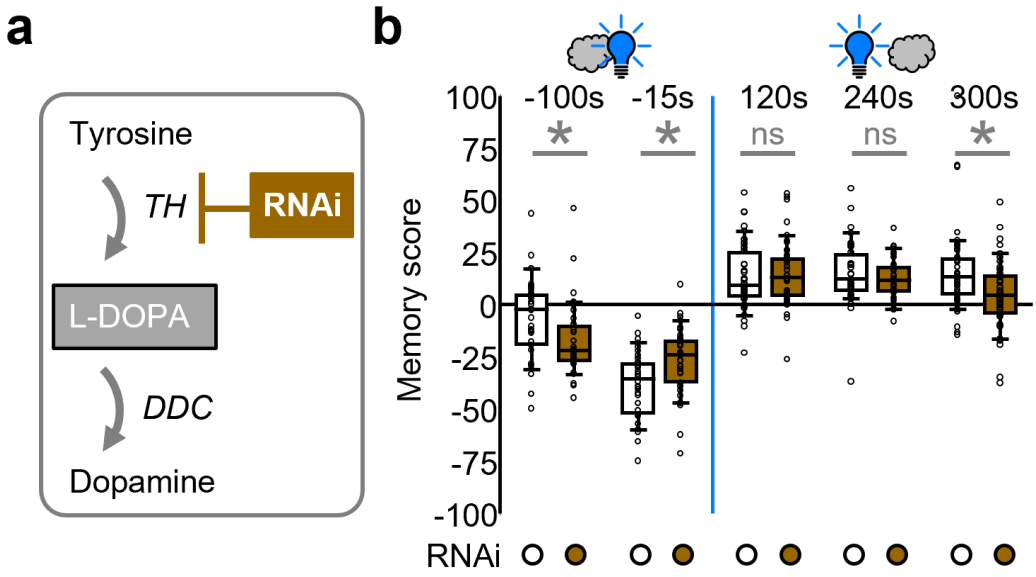

Figure 2.3 | The temporal profile of PPL1-01 reinforcement extends and blunts likewise upon local knock-down of TH.

a, Schematic of dopamine biosynthesis and of the inhibition of tyrosine hydroxylase (TH) by RNA interference (RNAi).

b, Mapping out the effect of TH-RNAi in the PPL1-01 neuron on the temporal profile of PPL1-01 reinforcement (N= 32, 32; 34, 34; 40, 40; 33, 34; 42, 42). Relative to controls, TH-RNAi promotes punishment memory upon trace conditioning (ISI -100s) and decreases punishment memory upon delay conditioning (ISI -15s). Relief memory is decreased (ISI 300s). Control flies were of the genotype PPL1-01>ChR2-XXL (open box plots and circles); flies for TH knock-down in the PPL1-01 neuron additionally carried the TH-RNAi construct (PPL1-01>ChR2-XXL/TH-RNAi) (box plots and circles with brown fill). Other details are as in the legend of Figure 2.1.

* indicates significance in MW-U tests at an error rate of 5%, adjusted according to Bonferroni-Holm, “ns” indicates non-significance in such tests. Statistical results are documented in Table 2.3, respectively. Underlying preference scores and memory scores separated by sex are shown in Extended Data Figure 2.6 and Extended Data Figure 2.7, respectively.

Table 2.3: Summary experimental design and statistics Figure 2.3

ISI	KKW test	MWU test			OSS test	
		Groups	*U*	*p*	Group	*p*
-100	H(9, N=363) =194.38; p<0.05	Control vs TH-RNAi	325	<0.05/3	Control	0.860
					TH-RNAi	<0.05/3
-15		Control vs TH-RNAi	350	<0.05/5	Control	<0.05/10
					TH-RNAi	<0.05/9
120		Control vs TH-RNAi	748	0.62	Control	<0.05/4
					TH-RNAi	<0.05/8
240		Control vs TH-RNAi	482	0.32	Control	<0.05/7
					TH-RNAi	<0.05/5
300		Control vs TH-RNAi	594	<0.05/4	Control	<0.05/6
					TH-RNAi	0.164

Sex based data separation

Separating behavioural data by sex is a major focus of our lab. But in aversive short-term memory so far never observed reliable differences between female and male flies. Indeed, for the control conditions summarized throughout the present study, memory scores do not differ between the sexes for trace, delay, or relief conditioning (Figure 2.4b). On examining the difference in memory scores of the TH-compromised cases minus the controls, however, it was surprising to find that specifically for trace conditioning (ISI -100s) the effect of compromising the TH function, which was significant in both sexes, was less pronounced in females than in males (Figure 2.4c). Two observations suggest that this sex difference is not a statistical artifact. Firstly, this sex difference can be discerned for both 3IY feeding as an acute, systemic (Extended Data Figure 2.4c, Extended Data Figure 2.4d) and for TH-RNAi as a constitutive, cell-specific intervention (Extended Data Figure 2.7). Secondly, when the brain-wide HPLC measurements of biogenic amines after 3IY feeding were separated by sex, this revealed only a non-significant tendency toward a decrease in dopamine levels in the females, whereas a significant decrease in dopamine levels was observed in the males (Extended Data Figure 2.5). This suggests that decreases in dopamine levels that in females remain below the significance threshold in brain-wide HPLC measurements (Extended Data Figure 2.5) can nevertheless have behavioural effects (Figure 2.4c), and that these behavioural effects are weaker in females than those produced by the more pronounced decreases in dopamine levels in males (Extended Data Figure 2.5, Figure 2.4c).

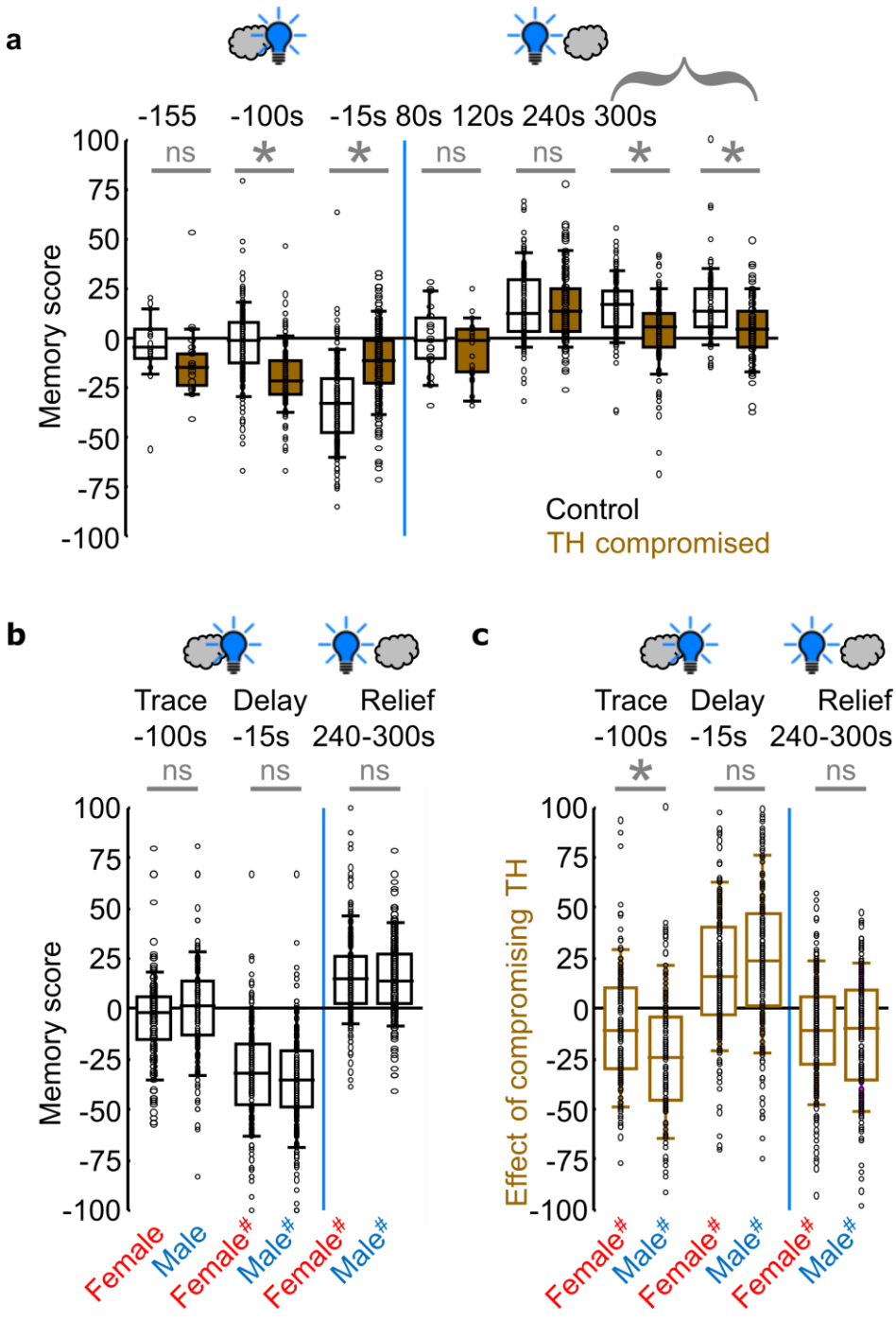

Figure 2.4 | Compromising TH function extends and blunts the temporal profile of PPL1-01 reinforcement.

a, Summary of the effects of compromising TH function on the temporal profile of PPL1-01 reinforcement, combined for 3IY and TH-RNAi, and across the present study. Shown are the memory scores of the respective control (open box plots) and TH-compromised cases (box plots with brown fill) (N= 20, 20, 120, 122, 159, 165, 20, 20, 101, 99, 108, 113, 62, 62).

b, Data for only the control cases shown in (a), separated by sex. Neither for trace conditioning (ISI -100s), nor for delay conditioning (ISI -15s), nor for relief conditioning (ISIs 240s and 300s) were sex-dependent differences observed (for a justification of why relief conditioning with ISIs of 80s and 120s is not included in this grouping see below) (N= 120, 120, 159, 157, 169, 169).

c, For the data in (a) the difference in memory scores of the TH-compromised cases minus the scores in the controls is plotted, separately for female and male flies, to quantify how strongly compromising TH function affects memory scores, in either sex. For trace conditioning (ISI -100s), the effect of compromising TH function was less pronounced in females than in males, whereas no such difference was observed for delay (ISI -15s) and relief conditioning (N= 118, 119, 159, 157, 168, 167). For relief conditioning, data were considered only for those ISIs for which compromising TH function had an effect to begin with (a: 240s and 300s).
Other details are as in the legend of Figure 2.1. * indicates significance in MW-U tests at an error rate of 5%, adjusted according to Bonferroni-Holm, “ns” indicates non-significance in such tests. “#” indicates significance in OSS-tests at an error rate of 5%, adjusted according to Bonferroni-Holm. Statistical results are documented in Table 2.4, respectively.

Table 2.4: Summary experimental design and statistics Figure 2.4

Figure	ISI	KKW test	MWU test			OSS test	
			Groups	*U*	*p*	Group	*p*
2.4a	-155	H(13, N=1191) =550.964; p<0.05	Control vs 3IY	112	0.018	Control	0.824
						3IY	<0.05/7
	-100		Control vs 3IY	3442	<0.05/7	Control	0.582
						3IY	<0.05/13
	-15		Control vs 3IY	6128	<0.05/5	Control	<0.05/14
						3IY	<0.05/9
	80		Control vs 3IY	161	0.298	Control	0.824
						3IY	1
	120		Control vs 3IY	4995	0.992	Control	<0.05/10
						3IY	<0.05/11
	240		Control vs 3IY	3687.5	<0.05/6	Control	<0.05/12
						3IY	<0.05/6
	300		Control vs 3IY	1267.5	<0.05/4	Control	<0.05/8
						3IY	0.04
2.4b	Trace	H(5, N=894) =431.922; p<0.05	Female vs Male	6195	0.062	Female	0.399
						Male	0.259
	Delay		Female vs Male	11158.5	0.103	Female	<0.05/6
						Male	<0.05/5
	Relief		Female vs Male	28199.5	0.62	Female	<0.05/4
						Male	<0.05/3
2.4c	Trace	H(5, N=888) =191.713; p<0.05	Female vs Male	5291	<0.05/3	Female	<0.05/1
						Male	<0.05/6
	Delay		Female vs Male	11164.5	0.105	Female	<0.05/5
						Male	<0.05/4
	Relief		Female vs Male	27708.5	0.695	Female	<0.05/3
						Male	<0.05/2

TPH enzyme inhibitor can reverse the effects of 3IY on trace conditioning

PPL1-01 is one of a total of 12-15 dopaminergic neurons in the PPL1 cluster, and specifically in the subset of six of these that innervate the mushroom body (Mao and Davis, 2009; Aso et al., 2014c, 2014a; Li et al., 2020). It has been reported that within the PPL1 cluster there is at least one neuron that is not only immunoreactive against TH but also against serotonin, and that constitutively compromising TH function by genetic means can both increase the number of anti-serotonin immunoreactive neurons in the PPL1 cluster and alter the pattern of anti-serotonin immunoreactivity in the mushroom body, specifically at the tips of the α and α' lobes, which receive both dopaminergic and serotonergic input (Niens et al., 2017). Preliminary results suggested that the used method for acutely lowering dopamine levels by 3IY left the number of anti-serotonin immunoreactive neurons in the PPL1 cluster unchanged but altered patterns of serotonin-immunoreactivity in a way similar to what was previously reported (Niens et al., 2017). This encouraged me to test whether downregulating serotonin synthesis would alter the effects we observed by feeding 3IY. To test for this possibility, I used para-chlorophenylalanine (PCPA), an inhibitor of the tryptophan hydroxylase enzyme (TPH) (Figure 2.5a).

For trace conditioning (ISI -100s), the increase in punishment memory caused by 3IY was fully reversed by an additional feeding of PCPA (Figure 2.5b). For delay conditioning (ISI -15s), the 3IY-induced decrease in punishment memory was only partially reversed by PCPA. For relief conditioning (ISI 240s), however, the decrease in relief memory through 3IY was not moderated by PCPA. Under low-dopamine conditions, the additional feeding of PCPA thus had a graded effect on memory scores, in the sense that it was strong for trace conditioning (ISI -100s) and tapered off as the ISIs were increased to -15s and 240s. Of note is that feeding PCPA alone, that is feeding PCPA under conditions of normal dopamine levels, had no effect on either form of conditioning (Figure 2.5c) (see Extended Data Figure 2.8 and Extended Data Figure 2.9 for the underlying preference scores and memory scores separated by sex, respectively).

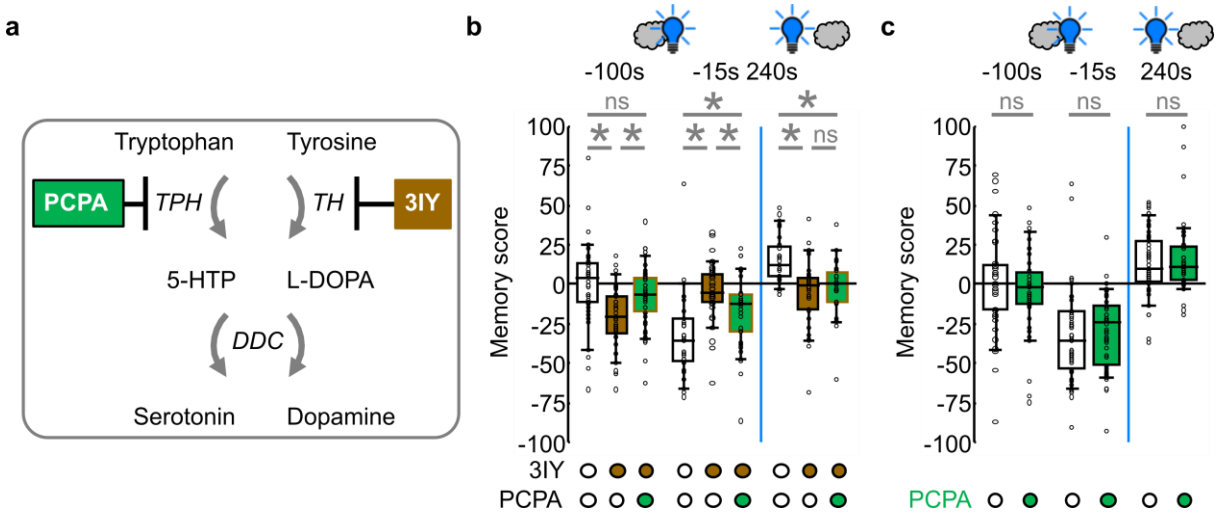

Figure 2.5 | Temporal profile of PPL1-01 reinforcement upon pharmacologically inhibiting the TPH and the TH enzyme.

a, Schematic of serotonin and dopamine biosynthesis, of the inhibition of tryptophan hydroxylase (TPH) by para-chlorophenylalanine (PCPA), and of the inhibition of tyrosine hydroxylase (TH) by 3-iodo-L-tyrosine (3IY), respectively. 5-HTP: 5-hydroxytryptophan; L-DOPA: 3,4-dihydroxy-L-phenylalanine; DDC: dopamine decarboxylase. Drug feeding was performed by the food method.

b, Relative to controls, punishment memory after odor→PPL1-01 trace conditioning (ISI -100s) is increased upon feeding of 3IY, an effect that is partially reversed by an additional feeding of PCPA (N= 38, 39, 45). For delay conditioning (ISI -15s), punishment memory is reduced by 3IY, an effect that is partially reversed by PCPA (N= 29, 33, 32). The reduction of relief memory (ISI 240s) by 3IY was not reversed by PCPA (N=25, 28, 29).

c, PCPA alone has no effect on punishment memory after trace conditioning (ISI -100s) (N= 39, 39) or delay conditioning (ISI -15s) (N= 45, 48) and leaves relief memory intact, too (ISI 240s) (N= 44, 41).
Open box plots and circles refer to the control condition, brown and green fill to groups fed with 3IY or with 3IY plus PCPA, respectively. Flies were of the genotype PPL1-01>ChR-2XXL. Other details are as in the legend of Figure 2.1.
indicates significance and “ns” non-significance in MW-U tests at an error rate of 5%, adjusted according to Bonferroni-Holm. Statistical results are documented in Table 2.5, respectively. Underlying preference scores and memory scores separated by sex are shown in Extended Data Figure 2.8 and Extended Data Figure 2.9, respectively.

Table 2.5: Summary experimental design and statistics Figure 2.5

Figure	ISI	KKW test	MWU test			OSS test	
			Groups	*U*	*p*	Group	*p*
2.5b	-100	H(2, N=122) =17.433; p<0.05/2	Control vs 3IY	358	<0.05/3	Control	0.871
			3IY vs 3IY+PCPA	556	<0.05/2	3IY	<0.05/3
			Control vs 3IY+PCPA	663	0.08	3IY+PCPA	<0.05/2
	-15	H(2, N=94) =21.727; p<0.05/3	Control vs 3IY	163	<0.05/3	Control	<0.05/3
			3IY vs 3IY+PCPA	340	<0.05/1	3IY	0.296
			Control vs 3IY+PCPA	283	<0.05/2	3IY+PCPA	<0.05/2
	240	H(2, N=82) =15.749; p<0.05/1	Control vs 3IY	156	<0.05/2	Control	<0.05/3
			3IY vs 3IY+PCPA	389	0.792	3IY	1
			Control vs 3IY+PCPA	163	<0.05/3	3IY+PCPA	0.851
2.5c	-100	H(5, N=255) =17.433; p<0.05	Control vs PCPA	656	0.389	Control	1
						PCPA	0.296
	-15		Control vs PCPA	956	0.342	Control	<0.05/5
						PCPA	<0.05/6
	240		Control vs PCPA	892.5	0.937	Control	<0.05/4
						PCPA	<0.05/3

Discussion

In this study, my results report that compromising TH function, either acutely by pharmacological means (Figure 2.1, Extended Data Figure 2.2, Figure 2.5) or by cell-specific RNAi (Figure 2.3), extends and blunts the temporal profile of PPL1-01 reinforcement. Specifically, it improves trace conditioning (ISI -100s), impairs delay conditioning (ISI -15s), and abolishes relief conditioning for longer intervals (ISIs 240s and 300s) (Figure 2.4a).

Relief conditioning in short versus long ISIs, and the relation to 'frustration' conditioning

The obtained results of the present study on relief conditioning with PPL1-01 reinforcement can reconcile earlier reports by König et al. (2018, loc. cit. figure 5) and Aso et al. (2019, loc. cit. figure 5, supplementary figure 3C). Those two studies differ in a number of ways, making it difficult to quantitatively relate the ISIs that were used. Differences include the use of a two-arm T-maze versus a horizontal, 4-field arena setup, and the use of ChR2XXL versus CsChrimson-Venus as the optogenetic effector, respectively. Nonetheless, by mapping out multiple ISIs, the present results confirm the TH-independence reported by König et al. (2018) for short relief ISIs, whereas for longer relief ISIs they are consistent with the TH-dependence reported by Aso et al. (2019).

The PPL1-01 neuron innervates the elongated axons of the mushroom body neurons as they pass through the γ1pedc compartment (Tanaka et al., 2008) (Figure 2.1a), one of the two known punishment compartments in the mushroom body. Upon delay conditioning with PPL1-01, a memory trace is established as a compartmentally local presynaptic depression of output synapses of those mushroom body neurons that are activated by odour, reducing drive to the approach-promoting compartmental output neuron (Hige et al., 2015). However, it is not clear whether upon relief conditioning with PPL1-01 the memory trace is likewise localized, and whether it would manifest, conversely, as synaptic potentiation. Using a single, short ISI, indeed, the results of Hige et al. (2015) did not suggest so. This prompted speculation that signalling from PPL1-01 to dopaminergic neurons outside the γ1pedc compartment may be involved in relief conditioning (König et al., 2018), possibly via multiple synaptic steps including the PAM-07 DANs (Aso et al., 2014; Li et al., 2020). Such heterotopy would contrast with the homotopy suggested by the results of Handler et al. (2019) for the other known punishment compartment (γ2) as well as for the two known reward compartments (γ4 and γ5) (the γ1pedc and γ3 compartments were not studied). That is, in these cases Handler et al. (2019) found that timing-dependent valence reversal manifests as depression/ potentiation within the same compartment.

A dissociation between trace versus delay conditioning

In this study, I showed a dissociation between trace and delay conditioning with PPL1-01 reinforcement. Trace conditioning, surprisingly, is improved by compromising TH function, whereas as expected (König et al., 2018; Aso et al., 2019) delay conditioning is impaired (Figure 2.4a, ISIs -100s versus -15s). This adds to earlier evidence that trace and delay procedures engage partially distinct downstream mechanisms in odour-shock associative learning. Mutants in the rutabaga gene, coding for the type I adenylate cyclase which acts as a molecular coincidence detector for this association, are unaffected in trace conditioning but are impaired in delay conditioning (Shuai et al., 2011). In turn, expression of a dominant-negative form of the Rac protein improves trace conditioning but leaves delay conditioning unaffected (Shuai et al., 2011). In addition, with a visual learning paradigm, (Grover et al., 2022) showed a selective role for the dopamine receptor Dop2R (CG33517) for trace but not delay conditioning.

Trace and delay conditioning certainly also share common features. For odour-shock associations these commonalities include impairment in mutants lacking Synapsin (Niewalda et al., 2015), the asymptotic memory strength upon repeated training trials (albeit reached at a slower rate for trace conditioning), the rate of memory decay, the profile of generalization (Galili et al., 2011), the likely site of the memory trace in the mushroom body, and their requirement of the dopamine receptor Dop1R1 (CG9652) (Shuai et al., 2011) (also see Grover et al., 2022).

Serotonin in trace conditioning – under low-dopamine conditions

Here I showed a decrease in brain-wide levels of dopamine rather than serotonin obtained by pharmacologically compromising TH function (Figure 2.2). Further, both this decrease in dopamine levels and the abovementioned effects on reinforcement learning were rescued by L-DOPA (Figure 2.1g, Figure 2.2). Interestingly, under low-dopamine conditions our results uncover a role for serotonin that is particularly strong for trace conditioning (ISI -100s), and that tapers off with increasing ISIs (Figure 2.5b). Under conditions of normal dopamine levels, however, these data do not provide evidence for a role of serotonin (Figure 2.5c); it is unclear whether this is at variance with the experiments reported by (Zeng et al., 2023), as these lacked critical genetic and procedural controls.

Implications

One may view, at a cognitive level, long-gap trace-conditioned cues as providing no evidence, and delay- and relief-conditioned cues as providing respectively evidence for and evidence against the causation of punishment. In a human subject at least, the temporal profile of reinforcement upon compromising TH function as found in the present study on flies (Figure 2.4a) would thus imply a state in which causality is attributed to cues that do not merit it, whereas credible evidence in favour of as well as credible evidence against the causation of punishment is not properly appreciated. Such a state may promote delusional beliefs about causal event structure, which are a hallmark symptom of schizophrenia (Garety et al., 2005; Moritz and Woodward, 2005; Moritz et al., 2005; Uhlhaas and Silverstein, 2005; Dudley et al., 2016; McCutcheon et al., 2019). Regarding flies, this study remains expressly agnostic as to whether their behaviour might be based on causal beliefs and whether schizophrenia-like states might be the result when the temporal profile of reinforcement is distorted as reported here.

In practical terms, the present study shows that mapping out the full 'fingerprint' of reinforcement across multiple temporal intervals may be required to understand how a given manipulation affects reinforcement learning. Indeed, my results (Figure 2.4a) provide a case of an experimental manipulation where focusing solely on any one single interval between odour and reinforcement will lead to drastically different conclusions, namely that memory is improved, impaired, or unaffected, depending on which interval is chosen. It therefore seems possible that apparent discrepancies in the literature can be resolved through mapping the full temporal profile of reinforcement.

Chapter 2 Extended Data Figures

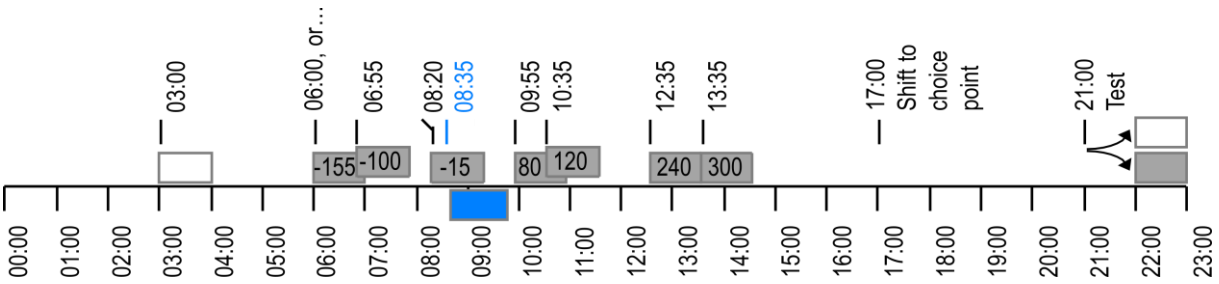

Extended Data Figure 2.1 | Timing of odour presentation and PPL1-01 activation by blue light.

At 0:00 min, the flies were gently loaded into the experimental setup. From 3:00 min on, the reference odour (white box) was presented for 1 min. For the optogenetic activation of the PPL1-01 neuron, blue light (blue box) was applied at 8:35 min for 1min with the help of 24 LEDs of 465 nm peak wavelength mounted on the inner surface of 2.5 cm-diameter and 4.5 cm-length hollow cylinders. These cylinders were fitted around transparent training tubes harbouring the flies. Blue light was applied as 12 pulses, each 1.2-sec long and followed by the next pulse with a 5 sec onset-to-onset interval. The absolute irradiance in the middle of the training tube during blue light pulses was 200 $\mu W/cm^2$ as measured with an STS-VIS Spectrometer (Ocean Optics). The paired odour (grey box) was presented for 1 min, too, at the onset-to-onset inter-stimulus-intervals (ISIs) from the blue light as indicated by the numbers within the grey boxes (s). Negative ISI values indicate that the presentation of the paired odour started before the blue light (ISIs -155s, -100s and -15s); positive ISIs indicate the reverse order of events (ISIs 80s, 120s, 240s and 300s). The onset times for all ISIs are indicated above. At 17:00 min the flies were shifted to the choice point between the odours. At 21:00 min the test started, and the flies were released into the T-maze. After 2 min the arms of the maze were closed, and the flies on each side were counted, separated by sex.

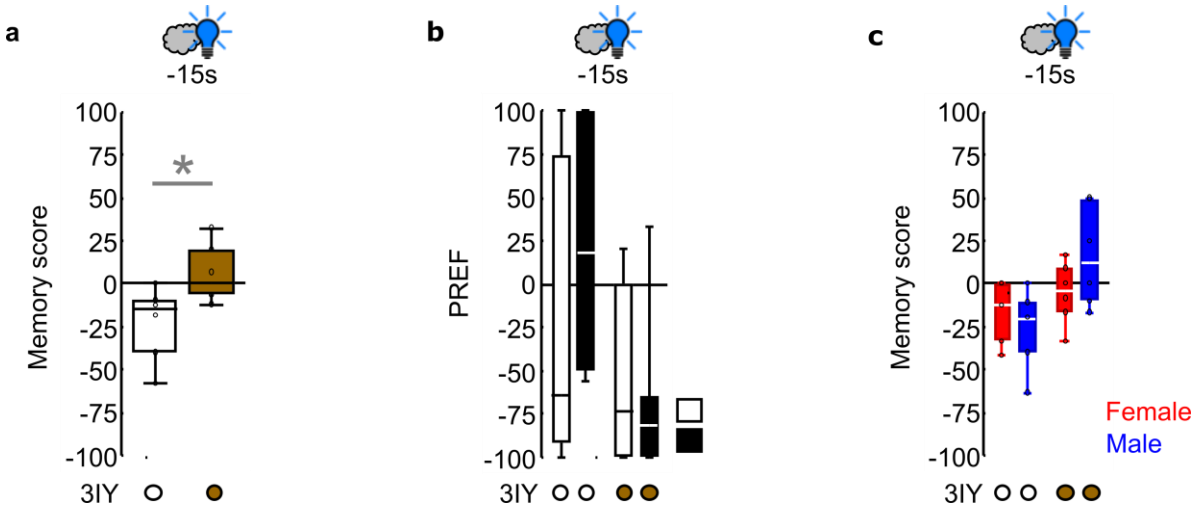

Extended Data Figure 2.2 | Repetition of the experiment in Figure 2.1d (ISI -15s).

(**a-c**) Repetition of the experiment shown in Figure 2.1d, for the ISI of -15s. Box plots represent the median as the middle line, 25%/75% quantiles as box boundaries, and 10%/90% quantiles as whiskers. The grey clouds depict the paired odor, and the blue light bulb PPL1-01 activation, presented with the indicated temporal relationship. (a) Memory scores, determined according to equation 2, for the control condition (open box plot, N= 6) and the 3IY-fed case (brown fill, N= 6). * Indicates significance in a MW-U test. (b) Preference scores, calculated according to equation 1, underlying the data from (a). Open box plots show benzaldehyde preference after BA was paired with PPL1-01 activation and OCT served as a reference odour (BA+); black fill indicates BA preference after OCT was paired with PPL1-01 activation and BA served as a reference odour (OCT+). (c) Data from (a), separated by sex. Red fill of the box plots refers to data from females, blue fill to data from males. Open circles below the panels refer to the control conditions, brown fill to the 3IY-fed cases. Other details as in the legend of Figure 2.1.

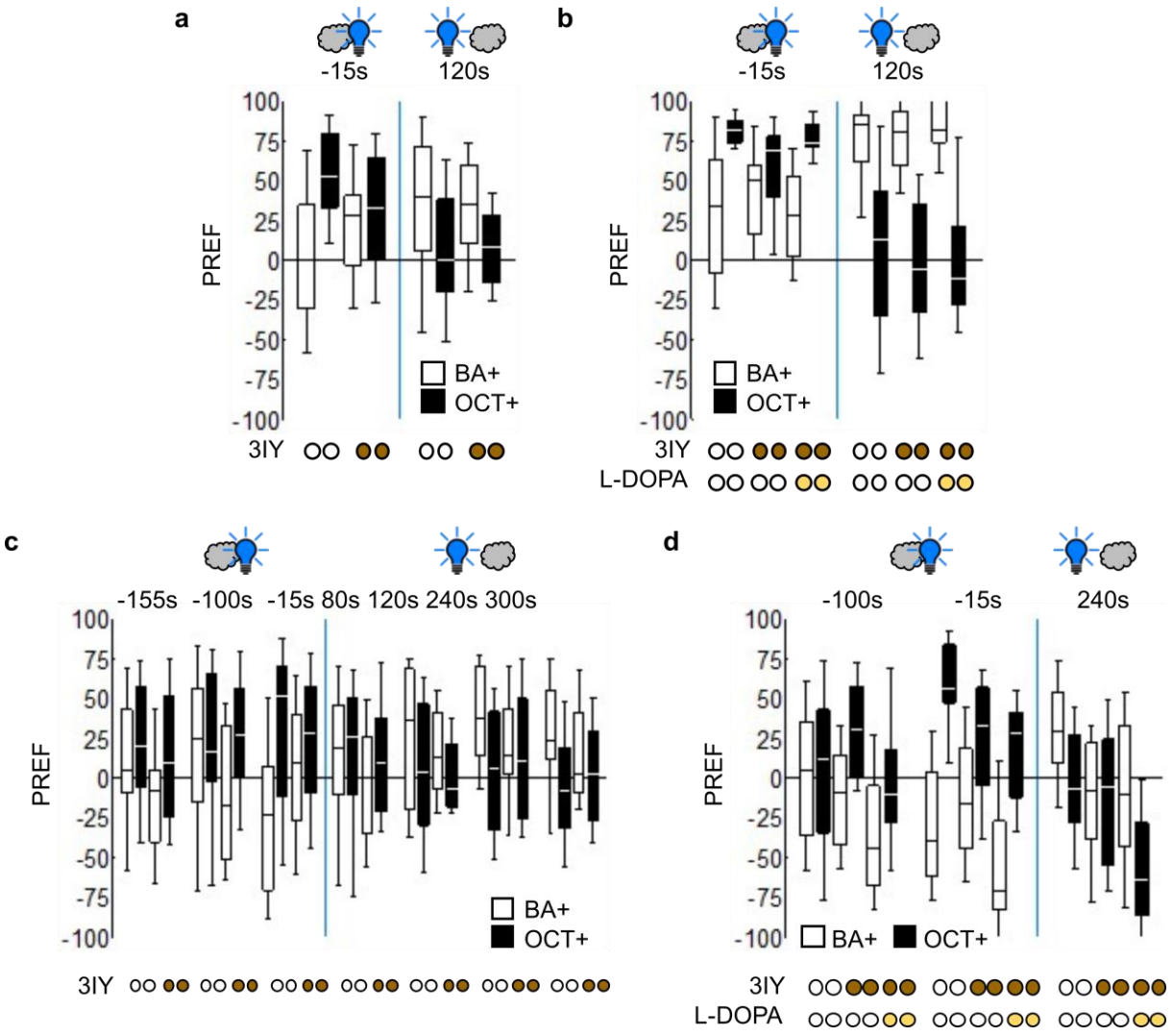

Extended Data Figure 2.3 | Underlying preference scores in Figure 2.1.

(a-d) Preference scores calculated from the choice between the odours benzaldehyde and octanol (BA, OCT) according to equation 1, and as underlying the memory scores in Figure 2.1d-g, respectively. Box plots represent the median as the middle line, 25%/75% quantiles as box boundaries, and 10%/90% quantiles as whiskers. Open box plots show benzaldehyde preference after BA was paired with PPL1-01 activation and OCT served as a reference odour (BA+); black fill indicates BA preference after OCT was paired with PPL1-01 activation and BA served as a reference odour (OCT+). The grey clouds depict the paired odour, and the blue light bulb PPL1-01 activation, presented with the indicated temporal relationship. Open circles below the panels refer to the control conditions, brown fill to the 3IY-fed cases, light brown fill to those additionally fed with L-DOPA. Other details as in the legend of Figure 2.1.

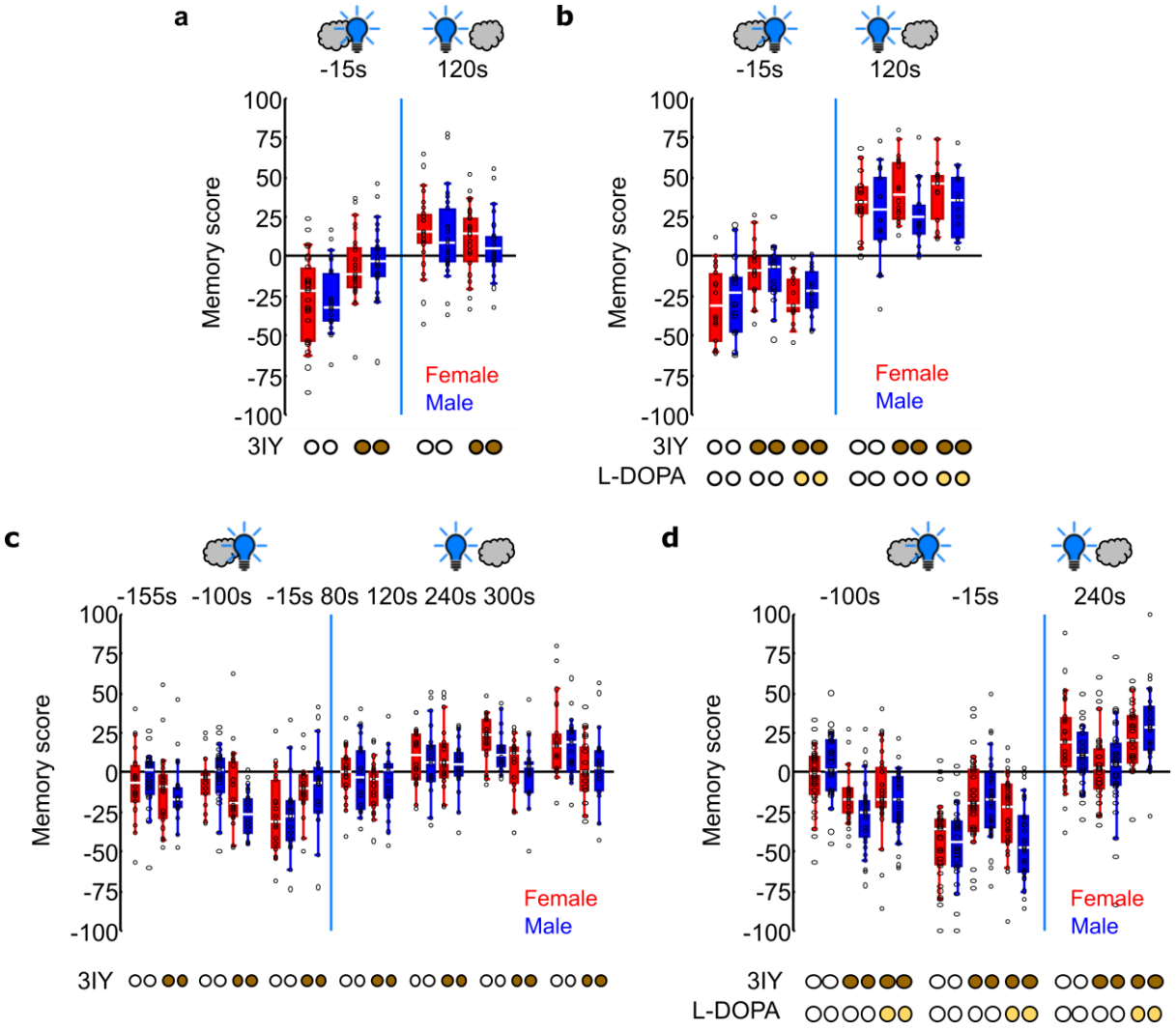

Extended Data Figure 2.4 | Memory scores from Figure 2.1 separated by sex.

(a-d) Memory scores from Figure 2.1d-g, respectively, separated by sex. Box plots represent the median as the middle line, 25%/75% quantiles as box boundaries, and 10%/90% quantiles as whiskers. Red fill of the box plots shows data from females; blue fill indicates data from males. The grey clouds depict the paired odour, and the blue light bulb PPL1-01 activation, presented with the indicated temporal relationship. Open circles below the panels refer to the control conditions, brown fill to the 3IY-fed cases, light brown fill to those additionally fed with L-DOPA. Other details as in the legend of Figure 2.1.

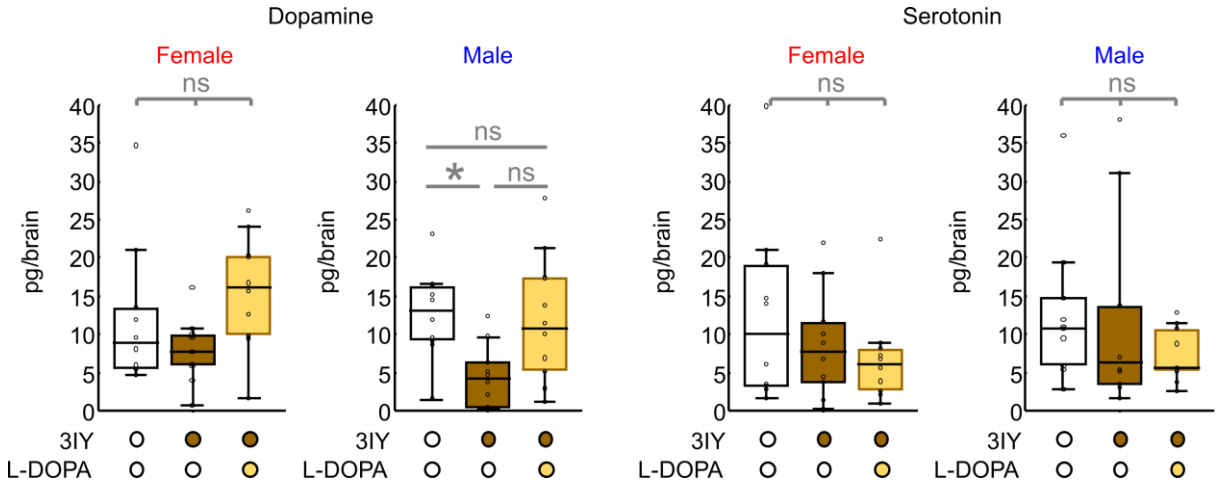

Extended Data Figure 2.5 | Levels of biogenic amines from Figure 2.2 separated by sex.

Brain-wide levels of dopamine (left) and serotonin (right) from Figure 2.2, separated for females and males as indicated. Box plots represent the median as the middle line, 25%/75% quantiles as box boundaries, and 10%/90% quantiles as whiskers. Open box plots and circles refer to the control condition, brown and light brown fill to groups fed with 3IY or with 3IY plus L-DOPA, respectively.
“ns” indicates non-significance in KW-tests, except for the case of dopamine measurements in males, where * and “ns” refer to significance and non-significance, respectively, in MW-U tests at an error rate of 5%, adjusted according to Bonferroni-Holm. Other details as in the legend of Figure 2.2.

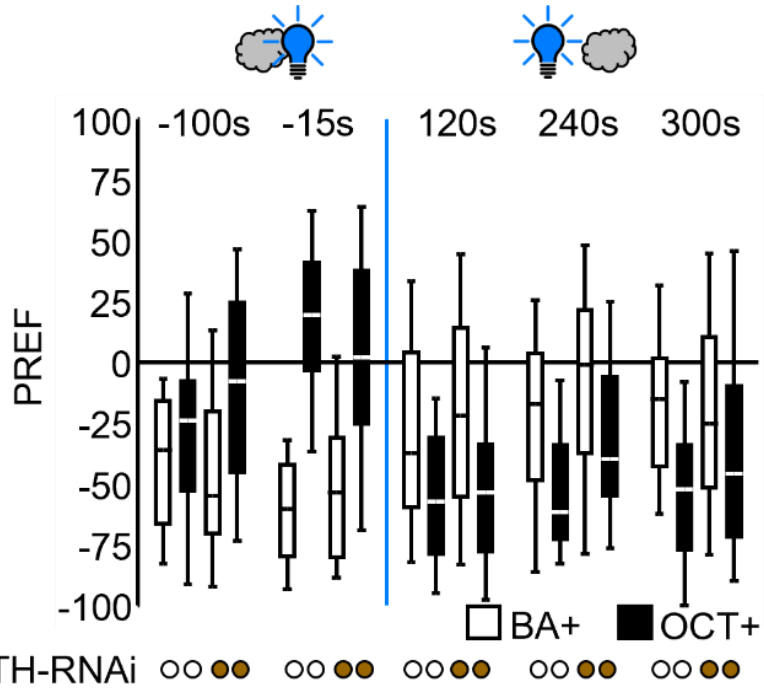

Extended Data Figure 2.6 | Underlying preference scores in Figure 2.3.

Preference scores calculated from the choice between the odours benzaldehyde and octanol (BA, OCT) according to equation 1, and as underlying the memory scores in Figure 2.3. Box plots represent the median as the middle line, 25%/75% quantiles as box boundaries, and 10%/90% quantiles as whiskers. Open box plots show benzaldehyde preference after BA was paired with PPL1-01 activation and OCT served as a reference odour (BA+); black fill indicates BA preference after OCT was paired with PPL1-01 activation and BA served as a reference odour (OCT+). The grey clouds depict the paired odour, and the blue light bulb PPL1-01 activation, presented with the indicated temporal relationship. Open circles below the panels refer to the control conditions, brown fill to the cases with RNAi against TH. Other details as in the legend of Figure 2.1.

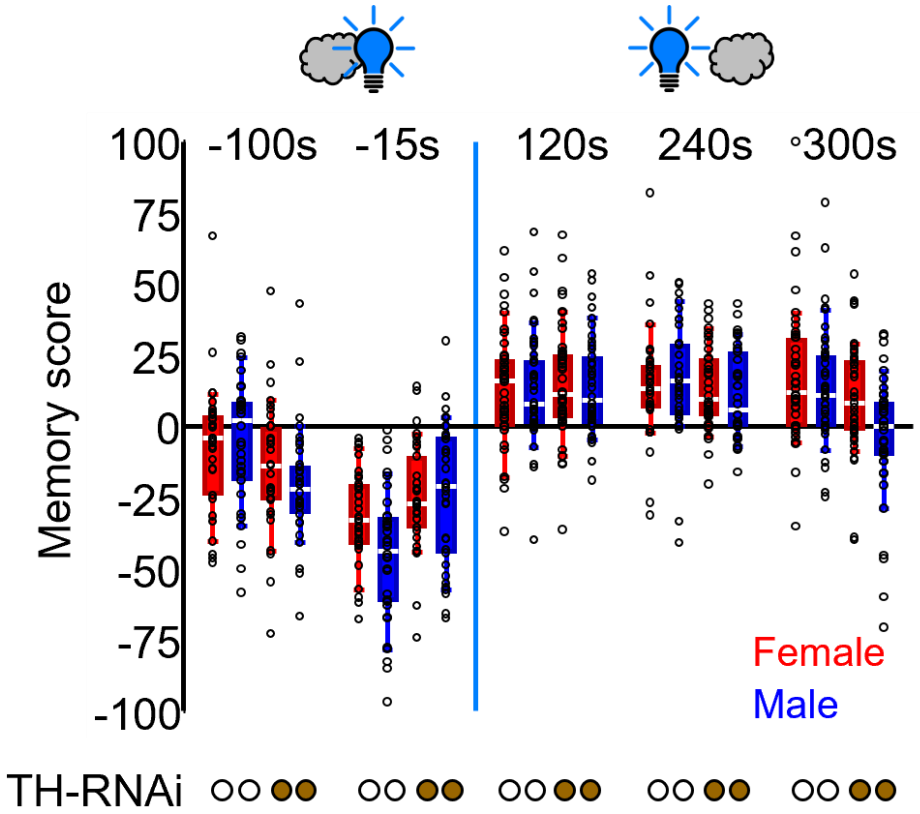

Extended Data Figure 2.7 | Memory scores from Figure 2.3 separated by sex.

Memory scores from Figure 2.3b, separated by sex. Box plots represent the median as the middle line, 25%/75% quantiles as box boundaries, and 10%/90% quantiles as whiskers. Box plots with red fill show data from females; blue fill indicates data from males. The grey cloud depicts the paired odour, and the blue light bulb PPL1-01 activation, presented with the indicated temporal relationship. Open circles below the panels refer to the control conditions, magenta fill to the cases with RNAi against TH. Other details as in the legend of Figure 2.1.

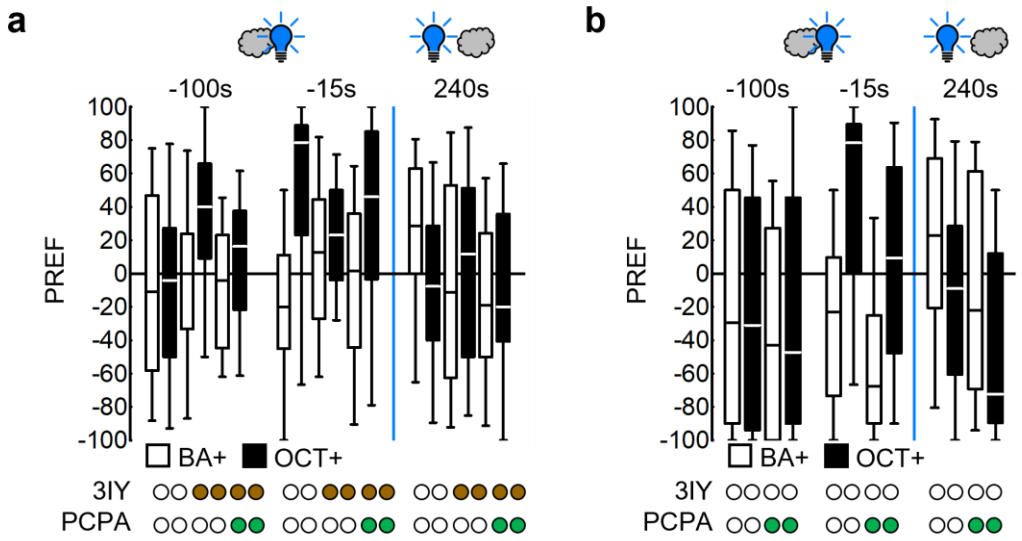

Extended Data Figure 2.8 | Preference scores underlying the memory scores in Figure 2.5.

(a-b) Preference scores calculated from the choice between the odours benzaldehyde and octanol (BA, OCT) according to equation 1, and as underlying the memory scores in Figure 2.5b and c, respectively. Box plots represent the median as the middle line, 25%/75% quantiles as box boundaries, and 10%/90% quantiles as whiskers. Open box plots show benzaldehyde preference after BA was paired with PPL1-01 activation and OCT served as a reference odour (BA+); black fill indicates BA preference after OCT was paired with PPL1-01 activation and BA served as a reference odour (OCT+). The grey clouds depict the paired odour, and the blue light bulb PPL1-01 activation, presented with the indicated temporal relationship. Open circles below the panels refer to the control conditions, brown fill refers to feeding with 3IY, and green fill to feeding with PCPA in addition. Other details as in the legend of Figure 2.1.

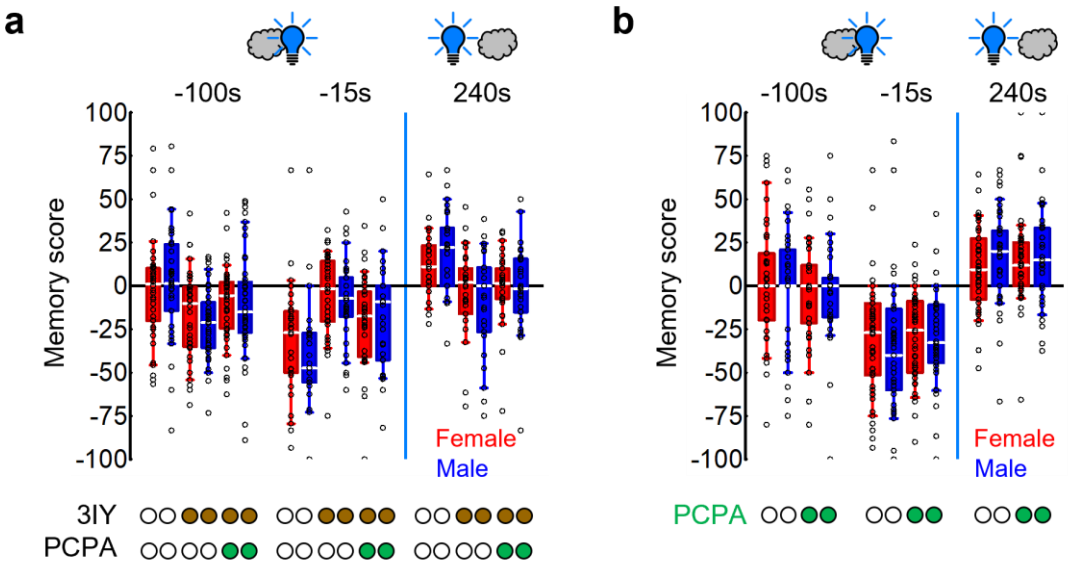

Extended Data Figure 2.9: Memory scores from Figure 2.5 separated by sex.

(a-b) Memory scores from Figure 2.5b and c, respectively, separated by sex. Box plots represent the median as the middle line, 25%/75% quantiles as box boundaries, and 10%/90% quantiles as whiskers. Red fill of the box plots shows data from females; blue fill indicates data from males. The grey clouds depict the paired odour, and the blue light bulb PPL1-01 activation, presented with the indicated temporal relationship. Open circles below the panels refer to the control conditions, brown fill refers to feeding with 3IY, and green fill to feeding with PCPA in addition (a) or PCPA alone (b). Other details as in the legend of Figure 2.1.

General discussion

In this thesis, my focus was to investigate the relationships between action, valence and dopamine in adult fruit flies, *Drosophila melanogaster* and to investigate the biomedical implications of this relationship.

In Chapter 1, I performed behavioural experiments, including novel paradigms developed in the course of this study, optogenetic and pharmacological manipulations and two photon *in vivo* calcium imaging and discovered how avoidance and in particular backward locomotion can confer negative valence by engaging punishing dopaminergic neurons. I further showed that re-afferent feedback is necessary for such dopamine neuron activation. With collaborators I further found by connectome analysis, computational modelling and behavioural optogenetics that the “moonwalker descending neurons” are a part of the memory efferent pathways for learned avoidance and that the uncovered processes can maintain successful learned avoidance as a counterforce of extinction learning. These findings, as I argue, can shed new light on the much-debated “avoidance paradox” as known in experimental psychology and, should similar processes be at work in humans, can have implications for exposure therapy in fear and anxiety disorder.

In Chapter 2, I investigated event timing as a fundamental aspect of valence processing. Specifically, I studied the role of dopamine by systemic pharmacological and neuron specific genetic manipulation in the punishing dopaminergic neuron PPL1-01. This revealed a complex profile of dopaminergic and non-dopaminergic mechanisms across the profile of event timings (i.e. trace, delay and relief conditioning), which prompted me to discuss a disturbed dopamine-serotonin balance as an endophenotype for both positive and cognitive symptoms in schizophrenia.

Both chapters were written in the intention to submit them for publication in space-restricted journals and hence include the kind contributions of my collaborators as acknowledged in both chapters. For the present General Discussion, I would like to take the opportunity to widen the discussion to provide a more comprehensive summary and outlook than is typically possible given the mentioned space restrictions.

Valence from action

Walking back to the moonwalker descending neurons (MDNs)

Animals usually move forwards. But when they fear or face any impediment or predator on their way, they typically slow down and switch to a situationally adaptive behaviour. Such adaptive behaviour can range from taking the risk and resuming the initial direction, removing the obstacle or fighting the threat, hiding, avoiding or escape. In *Drosophila*, such an escape consists of jumping and flight, if possible. However, when they encounter an unpassable obstacle e.g. dead end of a path, flies initiate backward walking to avoid the hindrance, turn and resume a novel walking direction. Backward walking is initiated by descending command neurons called the moonwalker descending neurons (MDNs) projecting from the brain to local motor circuits in the ventral nerve cord (Bidaye et al., 2014; Feng et al., 2020). Also activating MDNs by thermogenetics induces backward walking while silencing them abolished walking backward (Bidaye et al., 2014).

The MDNs comprise two pairs of DNs per hemisphere, having their soma in the medial posterior protocerebrum, with their bilateral dendritic arborization in the lateral accessory lobes (LALs) and projecting their axons until thoracic ganglia contralaterally (Bidaye et al., 2014; Namiki and Kanzaki, 2016). Pre and post synaptic sites of MDNs are observed in LALs as well as in leg neuropils, with postsynaptic sites mostly in the LAL and presynaptic sites mostly in the leg neuropils (Bidaye et al., 2014; Figure 1.1a, Extended Data Figure 1.1). Previously it was shown that the MDNs receive visual input and trigger backward walking. It has been demonstrated that visual projection neurons, the lobula columnar cells (LC16) induce backward walking by acting via MDNs (Sen et al., 2017) and silencing MDNs eliminates the LC16 triggered retreat in *Drosophila* (see Supplement Figure 15). Another interesting observation was that activating MDNs of one side causes contralateral backward turn. Hypothetically, visual threat from one side preferentially activates LC16 ipsilaterally, so as ipsilateral MDNs and thus causes contralateral turning. Accordingly bilateral activation of MDNs induces backward walking.

Similarly, mechanosensory cues can also initiate backward walking (Sen et al., 2019). The neurons conveying this mechanosensory input are still under investigation. However, a pair of ascending neurons named Two Lumps Ascending neurons (TLA) was identified as conveying feedforward mechanosensory stimuli to MDNs. Thus, TLAs can activate backward walking via the MDNs to mediate touch-evoked retreat. Accordingly, in darkness, activation of neurons expressing the mechanosensory channel NOMPC (No mechanoreceptor potential C) leads to

increased calcium response in TLAs and triggers backward walking (Walker et al., 2000; Ramdya et al., 2015; Sen et al., 2019).

The transition of forward to backward walking happens with a leg kinematics shift- from swing to stance phase in forward moving legs and stance to swing phase in backward moving legs. This kinematics is applicable in all 3 pairs of legs with the strongest impact on the hind legs T3 segment. The most prominent feature during the stance phase of backward walking is tibial flexion and femoral elevation in synchrony, leading to folding up the leg and pulling the body backwards. Anatomical and functional approaches have identified several dozens of candidates MDN target cells in the VNC. However, two of them have been identified as the most critical MDN-effector neurons for hindleg movements in backward walking: LBL40 mediating power stroke of the stance phase and LUL130 to mediate elevation at the beginning of the swing phase (Feng et al., 2020). Moreover, despite the differences in bodily organization and despite having different modes of locomotion in larval and adult Drosophila, these MDNs are present in both life stages (in the larval stage, they are known as mooncrawler neurons (Carreira-Rosario et al., 2018) and indeed persist through metamorphosis to conduct backward crawling or backward locomotion, respectively.

The trinity: Action, Valence, Dopamine

A central question of behavioural neuroscience is how perception, responsiveness and action selection are neuronally organized. Till today, our thinking is guided by the two philosophical approaches: 1) ethology – emphasizing the importance of evolutionarily inherited information, and 2) behaviourism- focusing on information collection through perception and action (Byrne, 2017). While ethology benefited from Darwin's theory of evolution providing a conceptual framework of information flow, behaviourism on the other hand, gained strength from laboratory-based experimentation. Yet, we are aware both of these approaches have their genuine merits, and limitations. Inspired in addition by research with a clinical background, the 'emergent new science of mind' (Kandel, 2007) employs mechanistic approaches to dealing with behaviour, theory and systematic functions of the brain. It also endeavours to understand psychological occurrences in neurobiological terms. In this context, I moved with a mechanistic approach to investigate the mutual causation between '*feeling bad'* from avoidance by backward locomotion and track down the role of dopamine in this process, which in this segment I would like to put into perspective.

The initial step was to get into whether inducing backward locomotion can convey negative reinforcement. To do so, backward locomotion was induced by optogenetically activating (either ChR2XXL^{A} or Chrimson^{A}) a broader set of moonwalker descending neurons driven by VT050660-Gal4 (Moonwalker^{A}) (Bidaye et al., 2014) (see Supplemental Table S1 for detail genotypes) and

found that odours presented during such backward locomotion can acquire negative valence (Figure 1.1, Figure 1.2a-b, Figure 1.4a, left). I also probed that the stability of this punishment memory was almost 2-4 hours (Figure 1.2a) and thus remained within the range of short term to intermediate term memory (review: Davis, 2023; early studies review: Tomchik and Davis, 2013). As the fundamental properties of reinforcer is that it has effects of opposite valence depending on timing (please see General Introduction and Chapter 2), I investigated the temporal reinforcement profile of moonwalker descending neurons by using different interstimulus intervals (Figure 1.3) and established a qualitatively similar temporal fingerprint of timing dependent valence reversal as shown previously for punishing dopaminergic neuron- PPL1-01(Aso and Rubin, 2016; König et al., 2018; Aso et al., 2019; Amin et al., 2025) and electric shock (Tanimoto et al., 2004; Yarali et al., 2008). Given that dopaminergic neurons are known to convey reinforcement signals across the animal kingdom and in flies (Schultz et al., 1997; Dickinson, 2001; Waddell, 2013; Schultz, 2015), next I investigated the role of dopamine for moonwalker reinforcement. With acute systemic pharmacological manipulation by 3IY, I found that moonwalker punishment- and relief-memory was dopamine biosynthesis dependent, and the reduction of both memories was reversible by additional L-Dopa feeding (Figure 1.4a). Odour choice was unaffected, and with our collaborators we could show that these treatments did not affect the backward locomotion of flies itself (Figure 1.4b, Extended Data Figure 1.2, performed in Bidaye lab).

Altogether, this showed that activation of the moonwalker neurons and thus inducing backward locomotion during odour presentation can establish aversive associative memory which is dopamine dependent. Together, these led me to address the question: ***why*** and ***how*** is activating MDNs that induce backward walking punishing and engaging the dopamine system?

To do so, I proceed with two working hypotheses:

1) MDNs are part of the output pathway from the mushroom body to learned avoidance behaviour, that is of memory – efferent circuits (see next section)

2) There is some form of feedback from MDNs to punishing DANs (see subsequent section).

A component of memory - efferent circuit: MBONs→LALs→MDNs

The mushroom bodies play a role as convergence site for associative learning. How this association takes place and gets implemented into learned behaviour, I have discussed in detail in the general introduction section. In short, the formation of associative memories in the mushroom body is that the coincidence of activation by odour and DAN signals is detected in the KCs, and this coincidence then is turned into a modification in the strength of the KC - MBON

synapses for those KCs that are part of the odour representation (see detail in General Introduction). As a general rule, punishing DANs entangle with approach promoting MBONs and rewarding DANs with avoidance promoting MBONs (Aso et al., 2014b; Owald et al., 2015). Fittingly, as a result of odour-shock coincidence, for example, the strength of the synapses between odour - coding KCs and approach - promoting MBONs get reduced, such that the unabated connection of the KCs with the avoidance - promoting MBONs leads to net learned avoidance behaviour (Hige et al., 2015).

So far, the only known efferent pathways of the mushroom body are MBONs (Tanaka et al., 2008; Aso et al., 2014a; Aso et al., 2014b). Although MBON efferent pathways are actively researched, the exact organization of the conditioned response pathways remains clouded. Let alone any evidence had found yet asking:

i) Are the MBONs connected to MDNs? and ii) Are MDNs part of the memory-efferent circuit?

In that regard, the prerequisite was to find a highly selective driver covering MDNs. Thus, I did a thorough systemic screening of highly selective MDNs driver (see supplement information section for additional parametric experiments, Supplement Figure 1-9, 12-14), and found activating a highly selective MDNs driver covering only 2 neurons per hemisphere convey punishing valence (Figure 1.5, Extended Data Figure 1.4c-d).

My finding paved the way for a collaborative connectome analysis (with the Ashok Litwin-Kumar and Salil Bidaye labs). Through that, we found, exclusively, 6 atypical MBON types: MBON30 coming out from (>) γ1γ2γ3, MBON35>γ2, MBON32>γ2, MBON27>γ5, MBON26>β'2d, MBON31>α'1a. These MBONs have significant innervation in 3 hubs of ventral neuropil LALs: LAL160,161; LAL171,172; LAL051 which put them in a bridging position to connect the MB to the MDNs (Figure 1.6b-e) (also see Chapter 1 result section and General Introduction for details). Importantly, a substantial share of these MBONs (MBON30, MBON35, MBON32) involve straightforwardly the three punishment processing compartments: γ1, γ2, γ3. Although, due to the unavailability of specific driver lines, the thorough systemic analyses of neurotransmitter effect could not be done, based on computational prediction (NeuPrint record), MBONs are classified as predicted cholinergic, glutamatergic and GABAergic. Acetylcholine has excitatory while GABA and likely also glutamate have inhibitory effects in insect central brain synapses (Liu and Wilson, 2013; Shiu et al., 2024). Under this assumption at least, after odour-shock association, KC-MBON synapses in these three punishment processing compartments: γ1, γ2, γ3 get depressed (Hige et al., 2015). In such situation, for example, the inhibitory MBON30 is less active, releasing the

excitatory LAL160,161 from inhibition, leading to an activation of MDNs, backward locomotion and avoidance (see Extended Data Figure 1.10, General Introduction and upcoming section). While for the other MBONs coming out from reward processing compartments (MBON27>γ5, MBON26>β'2d, MBON31>α'1a), have both excitatory and inhibitory input to the downstream LALs. Interestingly, among all the MBONs, MBON26 (β'2) receives both excitatory and inhibitory input and together with MBON31 (α'1), MBON32 (γ2) and MBON27 innervate contralateral LAL (Li et al., 2020) and provide potential convergent push-pull input to downstream targets (see Chapter 1 discussion for further detail). Also, MBON30 receives direct central complex input and thus also suggests a potential linking role in these two major regions of fly brain (Li et al., 2020) during navigation.

After finding ***how*** the mushroom body is connected to MDNs, I tested whether MDNs are part of memory-efferent pathway. To achieve this after classical olfactory conditioning with odour-electric shock, during retrieval MDNs were silenced optogenetically by GtACR1. This revealed that punishment memory retrieval was significantly reduced. This shows that MDNs are part of memory-efferent pathways, exclusively for learned aversive memory expression but neither for the behavioural expression of learned appetitive memory nor for naïve odour choice behaviour (Figure 1.7, Extended Data Figure 1.3, also see supplement information for the broader moonwalker driver, Supplement Figure 5-6).

A case of feedback: MDNs→ DANs

I next proceed to find out the mechanistic process of ***how*** MDNs engage dopaminergic punishment (Figure 1.8). In previous anatomical and functional studies, direct and indirect feedback loops from the MBONs towards the DANs have been observed, suggesting a modification of DAN activity by mushroom body efferent pathways (Aso et al., 2014a; Eichler et al., 2017; König et al., 2019; Li et al., 2020), which is particularly important for extinction learning (see General Introduction and Chapter 1).

In my thesis, I asked whether activation of MDNs indeed activates the punishing DANs by using *in vivo* two photon calcium imaging. I took advantage of genetic tools that allowed me to simultaneously activate the MDNs and image the DANs (see Chapter 1 for more details) and found that activation of MDNs strongly increased calcium responses in DANs of the known punishment processing compartments γ1 and γ2 in comparison to respective genetic controls (Figure 1.9a-d) (Claridge-Chang et al., 2009; Mao and Davis, 2009; Aso et al., 2010a, 2012a; Cohn et al., 2015; Hige et al., 2015).

As a next step, I searched for all the horizontal lobe compartments γ1-5 and β’2 by expressing GCaMP in all the dopaminergic neurons (DANs) (Figure 1.10a-f, see Supplemental Table S1 for detail genotypes). Now I observed strongest calcium response once again in punishment processing compartments: γ1, γ2 and the more lateral region of the γ3 compartment (Figure 1.10 and Extended data Figure 1.6a-c’’) and weak calcium response in the medial aspect of γ3 as well as in γ4,5 and β’2, the reward processing compartments (Figure 1.10, Extended Data Figure 1.6a-c’’). The observed weak calcium responses and the slow ramping dynamics in the rewarding compartments (γ4, 5 and β’2) suggest an indirect relay coming from the punishing compartments (Figure 1.10d-f). Possibly, the sub-segmental increased calcium response in γ3 (lateral to medial) is likely based on the shared input from punishing PPL1-DANs of γ1, γ2 or rewarding PAM-DANs of γ4 compartments (Extended data Figure 1.5; Extended Data Figure 1.6; Li et al., 2020, Figure 39). Also, previously shown observation was DANs of opposite valence participate in an indirect relay from the γ2α'1 to the β'2a compartment to encode omission of a negative outcome and MBON-γ2α'1 is an excitatory upstream element of PAM-β'2a (McCurdy et al., 2021). In addition, learned avoidance was shown to involve depressed activity in the MBON-γ1pedc (MBON-11) and subsequent release from inhibition in the downstream avoidance-promoting MBONs of the γ5 and β’2 compartments (MBON-01, MBON-03) (Owald et al., 2015; Perisse et al., 2016).

In sum, I found a functional feedback pathway from MDNs to DANs, with preferentially strong engagement of the punishing DANs, suggesting a mechanism of ***how*** MDNs induced backward locomotion feeds back to negative valence (Figure 1.9, Figure 1.10).

This prompted me to ask for- how does that feedback come about?

An attribution of re-afference principle

My initial hypothesis was that this feedback is a case of recurrent - internal feedback from MDNs to DANs, and so we proceeded with systemic connectome analysis within the brain but found no credible evidence (Scheffer et al., 2020; Dorkenwald et al., 2024; Schlegel 2024). Also, our current knowledge of ascending input from the VNC did not suggest any such connection from MDNs to DANs (Takemura et al., 2024; Azevedo et al., 2024; Cheong et al., 2024). Furthermore, our collaborative investigation in *explant* brain and brain together with VNC preparation, where we optogenetically activated MDNs and imaged the DANs (performed in David Owald's lab), did not show any increased calcium response (Extended Data Figure 1.7). A full fly brain together with VNC connectome may shed some new light in future which is yet not accessible (Simpson, 2024).

Next, inspired from - *Das Reafferenzprinzip* - I considered external sensory feedback or *re-afference* (The Reafference Principle, 1950, von Holst and Mittelstaedt; (Fukutomi and Carlson, 2020; Jékely et al., 2021). Therefore, I proceeded to test for a role of *re-afferent* feedback.

To do so, I used a piece of cotton wool to restrict leg movement ('trapping'). The experiment was a combined optogenetic activation of MDNs with two photon *in vivo* calcium imaging of DANs, as I performed before (Figure 1.10) but under three conditions *with-without-with* allowing the leg movement of fly (Figure 1.11a-e). This experiment confirmed that, before trapping, once again, strong activation of DANs in γ1, γ2, γ3 which went down during trapping and was significantly recovered after removal of cotton wool.

This result shows evidence that it is the '*action*'- the execution of MDN evoked leg movement, that is required for activating the γ1, γ2, γ3 DANs (Figure 1.11a-e). This result has been further strengthened by an analysis of the leg motion onset and calcium rise dynamics analysis (Extended Data Figure 1.8). The analysis showed that leg motion was initiated instantaneously (Extended Data Figure 1.8b-d) with optogenetic stimulation while calcium signals in DANs were gradual and took almost 500 ms (Extended Data Figure 1.8b). Generally, the presynaptic calcium influx for a single action potential is estimated to have a fast rise time of ~1 ms and a decay time of ~60 ms (Ali and Kwan, 2019). Such gradual calcium response in DANs thus, was consistent with sensory 'reafferent' feedback from the executed leg movement by MDN activation as the cause of these signals. While this leg movement onset and calcium signal dynamics was not fittingly plausible for an internal, recurrent, relatively faster MDN-to-DAN feedback. In addition, an interesting observation was increased calcium signals in the β'2 DANs after releasing from trapping which is fitting to the 'dopamine - ramps' in vertebrate when animals get closer to the reward (Lerner et al., 2021). Together, it was prudent to ask whether the MDN-induced *actuated*

movement is necessary for the observed punishing effect of MDN activation as I observed before (Figure 1.5). To test this, flies were mechanically trapped by cotton wool with the same principle as before and went through the differential conditioning following a choice test. This confirmed that it is 'action' by MDN induction, which is needed for punishment memory formation, too (Figure 1.12a-b). While punishment memory formation was unimpaired for activating known punishment DANs (PPL1-01) under such restricted situations showing the principle of olfactory aversive memory formation is possible under such conditions (Figure 1.12a, c).

In conjunction, my findings attributed a crucial aspect of central nervous system operation that the execution of MDN-evoked movement is essential for engaging the punishing γ1, γ2, γ3 DANs as well as for the MDN activation to have a punishing effect. In other words, action feedback to DANs is mostly and possibly exclusively, *re-afferent* (Figure 1.13). This prompted the question for the pathways mediating this reafference.

Generally, during running, hunting, flying, courting, fighting, foraging, building and grooming (Tuthill and Wilson, 2016) important sensory modalities for reafferent signalling are optic flow (Kim et al., 2015) and mechanosensation (Russell and Roberts, 1972). Previous studies showed that MDNs receive visual input (Sen et al., 2017) and mechanosensory input (Sen et al., 2019), thus can trigger backward locomotion. However, in the used experimental set-up (two photon *in vivo* and T-maze), experiments were conducted in darkness and therefore it is apparently far-fetched that optical flow is involved (indeed, during two photon imaging the flies did not actually move-over-ground such that even if vision were intact there was no optical flow for them to detect). Among the two types of mechanoreceptors, exteroceptors detect mechanical change in environment while position or body part movement is detected by proprioceptors. The defined insect proprioceptors are: chordotonal organs, campaniform sensilla and hair plate. A brief overview of the mechanoreceptors in *Drosophila* is provided below in Table 3.1 (Tuthill and Wilson, 2016; Tuthill and Azim, 2018; Medeiros et al., 2024).

Table 3.1: An overview of mechanoreceptors in *Drosophila*

Mechanoreceptors	Name	Location	Encoding property	Homologous in vertebrate
Proprioceptors	Chordotonal organ	Every joint, between joints within limbs and body segments	Direction and velocity of movement, resistant reflexes	Muscle spindle
	Campaniform sensilla	Close to joints	Detect mechanical load of the limbs	Golgi tendon
	Hair plate	Most leg joints (but not in antenna)	Threshold of joint movement	Joint receptors
Exteroceptors	Johnston's organ (also proprioceptor)	Distal segment of antenna	Detects sound, wind, gravity	Tympanal organs
	Tactile hair (Bristles)	Leg, thorax, head	Detecting mechanical cues: dust particles, parasites, wind	Merkel cells, Ruffini endings, Meissner's corpuscles

Based on the above-mentioned overview, the most plausible candidate for *re-afferent* feedback could be chordotonal organs and hair plates for monitoring the joint and leg movements. Although it has not yet been tested whether activating these proprioceptors itself would increase activity in punishing DANs in adult flies, a previous study in *Drosophila* larvae (Eschbach et al., 2020) showed that optogenetic activation of chordotonal organs selectively increase calcium signal in punishing DANs. Noticeably, larval connectome suggests 4-6 synaptic steps in between the chordotonal sensory neurons and these DANs. Considering the complexity of adult connectome and yet remaining full brain together with ventral nerve cord connectome stitching may make the investigation even more complex and need additional time.

What is it all about: A counterforce to extinction learning

Inspired by the theory of emotion (Darwin, 1872; James, 1884), I established a neurobiologically grounded study case in *Drosophila* for how avoidance can engage negative valence signalling. Specifically, I discovered that this aversive dopaminergic teaching signal possibly and exclusively coneys via a re-afferent feedback pathway. As a next step, it was prudent to ask for the biological significance of such positive feedback. At the conceptual level, my working hypothesis was that the punishing effect of avoidance may counteract extinction learning to rather maintain learned avoidance.

In olfactory classical conditioning, flies receive an odour associated with a punishing shock stimulus during training. Then encountering this odour during test will predict shock and will lead to learned avoidance behaviour (Quinn et al., 1974). If flies are repeatedly exposed to the previously punished odour without shock, extinction learning “should” occur because the odour is experienced, but the predicted shock is not (Myers and Davis, 2002, 2007). From comprehensive across species studies on extinction learning, there is ample evidence that much of the original memory survives extinction procedures (Rescorla 1972; McClelland and Rumelhart, 1985; McCloskey and Cohen, 1989; Bouton, 2002, 2004; Myers and Davis, 2002; Delamater, 2004; Todd et al., 2014). While so far, the notion was that these original memories in the extreme case remain untouched by extinction procedures, we wondered whether avoidance-to-punishment feedback may provide a mechanism for an active, memory-maintaining signal. This I believe is essential to investigate further as the basis of exposure therapy treatment to effectually annihilate maladaptive behaviours, thoughts or emotions (Bouton, 1988; Conklin and Tiffany, 2002; Craske et al., 2014). We specifically hypothesized that after olfactory classical conditioning with odour-electric shock, each time the fly shows successful learned avoidance of an odour, the moonwalker neurons are activated, and a punishing signal is generated. This signal would act on the representation of the just-avoided odour in the punishment compartments, effectively counteracting extinction learning as it takes place in the reward compartments. And indeed, what we observed both by behavioural experiments and by computational modelling supports such a scenario (Figure 1.14, Figure 1.15, Extended Data Figure 1.17). The obtained data showed that flies form a strong olfactory punishment memory because of CS-US association, but once they experience only CS without any US, they trigger extinction learning and thus learned avoidance is reduced. But only once the MDNs are also silenced while experiencing the CS alone, and thus feedback to punishing DANs is interrupted, the full potential of extinction learning is uncovered and learned avoidance is fully abolished (see Chapter 1 result section for more detail).

According to Pavlov (Pavlov, 1927), extinction learning disrupts the conditioned response but does not destroy it – which suggest a partial erasure of the original learning and thus a tendency to maintain the original learning and subsequent 'spontaneous recovery' or restoration. Maintaining the previous trace of learning is often referred to as 'adaptive conservatism' or 'anxiety conservation' in fear learning and is described as "better-safe-than-sorry approach" (Solomon and Wynne, 1954). That is, despite experiencing repeated presence of CS without US, animals often maintain avoidance even if there is hardly any recent reason to do so (Dunsmoor et al., 2015). Another important aspect to consider in CS-US association is the involvement of multiple independent components: sensory/perceptual, emotional, temporal, conceptual etc (Brandon et al., 2000; Delamater, 2012) Therefore, it is possible that conventional extinction learning only erasures the conditioned fear response but leaves the other element intact. This suggests a simultaneous erasure, maintenance or no effect on the separate aspect of the same memory (Lattal and Wood, 2013; Delamater and Westbrook, 2014). In avoidance-conditioning, this refers to a behavioural response that prevents the occurrence of CS associated with fear (Krypotos et al., 2018; Pittig et al., 2020). Clinical evidence showed that individuals suffering from anxiety-related disorders actively avoid the fear/anxiety related cue and hesitate to abolish the anxious memory (Nowakowski et al., 2013). This phenomenon of continued avoidance despite discontinued punishment is notorious in experimental psychology as the "avoidance paradox" (Bolles 1972; Le Doux et al., 2017).

Although several psychological factors have been previously suggested as a contributing factor for such maintenance of avoidance memory, there is only little laboratory and clinical evidence available (Lovibond, 2004). One of the very intriguing factor, fitting with our findings, is that - in extinction learning, if during the moment of experiencing the CS, a novel action is enabled that prevents the occurrence of the US, this novel action can prevent acquiring inhibitory properties for the original CS and thus will provide 'protection from extinction' (Dickinson and Burke, 1996; Rescorla, 2003; Dunsmoor et al., 2015). In our findings, it is suggestive that, at the moment of experiencing the CS without the US, the avoidance taken by MDN-driven backward locomotion by engaging punishing dopaminergic signal is thus providing the maintenance signal and protecting from full extinction. Therefore, once MDNs induced maintenance signals was taken away by silencing them, strengthening of the effects of extinction procedures "deepened extinction", (Rescorla, 2006) was achieved.

A variety of manipulations have been used to optimize extinction learning (counterconditioning: Wolpe, 1958; Scavio, 1974; Bouton, 1993; Pavlovian conditioning: Delamater, 1996; Rescorla,

1996; Instrumental conditioning: Rescorla, 1991, and indeed extinction learning is a highly complex phenomenon. As already mentioned briefly, prior work showed that extinction learning does not involve destruction of the original learning, rather parallel memories co-exist and compete to direct behaviour (Tovote et al., 2015; Felsenberg et al., 2017, 2018;). For example, olfactory aversive memory extinction requires activation of rewarding dopaminergic neurons (γ5 DANs) while olfactory appetitive memory extinction needs activation in punishing dopaminergic neurons (PPL1 DANs: MB-MP1(PPL1-γ1), perhaps MB-MV1 (PPL1-γ2α'1), PPL1-α 3). Here, the shown data demonstrates that, after odour-shock association, while acquisition of aversive extinction memory was taking place in rewarding compartment (γ5), in parallel, a counterforce of extinction learning by avoidance engaging maintenance signal was taking place in the punishment processing compartments (γ1, γ2, γ3). Strikingly, γ1pedc and γ2α′1-β′2a microcircuits are analogous to the roles of the amygdala and ventromedial prefrontal cortex (vmPFC) of mammals where amygdala encodes originally acquired fear memory and vmPFC encodes omission of the aversive outcome during reversal as reward. Interestingly, inhibiting vmPFC-VTA projection impairs shock omission extinction (McCurdy et al., 2021).Together, this suggests that during an extinction protocol, two parallel processes are going on in different places of the MB. Thus action-to-valence causation is a part of a system that maintains learned avoidance even if avoidance is successful. That is even when an expected punishment, because of avoidance behaviour, is precisely not received. Thus, my identification of avoidance-to-punishment feedback have significant impact because it identifies a hitherto elusive "counterforce" to extinction learning and as such may offer clinical perspectives that I will discuss next.

Implication in the field of clinical research

My findings put a new perspective on why the effects of exposure therapy of human anxiety disorders have such a relatively high rate of relapse (Craske and Mystkowski, 2006). An excellent example of successful translational research is fear extinction. Both laboratory studies and exposure based clinical trials for anxiety disorders have shown that conditioned fear behaviour is possible to extinguish but not fully, hence relapses easily (Vervliet et al., 2013). Prevention of relapses is thus the main motto. Effective pharmacological, cognitive behavioural therapy (CBT) and psychotherapeutic approaches have been used towards that end in the context of anxiety disorders, phobias, obsessive compulsive disorders, post-traumatic stress disorder (PTSD) and panic disorders for a while (Eddy et al., 2004; Mitte, 2005; Hoffman and Smits, 2008; Craske et al., 2014; Levy et al., 2022). Still, fear reduction is short-lived, incomplete and followed by relapse in a range from 19% to 62% (Eddy et al. 2004; Craske and Mystkowski 2006). This demands a developed treatment and a refined effort to re-think the overlooked mechanism that can maintain

aversive memories to return upon re-exposure to punishment (reinstatement), or contextual change (renewal) (Dunsmoor et al., 2015, Bouton et al., 2020). Below is provided an overview of therapeutic attempts of mixed outcomes in humans and rodents to prevent relapses in Table 3.2.

Table 3.2: An overview of therapeutic attempts to prevent relapses

Road to prevent relapse	Methods used	Findings	Source
By strengthening the extinction memory	Augmenting the number of extinction trials	Prevents relapse in rats	Denniston et al. 2003
	Compound extinction	Prevents relapses in rats but no reliable trials on human till date	Rescorla 2006
	Extinction retrieval cues	May prevent relapses in human, but exact conditions are unclear	Brooks and Bouton, 1994; Dibbets et al. 2008; Dibbets and Maes 2011; Vansteenwegen et al. 2006
	Mental reinstatement	Prevents relapse in human	Mystkowski et al. 2006
	Multiple contexts extinction	Conditionally works in rats and human	Bandarian Balooch et al. 2012
	Multiple stimulus extinction	Prevents relapse in human	Verveliet et al. 2004, 2005; Rowe and Craske, 1998
	US devaluation	Reduces fear and prevents return only in humans but not in rats	Storvse et al. 2010; Dibbets et al. 2012
	Cognitive enhancer: d-cycloserine	Boosts fear extinction, prevents reinstatement but leaves renewal and reacquisition intact	Walker et al. 2002; Richardson et al. 2004; Ledgerwood et al. 2005; Woods and Bouton 2006
By weakening the fear memory	Immediate extinction	Prevents relapse in rats but not reliable in human	Pavlov, 1927; Myers et al. 2006; Norrholm et al. 2008; Schiller et al. 2008
	Reconsolidation treatment	Unreliable results in rats and human	Nader et al. 2000

The overview shows that relapse is a fundamental hindrance to exposure-based therapy of anxiety disorders and very less is known about the prevention. Therefore, these finding of an action-based counterforce which hindrance the full potential of extinction learning to take effect should inspire a fresh start in neurobiological research to prevent the relapse after exposure therapies of anxiety disorders.

Backward locomotion across species

Backward locomotion is an important faculty for manoeuvrability across species. However, in comparison to forward locomotion or turning, it is not so well investigated yet in terms of the underlying neurons. Neurons resembling MDNs have been identified in crickets namely DBNc1-2 or DBNc2-2 (Schöneich et al., 2011) and DMIa-1or DMIb-1 in cockroaches (Burdohan and Comer, 1996). All of them seem to respond exclusively to mechanical stimuli in antennae, cephalic hairs and mouthparts with no apparent effect of visual stimuli. The function of these neurons is in general for short-latency evasive behaviour (Ye and Comer, 1996) and possibly separate from escape behaviour. In *Caenorhabditis elegans (C.elegans),* there are analogous command interneurons, AVA, AVD and AVE, controlling the reverse movement (Chalfie et al., 1985; Gray et al., 2005; Piggott et al., 2011). Among them, AVA is cholinergic (as MDNs) and is receiving mechanosensory input from head proprioceptors as well as upstream interneurons. As mentioned earlier, larval *Drosophila* also consist of mooncrawler neurons for backward crawling (Carreira-Rosario et al., 2018) as a part of the "dig and dive" behaviour in food (Kim et al., 2017).

In contexts other than evasion or escape, desert ants of the genus Cataglyphis and Myrmecia, they steer themselves backwards while carrying disproportionately large food items back home (Ardin et al., 2016; Pfeffer et al., 2016; Schwarz et al., 2017). That is, foraging ants usually walk forward while carrying large food items in a backward walking manner, time to time they let go of their food item, have a surrounding inspection period, followed by picking up the food again and resuming backward walking towards nest (Pfeffer et al., 2016). Another terrestrial animal, the dung beetle *Scarabaeus galenus,* forms an oversized dung ball and pushes it with their hind legs and head-down in a backward manner towards home to protect it from the other hungry beetles (Dacke and el Jundi, 2018). In this process, they also quite often let go of the ball to re-grip steadfastly. An example of using a similar manoeuvre namely 'cast and surge' has been described in flying insects e.g. hoverflies or wasps to locate odour source (van Breugel and Dickinson, 2014). In all these cases, it would be interesting to investigate whether there is an emotional experience in these animals while performing these actions.

Beyond the "moonwalk": descending neurons in other actions

Various transgenic drivers, combined with optogenetic and thermogenic effectors, have been used to characterize the behavioural changes resulting from descending neuron activity. According to behavioural changes the DNs are clustered into different groups (Figure 3.1), such as:

Forward walking: Forward walking is that one behaviour which animals need under diverse contexts and state. e.g. food search, mating, exploration, navigation or running away from a predator. Therefore, the command of DNs may convey a similar message under different circumstances with different motivation. DNp09 (Bidaye et al., 2020) for example mediates forward walking and turning to pursue courtship while BPN brain via other DNs (oDN1) elicit bolt, forward walking possibly to reach a food source or running away from a threat behind. I also performed a preliminary investigation with BPN-S1 (Bolt) neuron (Bidaye et al., 2020) for forward locomotion and Stop-1 neuron for halting locomotion in the supplementary section of my thesis (Supplement Figure 10, Supplement Figure 11, and Supplemental Table S2).

Backward walking: activation of moonwalker descending neurons (MDNs) makes flies walk backward (Bidaye et al., 2014) and MDNs are the central player of my thesis.

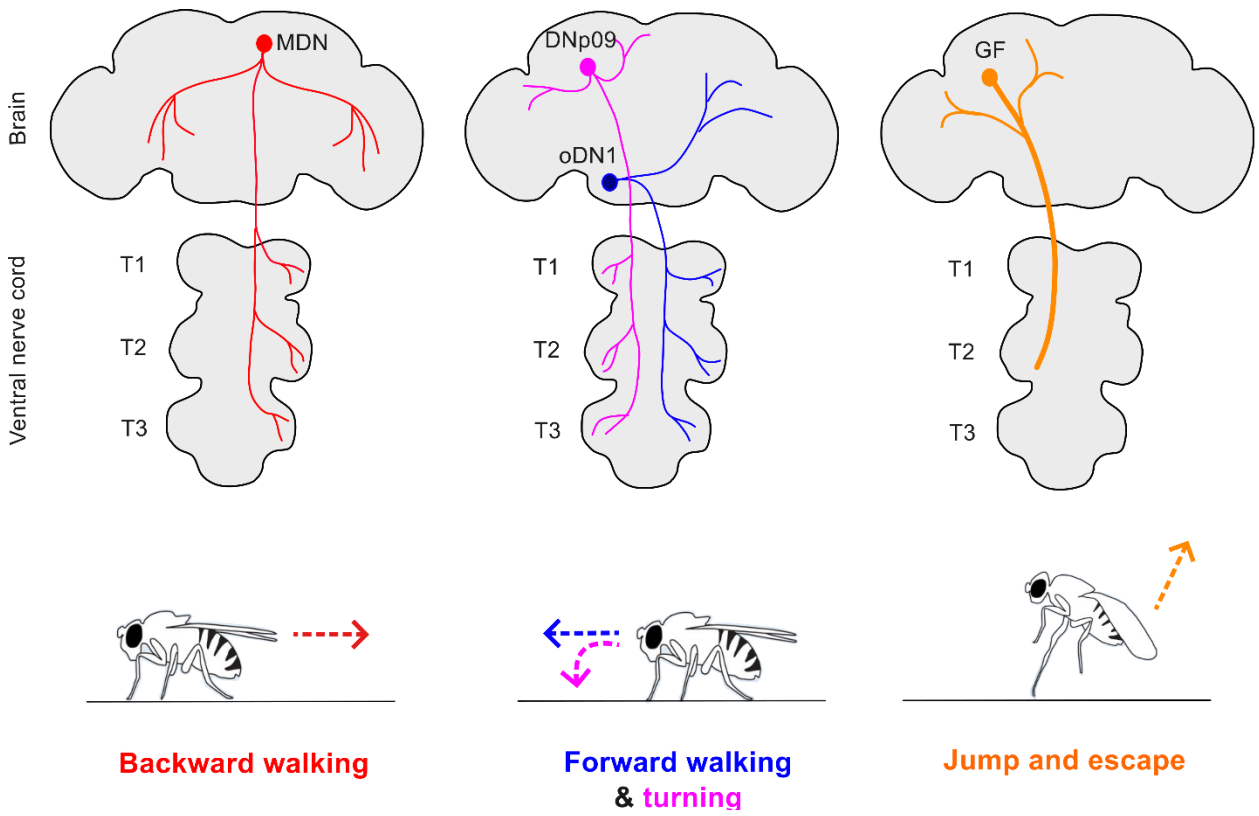

Figure 3.1 | Descending neurons in "fly's action".
Moonwalker descending neurons (MDNs) are responsible for backward walking; DNp09, oDN1 for forward walking and turning; the giant fiber (GF) initiates jump and escape of adult Drosophila melanogaster (modified figure from Simpson, 2024 and Ache et al., 2019).

Another classic example of commanded behaviour by descending neurons is jump take-off into flight (Bacon and Strausfeld, 1986). This type of rapid-adrift escape behaviour is elicited by giant fiber (GF) neurons (DNp01) (Simpson, 2024).

In contrast, a sequence of combinatorial motor programs is needed for grooming either for antennal cleaning (Hampel et al., 2015), wing cleaning (Zhang and Simpson, 2022), head cleaning or front leg rubbing (Guo et al., 2022). For example, activation of DNg12 can evoke alternative head sweeping or front leg rubbing to perform anterior grooming.

Altogether these give us food for thought about the ability of DNs to induce complex sequences of motor actions for diverse purposes. It would seem interesting to investigate not only the mechanistic process of how behaviours such as walking forward, turning, stopping, jumping or self-grooming are instructed by the brain, how they are actuated by the body but also how these actions feed back to the brain. Of particular interest would be to see how these processes are modulated by environmental, social and behavioural context – and whether they might have a valence component.

Valence to action

Timing-dependent valence reversal

Learning about life-threatening as well as life-saving situations are essential faculties across animal species. For that a proper representation of the causal structure of the world is mandatory. Hence, in a potentially changing environment, animals need the capacity to update these representations to predict such key events. In this respect, the temporal relationships between cues and events have been studied thoroughly (Shanks et al., 1989; Dickinson, 2001). For instance, this may comprise evidence in favour of a causal relationship with a punishment or evidence against it, and a proper judgement of this relationship is crucial for survival of animals and humans. In the General Introduction section, I discussed the importance of ‘contiguity’ and ‘contingency’. However, as discussed in Chapter 2, depending on the relative timing of contiguous events as defined by the inter-stimulus-interval (ISI), memories of opponent valence can be formed (Gerber et al., 2014, 2019). For example, aversive memories are formed when a cue comes before the punishment, whereas memories of appetitive valence are formed when a cue is presented upon the relieving termination of punishment (Tanimoto et al., 2004; Yarali et al., 2008; König et al., 2018; Aso and Rubin, 2016; Handler et al., 2019). Conversely, appetitive memories are formed when cue is presented with the occurrence of reward but when the cue is

presented upon the termination of reward presentation, a ‘frustration memory’ is formed. Such processe have been studied not only in *Drosophila* but also across species. A rich number of investigations have already been carried on “punishment” and “reward” learning in animals (punishment in *Drosophila*: Dubnau et al., 2001; Heisenberg, 2003; Gerber et al., 2004; Davis, 2005, 2023; Keene and Waddell, 2007; Aso et al., 2012; Aso and Rubin, 2016 in Aplysia: Lechner and Byrne, 1998; Baxter and Byrne, 2006 ; in rodents: Müller and Fendt, 2023 ; Review: Fendt and Fanselow, 1999; Maren, 2001; in monkeys: Davis et al., 2008; Monosov et al., 2015 ; and in humans: (Rosen and Schulkin, 1998; Öhman and Mineka, 2001); reward in flies: Tempel et al., 1983; Plaçais et al., 2013; Boto et al., 2020; Lin et al., 2024; rats: Schmid et al., 1995; and in humans: (Gottfried et al., 2003) . But much less is known about the underlying mechanism of “relief” and “frustration” learning (relief in *Drosophila*: Tanimoto et al., 2004; Yarali et al., 2008; Gerber et al., 2014; Vogt et al., 2015; Aso and Rubin, 2016; König et al., 2018; Handler et al., 2019; Thoener et al., 2021 ; in rats: Mohammadi and Fendt, 2015 and in humans: Andreatta et al., 2010, 2012; frustration in *Drosophila* larvae: Saumweber et al., 2018; Thoener et al., 2022 and in bees: Hellstern et al., 1998; Plath et al., 2012.

In addition, another form of associative learning can be achieved when there is a temporal gap between CS-US, known as trace conditioning (Galili et al., 2011) to discriminate it from the learning that takes place when there is no such gap, known as delay conditioning.

Given the potentially distinct mechanisms of all these mentioned forms of learning, a full characterization of ISI is an apt move to characterize learning, and the effects of any treatment might have on it.

Dopamine does it after all?

Previous studies showed the involvement of select sets of dopaminergic neurons in aversive associative memory formation, with the strongest evidence from PPL1-01 (Tanaka et al., 2008; Aso et al., 2010; Hige et al., 2015; König et al., 2018; Aso et al., 2016, 2019) (synonyms for PPL1-01 are PPL1-γ1pedc and MB-MP1). Nevertheless, the involvement of dopamine for relief memory upon termination PPL1-01 activation remained controversial and inconclusive (Aso and Rubin, 2016; König et al., 2018). Therefore, further investigations into the role of dopamine in timing dependent valence reversal seemed warranted. In Chapter 2 of the thesis, I investigated timing dependent valence reversal with optogenetic activation of PPL1-01 as US in adult *Drosophila* combined with acute pharmacological and neuron-specific genetic manipulation to compromise TH function. This revealed a complex temporal reinforcement profile of PPL1-01 dopaminergic neuron when TH function is compromised i) enhanced learning with a time gap between stimulus

and PPL1-01 punishment (trace conditioning), ii) impairs learning when the stimulus immediately precedes and overlaps PPL1-01 punishment (delay conditioning), and iii) prevents learning about a stimulus presented after PPL1-01 punishment has ceased (relief conditioning) (Figure 2.1f, Figure 2.3). Further, I found that all the compromised TH function effects were rescuable by additional by L-Dopa treatment (Figure 2.1g).

In addition, under conditions of low-dopamine (Figure 2.2) I uncovered a role of serotonin that is particularly strong for trace conditioning (ISI -100s), and that tapers off with increasing ISIs (Figure 2.5), my findings in Chapter 2 not only mapped out the full 'fingerprint' of reinforcement by the dopamine neuron PPL1-01 and resolve the apparent disparity among previous studies but also showed the plausible role of the dopamine-serotonin balance to shape the temporal profile of reinforcement learning. The possible clinical implications of these findings will be discussed below.

More generally the emerging across species picture is that the cellular and molecular mechanisms for trace versus delay conditioning only partially overlap (*Drosophila:* Duerr and Quinn, 1982; Dudai et al., 1983; Shuai et al., 2011; Grover et al., 2022; vertebrates: Bissonette and Roesch, 2016; Garritsen et al., 2023; Kong et al., 2023; Hou et al., 2024 and the same seems to be true for delay versus relief conditioning (*Drosophila*: Tanimoto et al., 2004; Yarali et al., 2008; Vogt et al., 2015; Gerber et al., 2014; Aso & Rubin et al. 2016; König et al., 2018; Handler et al., 2019; Grover et al., 2022; vertebrates: Andreatta et al., 2010, 2012; Mohammadi and Fendt, 2015; Bergado Acosta et al., 2017; Laing et al., 2024. Without discussing these findings in detail, I would like to stress that for the case of *Drosophila* it is as yet not clear whether relief learning with PPL1-01 or shock indeed takes place within the γ1 compartment (as would be suggested by the findings of Handler et al 2019 with respect to the appetitive domain and the γ4/5 compartments) or whether it involves some across-compartment signalling (Perisse et al., 2013, 2016; Hige et al., 2015; Hige, 2018; König et al., 2018).

A disturbed dopamine-serotonin balance: an endophenotype of Schizophrenia?

Although in flies we cannot speak of causality judgements in any strict sense, I find it tempting to consider the distortions in timing-dependent valence reversal that I observed under low-dopamine conditions in terms of causality. If, for the sake of the argument, we are doing so this suggests that they showed strong causal belief for a cue in the absence of evidence (better trace conditioning), impaired causal belief for cues as providing evidence for (impaired delay conditioning) and evidence against (impaired relief conditioning) the causation punishment, promoting systematically delusional beliefs about causal structure. In a human subject, such

delusional beliefs about causal event structure would be providing a hallmark symptom of schizophrenia (McCutcheon et al., 2019). Indeed, human schizophrenia patients tend to perceive cause-effect relationships where they do not exist and ‘jump to conclusions’ without sufficient evidence (Garety et al., 2005; Moritz and Woodward, 2005; Uhlhaas and Silverstein, 2005; Dudley et al., 2016). Behaviour that is based on causal belief structures that are thus insufficiently grounded in experience would also lead to poor performance in various memory tasks. The implication is that a dysfunction in dopaminergic reinforcement processing, or possibly a distorted dopamine-serotonin balance, is a common endophenotype of both positive symptoms (delusional causal beliefs) and cognitive symptoms (impaired memory performance) in schizophrenia.

Although our knowledge of the neurobiology of schizophrenia is yet rudimentary, it is continuously advancing. Clinical studies have provided evidence for dopaminergic abnormalities in schizophrenia (Laruelle et al., 1999; Howes and Kapur, 2009; Kegeles et al., 2010; Jones and Jahanshahi, 2011). On the other hand, it was shown that the serotonin system inhibits dopaminergic function in midbrain as well as in the forebrain and thus may alleviate the psychotic symptoms and enhance therapeutics in schizophrenia (albeit unclear properly) (American Journal of Psychiatry, Volume 153, Number 4, 1996). Interestingly, the male predominancy of the effect of compromising TH function in trace conditioning as I observed would seem to match the onset of incidence of schizophrenia is higher among male than woman with a ratio of 1.4:1 (Li et al., 2022; also see Figure 2.4c).

Conclusions

In this thesis, I investigated the mechanistic relationships between action, valence and dopamine in adult fruit fly, *Drosophila melanogaster* and the corresponding biomedical implications.

In Chapter 1, I discovered a process of acquiring negative valence from backward locomotion by using MDNs. Taking the lead in a collaborative enterprise, I found that MDNs are part of memory-efferent pathways from the mushroom body and required for learned aversive memory expression.

I developed novel experimental paradigms and by using them in functional imaging and behavioural experiments, I investigated how and why moving backward induces negative valence in the fly *Drosophila melanogaster*. In this process, I identified a novel re-afferent feedback pathway from this aversion which engages the punishing γ1,2,3 dopaminergic neurons.

Lastly, I showed the significance of this identified aversion engaging punishing DANs signals as a hitherto elusive “counterforce” to extinction learning that maintains avoidance, reducing the risk of further, possibly lethal, punishment. This offers a new perspective on re-evaluating the clinical implications on exposure therapy of human anxiety disorders to reduce the high rate of relapse. Together, this study provides a neurobiologically grounded argument for an integrated view of action, valence and memory organization.

Graphical summary of Chapter 1
Avoidance engages dopaminergic punishment in *Drosophila*

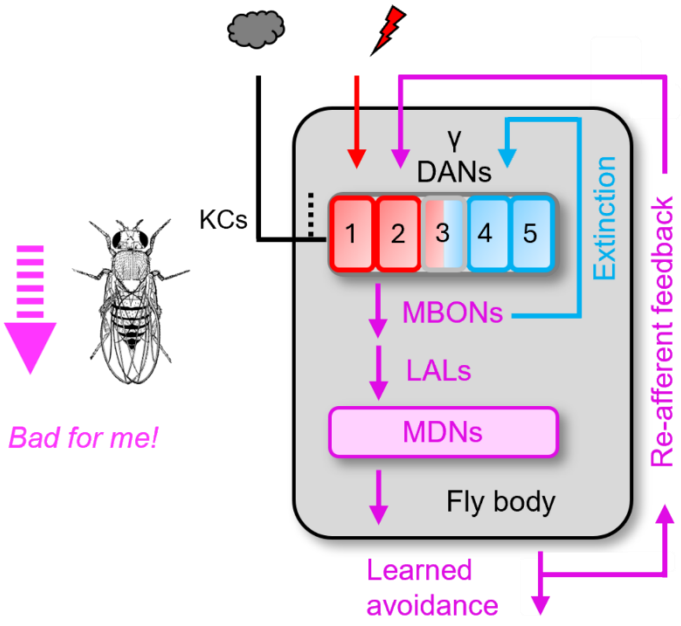

In Chapter 2, my findings demonstrated the full 'fingerprint' of reinforcement profile of PPL1-01 dopamine neuron, the complexity of the changes in reinforcement profile by a given manipulation and established a case for a delusion-like distortion of timing-dependent valence reversal. Specifically, I showed, under TH compromised condition, i) better trace conditioning, ii) impaired delay conditioning and iii) impaired relief conditioning.

I also found a compensatory role of serotonin in those states. For the practitioner this shows that for the interpretation of treatment effects a full characterization of the ISI function of memory scores can be critical. This also warrants considering possibly related psychiatric symptoms, in particular in schizophrenia. Given the role of dopamine across species, including humans, this may provide inspiration for experimentation and a better understanding of animal and human cognition under 'normal' and diseased conditions.

Graphical summary of Chapter 2
Temporal profile of reinforcement in *Drosophila*

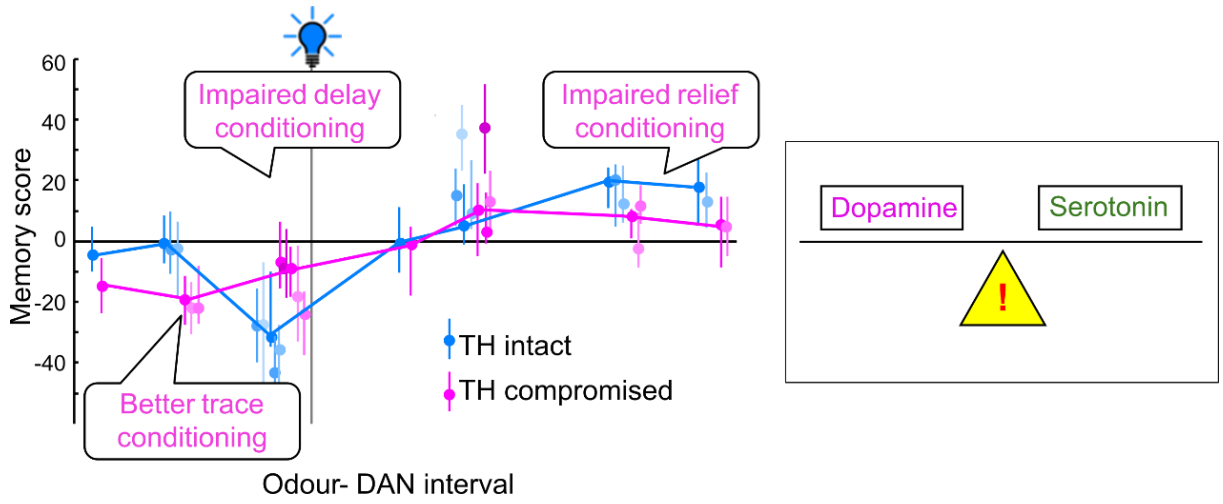

Appendix

List of abbreviations

DBD	DNA binding domain
AD	Activation domain
ChR	Channelrhodopsin
GtACR	Guillardia theta algae channelrhodopsin
ATR	All trans retinal
GFP	Green fluorescent protein
GECI	Genetically encoded calcium indicator
LED	Light-emitting diode
CS	Conditioned stimulus
US	Unconditioned stimulus
CR	Conditioned response
UR	Unconditioned response
OSN	Olfactory sensory neuron
OR	Olfactory receptor
AL	Antennal lobe
PN	Projection neuron
MB	Mushroom body
LH	Lateral horn
KC	Kenyon cell
CA	Calyx
DAN	Dopaminergic neuron
MBON	Mushroom body output neuron
PPL	Paired posterior lateral
PAM	Paired anterior medial
OAN	Octopaminergic neuron
APL	Anterior paired lateral
DPM	Dorsal paired medial
CRE	Crepine
SMP	Superior medial protocerebrum
SIP	Superior intermediate protocerebrum
LAL	Lateral accessory lobe
SEZ	Sub esophageal zone
LTD	Long term depression
DN	Descending neuron
VNC	Ventral nerve cord
PS	Posterior slope
GNG	Gnathal ganglion
MDN	Moonwalker descending neuron
ROI	Region of interest
RNAi	Ribonucleic acid interference
SUC	Sucrose
3IY	3-iodo-L-tyrosine
PCPA	Para-chlorophenylalanine
L-Dopa	3,4-dihydroxy-L-phenylalanine
KKW	Kruskal-Wallis
MWU	Mann-Whitney U
OSS	One sample sign
DA	Dopamine
5-HT	Serotonin
NT	Neurotransmitter
GPCR	G protein coupled receptor

References

Ache JM, Polsky J, Alghailani S, Parekh R, Breads P, Peek MY, Bock DD, von Reyn CR, Card GM (2019) Neural Basis for Looming Size and Velocity Encoding in the Drosophila Giant Fiber Escape Pathway. Current Biology 29:1073-1081.e4.

Akemann W, Mutoh H, Perron A, Park YK, Iwamoto Y, Knöpfel T (2012) Imaging neural circuit dynamics with a voltage-sensitive fluorescent protein. J Neurophysiol 108:2323–2337.

Albus JS (1971) A theory of cerebellar function. Math Biosci 10:25–61.

Ali F, Kwan AC (2019) Interpreting in vivo calcium signals from neuronal cell bodies, axons, and dendrites: a review. Neurophotonics 7:1.

Amato D, Canneva F, Cumming P, Maschauer S, Groos D, Dahlmanns JK, Grömer TW, Chiofalo L, Dahlmanns M, Zheng F, Kornhuber J, Prante O, Alzheimer C, von Hörsten S, Müller CP (2020) A dopaminergic mechanism of antipsychotic drug efficacy, failure, and failure reversal: the role of the dopamine transporter. Mol Psychiatry 25:2101–2118.

Amin F, König C, Zhang J, Kalinichenko LS, Königsmann S, Brunsberg V, Riemensperger TD, Müller CP, Gerber B (2025) Compromising tyrosine hydroxylase function extends and blunts the temporal profile of reinforcement by dopamine neurons in Drosophila. The Journal of Neuroscience:e1498242024.

Andreatta M, Fendt M, Mühlberger A, Wieser MJ, Imobersteg S, Yarali A, Gerber B, Pauli P (2012) Onset and offset of aversive events establish distinct memories requiring fear and reward networks. Learning & Memory 19:518–526.

Andreatta M, Mühlberger A, Yarali A, Gerber B, Pauli P (2010) A rift between implicit and explicit conditioned valence in human pain relief learning. Proceedings of the Royal Society B: Biological Sciences 277:2411–2416.

Ardin PB, Mangan M, Webb B (2016) Ant Homing Ability Is Not Diminished When Traveling Backwards. Front Behav Neurosci 10.

Aso Y et al. (2014b) Mushroom body output neurons encode valence and guide memory-based action selection in Drosophila. Elife 3.

Aso Y, Grübel K, Busch S, Friedrich AB, Siwanowicz I, Tanimoto H (2009) The Mushroom Body of Adult Drosophila Characterized by GAL4 Drivers. J Neurogenet 23:156–172.

Aso Y, Hattori D, Yu Y, Johnston RM, Iyer NA, Ngo T-T, Dionne H, Abbott L, Axel R, Tanimoto H, Rubin GM (2014b) The neuronal architecture of the mushroom body provides a logic for associative learning. Elife 3.

Aso Y, Herb A, Ogueta M, Siwanowicz I, Templier T, Friedrich AB, Ito K, Scholz H, Tanimoto H (2012) Three Dopamine Pathways Induce Aversive Odor Memories with Different Stability. PLoS Genet 8:e1002768.

Aso Y, Ray RP, Long X, Bushey D, Cichewicz K, Ngo T-T, Sharp B, Christoforou C, Hu A, Lemire AL, Tillberg P, Hirsh J, Litwin-Kumar A, Rubin GM (2019) Nitric oxide acts as a cotransmitter in a subset of dopaminergic neurons to diversify memory dynamics. Elife 8.

Aso Y, Rubin GM (2016) Dopaminergic neurons write and update memories with cell-type-specific rules. Elife 5.

Aso Y, Siwanowicz I, Bräcker L, Ito K, Kitamoto T, Tanimoto H (2010) Specific dopaminergic neurons for the formation of labile aversive memory. Curr Biol 20:1445–1451.

Azevedo A et al. (2024) Connectomic reconstruction of a female Drosophila ventral nerve cord. Nature 631:360–368.

Bacon JP, Strausfeld NJ (1986) The dipteran? Giant fibre? pathway: neurons and signals. Journal of Comparative Physiology A 158:529–548.

Balooch SB, Neumann DL, Boschen MJ. (2012). Extinction treatment in multiple contexts attenuates ABC renewal in humans. Behav Res Ther. 2012 Oct;50(10):604-9.

Barnstedt O, Owald D, Felsenberg J, Brain R, Moszynski J-P, Talbot CB, Perrat PN, Waddell S (2016) Memory-Relevant Mushroom Body Output Synapses Are Cholinergic. Neuron 89:1237–1247.

Baxter DA, Byrne JH (2006) Feeding behavior of Aplysia: A model system for comparing cellular mechanisms of classical and operant conditioning. Learning & Memory 13:669–680.

Benton R. 2006. On the ORigin of smell: odorant receptors in insects. Cellular and molecular life sciences 63: 1579-85

Bergado Acosta JR, Kahl E, Kogias G, Uzuneser TC, Fendt M (2017) Relief learning requires a coincident activation of dopamine D1 and NMDA receptors within the nucleus accumbens. Neuropharmacology 114:58–66.

Bidaye SS, Laturney M, Chang AK, Liu Y, Bockemühl T, Büschges A, Scott K (2020) Two Brain Pathways Initiate Distinct Forward Walking Programs in Drosophila. Neuron 108:469-485.e8.

Bidaye SS, Machacek C, Wu Y, Dickson BJ (2014) Neuronal Control of Drosophila Walking Direction. Science (1979) 344:97–101.

Bissonette GB, Roesch MR (2016) Development and function of the midbrain dopamine system: what we know and what we need to. Genes Brain Behav 15:62–73.

Böhm H, Schildberger K (1992) Brain Neurones Involved in the Control of Walking in the Cricket Gryllus Bimaculatus. Journal of Experimental Biology 166:113–130.

Bolles, R. C. (1972) The avoidance learning problem. Psychol. Learn. Motiv. 6, 97–145 (1972).

Boto T, Louis T, Jindachomthong K, Jalink K, Tomchik SM (2014) Dopaminergic Modulation of cAMP Drives Nonlinear Plasticity across the Drosophila Mushroom Body Lobes. Current Biology 24:822–831.

Boto T, Stahl A, Tomchik SM (2020) Cellular and circuit mechanisms of olfactory associative learning in Drosophila. J Neurogenet 34:36–46.

Boto T, Stahl A, Zhang X, Louis T, Tomchik SM (2019) Independent Contributions of Discrete Dopaminergic Circuits to Cellular Plasticity, Memory Strength, and Valence in Drosophila. Cell Rep 27:2014-2021.e2.

Bouton ME (1988) Context and ambiguity in the extinction of emotional learning: Implications for exposure therapy. Behaviour Research and Therapy 26:137–149.

Bouton, M. E. (1993). Context, time, and memory retrieval in the interference paradigms of Pavlovian learning. Psychological Bulletin, 114(1), 80–99.

Bouton ME (2002) Context, ambiguity, and unlearning: sources of relapse after behavioral extinction. Biol Psychiatry 52:976–986.

Bouton ME (2004) Context and Behavioral Processes in Extinction: Table 1. Learning & Memory 11:485–494.

Bouton ME, Maren S, McNally GP (2021) Behavioral and neurobiological mechanisms of pavlovian and instrumental extinction learning. Physiol Rev 101:611–681.

Bouvier J, Caggiano V, Leiras R, Caldeira V, Bellardita C, Balueva K, Fuchs A, Kiehn O (2015) Descending Command Neurons in the Brainstem that Halt Locomotion. Cell 163:1191–1203.

Bouzaiane E, Trannoy S, Scheunemann L, Plaçais P-Y, Preat T (2015) Two Independent Mushroom Body Output Circuits Retrieve the Six Discrete Components of Drosophila Aversive Memory. Cell Rep 11:1280–1292.

Boyden ES, Zhang F, Bamberg E, Nagel G, Deisseroth K (2005) Millisecond-timescale, genetically targeted optical control of neural activity. Nat Neurosci 8:1263–1268.

Brand AH, Perrimon N (1993) Targeted gene expression as a means of altering cell fates and generating dominant phenotypes. Development 118:401–415.

Brandon SE, Vogel EH, Wagner AR (2000) A componential view of configural cues in generalization and discrimination in Pavlovian conditioning. Behavioural Brain Research 110:67–72.

Brembs B (2009) Mushroom Bodies Regulate Habit Formation in Drosophila. Current Biology 19:1351–1355.

Brooks DC, Bouton ME. A retrieval cue for extinction attenuates spontaneous recovery (1993). J Exp Psychol Anim Behav Process. 1993 Jan;19(1):77-89. doi: 10.1037//0097-7403.19.1.77. PMID: 8418218.

Buhmann J, Sheridan A, Malin-Mayor C, Schlegel P, Gerhard S, Kazimiers T, Krause R, Nguyen TM, Heinrich L, Lee W-CA, Wilson R, Saalfeld S, Jefferis GSXE, Bock DD, Turaga SC, Cook M, Funke J (2021) Automatic detection of synaptic partners in a whole-brain Drosophila electron microscopy data set. Nat Methods 18:771–774.

Bullock, T., & Horridge, G.A. (1965). Structure and function in the nervous systems of invertebrates. Freeman: San Francisco.

Burdohan JA, Comer CM (1996) Cellular Organization of an Antennal Mechanosensory Pathway in the Cockroach, Periplaneta americana . The Journal of Neuroscience 16:5830–5843.

Burke CJ, Huetteroth W, Owald D, Perisse E, Krashes MJ, Das G, Gohl D, Silies M, Certel S, Waddell S (2012) Layered reward signalling through octopamine and dopamine in Drosophila. Nature 492:433–437.

Büschges A, Ache JM (2024) Motor Control on the Move - from Insights in Insects to General Mechanisms. Physiol Rev.

Byrne, J. H. (2017). Learning and memory: a comprehensive reference. Academic Press.

Byrne J, Kandel E (1996) Presynaptic facilitation revisited: state and time dependence. The Journal of Neuroscience 16:425–435.

Caggiano V, Leiras R, Goñi-Erro H, Masini D, Bellardita C, Bouvier J, Caldeira V, Fisone G, Kiehn O (2018) Midbrain circuits that set locomotor speed and gait selection. Nature 553:455–460.

Cannon, W. B. (1939). The wisdom of the body. New York: WW Norton and Company.

Capelli P, Pivetta C, Soledad Esposito M, Arber S (2017) Locomotor speed control circuits in the caudal brainstem. Nature 551:373–377.

Cardona A, Larsen C, Hartenstein V (2009) Neuronal fiber tracts connecting the brain and ventral nerve cord of the early Drosophila larva. Journal of Comparative Neurology 515:427–440.

Carpenter JK, Andrews LA, Witcraft SM, Powers MB, Smits JAJ, Hofmann SG (2018) Cognitive behavioral therapy for anxiety and related disorders: A meta-analysis of randomized placebo-controlled trials. Depress Anxiety 35:502–514.

Carreira-Rosario A, Zarin AA, Clark MQ, Manning L, Fetter RD, Cardona A, Doe CQ (2018) MDN brain descending neurons coordinately activate backward and inhibit forward locomotion. Elife 7.

Cassenaer S, Laurent G (2012) Conditional modulation of spike-timing-dependent plasticity for olfactory learning. Nature 482:47–52.

Cervantes-Sandoval I, Martin-Pena A, Berry JA, Davis RL (2013) System-Like Consolidation of Olfactory Memories in Drosophila. Journal of Neuroscience 33:9846–9854.

Chalasani SH, Chronis N, Tsunozaki M, Gray JM, Ramot D, Goodman MB, Bargmann CI (2007) Dissecting a circuit for olfactory behaviour in Caenorhabditis elegans. Nature 450:63–70.

Chalfie M, Sulston J, White J, Southgate E, Thomson J, Brenner S (1985) The neural circuit for touch sensitivity in Caenorhabditis elegans. The Journal of Neuroscience 5:956–964.

Chen T-W, Wardill TJ, Sun Y, Pulver SR, Renninger SL, Baohan A, Schreiter ER, Kerr RA, Orger MB, Jayaraman V, Looger LL, Svoboda K, Kim DS (2013) Ultrasensitive fluorescent proteins for imaging neuronal activity. Nature 499:295–300.

Cheong HS, Eichler K, Stürner T, Asinof SK, Champion AS, Marin EC, Oram TB, Sumathipala M, Venkatasubramanian L, Namiki S, Siwanowicz I, Costa M, Berg S, Jefferis GS, Card GM (2024) Transforming descending input into behavior: The organization of premotor circuits in the Drosophila Male Adult Nerve Cord connectome. eLife13:RP96084

Claridge-Chang A, Roorda RD, Vrontou E, Sjulson L, Li H, Hirsh J, Miesenböck G (2009) Writing Memories with Light-Addressable Reinforcement Circuitry. Cell 139:405–415.

Clark, E., Battistara, M., & Benton, M. A. (2022). A timer gene network is spatially regulated by the terminal system in the Drosophila embryo. Elife, 11, e78902.

Cognigni P, Felsenberg J, Waddell S (2018) Do the right thing: neural network mechanisms of memory formation, expression and update in Drosophila. Curr Opin Neurobiol 49:51–58.

Cohn R, Morantte I, Ruta V (2015) Coordinated and Compartmentalized Neuromodulation Shapes Sensory Processing in Drosophila. Cell 163:1742–1755.

Coles NA et al. (2022) A multi-lab test of the facial feedback hypothesis by the Many Smiles Collaboration. Nat Hum Behav 6:1731–1742.

Conklin CA, Tiffany ST (2002) Applying extinction research and theory to cue-exposure addiction treatments. Addiction 97:155–167.

Court R, Namiki S, Armstrong JD, Börner J, Card G, Costa M, Dickinson M, Duch C, Korff W, Mann R, Merritt D, Murphey RK, Seeds AM, Shirangi T, Simpson JH, Truman JW, Tuthill JC, Williams DW, Shepherd D (2020) A Systematic Nomenclature for the Drosophila Ventral Nerve Cord. Neuron 107:1071-1079.e2.

Craske MG, Hermans D, Vervliet B (2018) State-of-the-art and future directions for extinction as a translational model for fear and anxiety. Philosophical Transactions of the Royal Society B: Biological Sciences 373:20170025.

Craske MG, Mystkowski JL (2006) Exposure Therapy and Extinction: Clinical Studies. In: Fear and learning: From basic processes to clinical implications., pp 217–233. Washington: American Psychological Association.

Craske MG, Treanor M, Conway CC, Zbozinek T, Vervliet B (2014) Maximizing exposure therapy: An inhibitory learning approach. Behaviour Research and Therapy 58:10–23.

Crittenden JR, Skoulakis EM, Han KA, Kalderon D, Davis RL (1998) Tripartite mushroom body architecture revealed by antigenic markers. Learn Mem 5:38–51.

Dacke M, el Jundi B (2018) The Dung Beetle Compass. Current Biology 28:R993–R997.

Dag U, Lei Z, Le JQ, Wong A, Bushey D, Keleman K (2019) Neuronal reactivation during post-learning sleep consolidates long-term memory in Drosophila. Elife 8.

Darwin C (1872) The expression of the emotions in man and animals. London: John Murray.

Davis M, Antoniadis EA, Amaral DG, Winslow JT (2008) Acoustic Startle Reflex in Rhesus Monkeys: A Review. Rev Neurosci 19.

Davis RL (1993) Mushroom bodies and drosophila learning. Neuron 11:1–14.

Davis RL. (2005) Olfactory memory formation in Drosophila: from molecular to systems neuroscience. Annu Rev Neurosci. 2005;28:275-302.

Davis RL (2023) Learning and memory using Drosophila melanogaster: a focus on advances made in the fifth decade of research. Genetics 224.

Dawydow A, Gueta R, Ljaschenko D, Ullrich S, Hermann M, Ehmann N, Gao S, Fiala A, Langenhan T, Nagel G, Kittel RJ (2014) Channelrhodopsin-2–XXL, a powerful optogenetic tool for low-light applications. Proceedings of the National Academy of Sciences 111:13972–13977.

de Bruyne M, Clyne PJ, Carlson JR (1999) Odor Coding in a Model Olfactory Organ: The Drosophila Maxillary Palp. The Journal of Neuroscience 19:4520–4532.

de Bruyne M, Foster K, Carlson JR (2001) Odor Coding in the Drosophila Antenna. Neuron 30:537–552.

Deisseroth K (2011) Optogenetics. Nat Methods 8:26–29.

Denniston, James C., Raymond C. Chang, and Ralph R. Miller (2003) "Massive extinction treatment attenuates the renewal effect." Learning and motivation 34.1 (2003): 68-86.

Delamater AR (1996) Effects of several extinction treatments upon the integrity of Pavlovian stimulus-outcome associations. Anim Learn Behav 24:437–449.

Delamater AR (2004) Experimental extinction in Pavlovian conditioning: Behavioural and neuroscience perspectives. The Quarterly Journal of Experimental Psychology Section B 57:97–132.

Delamater AR (2012) Issues in the extinction of specific stimulus-outcome associations in Pavlovian conditioning. Behavioural Processes 90:9–19.

Delamater AR, Westbrook RF (2014) Psychological and neural mechanisms of experimental extinction: A selective review. Neurobiol Learn Mem 108:38–51.

Dickinson A (2001) The 28th Bartlett Memorial Lecture. Causal learning: an associative analysis. Q J Exp Psychol B 54:3–25.

Dickinson A, Burke J (1996) Within Compound Associations Mediate the Retrospective Revaluation of Causality Judgements. The Quarterly Journal of Experimental Psychology Section B 49:60–80.

Dibbets P, Havermans R, Arntz A. (2008). All we need is a cue to remember: the effect of an extinction cue on renewal. Behav Res Ther. 2008 Sep;46(9):1070-7. doi: 10.1016/j.brat.2008.05.007. Epub 2008 Jun 27. PMID: 18675398.

Dibbets P, J.H.R. (2011). Maes The effect of an extinction cue on ABA-renewal: does valence matter? Learning and Motivation, 42 (2011), pp. 133-144, 10.1016/j.lmot.2010.12.003

Dibbets P, Poort H, Arntz A. (2012). Adding imagery rescripting during extinction leads to less ABA renewal. J. Behav. Ther. Exp. Psychiatry 43:614–24

Dombeck DA, Harvey CD, Tian L, Looger LL, Tank DW (2010) Functional imaging of hippocampal place cells at cellular resolution during virtual navigation. Nat Neurosci 13:1433–1440.

Dorkenwald S et al. (2024) Neuronal wiring diagram of an adult brain. Nature 634:124–138.

Driscoll M, Buchert SN, Coleman V, McLaughlin M, Nguyen A, Sitaraman D (2021) Compartment specific regulation of sleep by mushroom body requires GABA and dopaminergic signaling. Sci Rep 11:20067.

Dubnau J, Grady L, Kitamoto T, Tully T (2001) Disruption of neurotransmission in Drosophila mushroom body blocks retrieval but not acquisition of memory. Nature 411:476–480.

Dudai Y, Uzzan A, Zvi S (1983) Abnormal activity of adenylate cyclase in the Drosophila memory mutant rutabaga. Neurosci Lett 42:207–212.

Dudley R, Taylor P, Wickham S, Hutton P (2016) Psychosis, Delusions and the “Jumping to Conclusions” Reasoning Bias: A Systematic Review and Meta-analysis. Schizophr Bull 42:652–665.

Duerr JS, Quinn WG (1982) Three Drosophila mutations that block associative learning also affect habituation and sensitization. Proceedings of the National Academy of Sciences 79:3646–3650.

Dunlap K (1967) The Emotions—By C.G. Lange and W. James, Hafner Publishing Co., New York (1967), pp. 5-7(Original work published 1922)

Dunsmoor JE, Niv Y, Daw N, Phelps EA (2015) Rethinking Extinction. Neuron 88:47–63.

Eckstein N et al. (2024) Neurotransmitter classification from electron microscopy images at synaptic sites in Drosophila melanogaster. Cell 187:2574-2594.e23.

Eddy KT, Dutra L, Bradley R, Westen D (2004) A multidimensional meta-analysis of psychotherapy and pharmacotherapy for obsessive-compulsive disorder. Clin Psychol Rev 24:1011–1030.

Eichler K, Li F, Litwin-Kumar A, Park Y, Andrade I, Schneider-Mizell CM, Saumweber T, Huser A, Eschbach C, Gerber B, Fetter RD, Truman JW, Priebe CE, Abbott LF, Thum AS, Zlatic M, Cardona A (2017) The complete connectome of a learning and memory centre in an insect brain. Nature 548:175–182.

ERBER J, MASUHR TH, MENZEL R (1980) Localization of short-term memory in the brain of the bee, Apis mellifera. Physiol Entomol 5:343–358.

Eschbach C, Fushiki A, Winding M, Schneider-Mizell CM, Shao M, Arruda R, Eichler K, Valdes-Aleman J, Ohyama T, Thum AS, Gerber B, Fetter RD, Truman JW, Litwin-Kumar A, Cardona A, Zlatic M (2020) Recurrent architecture for adaptive regulation of learning in the insect brain. Nat Neurosci 23:544–555.

Eschbach C, Fushiki A, Winding M, Afonso B, Andrade IV, Cocanougher BT, Eichler K, Gepner R, Si G, Valdes-Aleman J, Fetter RD, Gershow M, Jefferis GS, Samuel AD, Truman JW, Cardona A, Zlatic M. (2021) Circuits for integrating learned and innate valences in the insect brain. Elife. 2021 Nov 10;10:e62567.

Eyjolfsdottir E, Branson S, Burgos-Artizzu XP, Hoopfer ED, Schor J, Anderson DJ, Perona P (2014) Detecting Social Actions of Fruit Flies. In, pp 772–787.

Farris SM (2011) Are mushroom bodies cerebellum-like structures? Arthropod Struct Dev 40:368–379.

Felsenberg, J., Plath, J. A., Lorang, S., Morgenstern, L., & Eisenhardt, D. (2014). Short-and long-term memories formed upon backward conditioning in honeybees (Apis mellifera). Learning & Memory, 21(1), 37-45.

Felsenberg J, Barnstedt O, Cognigni P, Lin S, Waddell S (2017) Re-evaluation of learned information in Drosophila. Nature 544:240–244.

Felsenberg J, Jacob PF, Walker T, Barnstedt O, Edmondson-Stait AJ, Pleijzier MW, Otto N, Schlegel P, Sharifi N, Perisse E, Smith CS, Lauritzen JS, Costa M, Jefferis GSXE, Bock DD, Waddell S (2018) Integration of Parallel Opposing Memories Underlies Memory Extinction. Cell 175:709-722.e15.

Fendt M, Fanselow MS (1999) The neuroanatomical and neurochemical basis of conditioned fear. Neurosci Biobehav Rev 23:743–760.

Feng K, Sen R, Minegishi R, Dübbert M, Bockemühl T, Büschges A, Dickson BJ (2020) Distributed control of motor circuits for backward walking in Drosophila. Nat Commun 11:6166.

Fiala A (2007) Olfaction and olfactory learning in Drosophila: recent progress. Curr Opin Neurobiol 17:720–726.

Fletcher ML, Masurkar A V., Xing J, Imamura F, Xiong W, Nagayama S, Mutoh H, Greer CA, Knöpfel T, Chen WR (2009) Optical Imaging of Postsynaptic Odor Representation in the Glomerular Layer of the Mouse Olfactory Bulb. J Neurophysiol 102:817–830.

Frank DD, Jouandet GC, Kearney PJ, Macpherson LJ, Gallio M (2015) Temperature representation in the Drosophila brain. Nature 519:358–361.

Friggi-Grelin F, Coulom H, Meller M, Gomez D, Hirsh J, Birman S (2003) Targeted gene expression in Drosophila dopaminergic cells using regulatory sequences from tyrosine hydroxylase. J Neurobiol 54:618–627.

Friedman BH (2010). Feelings and the body: the Jamesian perspective on autonomic specificity of emotion. Biol Psychol. 2010 Jul;84(3):383-93. doi: 10.1016/j.biopsycho.2009.10.006. Epub 2009 Oct 29. PMID: 19879320

Fukutomi M, Carlson BA (2020) A History of Corollary Discharge: Contributions of Mormyrid Weakly Electric Fish. Front Integr Neurosci 14.

Gal R, Libersat F (2006) New vistas on the initiation and maintenance of insect motor behaviors revealed by specific lesions of the head ganglia. Journal of Comparative Physiology A 192:1003–1020.

Galili DS, Lüdke A, Galizia CG, Szyszka P, Tanimoto H (2011) Olfactory trace conditioning in Drosophila. J Neurosci 31:7240–7248.

Garety PA, Freeman D, Jolley S, Dunn G, Bebbington PE, Fowler DG, Kuipers E, Dudley R (2005) Reasoning, emotions, and delusional conviction in psychosis. J Abnorm Psychol 114:373–384.

Garritsen O, van Battum EY, Grossouw LM, Pasterkamp RJ (2023) Development, wiring and function of dopamine neuron subtypes. Nat Rev Neurosci 24:134–152.

Gerber B, Aso Y (2017) Localization, Diversity, and Behavioral Expression of Associative Engrams in Drosophila . In: Learning and Memory: A Comprehensive Reference, pp 463–473. Elsevier.

Gerber B, König C, Fendt M, Andreatta M, Romanos M, Pauli P, Yarali A (2019) Timing-dependent valence reversal: a principle of reinforcement processing and its possible implications. Curr Opin Behav Sci 26:114–120.

Gerber B, Scherer S, Neuser K, Michels B, Hendel T, Stocker RF, Heisenberg M (2004) Visual learning in individually assayed Drosophila larvae. Journal of Experimental Biology 207:179–188.

Gerber B, Yarali A, Diegelmann S, Wotjak CT, Pauli P, Fendt M (2014) Pain-relief learning in flies, rats, and man: basic research and applied perspectives. Learn Mem 21:232–252.

Gervasi N, Tchénio P, Preat T (2010) PKA Dynamics in a Drosophila Learning Center: Coincidence Detection by Rutabaga Adenylyl Cyclase and Spatial Regulation by Dunce Phosphodiesterase. Neuron 65:516–529.

Gluck, M. A., et al. (2016). Learning and memory. Worth Publishers.

Gottfried JA, O'Doherty J, Dolan RJ (2003) Encoding Predictive Reward Value in Human Amygdala and Orbitofrontal Cortex. Science (1979) 301:1104–1107.

Govorunova E. G., Sineshchekov O. A., Janz R., Liu X., Spudich J. L. (2015). NEUROSCIENCE. Natural light-gated anion channels: a family of microbial rhodopsins for advanced optogenetics. Science 349, 647–650. 10.1126/science.aaa7484

Govorunova EG, Sineshchekov OA, Rodarte EM, Janz R, Morelle O, Melkonian M, Wong GK-S, Spudich JL (2017) The Expanding Family of Natural Anion Channelrhodopsins Reveals Large Variations in Kinetics, Conductance, and Spectral Sensitivity. Sci Rep 7:43358.

Gray JM, Hill JJ, Bargmann CI (2005) A circuit for navigation in Caenorhabditis elegans. Proceedings of the National Academy of Sciences 102:3184–3191.

Grienberger C, Giovannucci A, Zeiger W, Portera-Cailliau C (2022) Two-photon calcium imaging of neuronal activity. Nature Reviews Methods Primers 2:67.

Grienberger C, Konnerth A (2012) Imaging Calcium in Neurons. Neuron 73:862–885.

Gronenberg W, Strausfeld NicholasJ (1991) Descending pathways connecting the male-specific visual system of flies to the neck and flight motor. Journal of Comparative Physiology A 169.

Grover D, Chen J-Y, Xie J, Li J, Changeux J-P, Greenspan RJ (2022) Differential mechanisms underlie trace and delay conditioning in Drosophila. Nature 603:302–308.

Gruntman E, Turner GC (2013) Integration of the olfactory code across dendritic claws of single mushroom body neurons. Nat Neurosci 16:1821–1829.

Guo L, Zhang N, Simpson JH (2022) Descending neurons coordinate anterior grooming behavior in Drosophila. Current Biology 32:823-833.e4.

Hammer M, Menzel R (1998) Multiple sites of associative odor learning as revealed by local brain microinjections of octopamine in honeybees. Learn Mem 5:146–156.

Hampel S, Franconville R, Simpson JH, Seeds AM (2015) A neural command circuit for grooming movement control. Elife 4.

Hancock, C. E., Bilz, F., Fiala, A. (2019). In Vivo Optical Calcium Imaging of Learning-Induced Synaptic Plasticity in Drosophila melanogaster. J. Vis. Exp. (152), e60288.

Handler A, Graham TGW, Cohn R, Morantte I, Siliciano AF, Zeng J, Li Y, Ruta V (2019) Distinct Dopamine Receptor Pathways Underlie the Temporal Sensitivity of Associative Learning. Cell 178:60-75.e19.

Hartenstein V, Omoto JJ, Ngo KT, Wong D, Kuert PA, Reichert H, Lovick JK, Younossi-Hartenstein A (2018) Structure and development of the subesophageal zone of the Drosophila brain. I. Segmental architecture, compartmentalization, and lineage anatomy. Journal of Comparative Neurology 526:6–32.

Harz H, Hegemann P (1991) Rhodopsin-regulated calcium currents in Chlamydomonas. Nature 351:489–491.

Hazelrigg T, Levis R, Rubin GM. Transformation of white locus DNA in drosophila: dosage compensation, zeste interaction, and position effects. Cell. 1984 Feb;36(2):469-81.

Hattori D, Aso Y, Swartz KJ, Rubin GM, Abbott LF, Axel R (2017) Representations of Novelty and Familiarity in a Mushroom Body Compartment. Cell 169:956-969.e17.

Hearn MG, Ren Y, McBride EW, Reveillaud I, Beinborn M, Kopin AS (2002) A Drosophila dopamine 2-like receptor: Molecular characterization and identification of multiple alternatively spliced variants. Proceedings of the National Academy of Sciences 99:14554–14559.

Heisenberg M (1980) Mutants of Brain Structure and Function: What is the Significance of the Mushroom Bodies for Behavior? In: Development and Neurobiology of Drosophila, pp 373–390. Boston, MA: Springer US.

Heisenberg M (2003) Mushroom body memoir: from maps to models. Nat Rev Neurosci 4:266–275.

Heisenberg M, Borst A, Wagner S, Byers D (1985) Drosophila Mushroom Body Mutants are Deficient in Olfactory Learning. J Neurogenet 2:1–30.

Heisenberg, M. and Gerber, B. (2008). Behavioral analysis of learning and memory in Drosophila. In Learning Theory and Behavior, R Menzel (Ed.). Vol. 1 of Learning and Memory: A Comprehensive Reference (J Byrne [Ed.]), pp. 549-559. Oxford: Elsevier.

Hellstern F, Malaka R, Hammer M (1998) Backward inhibitory learning in honeybees: a behavioral analysis of reinforcement processing. Learning & Memory 4:429–444.

Hige T (2018) What can tiny mushrooms in fruit flies tell us about learning and memory? Neurosci Res 129:8–16.

Hige T, Aso Y, Modi MN, Rubin GM, Turner GC (2015) Heterosynaptic Plasticity Underlies Aversive Olfactory Learning in Drosophila. Neuron 88:985–998.

Himmelreich S, Masuho I, Berry JA, MacMullen C, Skamangas NK, Martemyanov KA, Davis RL (2017) Dopamine Receptor DAMB Signals via Gq to Mediate Forgetting in Drosophila. Cell Rep 21:2074–2081.

Hoffman SG, Smits JAJ (2008) Cognitive-Behavioral Therapy for Adult Anxiety Disorders. J Clin Psychiatry 69:621–632.

Honegger KS, Campbell RAA, Turner GC (2011) Cellular-Resolution Population Imaging Reveals Robust Sparse Coding in the Drosophila Mushroom Body. The Journal of Neuroscience 31:11772–11785.

Holm S. (1979). A simple sequentially rejective multiple test procedure. Scand. J. Statist. 6, 65-70.

Hume, D. (1978). A treatise of human nature, edited by L. A. Selby-Bigge & P.H. Nidditch, Oxford: Clarendon Press. (Original published 1739-40).

Hou G, Hao M, Duan J, Han M-H (2024) The Formation and Function of the VTA Dopamine System. Int J Mol Sci 25.

Howes OD, Kapur S (2009) The Dopamine Hypothesis of Schizophrenia: Version III--The Final Common Pathway. Schizophr Bull 35:549–562.

Hsu CT, Bhandawat V (2016) Organization of descending neurons in Drosophila melanogaster. Sci Rep 6:20259.

Hsueh B et al. (2023) Cardiogenic control of affective behavioural state. Nature 615:292–299.

Huetteroth W, Perisse E, Lin S, Klappenbach M, Burke C, Waddell S (2015) Sweet Taste and Nutrient Value Subdivide Rewarding Dopaminergic Neurons in Drosophila. Current Biology 25:751–758.

Isabel G, Pascual A, Preat T (2004) Exclusive Consolidated Memory Phases in Drosophila. Science (1979) 304:1024–1027.

Israel S, Rozenfeld E, Weber D, Huetteroth W, Parnas M (2022) Olfactory stimuli and moonwalker SEZ neurons can drive backward locomotion in Drosophila. Current Biology 32:1131-1149.e7.

Ito I, Ong RC, Raman B, Stopfer M (2008) Sparse odor representation and olfactory learning. Nat Neurosci 11:1177–1184.

Jacob PF, Waddell S (2020) Spaced Training Forms Complementary Long-Term Memories of Opposite Valence in Drosophila. Neuron 106:977-991.e4.

James, W. (1884). What is an emotion? Mind 9, 188–205 (1884).

James, W. (1890). The principles of psychology, Vol. 1. Henry Holt and Co.

Jékely G, Godfrey-Smith P, Keijzer F (2021) Reafference and the origin of the self in early nervous system evolution. Philosophical Transactions of the Royal Society B: Biological Sciences 376:20190764.

Jhang J, Park S, Liu S, O'Keefe DD, Han S (2024) A top-down slow breathing circuit that alleviates negative affect in mice. Nat Neurosci 27:2455–2465.

Jiang L, Litwin-Kumar A (2021) Models of heterogeneous dopamine signaling in an insect learning and memory center. PLoS Comput Biol 17:e1009205.

Joiner WJ, Crocker A, White BH, Sehgal A (2006) Sleep in Drosophila is regulated by adult mushroom bodies. Nature 441:757–760.

Jones CRG, Jahanshahi M (2011) Dopamine Modulates Striato-Frontal Functioning during Temporal Processing. Front Integr Neurosci 5.

Kalinichenko LS et al. (2021) Neutral sphingomyelinase mediates the co-morbidity trias of alcohol abuse, major depression and bone defects. Mol Psychiatry 26:7403–7416.

Kandel, E. R. (2007). In search of memory: The emergence of a new science of mind. WW Norton & Company.

Keene AC, Waddell S (2007) Drosophila olfactory memory: single genes to complex neural circuits. Nat Rev Neurosci 8:341–354.

Kegeles LS, Abi-Dargham A, Frankle WG, Gil R, Cooper TB, Slifstein M, Hwang D-R, Huang Y, Haber SN, Laruelle M (2010) Increased Synaptic Dopamine Function in Associative Regions of the Striatum in Schizophrenia. Arch Gen Psychiatry 67:231.

Kim AJ, Fitzgerald JK, Maimon G (2015) Cellular evidence for efference copy in Drosophila visuomotor processing. Nat Neurosci 18:1247–1255.

Kim D, Alvarez M, Lechuga LM, Louis M (2017) Species-specific modulation of food-search behavior by respiration and chemosensation in Drosophila larvae. Elife 6.

Kim Y-C, Lee H-G, Han K-A (2007) D 1 Dopamine Receptor dDA1 Is Required in the Mushroom Body Neurons for Aversive and Appetitive Learning in Drosophila. The Journal of Neuroscience 27:7640–7647.

Kirkhart C, Scott K (2015) Gustatory Learning and Processing in the Drosophila Mushroom Bodies. The Journal of Neuroscience 35:5950–5958.

Klapoetke NC et al. (2014) Independent optical excitation of distinct neural populations. Nat Methods 11:338–346.

Kong M-S, Kim N, Jo KI, Kim S-P, Choi J-S (2023) Differential Encoding of Trace and Delay Fear Memory in the Entorhinal Cortex. Exp Neurobiol 32:20–30.

Kohler R E, (1994) Lords of the Fly. Drosophila Genetics and the Experimental Life. The University of Chicago Press, Chicago, London.

Konorski, J. (1948) Conditioned Reflexes and Neuron Organization. Cambridge University Press, Cambridge

König C, Khalili A, Ganesan M, Nishu AP, Garza AP, Niewalda T, Gerber B, Aso Y, Yarali A (2018) Reinforcement signaling of punishment versus relief in fruit flies. Learning & Memory 25:247–257.

König C, Khalili A, Niewalda T, Gao S, Gerber B (2019) An optogenetic analogue of second-order reinforcement in Drosophila. Biol Lett 15:20190084.

Krashes MJ, Keene AC, Leung B, Armstrong JD, Waddell S (2007) Sequential Use of Mushroom Body Neuron Subsets during Drosophila Odor Memory Processing. Neuron 53:103–115.

Krypotos A-M, Moscarello JM, Sears RM, LeDoux JE, Galatzer-Levy I (2018) A principled method to identify individual differences and behavioral shifts in signaled active avoidance. Learning & Memory 25:564–568.

Lai S-L, Lee T (2006) Genetic mosaic with dual binary transcriptional systems in Drosophila. Nat Neurosci 9:703–709.

Laing PAF, Vervliet B, Dunsmoor JE, Harrison BJ (2024) Pavlovian safety learning: An integrative theoretical review. Psychon Bull Rev.

Lammel S, Lim BK, Malenka RC (2014) Reward and aversion in a heterogeneous midbrain dopamine system. Neuropharmacology 76:351–359.

Lange, C. G. (1912). The mechanism of the emotions (B. Rand, Trans.). In B. Rand (Ed.), The classical psychologists (pp. 672–684). Copenhagen (Original work published 1885).

Larsson MC, Domingos AI, Jones WD, Chiappe ME, Amrein H, Vosshall LB (2004) Or83b Encodes a Broadly Expressed Odorant Receptor Essential for Drosophila Olfaction. Neuron 43:703–714.

Laruelle M, Abi-Dargham A, Gil R, Kegeles L, Innis R (1999) Increased dopamine transmission in schizophrenia: relationship to illness phases. Biol Psychiatry 46:56–72.

Lattal KM, Wood MA (2013) Epigenetics and persistent memory: implications for reconsolidation and silent extinction beyond the zero. Nat Neurosci 16:124–129.

Lechner HA, Byrne JH (1998) New Perspectives on Classical Conditioning: a Synthesis of Hebbian and Non-Hebbian Mechanisms. Neuron 20:355–358.

Ledgerwood L, Richardson R, Cranney J (2005). D-cycloserine facilitates extinction of learned fear: effects on reacquisition and generalized extinction. Biol Psychiatry. 2005 Apr 15;57(8):841-7.

LeDoux JE, Moscarello J, Sears R, Campese V (2017) The birth, death and resurrection of avoidance: a reconceptualization of a troubled paradigm. Mol Psychiatry 22:24–36.

Lerner TN, Holloway AL, Seiler JL (2021) Dopamine, Updated: Reward Prediction Error and Beyond. Curr Opin Neurobiol 67:123–130.

Levin LR, Han P-L, Hwang PM, Feinstein PG, Davis RL, Reed RR (1992) The Drosophila learning and memory gene rutabaga encodes a - adenylyl cyclase. Cell 68:479–489.

Levy HC, Stevens KT, Tolin DF (2022) Research Review: A meta-analysis of relapse rates in cognitive behavioral therapy for anxiety and related disorders in youth. Journal of Child Psychology and Psychiatry 63:252–260.

Liang H, Paxinos G, Watson C (2011) Projections from the brain to the spinal cord in the mouse. Brain Struct Funct 215:159–186

Li F et al. (2020) The connectome of the adult Drosophila mushroom body provides insights into function. Elife 9.

Li X, Zhou W, Yi Z (2022) A glimpse of gender differences in schizophrenia. Gen Psychiatr 35:e100823.

Lieu M-H, Vallejos MJ, Michael E, Tsunoda S (2012) Mechanisms Underlying Stage-1 TRPL Channel Translocation in Drosophila Photoreceptors. PLoS One 7:e31622.

Lieberman, D. A. (2020). Learning and Memory (2nd ed.). Cambridge: Cambridge University Press.

Lin AC, Bygrave AM, de Calignon A, Lee T, Miesenböck G (2014) Sparse, decorrelated odor coding in the mushroom body enhances learned odor discrimination. Nat Neurosci 17:559–568.

Lin H-H, Lai JS-Y, Chin A-L, Chen Y-C, Chiang A-S (2007) A Map of Olfactory Representation in the Drosophila Mushroom Body. Cell 128:1205–1217.

Lin Y-C, Wu T, Wu C-L (2024) The Neural Correlations of Olfactory Associative Reward Memories in Drosophila. Cells 13:1716.

Liu C, Plaçais P-Y, Yamagata N, Pfeiffer BD, Aso Y, Friedrich AB, Siwanowicz I, Rubin GM, Preat T, Tanimoto H (2012) A subset of dopamine neurons signals reward for odour memory in Drosophila. Nature 488:512–516.

Liu WW, Wilson RI (2013) Glutamate is an inhibitory neurotransmitter in the Drosophila olfactory system. Proceedings of the National Academy of Sciences 110:10294–10299.

Liu X, Davis RL (2009) The GABAergic anterior paired lateral neuron suppresses and is suppressed by olfactory learning. Nat Neurosci 12:53–59.

Livingstone MS, Sziber PP, Quinn WG (1984) Loss of calcium/calmodulin responsiveness in adenylate cyclase of rutabaga, a Drosophila learning mutant. Cell 37:205–215.

Lovibond PF (2004) Cognitive Processes in Extinction: Figure 1. Learning & Memory 11:495–500.

Luan H, Diao F, Scott RL, White BH (2020) The Drosophila Split Gal4 System for Neural Circuit Mapping. Front Neural Circuits 14.

Luan H, Peabody NC, Vinson CR, White BH (2006) Refined Spatial Manipulation of Neuronal Function by Combinatorial Restriction of Transgene Expression. Neuron 52:425–436.

Lütcke H (2010) Optical recording of neuronal activity with a genetically-encoded calcium indicator in anesthetized and freely moving mice. Front Neural Circuits.

Malaka R (1999) Models of Classical Conditioning. Bull Math Biol 61:33–83.

Mank M, Griesbeck O (2008) Genetically Encoded Calcium Indicators. Chem Rev 108:1550–1564.

Mao Z, Davis RL (2009) Eight different types of dopaminergic neurons innervate the Drosophila mushroom body neuropil: anatomical and physiological heterogeneity. Front Neural Circuits 3:5.

Maren S (2001) Neurobiology of Pavlovian Fear Conditioning. Annu Rev Neurosci 24:897–931.

Marin EC, Büld L, Theiss M, Sarkissian T, Roberts RJV, Turnbull R, Tamimi IFM, Pleijzier MW, Laursen WJ, Drummond N, Schlegel P, Bates AS, Li F, Landgraf M, Costa M, Bock DD, Garrity PA, Jefferis GSXE (2020) Connectomics Analysis Reveals First-, Second-, and Third-Order Thermosensory and Hygrosensory Neurons in the Adult Drosophila Brain. Current Biology 30:3167-3182.e4.

Marquis M, Wilson RI (2022) Locomotor and olfactory responses in dopamine neurons of the Drosophila superior-lateral brain. Current Biology 32:5406-5414.e5.

Marr D (1969) A theory of cerebellar cortex. J Physiol 202:437–470.

Martin JR, Ernst R, Heisenberg M (1998) Mushroom bodies suppress locomotor activity in Drosophila melanogaster. Learn Mem 5:179–191.

Masek P, Scott K (2010) Limited taste discrimination in Drosophila. Proceedings of the National Academy of Sciences 107:14833–14838.

McClelland JL, Rumelhart DE (1985) Distributed memory and the representation of general and specific information. J Exp Psychol Gen 114:159–188.

McCloskey M, Cohen NJ (1989) Catastrophic Interference in Connectionist Networks: The Sequential Learning Problem. In, pp 109–165.

McCurdy LY, Sareen P, Davoudian PA, Nitabach MN (2021) Dopaminergic mechanism underlying reward-encoding of punishment omission during reversal learning in Drosophila. Nat Commun 12:1115.

McCutcheon RA, Abi-Dargham A, Howes OD (2019) Schizophrenia, Dopamine and the Striatum: From Biology to Symptoms. Trends Neurosci 42:205–220.

McGuire SE, Le PT, Davis RL (2001) The Role of Drosophila Mushroom Body Signaling in Olfactory Memory. Science (1979) 293:1330–1333.

McGuire TR (1984) Learning in three species of diptera: The blow flyPhormia regina, the fruit flyDrosophila melanogaster, and the house flyMusca domestica. Behav Genet 14:479–526.

Medeiros AM, Hobbiss AF, Borges G, Moita M, Mendes CS (2024) Mechanosensory bristles mediate avoidance behavior by triggering sustained local motor activity in Drosophila melanogaster. Current Biology 34:2812-2830.e5.

Meinertzhagen IA, O'Neil SD (1991) Synaptic organization of columnar elements in the lamina of the wild type in Drosophila melanogaster. Journal of Comparative Neurology 305:232–263.

Menzel R (2022) In Search for the Retrievable Memory Trace in an Insect Brain. Front Syst Neurosci 16:876376.

Menzel, R., et al., in: Experimental Analysis of Insect Behavior, p. 195 (ed. L. Barton-Browne). Berlin-Heidelberg-New York: Springer 1974

Meschi E, Duquenoy L, Otto N, Dempsey G, Waddell S (2024) Compensatory enhancement of input maintains aversive dopaminergic reinforcement in hungry Drosophila. Neuron 112:2315-2332.e8.

Milad MR, Quirk GJ (2012) Fear Extinction as a Model for Translational Neuroscience: Ten Years of Progress. Annu Rev Psychol 63:129–151.

Mitte K (2005) Meta-Analysis of Cognitive-Behavioral Treatments for Generalized Anxiety Disorder: A Comparison With Pharmacotherapy. Psychol Bull 131:785–795.

Modi MN, Shuai Y, Turner GC (2020) The Drosophila Mushroom Body: From Architecture to Algorithm in a Learning Circuit. Annu Rev Neurosci 43:465–484.

Mohammadi M, Fendt M (2015) Relief learning is dependent on <scp>NMDA</scp> receptor activation in the nucleus accumbens. Br J Pharmacol 172:2419–2426.

Monosov IE, Leopold DA, Hikosaka O (2015) Neurons in the Primate Medial Basal Forebrain Signal Combined Information about Reward Uncertainty, Value, and Punishment Anticipation. The Journal of Neuroscience 35:7443–7459.

Moritz S, Woodward TS (2005) Jumping to conclusions in delusional and non-delusional schizophrenic patients. Br J Clin Psychol 44:193–207.

Moritz S, Woodward TS, Whitman JC, Cuttler C (2005) Confidence in Errors as a Possible Basis for Delusions in Schizophrenia. Journal of Nervous & Mental Disease 193:9–16.

Müller I, Fendt M (2023) Fear Conditioning in Laboratory Rodents. In, pp 119–160.

Myers KM, Davis M (2002) Behavioral and Neural Analysis of Extinction. Neuron 36:567–584.

Myers KM, Davis M (2007) Mechanisms of fear extinction. Mol Psychiatry 12:120–150.

Myers, K. M., Ressler, K. J., & Davis, M. (2006). Different mechanisms of fear extinction dependent on length of time since fear acquisition. Learning & memory, 13(2), 216-223.

Mystkowski, J. L., Craske, M. G., Echiverri, A. M., & Labus, J. S. (2006). Mental reinstatement of context and return of fear in spider-fearful participants. Behavior Therapy, 37(1), 49-60.

Nader K, Schafe GE, LeDoux JE. (2000). Fear memories require protein synthesis in the amygdala for reconsolidation after retrieval. Nature 406:722–26

Nagel G, Ollig D, Fuhrmann M, Kateriya S, Musti AM, Bamberg E, Hegemann P (2002) Channelrhodopsin-1: A Light-Gated Proton Channel in Green Algae. Science (1979) 296:2395–2398.

Nagel G, Szellas T, Huhn W, Kateriya S, Adeishvili N, Berthold P, Ollig D, Hegemann P, Bamberg E (2003) Channelrhodopsin-2, a directly light-gated cation-selective membrane channel. Proceedings of the National Academy of Sciences 100:13940–13945.

Nakai J, Ohkura M, Imoto K (2001) A high signal-to-noise Ca2+ probe composed of a single green fluorescent protein. Nat Biotechnol 19:137–141.

Namiki S, Dickinson MH, Wong AM, Korff W, Card GM (2018) The functional organization of descending sensory-motor pathways in Drosophila. Elife 7.

Namiki S, Kanzaki R (2016) Comparative Neuroanatomy of the Lateral Accessory Lobe in the Insect Brain. Front Physiol 7.

Niens J, Reh F, Çoban B, Cichewicz K, Eckardt J, Liu Y-T, Hirsh J, Riemensperger TD (2017) Dopamine Modulates Serotonin Innervation in the Drosophila Brain. Front Syst Neurosci 11:76.

Niewalda T, Michels B, Jungnickel R, Diegelmann S, Kleber J, Kähne T, Gerber B (2015) Synapsin determines memory strength after punishment- and relief-learning. J Neurosci 35:7487–7502.

Niewalda T, Singhal N, Fiala A, Saumweber T, Wegener S, Gerber B (2008) Salt Processing in Larval Drosophila: Choice, Feeding, and Learning Shift from Appetitive to Aversive in a Concentration-Dependent Way. Chem Senses 33:685–692.

Norrholm, S. D., Vervliet, B., Jovanovic, T., Boshoven, W., Myers, K. M., Davis, M., ... & Duncan, E. J. (2008). Timing of extinction relative to acquisition: a parametric analysis of fear extinction in humans. Behavioral neuroscience, 122(5), 1016.

Nowakowski ME, Rogojanski J, Antony MM (2013) Specific Phobia. In: The Wiley Handbook of Cognitive Behavioral Therapy, pp 979–1000. Wiley.

Öhman A, Mineka S (2001) Fears, phobias, and preparedness: Toward an evolved module of fear and fear learning. Psychol Rev 108:483–522.

Oltmanns S, Abben FS, Ender A, Aimon S, Kovacs R, Sigrist SJ, Storace DA, Geiger JRP, Raccuglia D (2020) NOSA, an Analytical Toolbox for Multicellular Optical Electrophysiology. Front Neurosci 14:712.

Otto N, Pleijzier MW, Morgan IC, Edmondson-Stait AJ, Heinz KJ, Stark I, Dempsey G, Ito M, Kapoor I, Hsu J, Schlegel PM, Bates AS, Feng L, Costa M, Ito K, Bock DD, Rubin GM, Jefferis GSXE, Waddell S (2020) Input Connectivity Reveals Additional Heterogeneity of Dopaminergic Reinforcement in Drosophila. Current Biology 30:3200-3211.e8.

Owald D, Felsenberg J, Talbot CB, Das G, Perisse E, Huetteroth W, Waddell S (2015) Activity of Defined Mushroom Body Output Neurons Underlies Learned Olfactory Behavior in Drosophila. Neuron 86:417–427.

Pai T-P, Chen C-C, Lin H-H, Chin A-L, Lai JS-Y, Lee P-T, Tully T, Chiang A-S (2013) Drosophila ORB protein in two mushroom body output neurons is necessary for long-term memory formation. Proceedings of the National Academy of Sciences 110:7898–7903.

Papadopoulou M, Cassenaer S, Nowotny T, Laurent G (2011). Normalization for sparse encoding of odors by a wide-field interneuron. Science. 2011 May 6;332(6030):721-5. doi: 10.1126/science.1201835. Erratum in: Science. 2011 Jun 10;332(6035):1263

Pascual A, Préat T (2001). Localization of long-term memory within the Drosophila mushroom body. Science. 2001 Nov 2;294(5544):1115-7.

Pavlov, I.P. (1927). Conditioned Reflexes: An Investigation of the Physiological Activity of the Cerebral Cortex (H. Milford.).

Perez-Orive J, Mazor O, Turner GC, Cassenaer S, Wilson RI, Laurent G (2002) Oscillations and Sparsening of Odor Representations in the Mushroom Body. Science (1979) 297:359–365.

Perisse E, Burke C, Huetteroth W, Waddell S (2013) Shocking Revelations and Saccharin Sweetness in the Study of Drosophila Olfactory Memory. Current Biology 23:R752–R763.

Perisse E, Owald D, Barnstedt O, Talbot CB, Huetteroth W, Waddell S (2016) Aversive Learning and Appetitive Motivation Toggle Feed-Forward Inhibition in the Drosophila Mushroom Body. Neuron 90:1086–1099.

Perron A, Mutoh H, Launey T, Knöpfel T (2009) Red-Shifted Voltage-Sensitive Fluorescent Proteins. Chem Biol 16:1268–1277.

Pfeffer SE, Wahl VL, Wittlinger M (2016) How to find home backwards? Locomotion and inter-leg coordination during rearward walking of Cataglyphis fortis desert ants. Journal of Experimental Biology 219:2110–2118.

Pfeiffer BD, Ngo T-TB, Hibbard KL, Murphy C, Jenett A, Truman JW, Rubin GM (2010) Refinement of Tools for Targeted Gene Expression in Drosophila. Genetics 186:735–755.

Phelps JS, Hildebrand DGC, Graham BJ, Kuan AT, Thomas LA, Nguyen TM, Buhmann J, Azevedo AW, Sustar A, Agrawal S, Liu M, Shanny BL, Funke J, Tuthill JC, Lee W-CA (2021) Reconstruction of motor control circuits in adult Drosophila using automated transmission electron microscopy. Cell 184:759-774.e18.

Piggott BJ, Liu J, Feng Z, Wescott SA, Xu XZS (2011) The Neural Circuits and Synaptic Mechanisms Underlying Motor Initiation in C. elegans. Cell 147:922–933.

Pittig A, Wong AHK, Glück VM, Boschet JM (2020) Avoidance and its bi-directional relationship with conditioned fear: Mechanisms, moderators, and clinical implications. Behaviour Research and Therapy 126:103550.

Plaçais P-Y, Trannoy S, Friedrich AB, Tanimoto H, Preat T (2013) Two Pairs of Mushroom Body Efferent Neurons Are Required for Appetitive Long-Term Memory Retrieval in Drosophila. Cell Rep 5:769–780.

Plath JA, Felsenberg J, Eisenhardt D (2012) Reinstatement in honeybees is context-dependent. Learning & Memory 19:543–549.

Pooryasin A, Fiala A (2015) Identified Serotonin-Releasing Neurons Induce Behavioral Quiescence and Suppress Mating in Drosophila. J Neurosci 35:12792–12812.

Quinn WG, Harris WA, Benzer S (1974) Conditioned Behavior in Drosophila melanogaster. Proceedings of the National Academy of Sciences 71:708–712.

Ramdya P, Lichocki P, Cruchet S, Frisch L, Tse W, Floreano D, Benton R (2015) Mechanosensory interactions drive collective behaviour in Drosophila. Nature 519:233–236.

Rescorla, RA (1966). Predictability and number of pairings in Pavlovian fear conditioning. Psychonomic Science, 4(11), 383–384

Rescorla, R. A. (1972). "Configural" conditioning in discrete-trial bar pressing. Journal of Comparative and Physiological Psychology, 79(2), 307–317.

Rescorla RA (1991) Associations of multiple outcomes with an instrumental response. J Exp Psychol Anim Behav Process 17:465–474.

Rescorla RA (2003) Protection from extinction. Learn Behav 31:124–132.

Rescorla RA (2006) Deepened extinction from compound stimulus presentation. J Exp Psychol Anim Behav Process 32:135–144.

Rescorla, RA (1996). Preservation of Pavlovian Associations through Extinction. The Quarterly Journal of Experimental Psychology Section B, 49(3b), 245-258.

Richardson R, Ledgerwood L, Cranney J. (2004). Facilitation of fear extinction by D-cycloserine: theoretical and clinical implications. Learn. Mem. 11:510–16

Riemensperger T, Issa A-R, Pech U, Coulom H, Nguyễn M-V, Cassar M, Jacquet M, Fiala A, Birman S (2013) A single dopamine pathway underlies progressive locomotor deficits in a Drosophila model of Parkinson disease. Cell Rep 5:952–960.

Riemensperger T, Kittel RJ, Fiala A (2016) Optogenetics in Drosophila Neuroscience. In, pp 167–175.

Riemensperger T, Völler T, Stock P, Buchner E, Fiala A (2005) Punishment Prediction by Dopaminergic Neurons in Drosophila. Current Biology 15:1953–1960.

Rosen JB, Schulkin J (1998) From normal fear to pathological anxiety. Psychol Rev 105:325–350.

Rowe MK, Craske MG. (1998). Effects of varied-stimulus exposure training on fear reduction and return of fear. Behav. Res. Ther. 36:719–34

Russell IJ, Roberts BL (1972) Inhibition of Spontaneous Lateral-Line Activity by Efferent Nerve Stimulation. Journal of Experimental Biology 57:77–82.

Salcedo E, Huber A, Henrich S, Chadwell L V., Chou W-H, Paulsen R, Britt SG (1999) Blue- and Green-Absorbing Visual Pigments of Drosophila : Ectopic Expression and Physiological Characterization of the R8 Photoreceptor Cell-Specific Rh5 and Rh6 Rhodopsins. The Journal of Neuroscience 19:10716–10726.

Sapkal N, Mancini N, Kumar DS, Spiller N, Murakami K, Vitelli G, Bargeron B, Maier K, Eichler K, Jefferis GSXE, Shiu PK, Sterne GR, Bidaye SS (2024) Neural circuit mechanisms underlying context-specific halting in Drosophila. Nature 634:191–200.

Saumweber T, Rohwedder A, Schleyer M, Eichler K, Chen Y, Aso Y, Cardona A, Eschbach C, Kobler O, Voigt A, Durairaja A, Mancini N, Zlatic M, Truman JW, Thum AS, Gerber B (2018) Functional architecture of reward learning in mushroom body extrinsic neurons of larval Drosophila. Nat Commun 9:1104.

Scavio MJ (1974) Classical-classical transfer: Effects of prior aversive conditions upon appetitive conditioning in rabbits (Oryctolagus cuniculus). J Comp Physiol Psychol 86:107–115.

Scheffer LK et al. (2020) A connectome and analysis of the adult Drosophila central brain. Elife 9.

Schlegel P et al. (2024) Whole-brain annotation and multi-connectome cell typing of Drosophila. Nature 634:139–152.

Schleyer M, Reid SF, Pamir E, Saumweber T, Paisios E, Davies A, Gerber B, Louis M (2015) The impact of odor–reward memory on chemotaxis in larval Drosophila. Learning & Memory 22:267–277.

Schmid A, Koch M, Schnitzler HU (1995) Conditioned Pleasure Attenuates the Startle Response in Rats. Neurobiol Learn Mem 64:1–3.

Schiller D, Cain CK, Curley NG, Schwartz JS, Stern SA. et al. 2008. Evidence for recovery of fear following immediate extinction in rats and humans. Learn. Mem. 15:394–402

Schöneich S, Schildberger K, Stevenson PA (2011) Neuronal organization of a fast-mediating cephalothoracic pathway for antennal-tactile information in the cricket (Gryllus bimaculatus DeGeer). Journal of Comparative Neurology 519:1677–1690.

Schachter, S., & Singer, J. (1962). Cognitive, social, and physiological determinants of emotional state. Psychological Review, 69(5), 379–399

Schroll C, Riemensperger T, Bucher D, Ehmer J, Völler T, Erbguth K, Gerber B, Hendel T, Nagel G, Buchner E, Fiala A (2006) Light-Induced Activation of Distinct Modulatory Neurons Triggers Appetitive or Aversive Learning in Drosophila Larvae. Current Biology 16:1741–1747.

Schultz W (2006) Behavioral Theories and the Neurophysiology of Reward. Annu Rev Psychol 57:87–115.

Schultz W (2015) Neuronal Reward and Decision Signals: From Theories to Data. Physiol Rev 95:853–951.

Schultz W, Dayan P, Montague PR (1997) A Neural Substrate of Prediction and Reward. Science (1979) 275:1593–1599.

Schwaerzel M, Heisenberg M, Zars T (2002) Extinction Antagonizes Olfactory Memory at the Subcellular Level. Neuron 35:951–960.

Schwaerzel M, Monastirioti M, Scholz H, Friggi-Grelin F, Birman S, Heisenberg M (2003) Dopamine and Octopamine Differentiate between Aversive and Appetitive Olfactory Memories in Drosophila. The Journal of Neuroscience 23:10495–10502.

Schwarz S, Wystrach A, Cheng K (2017) Ants' navigation in an unfamiliar environment is influenced by their experience of a familiar route. Sci Rep 7:14161.

Séjourné J, Plaçais P-Y, Aso Y, Siwanowicz I, Trannoy S, Thoma V, Tedjakumala SR, Rubin GM, Tchénio P, Ito K, Isabel G, Tanimoto H, Preat T (2011) Mushroom body efferent neurons responsible for aversive olfactory memory retrieval in Drosophila. Nat Neurosci 14:903–910.

Seki Y, Dweck HKM, Rybak J, Wicher D, Sachse S, Hansson BS (2017) Olfactory coding from the periphery to higher brain centers in the Drosophila brain. BMC Biol 15:56.

Sen R, Wang K, Dickson BJ (2019) TwoLumps Ascending Neurons Mediate Touch-Evoked Reversal of Walking Direction in Drosophila. Current Biology 29:4337-4344.e5.

Sen R, Wu M, Branson K, Robie A, Rubin GM, Dickson BJ (2017) Moonwalker Descending Neurons Mediate Visually Evoked Retreat in Drosophila. Current Biology 27:766–771.

Shanks, D. R., Pearson, S. M. and Dickinson, A. (1989). Temporal contiguity and the judgement of causality by human subjects. Q. J. Exp. Psychol. (B) 41, 139-159.

Shiu PK et al. (2024) A Drosophila computational brain model reveals sensorimotor processing. Nature 634:210–219.

Shuai Y, Hu Y, Qin H, Campbell RAA, Zhong Y (2011) Distinct molecular underpinnings of Drosophila olfactory trace conditioning. Proc Natl Acad Sci U S A 108:20201–20206.

Siju KP, De Backer J-F, Grunwald Kadow IC (2021) Dopamine modulation of sensory processing and adaptive behavior in flies. Cell Tissue Res 383:207–225.

Silver D et al. (2016) Mastering the game of Go with deep neural networks and tree search. Nature 529:484–489.

Simpson JH (2024) Descending control of motor sequences in. Curr Opin Neurobiol 84:102822.

Sitaraman D, Aso Y, Jin X, Chen N, Felix M, Rubin GM, Nitabach MN (2015) Propagation of Homeostatic Sleep Signals by Segregated Synaptic Microcircuits of the Drosophila Mushroom Body. Current Biology 25:2915–2927.

Solomon RL (1980) The opponent-process theory of acquired motivation: The costs of pleasure and the benefits of pain. American Psychologist 35:691–712.

Solomon RL, Corbit JD (1973) An opponent-process theory of motivation: II. Cigarette addiction. J Abnorm Psychol 81:158–171.

Solomon RL, Corbit JD (1974) An opponent-process theory of motivation: I. Temporal dynamics of affect. Psychol Rev 81:119–145.

Solomon RL, Wynne LC (1954) Traumatic avoidance learning: the principles of anxiety conservation and partial irreversibility. Psychol Rev 61:353–385.

Sosulski DL, Bloom ML, Cutforth T, Axel R, Datta SR (2011) Distinct representations of olfactory information in different cortical centres. Nature 472:213–216.

Staudacher E, Schildberger K (1998) Gating of Sensory Responses of Descending Brain Neurones During Walking in Crickets. Journal of Experimental Biology 201:559–572.

Steinfeld, M. R., & Bouton, M. E. (2020). Context and renewal of habits and goal-directed actions after extinction. Journal of Experimental Psychology: Animal Learning and Cognition, 46(4), 408.

Stettler DD, Axel R (2009) Representations of Odor in the Piriform Cortex. Neuron 63:854–864.

Stocker RF (1994) The organization of the chemosensory system in Drosophila melanogaster: a rewiew. Cell Tissue Res 275:3–26.

Stocker RF, Heimbeck G, Gendre N, de Belle JS (1997) Neuroblast ablation in Drosophila P[GAL4] lines reveals origins of olfactory interneurons. J Neurobiol 32:443–456.

Storvse AB, McNally GP, Richardson R. 2010. US habituation, like CS extinction, produces a decrement in conditioned fear that is NMDA dependent and subject to renewal and reinstatement. Neurobiol. Learn. Mem. 93:463–71

Strack F, Martin LL, Stepper S (1988) Inhibiting and facilitating conditions of the human smile: A nonobtrusive test of the facial feedback hypothesis. J Pers Soc Psychol 54:768–777.

Strausfeld NJ, Hansen L, Li Y, Gomez RS, Ito K (1998) Evolution, discovery, and interpretations of arthropod mushroom bodies. Learn Mem 5:11–37.

Stuber GD (2023) Neurocircuits for motivation. Science (1979) 382:394–398.

Sugamori KS, Demchyshyn LL, McConkey F, Forte MA, Niznik HB (1995) A primordial dopamine D1-like adenylyl cyclase-linked receptor from Drosophila melanogaster displaying poor affinity for benzazepines. FEBS Lett 362:131–138.

Sun Y, Qiu R, Li X, Cheng Y, Gao S, Kong F, Liu L, Zhu Y (2020) Social attraction in Drosophila is regulated by the mushroom body and serotonergic system. Nat Commun 11:5350.

Sutton, R. S. & Barto, A. G. Reinforcement learning: An introduction (MIT Press, 2018).

Takemura, S. Y., Aso, Y., Hige, T., Wong, A., Lu, Z., Xu, C. S., ... & Scheffer, L. K. (2017). A connectome of a learning and memory center in the adult Drosophila brain. Elife, 6, e26975.

Takemura, S. Y. (2024). A connectome of the male Drosophila ventral nerve cord. eLife 13. RP97769.

Tanaka NK, Tanimoto H, Ito K (2008) Neuronal assemblies of the Drosophila mushroom body. Journal of Comparative Neurology 508:711–755.

Tang S, Guo A (2001) Choice Behavior of Drosophila Facing Contradictory Visual Cues. Science (1979) 294:1543–1547.

Tanimoto H, Heisenberg M, Gerber B (2004) Event timing turns punishment to reward. Nature 430:983–983.

Taylor SS, Buechler JA, Yonemoto W (1990) Taylor SS, Buechler JA, Yonemoto W. cAMP-dependent protein kinase: framework for a diverse family of regulatory enzymes. Annu Rev Biochem. 1990;59:971-1005

Technau GM (1984) Fiber number in the mushroom bodies of adult Drosophila melanogaster depends on age, sex and experience. J Neurogenetics 1:113–126

Tempel BL, Bonini N, Dawson DR, Quinn WG (1983) Reward learning in normal and mutant Drosophila. Proceedings of the National Academy of Sciences 80:1482–1486.

The American Journal of Psychiatry. (1996). American Journal of Psychiatry, 153(4), A52A52.

Thoener J, König C, Weiglein A, Toshima N, Mancini N, Amin F, Schleyer M (2021) Associative learning in larval and adult Drosophila is impaired by the dopamine-synthesis inhibitor 3-Iodo-L-tyrosine. Biol Open 10.

Thoener J, Weiglein A, Gerber B, Schleyer M (2022) Optogenetically induced reward and ‘frustration’ memory in larval Drosophila melanogaster. Journal of Experimental Biology 225.

Tian L, Hires SA, Mao T, Huber D, Chiappe ME, Chalasani SH, Petreanu L, Akerboom J, McKinney SA, Schreiter ER, Bargmann CI, Jayaraman V, Svoboda K, Looger LL (2009) Imaging neural activity in worms, flies and mice with improved GCaMP calcium indicators. Nat Methods 6:875–881.

Todd TP, Vurbic D, Bouton ME (2014) Mechanisms of renewal after the extinction of discriminated operant behavior. J Exp Psychol Anim Learn Cogn 40:355–368.

Tomchik SM, Davis RL (2009) Dynamics of Learning-Related cAMP Signaling and Stimulus Integration in the Drosophila Olfactory Pathway. Neuron 64:510–521.

Tomchik SM, Davis RL (2013) Drosophila Memory Research through Four Eras. In, pp 359–377.

Toshima N, Tanimura T (2012) Taste preference for amino acids is dependent on internal nutritional state in Drosophila melanogaster. Journal of Experimental Biology 215:2827–2832.

Tovote P, Fadok JP, Lüthi A (2015) Neuronal circuits for fear and anxiety. Nat Rev Neurosci 16:317–331.

Tsien RY (1998) The green fluorescent protein. Annu Rev Biochem. 1998;67:509-44.

Tully T (1984) Drosophila Learning: Behavior and biochemistry. Behav Genet 14:527–557.

Tully T, Cambiazo V, Kruse L (1994a) Memory through metamorphosis in normal and mutant Drosophila. The Journal of Neuroscience 14:68–74.

Tully T, Preat T, Boynton SC, Del Vecchio M (1994b) Genetic dissection of consolidated memory in Drosophila. Cell 79:35–47.

Tully T, Quinn WG (1985) Classical conditioning and retention in normal and mutantDrosophila melanogaster. Journal of Comparative Physiology A 157:263–277.

Turner GC, Bazhenov M, Laurent G (2008) Olfactory Representations by Drosophila Mushroom Body Neurons. J Neurophysiol 99:734–746.

Tuthill JC, Azim E (2018) Proprioception. Current Biology 28:R194–R203.

Tuthill JC, Wilson RI (2016) Mechanosensation and Adaptive Motor Control in Insects. Current Biology 26:R1022–R1038.

Uhlhaas PJ, Silverstein SM (2005) Perceptual Organization in Schizophrenia Spectrum Disorders: Empirical Research and Theoretical Implications. Psychol Bull 131:618–632.

van Breugel F, Dickinson MH (2014) Plume-Tracking Behavior of Flying Drosophila Emerges from a Set of Distinct Sensory-Motor Reflexes. Current Biology 24:274–286.

Vervliet B, Craske MG, Hermans D (2013) Fear Extinction and Relapse: State of the Art. Annu Rev Clin Psychol 9:215–248.

Vervliet B, Vansteenwegen D, Eelen P. 2004. Generalization of extinguished skin conductance responding in human fear conditioning. Learn. Mem. 11:555–58

Vansteenwegen D, B. Vervliet, D. Hermans, T. Beckers, F. Baeyens, P. Eelen. Stronger renewal in human fear conditioning when tested with an acquisition retrieval cue than with an extinction retrieval cue Behaviour Research and Therapy, 44 (2006), pp. 1717-1725, 10.1016/j.brat.2005.10.014

Vogt K, Aso Y, Hige T, Knapek S, Ichinose T, Friedrich AB, Turner GC, Rubin GM, Tanimoto H (2016) Direct neural pathways convey distinct visual information to Drosophila mushroom bodies. Elife 5.

Vogt K, Yarali A, Tanimoto H (2015) Reversing Stimulus Timing in Visual Conditioning Leads to Memories with Opposite Valence in Drosophila. PLoS One 10:e0139797.

von Holst E, Mittelstaedt H. (1950). Das Reafferenzprinzip. Naturwissenschaften 37, 464-476. (10.1007/bf00622503)

Vosshall LB, Wong AM, Axel R (2000) An Olfactory Sensory Map in the Fly Brain. Cell 102:147–159.

Vosshall, L. B. (2003). Diversity and expression of odorant receptors in Drosophila. In Insect Pheromone Biochemistry and Molecular Biology (pp. 567-591). Academic Press.

Vosshall LB, Stocker RF (2007) Molecular Architecture of Smell and Taste in Drosophila. Annu Rev Neurosci 30:505–533.

Waddell, S., Armstrong, J. D., Kitamoto, T., Kaiser, K., & Quinn, W. G. (2000). The amnesiac gene product is expressed in two neurons in the Drosophila brain that are critical for memory. Cell, 103(5), 805-813.

Waddell S (2013) Reinforcement signalling in Drosophila; dopamine does it all after all. Curr Opin Neurobiol 23:324–329.

Walker RG, Willingham AT, Zuker CS (2000) A Drosophila mechanosensory transduction channel. Science. 2000 Mar 24;287(5461):2229-34.

Walker DL, Ressler KJ, Lu K, Davis M. (2002). Facilitation of conditioned fear extinction by systemic administrator or intra-amygdala infusions of D-cycloserine as assessed with fear-potentiated startle in rats. J. Neurosci. 22:62343–51

Wagner A. R. (1981). SOP: A model of automatice memory processing in animal behavior. In Spear N. E. & Miller R. R. (Eds.), Information processing in animals: Memory mechanisms (pp. 5–47). Hillsdale, NJ: Erlbaum Inc

Wang JW, Wong AM, Flores J, Vosshall LB, Axel R (2003) Two-Photon Calcium Imaging Reveals an Odor-Evoked Map of Activity in the Fly Brain. Cell 112:271–282.

Winding M et al. (2023) The connectome of an insect brain. Science (1979) 379.

Woods, A. M., & Bouton, M. E. (2006). D-cycloserine facilitates extinction but does not eliminate renewal of the conditioned emotional response. Behavioral Neuroscience, 120(5), 1159–1162

Wolpe, J. (1958). Psychotherapy by Reciprocal Inhibition. (Stanford: Stanford University Press)

Wu M, Nern A, Williamson WR, Morimoto MM, Reiser MB, Card GM, Rubin GM (2016) Visual projection neurons in the Drosophila lobula link feature detection to distinct behavioral programs. Elife 5.

Yamagata N, Hiroi M, Kondo S, Abe A, Tanimoto H (2016) Suppression of Dopamine Neurons Mediates Reward. PLoS Biol 14:e1002586.

Yamamoto K, Vernier P (2011) The Evolution of Dopamine Systems in Chordates. Front Neuroanat 5.

Yarali A, Niewalda T, Chen Y, Tanimoto H, Duerrnagel S, Gerber B (2008) 'Pain relief' learning in fruit flies. Anim Behav 76:1173–1185.

Ye S, Comer CM (1996) Correspondence of Escape-Turning Behavior with Activity of Descending Mechanosensory Interneurons in the Cockroach, Periplaneta americana. The Journal of Neuroscience 16:5844–5853.

Zeng J, Li X, Zhang R, Lv M, Wang Y, Tan K, Xia X, Wan J, Jing M, Zhang X, Li Y, Yang Y, Wang L, Chu J, Li Y, Li Y (2023) Local 5-HT signaling bi-directionally regulates the coincidence time window for associative learning. Neuron 111:1118-1135.e5.

Zhang K, Guo JZ, Peng Y, Xi W, Guo A (2007) Dopamine-Mushroom Body Circuit Regulates Saliency-Based Decision-Making in Drosophila. Science (1979) 316:1901–1904.

Zhang N, Simpson JH (2022) A pair of commissural command neurons induces Drosophila wing grooming. iScience 25:103792.

Zhang Y et al. (2023) Fast and sensitive GCaMP calcium indicators for imaging neural populations. Nature 615:884–891.

Zhao B, Sun J, Zhang X, Mo H, Niu Y, Li Q, Wang L, Zhong Y (2019) Long-term memory is formed immediately without the need for protein synthesis-dependent consolidation in Drosophila. Nat Commun 10:4550.

Zheng Z et al. (2018) A Complete Electron Microscopy Volume of the Brain of Adult Drosophila melanogaster. Cell 174:730-743.e22.

Zolin A, Cohn R, Pang R, Siliciano AF, Fairhall AL, Ruta V (2021) Context-dependent representations of movement in Drosophila dopaminergic reinforcement pathways. Nat Neurosci 24:1555–1566.

Zorović M, Hedwig B (2011) Processing of species-specific auditory patterns in the cricket brain by ascending, local, and descending neurons during standing and walking. J Neurophysiol 105:2181–2194.

Supplementary Information

1. Supplemental Table S1
2. Supplemental Data Table S1
3. Supplement figures 1-16 includes all the additionally performed experiments. See Supplemental Table S2 for corresponding Genotype information and Supplemental Data Table S2 for statistical results.

Supplemental Table S1

Abbreviated genotype	Genotype	Source	Used in
Moonwalker^{A}	VT050660-Gal4 (attp2)	Bidaye et al. 2014	Figure 1.1 - 1.4. Ext Data Figure 1.1a,1.2, 1.11-1.13
Moonwalker^{B}	VT044845-lexA (attp40) /CyO; sb/TM3	Kindly provided by David Owald	Ext Data Figure 1.4b,1.5,1.6b-d"
MDN1^{A}	VT044845-Gal4-DBD (attp40); VT050660-Gal4-AD (attp2)	Bidaye et al., 2014	Figure 1.5, 1.6a, 1.7, 1.12b, 1.15d. Ext Data Figure 1.1b-c, 1.3, 1.9b, 1.14, 1.15, 1.17
MDN1^{B}	VT049484-lexA DBD (JK22c); VT050660 AD (attp2)/TM3 (ser)	Kindly provided by Salil. S. Bidaye	Figure 1.9, 1.10, 1.11a-e Ext Data Figure 1.4a,c,d, 1.6c-c", 1.7, 1.8b-f
DANs	Sp/CyO; R58E02-Gal4, TH-Gal4/TM3 (sb)	Kindly provided by David Owald	Figure 1.10, 1.11a-e Ext Data Figure 1.5, 1.6c-d", 1.7, 1.8b-f
γ1	MB320C-Gal4	BDSC#68253	Figure 1.9c, 1.12c Ext Data Figure 1.16b
γ2	MB296B-Gal4	BDSC#68308	Figure 1.9d
ChR2XXL^{A}	UAS-ChR2XXL	BDSC#58374	Figure 1.1, 1.2a, c, 1.3, 1.4, 1.5, 1.12b, c Ext Data Figure 1.2a, 1.12d
ChR2XXL^{B}	lexAop-ChR2XXL	Kindly provided by David Owald	Ext Data Figure 1.4c
Chrimson^{A}	20x-UAS-CsChrimson-mVenus (attp2)	BDSC#55136	Figure 1.2b, 1.3 Ext Data Figure 1.2b, c
Chrimson^{B}	lexAop-CsChrimson	Kindly provided by David Owald	Ext Data Figure 1.4d
Chrimson^{C} GCaMP	lexAop-CsChrimson-tdtomato, UAS-GCaMP6f; VT1211-lexA*/CyO; MKRS/TM6B	Kindly provided by David Owald	Figure 1.9, 1.10, 1.11 Ext Data Figure 1.5b-g, 1.6, 1.7, 1.8b-f
Chrimson^{D}	lexAop-ChrimsonR::mCherry	Kindly provided by Vivek Jayaraman	Ext Data Figure 1.4a,b
GtACR1	UAS-GtACR1	Kindly provided by Robert J. Kittel	Fig. 1.7, 1.15d Ext Data Figure 1.3b, 1.9b, 1.17
CantonS	CS_{gpuLIN}	Kindly provided by Troy D. Zars	Ext Data Figure 1.9a
W^{1118}**	white null-mutant	Hazelrigg et al., 1984	Figure 1.1, 1.2b-c, 1.3, 1.5, 1.7 Ext Data Figure 1.3, 1.4, 1.9b
dgG4**	Enhancerless Gal4: w[1118]; P{y[+t7.7] w[+mC]=GAL4.1Uw}attP2	BDSC#68384	Figure 1.5, 1.7 Ext Data Figure 1.3, 1.9b

* Removed during crossings that establish experimental genotypes.

** Used to create heterozygous driver (Dri Ctrl) and effector controls (Eff Ctrl).

Supplemental Data Table S1

Figure	Statistical Analysis		
Figure 1.1	*KKW test*		
	H(2, N=56)=36.014;	p<0.0	*
	MWU test		
	Exp vs Eff	U=0; p<0.05/2	*
	Exp vs Dri	U=12; p<0.05/1	*
	OSS test		
	Exp	p<0.05/3	*
	Dri	p=1	ns
	Eff	p=0.332	ns
Figure 1.2a	*KKW test*		
	H(5, N=118)=44.197;	p<0.05	*
	MWU test		
	Immediate vs 8h	U=35.5; p<0.05/5	*
	Immediate vs 4h	U=56,5; p<0.05/4	*
	Immediate vs 2h	U=82.5; p<0.05/2	*
	Immediate vs 1h	U=78; p<0.05/3	*
	Immediate vs 30min	U=137; p=0.14	ns
	OSS test		
	Immediate	p<0.05/3	*
	30min	p<0.05/6	*
	1h	p<0.05/5	*
	2h	p<0.05/4	*
	4h	p<0.05/2	*
	8h	p=0.648	ns
Figure 1.2b	*KKW test*		
	H(2, N=52)=16.611;	p<0.05	*
	MWU test		
	Exp vs Eff	U=69; p<0.05/1	*
	Exp vs Dri	U=31; p<0.05/2	*
	OSS test		
	Exp	p<0.05/3	*
	Dri	p=0.332	ns
	Eff	p=0.455	ns
Figure 1.2c	*KKW test*		
	H(2, N=48)=13.579;	p<0.05	*
	MWU test		
	Exp vs Eff	U=47; p<0.05/2	*
	Exp vs Dri	U=50; p<0.05/1	*
	OSS test		
	Exp	p<0.05/3	*
	Dri	p=1	ns
	Eff	p=1	ns

Figure 1.4a	*KKW test*				
	-15	H(2, N=70)=8.993;	p<0.05/1	*	
	120	H(2, N=59)=11.433;	p<0.05/2	*	
	MWU test				
	-15	SUC vs 3IY + L-DOPA	U=249; p=0.742	ns	
	-15	SUC vs 3IY	U=159; p<0.05/2	*	
	-15	3IY vs 3IY + L-DOPA	U=151; p<0.05/3	*	
	120	SUC vs 3IY + L-DOPA	U=178; p=0.561	ns	
	120	SUC vs 3IY	U=87; p<0.05/2	*	
	120	3IY vs 3IY + L-DOPA	U=86; p<0.05/3	*	
	OSS test				
	-15	SUC	p<0.05/2	*	
	-15	3IY	p<0.05/1	*	
	-15	3IY + L-DOPA	p<0.05/3	*	
	120	SUC	p<0.05/3	*	
	120	3IY	p=0.648	ns	
	120	3IY + L-DOPA	p<0.05/2	*	
Figure 1.5	*KKW test*				
	H(2, N=55)=8.273;		p<0.05	*	
	MWU test				
	Exp vs Eff		U=92; p<0.05/2	*	
	Exp vs Dri		U=99; p<0.05/1	*	
	OSS test				
	Exp		p<0.05/3	*	
	Dri		p=1	ns	
	Eff		p=0.804	ns	
Figure 1.7a	*KKW test*				
	H(3, N=77)=36.014;		p<0.05	*	
	MWU test				
	Exp vs Dark		U=24; p<0.05/3	*	
	Exp vs Dri		U=130; p<0.05/1	*	
	Exp vs Eff		U=112; p<0.05/2	*	
	OSS test				
	Dark		p<0.05/3	*	
	Exp		p<0.05/1	*	
	Dri		p<0.05/2	*	
	Eff		p<0.05/4	*	
Figure 1.7b	*KKW test*				
	H(3, N=35)=3.58;		p=0.311	ns	
	OSS test				
	All groups		p<0.05	*	
Figure 1.9c	*MWU test*				
	Chrimson vs Control		U=1; p<0.05	*	

Figure 1.9d

MWU test

Chrimson vs Control U=0; p<0.05 *

Figure 1.10f

KKW test

H(11, N=107)=66.284; p<0.05 *

MWU test

γ1	Chrimson vs Control	U=0; p<0.05/5	*
γ2	Chrimson vs Control	U=8; p<0.05/4	*
γ3	Chrimson vs Control	U=0; p<0.05/6	*
γ4	Chrimson vs Control	U=15; p<0.05/1	*
γ5	Chrimson vs Control	U=11; p<0.05/2	*
β'2	Chrimson vs Control	U=8; p<0.05/3	*

Figure 1.11e

Wilcoxon signed-rank test

RM ANOVA

	Source	SS	ddof1	ddof2	MS	F	p-unc	p-GG-corr	ng2	eps
0	trapping	0.457	2	18	0.229	10.455	0.001	0.002	0.136	0.868
1	compartment	0.448	5	45	0.090	4.681	0.002	0.023	0.134	0.400
2	trapping * compartment	0.462	10	90	0.046	4.775	0.000	0.014	0.137	0.245

γ1

	Contrast	A	B	Paired	Parametric	W-val	alternative	p-unc	p-corr	p-adjust	hedges	
0	trapping	after	before	TRUE	FALSE	15	two-sided	0.232	0.232	holm	-0.708	ns
1	trapping	after	trapped	TRUE	FALSE	0	two-sided	0.002	0.006	holm	1.606	*
2	trapping	before	trapped	TRUE	FALSE	1	two-sided	0.004	0.008	holm	1.719	*

γ2

	Contrast	A	B	Paired	Parametric	W-val	alternative	p-unc	p-corr	p-adjust	hedges	
0	trapping	after	before	TRUE	FALSE	20	two-sided	0.492	0.492	holm	-0.355	ns
1	trapping	after	trapped	TRUE	FALSE	1	two-sided	0.004	0.012	holm	1.656	*
2	trapping	before	trapped	TRUE	FALSE	3	two-sided	0.010	0.020	holm	1.590	*

γ3

	Contrast	A	B	Paired	Parametric	W-val	alternative	p-unc	p-corr	p-adjust	hedges	
0	trapping	after	before	TRUE	FALSE	17	two-sided	0.322	0.322	holm	-0.498	ns
1	trapping	after	trapped	TRUE	FALSE	10	two-sided	0.084	0.168	holm	0.764	ns
2	trapping	before	trapped	TRUE	FALSE	4	two-sided	0.014	0.041	holm	1.269	*

γ4

	Contrast	A	B	Paired	Parametric	W-val	alternative	p-unc	p-corr	p-adjust	hedges	
0	trapping	after	before	TRUE	FALSE	26	two-sided	0.922	0.922	holm	-0.010	ns
1	trapping	after	trapped	TRUE	FALSE	10	two-sided	0.084	0.252	holm	0.391	ns
2	trapping	before	trapped	TRUE	FALSE	13	two-sided	0.160	0.320	holm	0.432	ns

γ5

	Contrast	A	B	Paired	Parametric	W-val	alternative	p-unc	p-corr	p-adjust	hedges	
0	trapping	after	before	TRUE	FALSE	5	two-sided	0.020	0.059	holm	0.481	ns
1	trapping	after	trapped	TRUE	FALSE	5	two-sided	0.020	0.059	holm	0.645	ns
2	trapping	before	trapped	TRUE	FALSE	20	two-sided	0.492	0.492	holm	0.105	ns

β'2

	Contrast	A	B	Paired	Parametric	W-val	alternative	p-unc	p-corr	p-adjust	hedges	
0	trapping	after	before	TRUE	FALSE	1	two-sided	0.004	0.012	holm	1.089	*
1	trapping	after	trapped	TRUE	FALSE	4	two-sided	0.014	0.027	holm	0.842	*
2	trapping	before	trapped	TRUE	FALSE	10	two-sided	0.084	0.084	holm	-0.402	ns

Figure 1.12b

MWU test
Open vs Trapped U=225; p<0.05 *

OSS test
Open p<0.05/2 *
Trapped p=1 ns

Figure 1.12c

MWU test
Open vs Trapped U=213.5; p=0.127 ns

OSS test
Open p<0.05/2 *
Trapped p<0.05/1 *

Figure 1.15b	*KKW test*			
	H(4, N=100)=58.991;		p<0.05	*
	MWU test			
	air vs. odor: MDN1 intact vs MDN1 silenced		U=75.5; p<0.05/1	*
	odor vs. odor: MDN1 intact vs MDN1 silenced		U=27.5; p<0.05/2	*
	OSS test			
	air vs. air: MDN1 intact		p<0.05/5	*
	air vs. odor: MDN1 intact		p<0.05/3	*
	air vs. odor: MDN1 silenced		p<0.05/2	*
	odor vs. odor: MDN1 intact		p<0.05/4	*
	odor vs. odor: MDN1 silenced		p<0.05/1	*
Figure 1.15d	*KKW test*			
	H(4, N=149)=59.761;	p<0.05		*
	MWU test			
	air vs. odor: MDN1^{A} intact vs MDN1^{A} silenced		U=245; p<0.05/2	*
	odor vs. odor: MDN1^{A} intact vs MDN1^{A} silenced		U=84.5; p<0.05/1	*
	OSS test			
	air vs. air: MDN1^{A} intact	p<0.05/5		*
	air vs. odor: MDN1^{A} intact	p<0.05/4		*
	air vs. odor: MDN1^{A} silenced	p=1		ns
	odor vs. odor: MDN1^{A} intact	p<0.05/3		*
	odor vs. odor: MDN1^{A} silenced	p=0.302		ns
ExtData Figure 1.3	*KKW test*			
	H(3, N=82)=3.373;	p=0.338		ns
	OSS test			
	All groups	p<0.05		*
ExtData Figure 1.4c	*KKW test*			
	H(2, N=34)=9.248;	p<0.05		*
	MWU test			
	Exp vs Eff	U=22; p<0.05/1		*
	Exp vs Dri	U=27; p<0.05/2		*
	OSS test			
	Exp	p<0.05/3		*
	Dri	p=0.774		ns
	Eff	p=1		ns
ExtData Figure 1.4d	*KKW test*			
	H(2, N=33)=7.981;	p<0.05		*
	MWU test			
	Exp vs Eff	U=26; p<0.05/2		*
	Exp vs Dri	U=25; p<0.05/1		*
	OSS test			
	Exp	p=0.039		ns
	Dri	p=1		ns
	Eff	p=1		ns

ExtData Figure 1.5f	*KKW test*		
	H(9, N=60)=25.331; p<0.05		*
	MWU test		
	γ2 Chrimson vs Control	U=1; p<0.05/5	*
	γ3 Chrimson vs Control	U=6; p=0.038	ns
	γ4 Chrimson vs Control	U=6; p=0.1	ns
	γ5 Chrimson vs Control	U=6; p=0.054	ns
	β'2 Chrimson vs Control	U=6; p=0.093	ns
ExtData Figure 1.6c"	*Friedman test*		
	W(4)= 0.381, P= 0.016, N= 8 ,	p<0.05	*
ExtData Figure 1.6d"	*Friedman test*		
	W(4)= 0.011, P= 0.99, N= 7,	p>0.05	ns
ExtData Figure 1.7	*MWU test*		
	γ3 vs γ3 control U=7	p<0.05/6	*
ExtData Figure 1.9a	*OSS test*		
	Canton S	p=0.774	ns
ExtData Figure 1.9b	*KKW test*		
	H(2, N=36)=0.195;	p=0.907	ns
	OSS test		
	All groups	p=0.061	ns

Supplement Figures

(Supplement figures 1-16 includes all the additionally performed experiments.

All experiments were conducted with 3 training trials unless mentioned otherwise.

See Supplemental Table S2 for additional Genotype information and Supplemental Data Table S2 for statistical results.

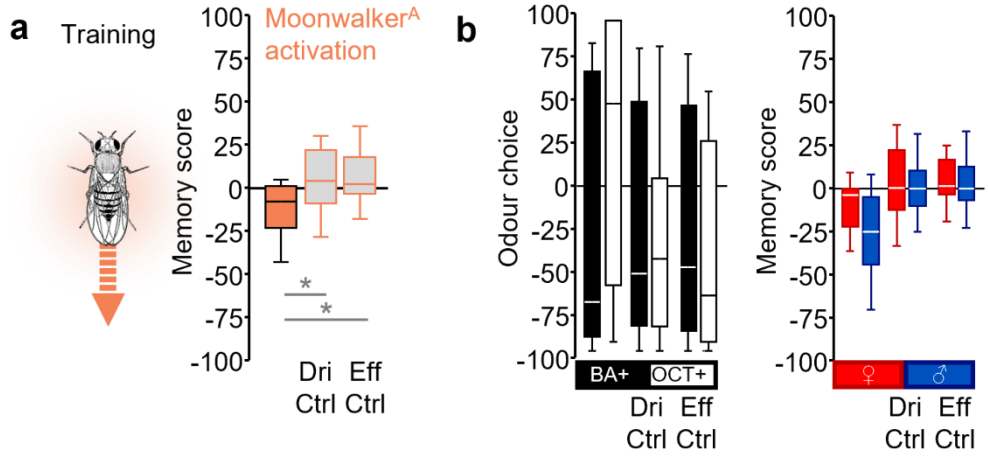

Supplement Figure 1 | Moonwalker^A activation with Chrimson^A and testing in ambient light conveys weak negative valence. BA preference and memory scores are separated by sex.

a, Aversive memory by pairing odour with moonwalker neuron activation, see rationale in Figure 1.1b. (orange: Moonwalker^A>Chrimson^A, grey: Driver control: Moonwalker^A>+, Effector control: +>Chrimson^A, +: absence of driver or effector construct) (N= 27,26,26). Data were analysed across groups by Kruskal-Wallis tests (P< 0.05), followed by pairwise comparisons (Mann-Whitney U-tests, *P< 0.05 with Bonferroni-Holm correction) (ns: P> 0.05). Box-whisker plots show median, interquartile range (box) and 10th/90th percentiles (whiskers).

b, BA preference and memory scores respectively, separated by sex. Box plots represent the median as the middle line, 25%/75% quantiles as box boundaries, and 10%/90% quantiles as whiskers. Black fill of the box plots show BA preference when BA (Benzaldehyde) was associated with optogenetic, and white fill of the box indicates BA preference when OCT (3-octanol) was associated with optogenetic. Red fill of the box plots shows data from females; blue fill indicates data from males. The orange glowing fly indicates when red light was used for moonwalker activation. See Supplement Table S2 for additional Genotype information and Supplement Data Table S2 for statistical results.

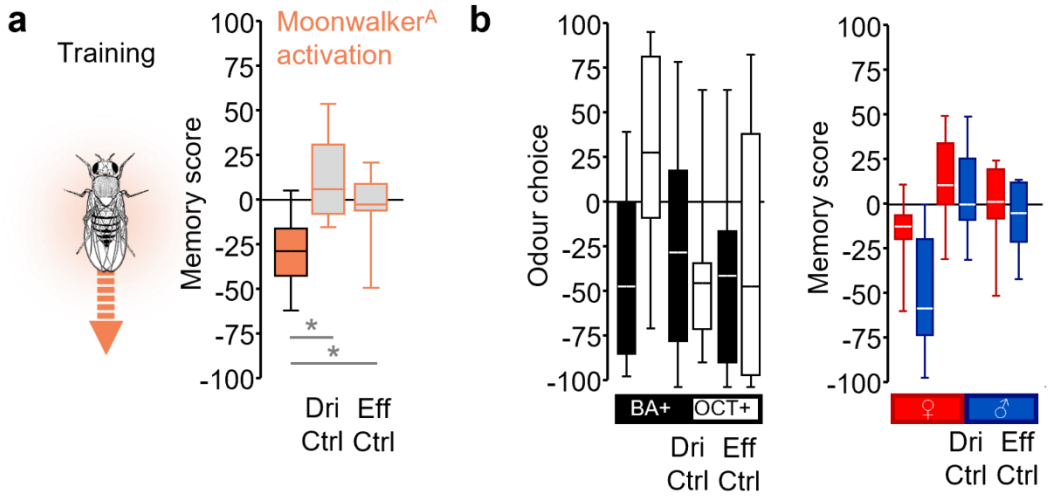

Supplement Figure 2 | Moonwalker^A activation with Chrimson^A and testing in complete darkness conveys stronger negative valence. BA preference and memory scores are separated by sex.

a, Aversive memory by pairing odour with moonwalker neuron activation (orange: Moonwalker^{A}>Chrimson^{A}, grey: Driver control: Moonwalker^{A}>+, Effector control: +>Chrimson^{A}, +: absence of driver or effector construct) (N= 11,10,11). Data were analysed across groups by Kruskal-Wallis tests (P< 0.05), followed by pairwise comparisons (Mann-Whitney U-tests, *P< 0.05 with Bonferroni-Holm correction) (ns: P> 0.05). Box-whisker plots show median, interquartile range (box) and 10th/90th percentiles (whiskers).

b, BA preference and Memory scores respectively, separated by sex. Box plots represent the median as the middle line, 25%/75% quantiles as box boundaries, and 10%/90% quantiles as whiskers. Black fill of the box plots show BA preference when BA (Benzaldehyde) was associated with optogenetic, and white fill of the box indicates BA preference when OCT (3-octanol) was associated with optogenetic. Red fill of the box plots shows data from females; blue fill indicates data from males. The orange glowing fly indicates when red light was used for moonwalker activation. See Supplement Table S2 for additional Genotype information and Supplement Data Table S2 for statistical results.

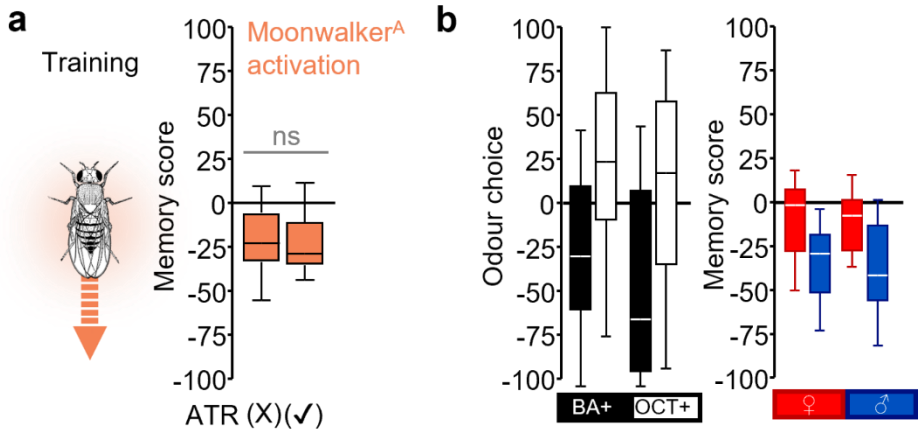

Supplement Figure 3 | Moonwalker^{A} activation with Chrimson^{A} (raised with or without ATR containing food) conveys similar strength of negative valence. BA preference and memory scores are separated by sex.

a, Aversive memory by pairing odour with moonwalker neuron activation, see rationale in Figure 1.1b (orange: Moonwalker^{A}>Chrimson^{A}) (N= 30,30). Data were analysed across groups by Kruskal-Wallis tests (P< 0.05), followed by pairwise comparisons (Mann-Whitney U-tests, *P< 0.05 with Bonferroni-Holm correction) (ns: P> 0.05). X: absence of ATR; ✓: presence of ATR. Box-whisker plots show median, interquartile range (box) and 10th/90th percentiles (whiskers).

b, BA preference and Memory scores respectively, separated by sex. Box plots represent the median as the middle line, 25%/75% quantiles as box boundaries, and 10%/90% quantiles as whiskers. Black fill of the box plots show BA preference when BA (Benzaldehyde) was associated with optogenetic, and white fill of the box indicates BA preference when OCT (3-octanol) was associated with optogenetic. Red fill of the box plots shows data from females; blue fill indicates data from males. The orange glowing fly indicates when red light was used for moonwalker activation. See Supplement Table S2 for additional Genotype information and Supplement Data Table S2 for statistical results.

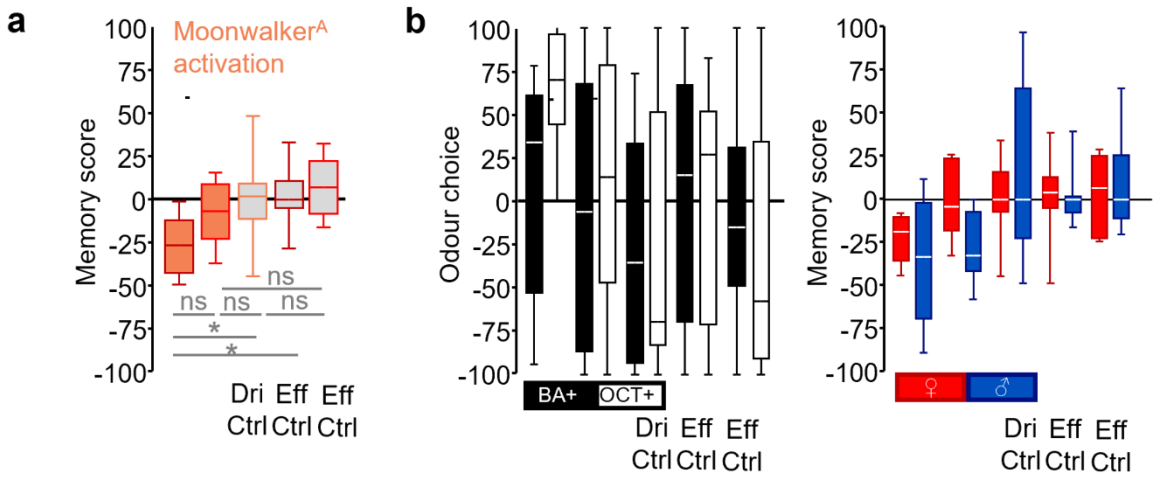

Supplement Figure 4 | Parametric analysis of Moonwalker^{A} activation with Chrimson^{E}/Chrimson^{F} effector. BA preference and memory scores are separated by sex.

a, Aversive memory by pairing odour with moonwalker neuron activation, see rationale in Figure 1.1b. (dark red: Moonwalker^{A}>Chrimson^{E}; light red: Moonwalker^{A}>Chrimson^{F}; grey: Driver control: Moonwalker^{A}>+, Effector control: +>Chrimson^{E} and +>Chrimson^{F}, +: absence of driver or effector construct) (N= 12,12,12,12,12). Data were analysed across groups by Kruskal-Wallis tests (P< 0.05), followed by pairwise comparisons (Mann-Whitney U-tests, *P< 0.05 with Bonferroni-Holm correction) (ns: P> 0.05). Box-whisker plots show median, interquartile range (box) and 10th/90th percentiles (whiskers).

b, BA preference and Memory scores respectively, separated by sex. Box plots represent the median as the middle line, 25%/75% quantiles as box boundaries, and 10%/90% quantiles as whiskers. Black fill of the box plots show BA preference when BA (Benzaldehyde) was associated with optogenetic, and white fill of the box indicates BA preference when OCT (3-octanol) was associated with optogenetic. Red fill of the box plots shows data from females; blue fill indicates data from males. See Supplement Table S2 for additional Genotype information and Supplement Data Table S2 for statistical results.

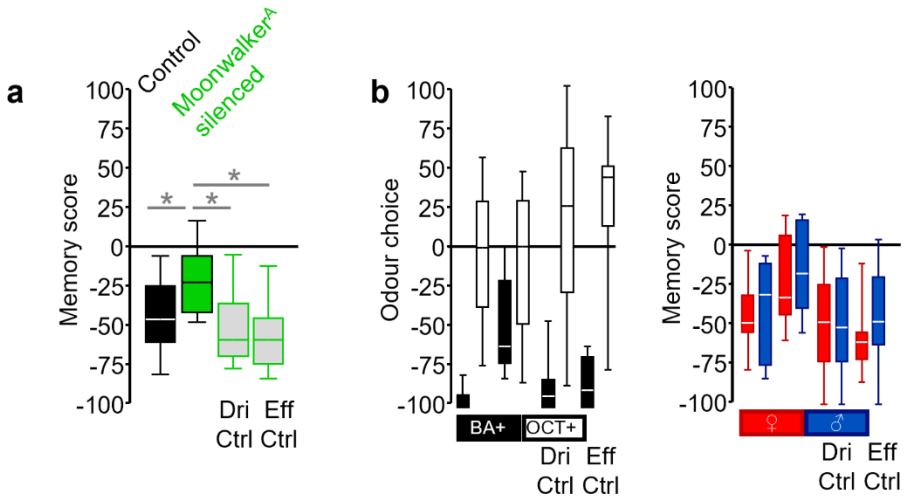

Supplement Figure 5 | Moonwalker^{A} contributes to memory-efferent circuits for learned avoidance memory expression. BA preference and memory scores are separated by sex.

a, Outcome of odour-shock learning experiments (see Rationale as Figure 1.7a). Relative to the Control condition (black), silencing all moonwalker neurons during the test reduced odour-shock memory scores (Moonwalker^{A} silenced, green) (genotype in both cases: Moonwalker^{A}>GtACR1) to levels less than in genetic controls (grey: Driver control: Moonwalker^{A}>+, Effector control: +>GtACR1) (N= 16,19,20,17).

b, BA preference and Memory scores, respectively, separated by sex. Box plots represent the median as the middle line, 25%/75% quantiles as box boundaries, and 10%/90% quantiles as whiskers. Black fill of the box plots show BA preference when BA (Benzaldehyde) was associated with electric shock, and white fill of the box indicates BA preference when OCT (3-octanol) was associated with electric shock. Red fill of the box plots shows data from females; blue fill indicates data from males. Rationale and other details as in the legend of Figure 1.7a. See Supplement Table S2 for additional Genotype information and Supplement Data Table S2 for statistical results.

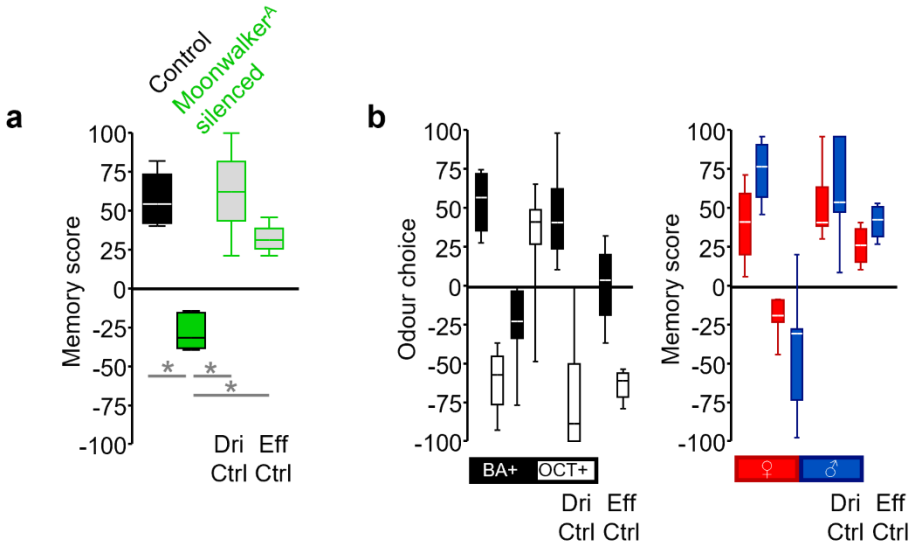

Supplement Figure 6 | Moonwalker^{A} contributes to memory-efferent circuits for learned approach memory expression, too. BA preference and memory scores are separated by sex.

a, Outcome of odour-sugar learning experiments (see Rationale as Figure 1.7b). Relative to the Control condition (black), silencing all moonwalker neurons during the test reduced odour-shock memory scores (Moonwalker^{A} silenced, green) (genotype in both cases: Moonwalker^{A}>GtACR1) to levels less than in genetic controls (grey: Driver control: Moonwalker^{A}>+, Effector control: +>GtACR1) (N= 16,14,14,13).

b, BA preference and Memory scores, respectively, separated by sex. Box plots represent the median as the middle line, 25%/75% quantiles as box boundaries, and 10%/90% quantiles as whiskers. Black fill of the box plots show BA preference when BA (Benzaldehyde) was associated with electric shock, and white fill of the box indicates BA preference when OCT (3-octanol) was associated with electric shock. Red fill of the box plots shows data from females; blue fill indicates data from males. Rationale and other details as in the legend of Figure 1.7b. See Supplement Table S2 for additional Genotype information and Supplement Data Table S2 for statistical results.

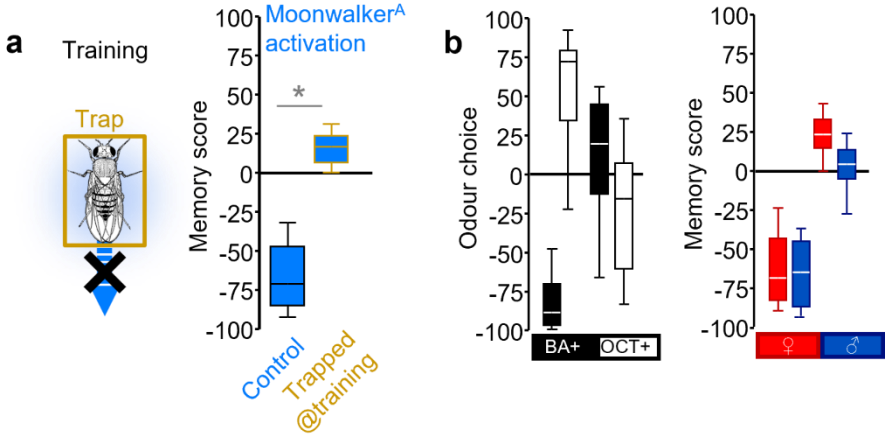

Supplement Figure 7 | Moonwalker^{A}-evoked movement is required for moonwalking punishment. BA preference and memory scores are separated by sex.

a, Pairing odour with optogenetic activation of all moonwalker neurons establishes aversive memory under Control conditions but not when locomotion was restrained during the training period. Restraining locomotion during training causes not only complete abolishment of punishment memory but also create mild reward memory (see Figure 1.12a-b for rationale). Genotypes: Moonwalker^{A}>ChR2XXL^{A} (N= 12,13). Data were analysed across groups by Kruskal-Wallis tests (P< 0.05), followed by pairwise comparisons (Mann-Whitney U-tests, *P< 0.05 with Bonferroni-Holm correction) (ns: P> 0.05). Box-whisker plots show median, interquartile range (box) and 10th/90th percentiles (whiskers).

b, BA preference and Memory scores respectively, separated by sex. Box plots represent the median as the middle line, 25%/75% quantiles as box boundaries, and 10%/90% quantiles as whiskers. Black fill of the box plots show BA preference when BA (Benzaldehyde) was associated with optogenetic, and white fill of the box indicates BA preference when OCT (3-octanol) was associated with optogenetic. Red fill of the box plots shows data from females; blue fill indicates data from males.
See Supplement Table S2 for additional Genotype information and Supplement Data Table S2 for statistical results.

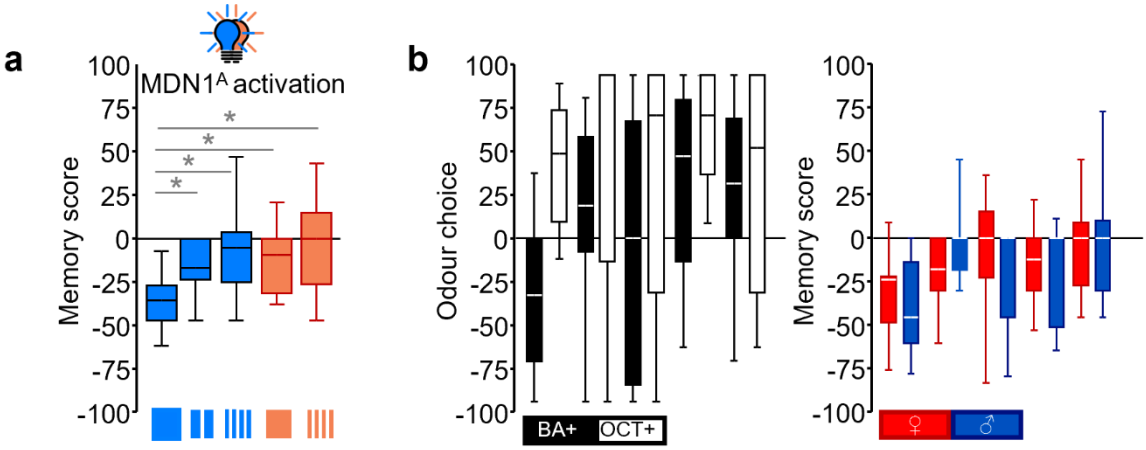

Supplement Figure 8 | Parametric analysis of MDN1^{A} activation with ChR2-XXL^{A} and Chrimson^{E} with different light regime. BA preference and memory scores are separated by sex.

a, Aversive memory by pairing odour with moonwalker neuron activation. Blue: Moonwalker^{A}>ChR2-XXL^{A}, either with continuous light with highest intensity (4.99s ON/0.01s OFF) (thick blue bar) or intermediate intensity (1.2s ON/3.8s OFF) (thin two blue bars) or pulsed low intensity (0.01s ON/0.01s OFF) (multiple thin blue bars). Orange: MoonwalkerA>Chrimson^{E}, either with continuous light with highest intensity (thick orange bar) or pulsed low intensity (multiple thin orange bars). N= 20,20,20,32,24. Data were analysed across groups by Kruskal-Wallis tests (P< 0.05), followed by pairwise comparisons (Mann-Whitney U-tests, *P< 0.05 with Bonferroni-Holm correction) (ns: P> 0.05). Box-whisker plots show median, interquartile range (box) and 10th/90th percentiles (whiskers).

b, BA preference and Memory scores respectively, separated by sex. Box plots represent the median as the middle line, 25%/75% quantiles as box boundaries, and 10%/90% quantiles as whiskers. Black fill of the box plots show BA preference when BA (Benzaldehyde) was associated with optogenetic, and white fill of the box indicates BA preference when OCT (3-octanol) was associated with optogenetic. Red fill of the box plots shows data from females; blue fill indicates data from males.
See Supplement Table S2 for additional Genotype information and Supplement Data Table S2 for statistical results.

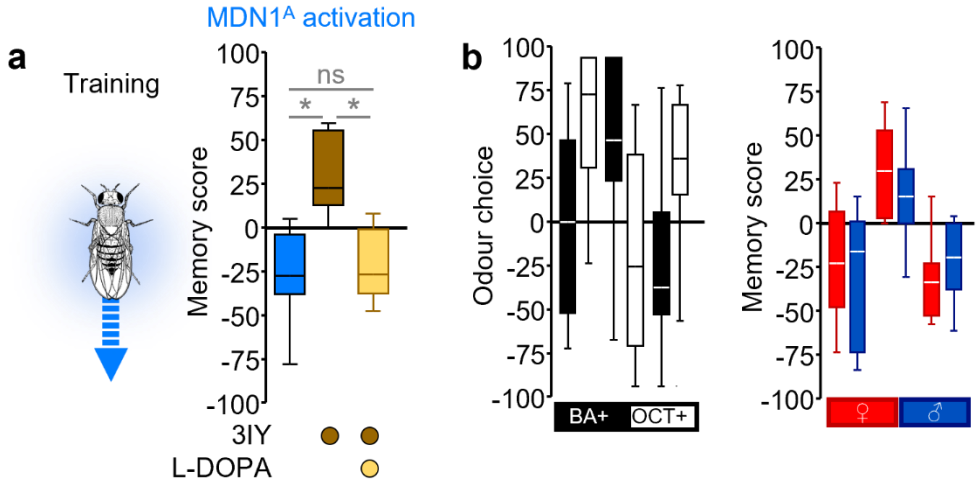

Supplement Figure 9 | Role of DA in MDN1^{A} reinforcement. BA preference and memory scores are separated by sex.

a, Inhibition of dopamine biosynthesis by 3-iodo-L-tyrosine (3IY), and effects of 3IY on learning from moonwalker activation (see Figure 1.4a for rationale). (Genotype: MDN1^{A}>ChR2XXL^{A}, intervals -15s; blue: control, brown: 3IY, light brown: additional supply of 3,4-dihydroxy-L-phenylalanine (L-DOPA)) (N= 15,15,13). DDC: dopamine decarboxylase. TH: tyrosine hydroxylase. Clouds and light bulbs represent odours and optogenetic activation in all experiments. Data were analysed across groups by Kruskal-Wallis tests (P< 0.05), followed by pairwise comparisons (Mann-Whitney U-tests, *P< 0.05 with Bonferroni-Holm correction) (ns: P> 0.05). Box-whisker plots show median, interquartile range (box) and 10th/90th percentiles (whiskers).

b, BA preference and Memory scores respectively, separated by sex. Box plots represent the median as the middle line, 25%/75% quantiles as box boundaries, and 10%/90% quantiles as whiskers. Black fill of the box plots show BA preference when BA (Benzaldehyde) was associated with optogenetic, and white fill of the box indicates BA preference when OCT (3-octanol) was associated with optogenetic. Red fill of the box plots shows data from females; blue fill indicates data from males. The blue glowing fly indicates when blue light was used for moonwalker activation. No circles below the panels refer to the control

conditions, brown fill refers to feeding with 3IY, and yellow fill to feeding with L-DOPA in addition. See Supplement Table S2 for additional Genotype information and Supplement Data Table S2 for statistical results.

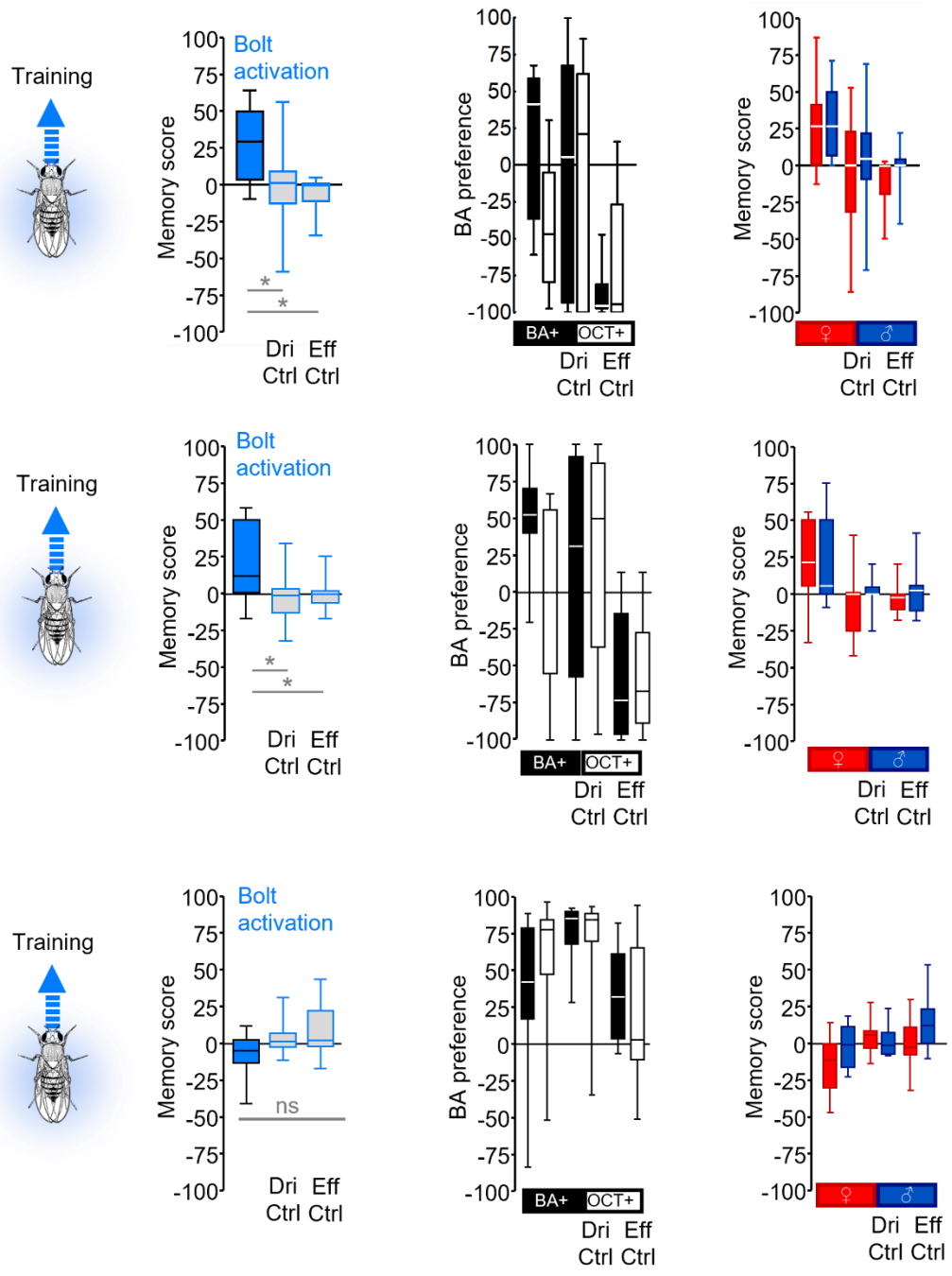

Supplement Figure 10 | Forward locomotion inducing Bolt neuron (BPN-S1) activation have complex valence profile. BA preference and memory scores are separated by sex.

(**Top**) Showing reward memory through Bolt activation (blue: Bolt>ChR2XXL^{A}, grey: Driver control: Bolt>+, Effector control: +>ChR2XXL^{A}) (N= 20,20,21). see rationale in Figure 1.1b, while Bolt activation induces forward locomotion.
(**Middle**) Similar as (top) (N=17,17,17).

(**Bottom**) Showing no valence through Bolt activation. Leading to complex and inconclusive result. (N=14,8,9). Data were analysed across groups by Kruskal-Wallis tests (P< 0.05), followed by pairwise comparisons (Mann-Whitney U-tests, *P< 0.05 with Bonferroni-Holm correction) (ns: P> 0.05). Box-whisker plots show median, interquartile range (box) and 10th/90th percentiles (whiskers).

Corresponding (**top, middle, bottom**) BA preference and Memory scores respectively, separated by sex. Box plots represent the median as the middle line, 25%/75% quantiles as box boundaries, and 10%/90% quantiles as whiskers. Black fill of the box plots show BA preference when BA (Benzaldehyde) was associated with optogenetic, and white fill of the box indicates BA preference when OCT (3-octanol) was associated with optogenetic. Red fill of the box plots shows data from females; blue fill indicates data from males. The blue glowing fly indicates when blue light was used for Bolt activation. See Supplement Table S2 for additional Genotype information and Supplement Data Table S2 for statistical results.

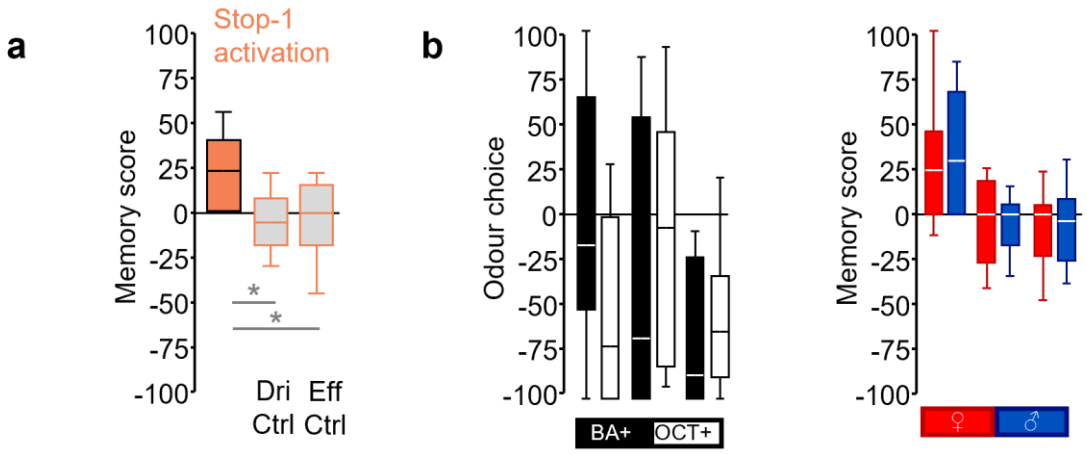

Supplement Figure 11 | Halting inducing Stop-1 neuron activation with Chrimson^{A} conveys weak positive valence. BA preference and memory scores are separated by sex.

a, Reward memory by pairing odour with Stop-1 activation, see rationale in Figure 1.1b while Stop-1 activation induces halting/stopping behaviour (orange: Stop-1>Chrimson^{A}, grey: Driver control: Stop-1>+, Effector control: +>Chrimson^{A}, +: absence of driver or effector construct) (N= 16, 16, 15). Data were analysed across groups by Kruskal-Wallis tests (P< 0.05), followed by pairwise comparisons (Mann-Whitney U-tests, *P< 0.05 with Bonferroni-Holm correction) (ns: P> 0.05). Box-whisker plots show median, interquartile range (box) and 10th/90th percentiles (whiskers).

b, BA preference and Memory scores respectively, separated by sex. Box plots represent the median as the middle line, 25%/75% quantiles as box boundaries, and 10%/90% quantiles as whiskers. Black fill of the box plots show BA preference when BA (Benzaldehyde) was associated with optogenetic, and white fill of the box indicates BA preference when OCT (3-octanol) was associated with optogenetic. Red fill of

the box plots shows data from females; blue fill indicates data from males. See Supplement Table S2 for additional Genotype information and Supplement Data Table S2 for statistical results.

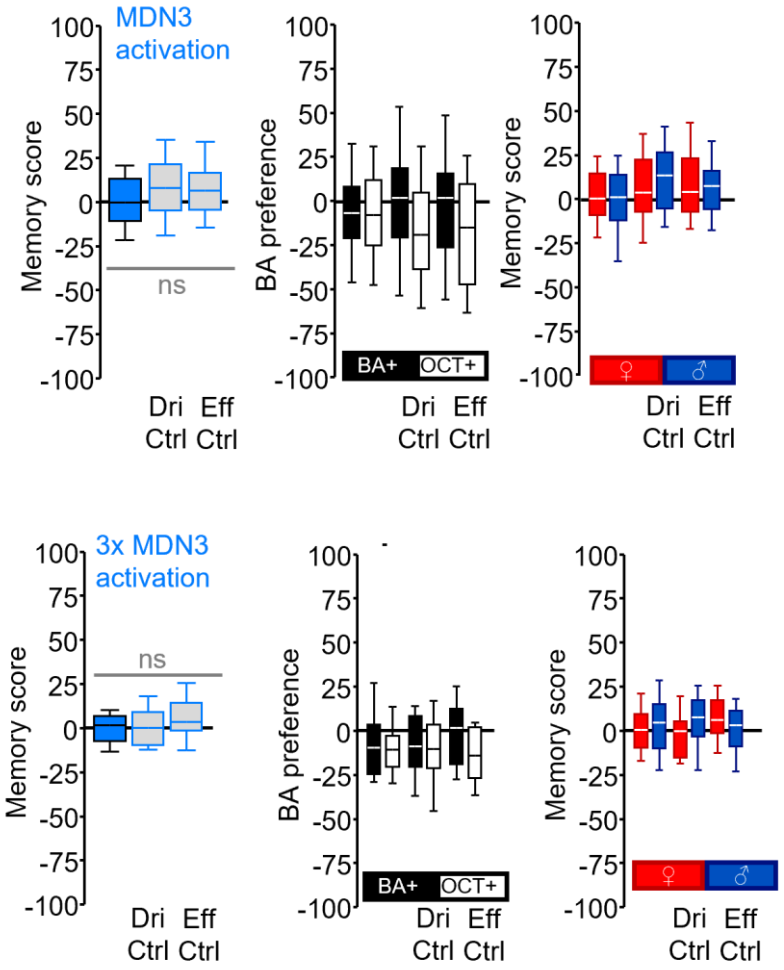

Supplement Figure 12 | Activating MDN3 does not convey negative valence. BA preference and memory scores are separated by sex.

(**Top**) Showing no memory through 1 trial of MDN3 activation or **(Bottom**) 3 trials of activation, see rationale in Figure 1.5 (blue: MDN3>ChR2XXL^{A}, grey: Driver control: MDN3>+, Effector control: +>ChR2XXL^{A}) (N= 58,59,43) or (N= 32,30,32). Data were analysed across groups by Kruskal-Wallis tests (P< 0.05), followed by pairwise comparisons (Mann-Whitney U-tests, *P< 0.05 with Bonferroni-Holm correction) (ns: P> 0.05). Box-whisker plots show median, interquartile range (box) and 10th/90th percentiles (whiskers).

Corresponding (top, bottom) BA preference and Memory scores respectively, separated by sex. Box plots represent the median as the middle line, 25%/75% quantiles as box boundaries, and 10%/90% quantiles as whiskers. Black fill of the box plots show BA preference when BA (Benzaldehyde) was associated with optogenetic, and white fill of the box indicates BA preference when OCT (3-octanol) was associated with optogenetic. Red fill of the box plots shows data from females; blue fill indicates data from males. See Supplement Table S2 for additional Genotype information and Supplement Data Table S2 for statistical results.

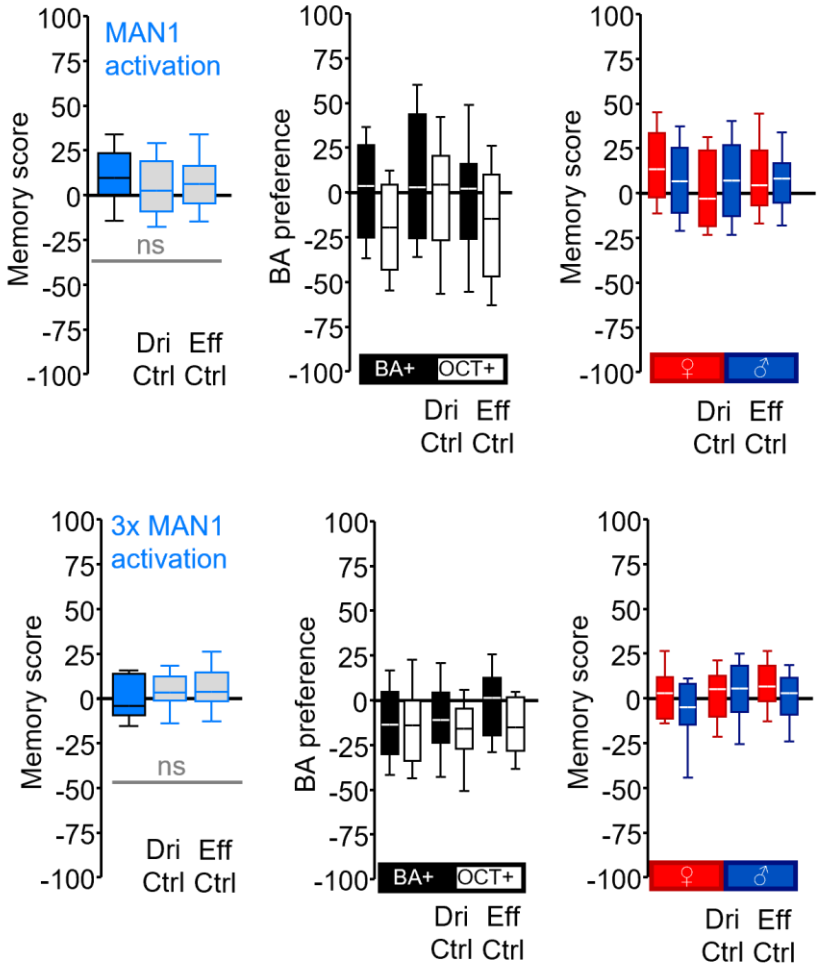

Supplement Figure 13 | Activating moonwalker ascending neurons MAN1 does not convey negative valence. BA preference and memory scores are separated by sex.
(**Top**) Showing no memory through 1 trial of MAN1 activation or (**Bottom**) 3 trials of activation, see rationale in Figure 1.5. (blue: MAN1>ChR2XXL^{A}, grey: Driver control: MAN1>+, Effector control: +>ChR2XXL^{A}) (N= 31,31,18) or (N= 31,30,32). Data were analysed across groups by Kruskal-Wallis tests (P< 0.05), followed by pairwise comparisons (Mann-Whitney U-tests, *P< 0.05 with Bonferroni-Holm correction) (ns: P> 0.05). Box-whisker plots show median, interquartile range (box) and 10th/90th percentiles (whiskers).

Corresponding (**top,bottom**) BA preference and Memory scores respectively, separated by sex. Box plots represent the median as the middle line, 25%/75% quantiles as box boundaries, and 10%/90% quantiles as whiskers. Black fill of the box plots show BA preference when BA (Benzaldehyde) was associated with optogenetic, and white fill of the box indicates BA preference when OCT (3-octanol) was associated with optogenetic. Red fill of the box plots shows data from females; blue fill indicates data from males. See Supplement Table S2 for additional Genotype information and Supplement Data Table S2 for statistical results.

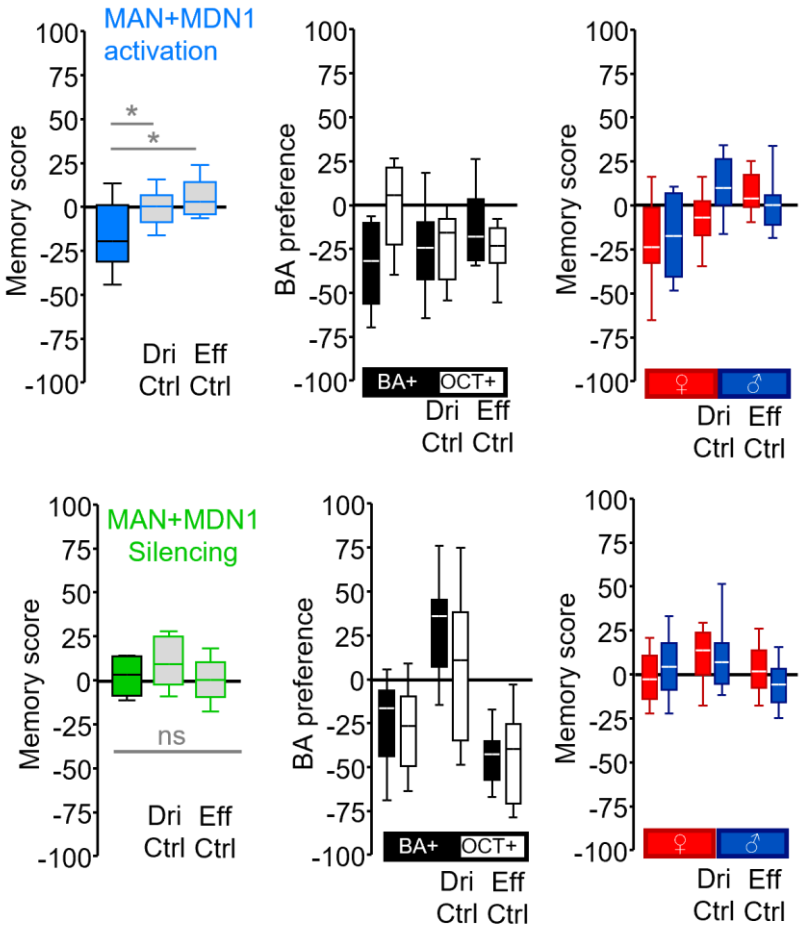

Supplement Figure 14 | Activating combination of moonwalker descending and ascending neurons MAN+MDN1 convey negative valence and silencing does not. BA preference and memory scores are separated by sex.

(**Top**) Showing aversive memory through MAN+MDN1 activation, see rationale in Figure 1.5 (blue: MAN+MDN1>ChR2XXL^{A}, grey: Driver control: MAN+MDN1>+, Effector control: +>ChR2XXL^{A}) (N= 20,22,18).

(Bottom) showing no memory silencing MAN+MDN1, see rationale in Extended Data Figure 1.9b (green: MAN+MDN1>GtACR1, grey: Driver control: MAN+MDN1>+, Effector control: +>GtACR1) (N= 22,22,24). Data were analysed across groups by Kruskal-Wallis tests (P< 0.05), followed by pairwise comparisons (Mann-Whitney U-tests, *P< 0.05 with Bonferroni-Holm correction) (ns: P> 0.05). Box-whisker plots show median, interquartile range (box) and 10th/90th percentiles (whiskers).

Corresponding (top, bottom) BA preference and Memory scores respectively, separated by sex. Box plots represent the median as the middle line, 25%/75% quantiles as box boundaries, and 10%/90% quantiles as whiskers. Black fill of the box plots show BA preference when BA (Benzaldehyde) was associated with optogenetic, and white fill of the box indicates BA preference when OCT (3-octanol) was associated with optogenetic. Red fill of the box plots shows data from females; blue fill indicates data from males. See Supplement Table S2 for additional Genotype information and Supplement Data Table S2 for statistical results.

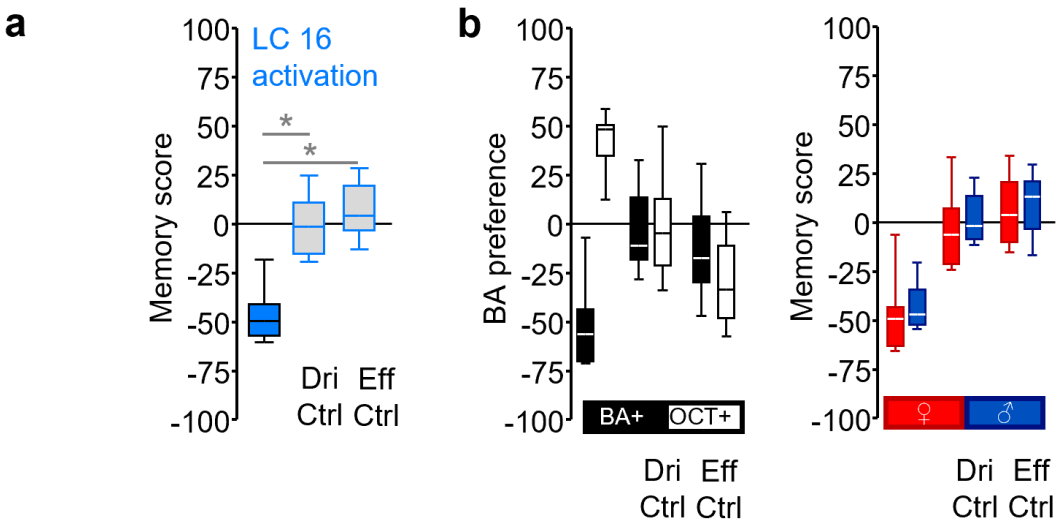

Supplement Figure 15 | Activating visual projection neuron, Lobular columnar cell (LC16) conveys negative valence. BA preference and memory scores are separated by sex.
a, Showing aversive memory through LC16 activation, see rationale in Figure 1.1b. (blue: LC16>ChR2XXL^{A}, grey: Driver control: LC16>+, Effector control: +>ChR2XXL^{A}) (N= 13,12,24)
Data were analysed across groups by Kruskal-Wallis tests (P< 0.05), followed by pairwise comparisons (Mann-Whitney U-tests, *P< 0.05 with Bonferroni-Holm correction) (ns: P> 0.05). Box-whisker plots show median, interquartile range (box) and 10th/90th percentiles (whiskers).

b, BA preference and Memory scores respectively, separated by sex. Box plots represent the median as the middle line, 25%/75% quantiles as box boundaries, and 10%/90% quantiles as whiskers. Black fill of the box plots show BA preference when BA (Benzaldehyde) was associated with optogenetic, and white fill of the box indicates BA preference when OCT (3-octanol) was associated with optogenetic. Red fill of the box plots shows data from females; blue fill indicates data from males. See Supplement Table S2 for additional Genotype information and Supplement Data Table S2 for statistical results.

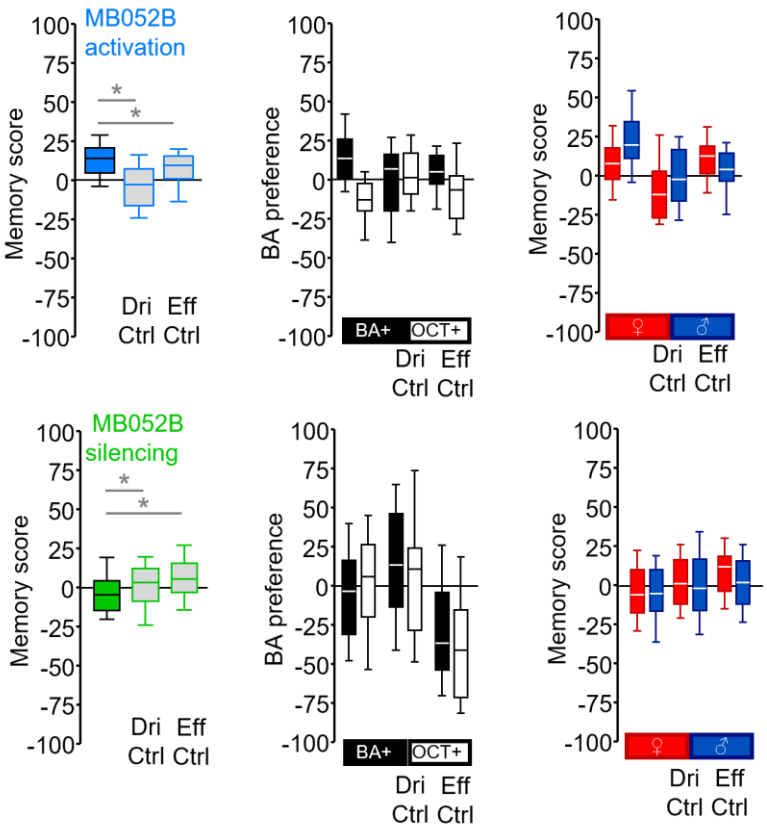

Supplement Figure 16 | Activating mushroom body output neuron MB052B (corresponding to α'1, α2 and α'3 compartments) conveys positive valence and silencing conveys negative valence. BA preference and memory scores are separated by sex.

(**Top**) Showing reward memory through MB052B activation. (blue: MB052B>ChR2XXL^{A}, grey: Driver control: MB052B>+, Effector control: +>ChR2XXL^{A}) (N= 35,34,29)

(**Bottom**) showing aversive memory through silencing MBON052B (green: MB052B>GtACR1, grey: Driver control: MB052B>+, Effector control: +>GtACR1) (N= 60,58,58).

Data were analysed across groups by Kruskal-Wallis tests (P< 0.05), followed by pairwise comparisons (Mann-Whitney U-tests, *P< 0.05 with Bonferroni-Holm correction) (ns: P> 0.05). Box-whisker plots show median, interquartile range (box) and 10th/90th percentiles (whiskers).

Corresponding (top, bottom) BA preference and Memory scores respectively, separated by sex. Box plots represent the median as the middle line, 25%/75% quantiles as box boundaries, and 10%/90% quantiles as whiskers. Black fill of the box plots show BA preference when BA (Benzaldehyde) was associated with optogenetic, and white fill of the box indicates BA preference when OCT (3-octanol) was associated with optogenetic. Red fill of the box plots shows data from females; blue fill indicates data from males. See Supplement Table S2 for additional Genotype information and Supplement Data Table S2 for statistical results.

Supplemental Table S2

Abbreviated Genotype	Genotype	Source	Used in
Moonwalker[A]	VT050660-Gal4 (attp2)	Bidaye et al. 2014	Supplement Figure 1-7
MDN1[A]	VT044845-Gal4-DBD (attp40); VT050660-Gal4-AD (attp2)	Bidaye et al., 2014	Supplement Figure 8-9
Bolt (BPN-S1)	R11H10-p65ADZp(attp40)/CyO ; VT025925-ZpGal4DBD(attp2)/TM2	Bidaye et al., 2020	Supplement Figure 10
Stop-1	W1118; VT009650AD/CyO; R36GO0/TM6B	Kindly provided by Salil.S.Bidaye	Supplement Figure 11
MDN3	MDN3- Gal4	Bidaye et al., 2014	Supplement Figure 12
MAN1	MAN1-Gal4	Bidaye et al., 2014	Supplement Figure 13
MDN+MAN1	MDN+MAN1- Split - Gal4	Bidaye et al., 2014	Supplement Figure 14
LC16.1	R26A03-p65ADZp (attP40); R54A05-ZpGAL4DBD (attP2)	BDSC # 68331	Supplement Figure 15
MB052B	MB052B-Gal4	Aso et al., 2014	Supplement Figure 16
ChR2XXL[A]	UAS-ChR2XXL	BDSC#58374	Supplement Figure 7-10, 12,13, 14(top), 15, 16(top)
GtACR1	UAS-GtACR1	Kindly provided by Robert J. Kittel	Supplement Figure 5-6, 14(bottom), 16(bottom)
Chrimson[A]	20x-UAS-CsChrimson-mVenus (attp2)	BDSC#55136	Supplement Figure 1-3, 11
Chrimson[E]	20x-UAS-ChrimsonR-mCherry (attp18)	Kindly provided by Salil.S.Bidaye	Supplement Figure 4, 8
Chrimson[F]	20x-UAS-ChrimsonR-mVenus (attp18)	Kindly provided by Salil.S.Bidaye	Supplement Figure 4
W^{1118}**	white null-mutant strain	Hazelrigg et al., 1984	Supplement Figure 1-2,4-6,10-16
dgG4**	Enhancerless Gal4: w[1118]; P{y[+t7.7] w[+mC]=GAL4.1Uw}attP2	BDSC#68384	Supplement Figure 12-16

** Used to create heterozygous driver (Dri Ctrl) and effector controls (Eff Ctrl).

Supplemental Data Table S2

Figure No	Statistical analysis		
SupFig1	*KKW test*		
	H (2, N= 79) =11.98143;	p =0.0025	*
	MWU test		
	Exp vs Eff	U=169; p<0.05/2	*
	Exp vs Dri	U=200,5 ; p<0.05/1	*
	OSS test		
	Exp	p<0.05/3	*
	Dri	p=0.845	ns
	Eff	p=0.524	ns
SupFig2	*KKW test*		
	H (2, N= 32) =13,23027	p =0.0013	*
	MWU test		
	Exp vs Eff	U=6; p<0.05/2	*
	Exp vs Dri	U=26 ; p<0.05/1	*
	OSS test		
	Exp	p<0.05/3	*
	Dri	p=0.3323	ns
	Eff	p=0.4545	ns
SupFig3	*MWU test*		
	No Retinal (ATR) vs with Retinal	U=406; p>0.05	ns
	OSS test		
	No Retinal (ATR)	p<0.05	*
	with Retinal (ATR)	p<0.05	*
SupFig4	*KKW test*		
	H (4, N= 60) =12,91674	p =0.0117	*
	MWU test		
	Exp vs Eff (Chrimson^{E})	U=24; p<0.05/6	*
	Exp vs Dri (Chrimson^{E})	U=31 ; p<0.05/5	*
	Exp vs Eff (Chrimson^{F})	U=43.5; p>0.05	ns
	Exp vs Dri (Chrimson^{F})	U=62 ; p>0.05	ns
	Exp vs Exp	U=38; p>0.05	ns
	OSS test		
	Exp (Moonwalker^{A} x Chrimson^{E})	p<0.05/5*	
	Exp (Moonwalker^{A} x Chrimson^{F})	p=0.5488	ns
	Dri	p=1	ns
	Eff (ChrimsonE)	p=1	ns
	Eff(ChrimsonF)	p=1	ns
SupFig5	*KKW test*		
	H(3, N=72)=17,51744;	p=0.0006	*
	MWU test		
	Exp vs Dark	U=78; p<0.05/1	*
	Exp vs Dri	U=69; p<0.05/2	*
	Exp vs Eff	U=46; p<0.05/3	*
	OSS test		
	Dark	p<0.05/2	*

	Exp	p<0.05/1	*
	Dri	p<0.05/4	*
	Eff	p<0.05/3	*
SupFig6	*KKW test*		
	H(3, N=21)=14,54638;	p=0.0022	*
	MWU test		
	Exp vs Dark	U=0; p<0.05/2	*
	Exp vs Dri	U=0; p<0.05/3	*
	Exp vs Eff	U=0; p<0.05/1	*
	OSS test		
	Dark	p<0.05/2	ns
	Exp	p<0.05/1	*
	Dri	p<0.05/4	*
	Eff	p<0.05/3	ns
SupFig7	*MWU test*		
	Control vs Trapped	U=0; p<0.05/2	*
	OSS test		
	Control	p<0.05/2	*
	Trapped	p<0.05/1	*
SupFig8	*KKW test*		
	H (4, N= 110) =16.99635; p =0.001	*	
	MWU test		
	$MDN1^A$x $ChR2\text{-}XXL^A$ (Continuous vs Intermediate)	U=85.5; p<0.05/3	*
	$MDN1^A$x $ChR2\text{-}XXL^A$ (Continuous vs Pulsed)	U=68 ; p<0.05/2	*
	$MDN1^A$ x $ChR2\text{-}XXL^A$ vs $MDN1^A$ x $Chrimson^E$ (Continuous vs Continuous))	U=144; p<0.05/4	*
	$MDN1^A$ x $ChR2\text{-}XXL^A$ vs $MDN1^A$ x $Chrimson^E$ (Continuous vs pulsed))	U=96.5; p<0.05/5	*
	OSS test		
	$MDN1^A$x $ChR2\text{-}XXL^A$ (Continuous)	p<0.05/5	*
	$MDN1^A$x $ChR2\text{-}XXL^A$ (Intermediate)	p<0.05/4	*
	$MDN1^A$x $ChR2\text{-}XXL^A$ (Pulsed)	p=0.387	ns
	$MDN1^A$x $Chrimson^E$ (Continuous)	p<0.05/3	*
	$MDN1^A$x $Chrimson^E$ (Pulsed)	p=0.8238	ns
SupFig9	*KKW test*		
	H(2, N=43)=23,71427;	p=0.0000	*
	MWU test		
	SUC vs 3IY + L-DOPA	U=93; p=0.853	ns
	SUC vs 3IY	U=10; p<0.05/3	*
	3IY vs 3IY + L-DOPA	U=9; p<0.05/2	*
	OSS test		
	SUC	p<0.05/2	ns
	3IY	p<0.05/3	*
	3IY + L-DOPA	p<0.05/1	ns
SupFig10 (top)	*KKW test*		
	H (2, N= 61) =13.05162;	p =0.0015	*
	MWU test		
	Exp vs Eff	U=74.5; p<0.05/2	*
	Exp vs Dri	U=110 ; p<0.05/1	*

	OSS test		
	Exp	p<0.05/3	*
	Dri	p=0.8145	ns
	Eff	p=0.481	ns
SupFig10 (middle)	*KKW test*		
	H (2, N= 50) =7.644942;	p =0.0219	*
	MWU test		
	Exp vs Eff	U=68,5; p<0.05/2	*
	Exp vs Dri	U=71 ; p<0.05/1	*
	OSS test		
	Exp	p<0.03/3	ns
	Dri	p=0.61	ns
	Eff	p=0.804	ns
SupFig10 (bottom)	*KKW test*		
	H (2, N= 31) =3.372;	p =0.1853	ns
SupFig11	*KKW test*		
	H (2, N= 47) =12.1943;	p =0.0022	*
	MWU test		
	Exp vs Eff	U=48; p<0.05/1	*
	Exp vs Dri	U=45 ; p<0.05/2	*
	OSS test		
	Exp	p<0.05/3	*
	Dri	p=0.455	ns
	Eff	p=1	ns
SupFig12 (1 trial)	*KKW test*		
	H (2, N= 178) =5.48244;	p =0.0645	ns
SupFig12 (3 trial)	*KKW test*		
	H (2, N= 94) =2.979997;	p =0.2254	ns
SupFig13 (1 trial)	*KKW test*		
	H (2, N= 123) =2.3066;	p =0.0645	ns
SupFig13 (3 trial)	*KKW test*		
	H (2, N= 93) =4,2533;	p =0.0645	ns
SupFig14 (activation)	*KKW test*		
	H (2, N= 60) =12.11.4856;	p =0.0032	*
	MWU test		
	Exp vs Eff	U=73; p<0.05/1	*
	Exp vs Dri	U=125.5 ; p<0.05/2	*
	OSS test		
	Exp	p<0.05/3	*
	Dri	p=1	ns
	Eff	p=0.48	ns
SupFig14 (silencing)	*KKW test*		
	H (2, N= 68) =4.86808;	p =0.08	ns

SupFig15	*KKW test*		
	H (2, N= 49) =26.35385;	p =0.0000	*
	MWU test		
	Exp vs Eff	U=4; p<0.05/2	*
	Exp vs Dri	U=8 ; p<0.05/1	*
	OSS test		
	Exp	p<0.05/3	*
	Dri	p=0.774	ns
	Eff	p=0.1516	ns
SupFig16 (activation)	*KKW test*		
	H (2, N= 98) =21.34925;	p =0.0000	*
	MWU test		
	Exp vs Eff	U=352; p<0.05/1	*
	Exp vs Dri	U=229 ; p<0.05/2	*
	OSS test		
	Exp	p<0.05/3	*
	Dri	p=0.229	ns
	Eff	p<0.05/2	*
SupFig16 (silencing)	*KKW test*		
	H (2, N= 176) =12.63377;	p =0.0018	*
	MWU test		
	Exp vs Eff	U=1083; p<0.05/2	*
	Exp vs Dri	U=1256 ; p<0.05/1	*
	OSS test		
	Exp	p<0.05/2	*
	Dri	p=0.237	ns
	Eff	p<0.05/3	*

Declaration of Honour

“I hereby declare that I prepared this thesis without the impermissible help of third parties and that none other that the aids indicated have been used; all sources of information are clearly marked, including my own publications.

In particular I have not consciously:

- fabricated data or rejected undesirable results,
- misused statistical methods with the aim of drawing other conclusions than those warranted by the available data,
- plagiarized external data or publications,
- presented the results of other researchers in a distorted way.

I am aware that violations of copyright may lead to injunction and damage claims by the author and also to prosecution by law enforcement authorities.

I hereby agree that the thesis may be electronically reviewed with the aim of identifying plagiarism.

This work has not been submitted as a doctoral thesis in the same or a similar form in Germany, nor in any other country. It has not yet been published as a whole.”

Fatima Amin